PROCEEDINGS OF THE ACADEMY OF SCIENCES OF THE USSR

Physical Chemistry Section

Volume 133, Numbers 1-6 July-August, 1960

CONTENTS

	PAGE	RUSS. ISSUE	RUSS. PAGE
Differences in the Mechanism of Liquid and Gaseous Phase Oxidation of Ethyl Alcohol. É. A. Blyumberg, G. E. Zaikov, Z. K. Maizus, and N. M. Émanuél'.	575	1	144
The Effect of Water Vapor on the Interaction of Germanium and Oxygen. R. Kh. Burshtein, L. A. Larin, and G. F. Voronina	579	1	148
Investigation of the Strength of C–O Bonds by Isotopic Exchange. V. G. Vasil'ev and E. N. Kharlamova	583	1	152
Measurement of Sound Velocity in Detonation Products. V. M. Zaitsev, P. F. Pokhil, and K. K. Shvedov	587	1	155
Adiabatic Theory for Electron Transfer Processes in Solution. V. G. Levich and R. R. Dogonadze	591	1	158
Nature of the Current Fall on Polarographic Waves Limited by a Preceding Chemical Reaction. S. G. Mairanovskii	595	1	162
Electrical Properties of Inner Complexes. O. A. Osipov and V. M. Artemova	599	1	166
Kinetics of Electrode Processes on a Silicon Electrode in Acid and Alkaline Solutions. E. N. Paleolog, K. S. Korotkova, and N. D. Tomashov	603	1	170
Conditions for the Stability of a Plane Solid-Liquid Interface during Crystallization of a Binary Melt. D. E. Temkin	607	1	174
The Nature of Secondary Chemical Bonds. D. N. Shigorin, A. N. Rodionov, T. V. Talalaeva, and K. A. Kocheshkov	611	1	178
Anodic Dissolution of Germanium with a p-n Junction. O. G. Deryagina, E. N. Paleolog and N. D. Tomashov	615	2	388
Electrochemical and Photoelectrochemical Behavior of the Silicon Electrode. S. U. Izidinov, T. I. Borisova and V. I. Veselovskii	619	2	392
The Operation of a Galvanic Cell with a Solid Electrolyte Exhibiting Mixed Conductivity. S. V. Karpachev and S. F. Pal'guev	623	2	396
The Mechanism of the Combustion of Powders. G. B. Manelis, A. G. Merzhanov, and F. I. Dubovitskii	627	2	399
The Interaction Between a Microimpurity and the Surface of Crystals. I. V. Melikhov, Chiu Hsiao-Hsi and M. S. Merkulova	629	2	401
Molecular Mechanism in the Deformations of Polymer Substances. G. A. Patrikeev	635	2	405
Equilibrium Potentials of Zirconium in Mixed Fluoride-Chloride Melts. M. V. Smirnov, V. E. Komarov, and A. N. Baraboshkin	639	2	409
Catalytic Decomposition of Hydrazine on Nickel Sulfide and its Solid Solutions. Huang Yu-mei, N. P. Keier, and S. Z. Roginskii	643	2	413
Effect of Adsorption of Anions on the Discharge of Hydrogen on Palladium and the Ionization of Hydrogen Dissolved in Palladium . L. T. Shanina	647	2	417
The Luminescence Spectra of Haloanthraquinones Frozen in Solution. D. N. Shigorin, N. A. Shcheglova, and N. S. Dokunikhin	651	2	420

CONTENTS (continued)

	PAGE	RUSS. ISSUE	RUSS. PAGE
The Paramagnetic Resonance of Various Forms of α, α-Diphenyl- β-picrylhydrazyl Yu. V. Yablokov	655	2	424
Electrochemical and Photoelectrochemical Processes on p- and n-Germanium at Cathodic Polarization	659	3	620
Fine Structure of the Rayleigh Scattering Line in Solutions and Hyperacoustic Dispersion. L. V. Lanshina and M. I. Shakhparonov	663	3	624
Initiating Action of Nitrosyl Chloride in the Oxidation of Propane. Z. K. Maizus and N. M. Émanuél'	667	3	627
The Mechanism of the Influence of Small Quantities of Added Electrolytes on the Strength of a Crystallization Hardened Structure. E. E. Segalova, Z. N. Markina, and P. A. Rebinder	671	3	630
Stationary States of Dispersed Electrochemical Systems and their Stability. V. P. Smilga and Yu. A. Chizmadzhev	675	3	633
Dependence of Normal and Shearing Stresses Upon the Value of Deformation at the Transition from the Rest State to the Stationary Flow of a Gel of Aluminum Naphthenate. A. A. Trapeznikov, A. S. Morozov, and G. G. Petrzhik	679	3	637
Chemisorption on Pure and Doped NiS. Huang Yu-mei, N. P. Keier and S. Z. Roginskii	683	3	641
Effect of Metal and Solvent on the Formation of Aromatic Anion-Radical Polymerization Initiators. E. A. Yakovleva, E. S. Petrov, S. P. Solodovnikov, V. V. Voevodskii, and A. I. Shatenshtein	689	3	645
Effect of Specific Radioactivity of Cerium Oxalate on its Solubility. Vikt. I. Spitsyn and N. G. Moshchanskaya	693	4	859
The Influence of the State of the Diffusion Side of an Iron Membrane on the Rate of Diffusion of Electrolytic Hydrogen. I. A. Bagotskaya and L. D. Kovba	697	4	862
The Effect of Particle Size on the Rate of Combustion of Mixtures Containing Potassium Perchlorate. N. N. Bakhman and A. F. Belyaev	701	4	866
The Mechanism of the Electrolytic Polishing of Metals, in the Light of Electron Microscope Studies of the Surface at Different Stages in the Treatment. G. S. Vozdvizhenskii, G. A. Gorbachuk, and G. P. Dezider'ev	705	4	869
On the Nonequilibrium State behind a Shock Wave in Air. S. A. Losev and N. A. Generalov	709	4	872
The Influence of Selenium and Tellurium on the Catalytic Action of Silver in the Oxidation of Ethylene. V. E. Ostrovskii, N. V. Kul'kova, and A.D. Nedbaeva	713	4	875
A Rapid Chromatographic Method of Measuring Gas and Vapor Isotherms. S. Z. Roginskii, M. I. Yanovskii, Lu Pei-chzhan, G. A. Gaziev, G. M. Zhabrova, B. M. Kadenatsi and V. V. Brazhnikov	717	4	878
Kinetics of the Hydrolysis of Pyridine-Sulfur Trioxide. I. G. Ryss and D.B. Donskaya.	721	4	882
The Effect of Temperature on the Corrosion Rate of Metals in Acid Media. V. A. Khitrov, V. I. Shatalova, I. S. Smol'yaninov, and Yu. I. Sadovskaya	725	4	886
The Effects of Light on Polarized Germanium Anodes A. A. Yakovleva, T. I. Borisova, and V. I. Veselovskii	729	4	889
The Mechanism of the Reciprocal Transfer of Copper during Friction between Bronze and Steel. D. N. Garkunov, V. N. Lozovskii, and A. A. Polyakov.	733	5	1128
The Problem of Measuring the Condensation Coefficient. R. Ya. Kucherov and L. É. Rikenglaz	735	5	1130
Morphology of Molecular Packing in Linear Polyesters. Yu. V. Mnyukh, E. M. Belavtseva, and A. I. Kitaigorodskii	739	5	1132

CONTENTS (continued)

	PAGE	RUSS. ISSUE	RUSS. PAGE
Autooscillation Processes in Some Electrochemical Systems. Yu. A. Chizmadzhev	745	5	1136
Specific Catalytic Activity of Iron Films toward Isotopic Exchange in Molecular Hydrogen. M. A. Avdeenko, G. K. Boreskov, and K. N. Zhavoronkova	749	6	1354
Effect of Molecular Weight on the Luminescence of High-Molecular Compounds. V. F. Gachkovskii	753	6	1358
A Study of the Spontaneous Contraction of Polymers with a Branched Spatial Structure during Their Breakdown. V. E. Gul', V. V. Kovriga, and A. N. Kamenskii.	761	6	1364
The Rate of Electron Exchange Reactions in Solutions. R. R. Dogonadze	765	6	1368
Emission of Chemically Active Particles during the Oxidation of Aluminum. M. Ya. Gen and Yu. I. Petrov	767	6	1361
The Detonation of Nitromethane Close to the Limit. A. N. Dremin, G. A. Adadurov, and O. K. Rozanov.	771	6	1372
The Mechanism by Which Modifying Admixtures Influence the Selectivity of Zinc Oxide for the Dehydrogenation and the Dehydration of Isopropyl Alcohol. G. M. Zhabrova, V. I. Vladimirova and O. M. Vinogradova	775	6	1375
Capillary Rise of a Liquid in Porous Media and Capillary Hysteresis. D. N. Nekrasov and M. M. Kusakov	779	6	1379
Effect of β-Radiation of S^{35} on Isotopic Exchange of Oxygen in the System $Na_2SO_4^{16}-O_2^{18}$. Vikt. I. Spitsyn and V. G. Finikov	781	6	1381
The Mobility of Modifying Additives in Silver. Yu. N. Stepanov, L. Ya. Margolis, and S. Z. Roginskii	785	6	1384
The Thermodynamic Properties of Chlorinated Silanes. M. L. Shakhparonov, S. L. Lel'chuk and K. M. Korchemskaya	789	6	1388

DIFFERENCES IN THE MECHANISM OF LIQUID AND GASEOUS PHASE OXIDATION OF ETHYL ALCOHOL

É. A. Blyumberg, G. E. Zaikov, Z. K. Maizus, and N. M. Émanuél',

Corresponding Member, Acad. Sci. USSR

Institute of Chemical Physics, Academy of Sciences, USSR
Translated from Doklady Akademii Nauk SSSR, Vol. 133, No. 1, pp. 144-147,
July, 1960
Original article submitted March 29, 1960

The oxidation of compressed n-butane in the neighborhood of critical temperature and pressure has established the superiority of liquid phase oxidation over oxidation in the gaseous state [1, 2].

Oxidation takes place at considerably lower temperatures in the liquid state and is characterized by high selectivity and rate of reaction, and by an almost complete absence of those products of deep oxidation which arise in the gaseous phase. The explanation of these differences is a problem of considerable technical and theoretical importance.

N. N. Semenov [3] explained the relation between the composition of the products from gaseous oxidation of the hydrocarbons and the oxidation conditions in terms of two competing radical reactions: isomerization of the $RO_2\cdot$ radical with subsequent monomolecular breakdown

$$RO_2\cdot \rightarrow R'O\cdot + R''OH \qquad (1)$$

and a bimolecular reaction between the $RO_2\cdot$ and the hydrocarbon in question

$$RO_2\cdot + RH \rightarrow RO_2H + R\cdot \qquad (2)$$

Reaction (1) is favored by an elevation of the temperature and a reduction of the pressure, while Reaction (2) is favored by a reduction in the temperature and an elevation of the pressure.

If these concepts are applied to liquid phase oxidation of hydrocarbons at high density it should be assumed that the principal reaction is that leading to the formation of the hydroperoxides, i.e., Reaction (2). It is not impossible that the differences in the gas phase and liquid phase oxidations arise not only from the concentration changes accompanying alteration in the state of aggregation but from still more profound factors associated with differences in the oxidation mechanisms. A comparative study of the liquid phase and gas phase oxidations of a single substance under comparable conditions would be instructive in this connection.

Ethyl alcohol is a suitable material for such study since its relatively high critical temperature of 243° permits investigations to be extended over a wide temperature interval.

High pressure liquid phase oxidation of ethyl alcohol is also of interest in itself since the literature contains no data at all on the kinetics of this reaction and patents give only fragmentary indication of the possibility that this process can be carried out in the presence of catalysts.

The present study of the oxidation of ethyl alcohol employed a stainless steel autoclave system having a cylindrical reactor equipped with a thermocouple and various tubes for the introduction of bubbling air and removal of the reaction products. The vaporizing alcohol was returned to the reactor as a condensate from a reflux condenser [2].

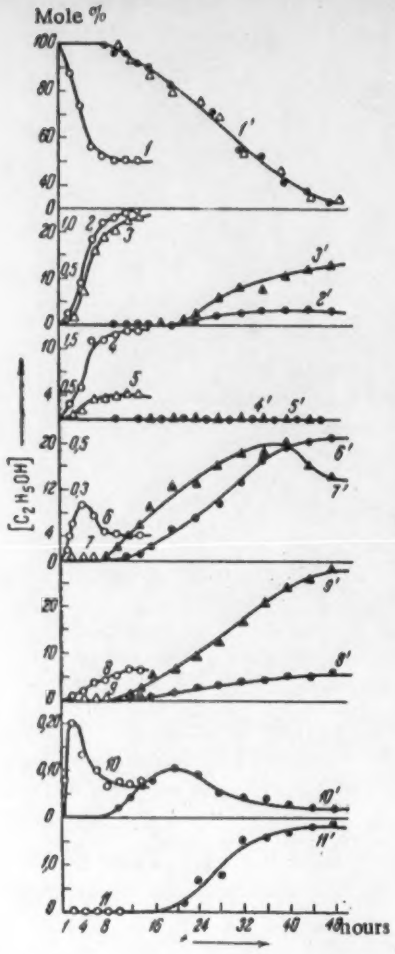

Fig. 1. Kinetic curves for the formation of reaction products during oxidation of ethyl alcohol at 200° in the liquid phase (unprimed numerals) and in the gaseous phase at an initial alcohol concentration of $2.6 \cdot 10^{-3}$ moles/ cm^3 (primed numerals). 1 and 1') Consumption of ethyl alcohol (the triangulated points on Curve 1' correspond to data from the kinetic curve for the alcohol consumption in experiments at an initial concentration of $0.54 \cdot 10^{-3}$ moles/ cm^3 after arbitrary displacement to that same induction period as for the experiments at $2.6 \cdot 10^{-3}$ moles/ cm^3); 2 and 2') acetic acid; 3 and 3') formic acid(right-hand scale); 4 and 4') ethyl acetate; 5 and 5') ethyl formate (right-hand scale); 6 and 6') acetaldehyde; 7 and 7') formaldehyde (right-hand scale); 8 and 8') CO_2; 9 and 9') CO; 10 and 10') peroxide; 11 and 11') methyl alcohol.

Identification and quantitative determination of the various reaction products was made by the usual methods of chemical analysis supplemented by a specially developed technique of paper chromatography for the separation of alcohols and carbonyl compounds [4].

Liquid phase oxidation was carried out at 200° under a pressure of 50 atm with an air feed of 20 liters/hr. Passage to gas phase oxidation at the same temperature was brought about by lowering the pressure in the reactor to 20 atm.

Kinetic curves for the consumption of ethyl alcohol and the formation of the oxidation products are given in the Figure for both the gas phase and the liquid phase oxidations. For ease of comparison, all of the results included in this figure have been reduced to unit quantity of reacting alcohol. The liquid phase oxidation is characterized by the almost complete absence of an induction period. There is an extended induction period of the order of 10 hours in the gas phase oxidation and the rate of reaction at the end of this period is much less than that for oxidation in the liquid.

Detailed analysis shows that there is a marked difference in the composition of the products obtained from the oxidation of ethyl alcohol in the gas phase and in the liquid phase. Although acetic acid and ethyl acetate are the principal products obtained from the liquid phase oxidation, these substances are almost completely lacking in the gas phase oxidation. Considerable quantities of carbon monoxide are produced, but only in the gas phase oxidation. Acetaldehyde, the second basic product from the gaseous oxidation, is detectable in only very small quantities in the liquid phase oxidation, and appears there as an intermediate reaction product.

Formic acid and peroxides are unstable under the experimental conditions and were detected in very small amounts in both processes. The formic acid undergoes thermal decomposition into CO and water, while the peroxides break down under the catalytic action of the metallic walls of the reactor. Formaldehyde and methyl alcohol were observed as reaction products only in the gaseous oxidation.

At first glance it would seem that this marked change in the direction of reaction in passing from liquid to gaseous oxidation would be consistent with the Semenov concept of competing radical reactions. The principal reaction in the liquid phase oxidation of ethyl alcohol can be represented by:

$$CH_3CH_2OH + O_2 \rightarrow CH_3\dot{C}HOH + HO_2$$

$$CH_3\dot{C}HOH + O_2 \rightarrow CH_3CHOH \quad (O-O\bullet)$$

$$CH_3CH(O-O\bullet)-OH + CH_3CH_2OH \rightarrow CH_3CH(OOH)OH + CH_3\dot{C}HOH$$

$$CH_3CH(OOH)OH \rightarrow CH_3COH + H_2O_2;\ CH_3COH \xrightarrow{O_2} CH_3COOH.$$

Here, acetic acid should be the major reaction product, just as has been shown to be the case in the present work. (Ethyl acetate can be looked upon as the product of further interaction between the acetic acid and ethyl alcohol.)

Passage to the gas phase oxidation at the same temperature involves a diminution of the density of the reacting mixture and thus increases the probability of monomolecular breakdown of the peroxide radical. Thus, there are two possible paths for isomerization of the radical

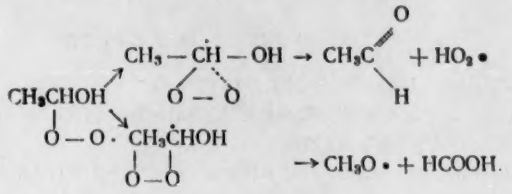

with the formation of acetaldehyde and formic acid (carbon monoxide), the actually observed products from gas phase oxidation.

The acetaldehyde is here a final reaction product, further oxidation to acetic acid being possibly prevented by the inhibiting action of the ethyl alcohol which is characteristic of the gaseous reaction. Differences in the density of the ethyl alcohol cannot, however, account entirely for the observed difference in mechanisms in the liquid and gas phase oxidations. Under our experimental conditions, the alcohol concentration changed by a factor of five in passing from the one state of aggregation to the other, going from $1.26 \cdot 10^{-2}$ moles/cm^3 in the liquid phase to $2.6 \cdot 10^{-3}$ moles/cm^3 in the gaseous phase, and this could not lead to so marked an alteration in the direction of reaction. The ratio of the rates of Reactions (1) and (2) at fixed temperature should, in fact, be proportional to the concentration of the oxidizing alcohol

$$\frac{w_1}{w_2} = \frac{k_1 (R)}{k_2 (R)\,(ROH)},$$

so that the ratio w_2/w_1 in our case would be five times greater for oxidation in the liquid phase than for oxidation in the gaseous phase. In evaluating the quantity k_2/k_1 from the experimental data we introduced the concept of the specific fraction of products formed along each of the two reaction paths, setting $\alpha_1 = w_1/w_{form}$ for the breakdown of the peroxide radical, and $\alpha_2 = w_2/w_{form}$ for the interaction of this radical with the alcohol, w_{form} being the sum, $w_1 + w_2$, of the rates of formation of products in the gas phase oxidation and in the liquid oxidation. A relation between α_1, α_2, and the ratio k_2/k_1 can be obtained by imposing the condition that the radical concentration, (R), have a stationary value,

$$\frac{d(R\cdot)}{dt} = w_{form} - k_1 (R) - k_2 (R)\,(ROH) = 0. \qquad (I)$$

Setting the value of (R) from Equation (I) into the expressions for w_1 and w_2 gives

$$w_1 = \frac{w_{form}}{1 + \frac{k_2}{k_1}(ROH)} \quad \text{and} \quad w_2 = \frac{w_{form}(ROH)}{\frac{k_1}{k_2} + (ROH)}$$

or

$$\alpha_1 = 1 \Big/ \left[1 + \frac{k_2}{k_1}(ROH)\right]; \quad \alpha_2 = (ROH) \Big/ \left[\frac{k_1}{k_2} + (ROH)\right].$$

The values of the ratio k_2/k_1 for gas and liquid phase alcohol oxidations can be determined as soon as the α's have been obtained from the experimental data. In the first case $k_2/k_1 = 0.37$ and in the second, $k_2/k_1 = 4.8 \cdot 10^{-4}$, so that the rate ratio for Reactions (1) and (2) alters, not by a factor of five, but by 10^3, in passing from the liquid phase to the gaseous phase oxidation.

A five-fold alteration in the alcohol concentration (from $2.6 \cdot 10^{-3}$ moles/cm^3 to $0.54 \cdot 10^{-3}$ moles/cm^3) in the gaseous phase oxidation at 200° and 20 atm pressure increases the induction period from 10 to 24 hours, but

is almost without effect on the rate of consumption of the alcohol at the end of this period (open circles in the Figure), or on the composition of the oxidation products. These changes alter α_1 and α_2 by several fold.

Thus, the conclusion can be drawn that the rate and direction of reaction in the liquid phase oxidation of ethyl alcohol are fixed, not by the high density alone, but also by the specific characteristics of the liquid state. Such specific characteristics could arise from the presence of intermolecular hydrogen bonding or from reactions involving ions which are lacking in the gaseous phase.

LITERATURE CITED

1. N. M. Émanuél', Doklady Akad. Nauk SSSR 110, 245 (1956).*
2. É. A. Blyumberg, Z. K. Maizus, and N. M. Émanuél', Collection, Oxidation of Hydrocarbons in the Liquid Phase [in Russian] (Izd. AN SSSR, 1959) p. 125.
3. N. N. Semenov, Certain Problems in Chemical Kinetics and Reactivity [in Russian] (Izd. AN SSSR, 1958) p. 131.
4. G. E. Zaikov, Zhur. Anal. Khim. 15, 104 (1960).*

* Original Russian pagination. See C. B. translation.

THE EFFECT OF WATER VAPOR ON THE INTERACTION OF GERMANIUM AND OXYGEN

R. Kh. Burshtein, L. A. Larin, and G. F. Voronina

Institute of Electrochemistry, Academy of Sciences, USSR
(Presented by Academician A. N. Frumkin, January 28, 1960)
Translated from Doklady Akademii Nauk SSSR, Vol. 133, No. 1, pp. 148-151, July, 1960
Original article submitted January 25, 1960

Our earlier investigations [1, 2] on the mechanism of the chemisorption of oxygen on germanium have shown that a protective film involving two adsorbed oxygens per germanium atom is formed when a germanium surface is brought into contact with dry oxygen at room temperature. Comparison with data on the effect of adsorbed oxygen on the electronic work function of germanium permits the conclusion that the germanium surface becomes covered with a monolayer of composition GeO during the rapid stage of the adsorption and with a monolayer of composition GeO_2 during the slow stage.

It is known from a number of sources that contact with atmospheric air containing water vapor will alter the characteristics of semiconducting germanium devices [3]. Interest attaches to a study of the mechanism of this process and to the elucidation of the effect of water vapor on clean germanium surfaces and on germanium surfaces covered with oxide films. The following experiments were carried out in this connection. A germanium surface was freed of its oxide film by reduction with hydrogen and subsequent degasification, using the technique which we have described earlier [1]; small amounts of oxygen sufficient for completion of either the slow or the rapid stage of the adsorption were then adsorbed on this surface. Following this, the germanium surface was brought into contact with water vapor. The water vapors were either frozen out or pumped away after the lapse of a definite period, and the kinetics of oxygen adsorption studied once more.

The results of these experiments are presented in Fig. 1 where the reciprocal time for half-adsorption of each portion of oxygen has been plotted on the axis of ordinates and the total quantity of adsorbed oxygen, on the axis of abscissas. These data make it clear that the rate of adsorption is increased by removal of water vapors from a germanium surface on which the rapid and slow stages of adsorption (as represented by Curve 1) had been completed and contact then made with water vapor. The process rate diminishes once more as the germanium is acted on by new portions of oxygen (Fig. 1, 2). On the other hand, subsequent interaction of water vapor with germanium covered by a newly formed passive oxide film leads to an increase in the rate of reaction with oxygen, and the surface can, in this case, be rendered passive by additional oxygen adsorption (Fig. 1, 3). Thus, these experiments show that adsorption of water vapor on a germanium surface covered with an oxide film leads to a breakdown in the passivity of this film with the formation of a thick oxide layer.

This breakdown in the passivity of the oxide film under the action of water vapor could be observed clearly when the effect was studied through measurements on differences in contact potentials. These measurements were carried out by the vibrating condensor method in a fused glass apparatus with a reference electrode such as we described earlier in [4]. The effect of the adsorption of water vapor on the electronic work function of a clean germanium surface is shown by Fig. 2, 1. These data indicate that there is a linear relation between log P_{H_2O} and the alteration in the work function over the pressure range from $1 \cdot 10^{-3}$ to 7 mm of Hg. The electronic work function increases by 0.16 v over this pressure interval. There is, however, a sharp increase in the work

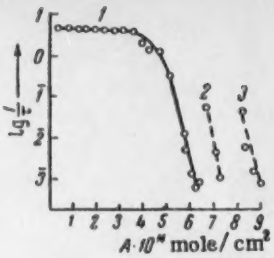

Fig. 1. Relation between the degree of surface coverage of germanium and the rate of oxygen adsorption. 1) On a clean surface; 2) after adsorption of water vapor.

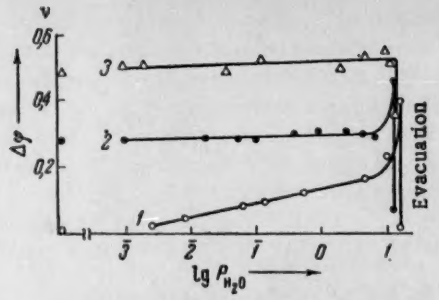

Fig. 2. Relation between log P_{H_2O} and the difference in contact potentials: 1) on a clean surface; 2) on germanium covered with an oxide film; 3) after repeated treatment.

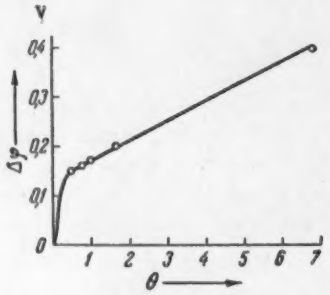

Fig. 3. Relation between the amount of adsorbed water vapor and the difference in contact potentials. θ designates the number of molecular layers.

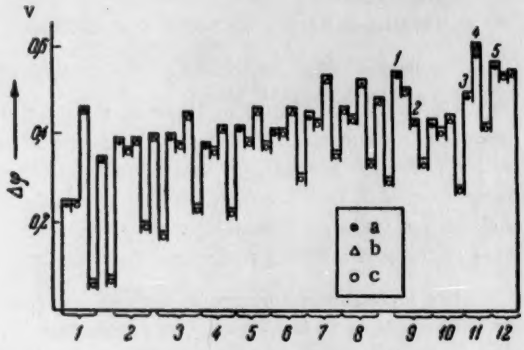

Fig. 4. Alteration of the difference in contact potentials under repeated treatment of a germanium surface with oxygen, water wapor, and in vacuum. a) Oxygen; b) water; c) in vacuum. 1) P_{O_2} = = 12 mm; 2) τ = 120 min; 3) P_{O_2} = 3 mm; 4) simultaneous action of water vapor (P_{H_2O} =15 mm) and oxygen (P_{O_2} = 3 mm); 5) P_{O_2} = 1.5 mm, τ = 1000 min.

function by 0.24 v when the partial pressure of the water vapor is increased by raising the humidity from 50 to 100%. Thus, the work function can be increased by 0.4 v through adsorption of water vapor. This alteration in work function is reversible, the work function falling to the value characteristic of a clean germanium surface when the water vapor is pumped away.

The effect of water vapor on the work function of germanium covered with an oxide film is of a different type. The results of experiments on this point are illustrated in Fig. 2, 2. Here the oxygen was allowed to adsorb on the germanium for 15 hours at a pressure of 0.1 mm of Hg. Under these conditions, the resulting alteration of 0.15 v of the difference in contact potentials is principally due to the rapid adsorption of oxygen and only partially due to the slow adsorption, conclusions which are consistent with the earlier results. Figure 2, 2 shows that there is an increase of 0.28 v in the work function from the chemisorption of oxygen under these conditions. Adsorption of water vapor under an alteration in pressure from $1 \cdot 10^{-3}$ to 7 mm changes the contact difference of a germanium surface covered with an oxide film by only 0.02 v. The difference in contact potentials rises by 0.16 v when the water vapor pressure is increased from 7 to 15 mm. Thus, the alteration in the difference in contact potentials caused by adsorption of water vapor is twice as great on a surface which is covered with an oxide film.

Figure 2 (Curves 1 and 2) shows that there is a sharp alteration in the difference of contact potentials over the interval of water vapor pressures from 7 to 15 mm (log P_{H_2O} = 0.84 – 1.18). These results can be explained

on the basis of [5, 6] where it was shown that the water vapor adsorption resulting from an increase in the humidity up to 80% is associated with the formation of three molecular layers, while an elevation of the humidity from 80 to 100% increases the depth of the water film to seven molecules. Our results have been compared with those of certain Japanese investigators [6] in Fig. 3, where the relation between the value of $\Delta\varphi$ and the number of molecular water layers adsorbed on the germanium is presented. This figure makes it clear that the pronounced increase in difference of contact potentials which is met at the higher pressures is related to the marked rise in the amount of water vapor which is taken up under these conditions.

In distinction to the case of adsorption of water vapor on a clean surface, Fig. 2 shows the adsorption of an oxide-covered germanium surface to be irreversible.

This is indicated by the fact that the difference in contact potentials does not return to its original value after desorption of the water vapors, but takes on a value some 0.07 v higher than the work function for a clean germanium surface. The implication is that there is a breakdown in the structure of the oxide film and an alteration in its protective action.

The fact that the diminution in the difference in contact potentials under the action of water vapor is less on an oxidized germanium surface than on a clean surface is possibly due to a decrease of the work function resulting from breakdown in the structure of the oxide film which proceeds simultaneously with the increase in the work function resulting from the water vapor adsorption itself.

The data of Fig. 1 indicate that the germanium surface acquires the ability to adsorb additional quantities of oxygen as a result of such structural breakdown. The work function of the germanium once more rises to 0.4 v after these additional quantities of oxygen have been taken up. The effect of successive action of oxygen, water vapor, and vacuum on the surface properties of germanium was followed through 12 cycles. The results of these experiments are presented in Fig. 4. Except for those special cases which are noted in the figure, the oxygen was adsorbed on the germanium at a pressure of the order of $1 \cdot 10^{-1}$ mm for 15-30 min, and the water vapor adsorbed at 100% humidity for 10-30 min. The specimens were held in vacuum for approximately 30 min. The data of Figs. 1 and 4 show that a germanium surface which is in contact with water vapor cannot be brought into a stable state. The data on the value of the work function after desorption indicate that the protective action of the oxide film is broken down in every case where the germanium surface is oxidized in contact with water vapor.

Results from a study of the effect of various pressures of water vapor on the difference of contact potentials of germanium which had been subjected to repeated action of oxygen and water vapor (11 cycles) are shown in Fig. 2, 3. It follows from these data that the adsorption of water vapor, even at high humidity, will increase the work function of the germanium by only 0.03 v if the conditions are such that a thick oxide film has been formed on the surface. This alteration is considerably less than that which occurs in the first cycle. The work function continues to change appreciably as the water vapors are pumped off, although the alteration here is much less pronounced than in the first cycle. Thus, the alteration of the work function resulting from evacuation of the water vapors is 0.4 v in the first cycle and only 0.16 v in the tenth cycle.

A study of the joint action of oxygen and water vapor on the work function of germanium was carried out earlier by Brattain and Bardeen [7]. These experiments were performed with germanium which had been treated with oxygen in a spark discharge and showed the work function to diminish, regardless of whether the metal was held in an atmosphere of oxygen alone or in an atmosphere of oxygen saturated with water vapor. Our own results prove that there is an increase in the work function from the adsorption of either oxygen or water vapor on a clean germanium surface or on a germanium surface which is covered with a rather thin oxide film. The divergences in these conclusions clearly result from the fact that treatment of germanium with oxygen in a spark discharge brings about a profound alteration in the surface properties of the metal.

It also follows from our data that the adsorption of water vapor leads to a breakdown of the protective oxide film on the germanium surface. This, in turn, results in the formation of thick oxide layers on the surface. It is possible that the formation of these thick oxide layers is responsible for the deterioration of the characteristics of semiconducting devices which are in contact with the atmosphere.

It would be advisable to render the germanium surface hydrophobic in order to impede the formation of these thick oxide films. This was achieved by the adsorption of trichloromethylsilane vapors on the germanium at the end of the rapid and slow stages of adsorption. Hydrolysis was then carried out, with polymerization of

the trichloromethylsilane, in the presence of water vapor at 150° for 1.5 hr.

The activating action of water vapor for the oxygen adsorption practically ceased once the germanium surface had been covered with this hydrophobic film.

The stability of this hydrophobic surface with respect to the adsorption of oxygen was maintained even after repeated interaction with water vapor and oxygen. Preliminary experiments have shown that treatment with the silane has a beneficient effect on the characteristics of semiconducting devices.

We wish to express our thanks to Academician A. N. Frumkin for his interest in this work.

LITERATURE CITED

1. R. Kh. Burshtein, L. A. Larin, and G. F. Voronina, Doklady Akad. Nauk SSSR 130, 4, 801 (1960).•
2. R. Kh. Burshtein and L. A. Larin, Doklady Akad. Nauk SSSR 130, 3, 565 (1960).•
3. E. N. Clarke, Phys. Rev. 99, 1899 (1955).
4. R. Kh. Burshtein and L. A. Larin, Zhur. Fiz. Khim. 32, 194 (1958).
5. J. T. Law, J. Phys. Chem. 59, 67 (1955).
6. K. Kawasaki, K. Kanou, and Y. Sekita, J. Phys. Soc. Japan 14, 233 (1959).
7. W. H. Brattain and J. Bardeen, Bell Syst. Techn. J. 32, 1 (1953).

• Original Russian pagination. See C. B. translation.

INVESTIGATION OF THE STRENGTH OF C – O BONDS BY ISOTOPIC EXCHANGE

V. G. Vasil'ev and E. N. Kharlamova

L. Ya. Karpov Physicochemical Scientific Research Institute

(Presented by Academician S. S. Medvedev, March 4, 1960)
Translated from Doklady Akademii Nauk SSSR, Vol. 133, No. 1, pp. 152-154, July, 1960
Original article submitted March 4, 1960

The strength of C – O bonds in ethers and esters is of both theoretical and practical interest as it plays a certain role in the thermal stability of polyester resins.

The authors investigated the comparative strength of bonds in ethers and esters of various structures by the isotopic exchange method with C^{14}. The degree of exchange (in percent of equilibrium) reached under given experimental conditions after a certain constant time interval was taken as a relative measure of the strength. The conditions were selected such that the degree of exchange was small and in any case did not exceed 20-40%; the degrees of exchange therefore corresponded approximately to the rate constants. The experiments were carried out in ampoules. The exchanging mixtures were equimolecular; one of the components was labeled with C^{14} in the C*–O bond. After being heated at the given temperature, the mixture was extracted from the ampoule and separated. In the first two series, the degree of exchange was determined from the radioactivity acquired by the unlabeled component (qualitative) and in the third series it was determined from the fall in isotope content of the labeled acid (quantitative). The completeness of separation of the mixture was checked by a "blank" experiment which was carried out with the same mixture without heating and was always quite satisfactory.

EXPERIMENTAL

Series 1. Test experiments with ethers. These experiments showed that p-nitrophenetole, p-chlorophenetole, p-diethoxybenzene, and the ethyl ether of p-cresol do not exchange with C^{14}-ethyl ether when heated to 300° for 20 hours (only traces of exchange were observed). Phenetole gave very slight exchange with ether under the same conditions. Test experiments on the exchange of phenetole and p-nitrophenetole with C^{14}-ethanol under the same conditions also showed that there was no exchange. This indicates the strength of the C–O bond in these systems.

Series 2. Qualitative experiments on exchange in carboxyl and carbonyl compounds. The results of experiments on exchange at 200° for 15 hours are given in the Table.

Mixture components	Exchange	Mixture components	Exchange
$CH_3C^*OOH + CH_3COOC_6H_5$	Slight	$(CH_3C^*O)_2O + CH_3COOC_6H_5$	Slight
$C_6H_5C^*OOH + C_6H_5COOC_2H_5$	None	$(CH_3C^*O)_2O + CH_3COC_6H_5$	None
$C_6H_5C^*OOH + C_6H_5COOC_6H_5$	Considerable	$(C_6H_5C^*O)_2O + C_6H_5COOC_6H_5$	Slight
The same, 300°	Equilibrium	$(C_6H_5C^*O)_2O + C_6H_5COC_6H_5$	None

As the Table shows, ketones do not exchange with anhydrides; the C–CO bond evidently does not undergo exchange under these conditions.

On the basis of these test experiments, the system $C_6H_5COOC_6H_5 + C_6H_5C^*OOH$ was chosen for subsequent quantitative experiments.

Series 3. Quantitative investigation of exchange in the system phenyl benzoate + benzoic acid and determination of the position of bond rupture during exchange. With the given system the authors investigated the relative strength of the two C–O bonds in esters by the double isotopic exchange method they developed. The principle of this method is that an exchange experiment in the given system is carried out twice under identical conditions (temperature, time, amounts, etc.), but with the difference that in the first experiment an acid labeled with C^{14} in the carboxyl is used and in the second experiment it is labeled with O^{18} in both O atoms of the carboxyl.

If exchange occurs at the first C–O bond, i.e., according to scheme 1

$$\left.\begin{array}{l} C_6H_5CO-OC_6H_5 \\ + \\ C_6H_5C^*\overset{\vee}{O}-\overset{\vee}{O}H \end{array}\right\}\rightarrow \begin{array}{l} C_6H_5C^*\overset{\vee}{O}-OC_6H_5 \\ + \\ C_6H_5CO-\overset{\vee}{O}H, \end{array} \qquad (1)$$

then one would expect that the degree of exchange of C^{14} would be twice as great as that of O^{18}.

If exchange occurs at the second C–O bond, i.e., according to scheme 2

$$\left.\begin{array}{l} C_6H_5COO-C_6H_5 \\ + \\ C_6H_5C^*\overset{\vee}{O}\overset{\vee}{O}-H \end{array}\right\}\rightarrow \begin{array}{l} C_6H_5C^*\overset{\vee}{O}\overset{\vee}{O}-C_6H_5 \\ + \\ C_6H_5COO-H, \end{array} \qquad (2)$$

then one would expect equal degrees of exchange of C^{14} and O^{18}.

Finally, if both mechanisms occur, then by comparing the results of the two experiments the degree of each may be determined. By this method it is possible to determine at which of the two bonds there is exchange in an ester, i.e., to determine their relative strength.

O^{18}-Benzoic acid was synthesized according to the scheme

$$C_6H_5COCl + H_2O^{18} \rightarrow C_6H_5COO^{18}H + HCl.$$

Since equilibrium distribution of O^{18} between the oxygen atoms in the carboxyl is reached only in the state of the benzoate ion, the benzoic acid synthesized was converted into sodium benzoate and then back into the acid:

$$C_6H_5C\overset{\vee}{O}O\overset{\vee}{H} + Na\overset{\vee}{O}H \rightarrow C_6H_5C\overset{\vee}{O}\overset{\vee}{O}Na \xrightarrow[\text{dry benzene}]{HCl} C_6H_5C\overset{\vee}{O}\overset{\vee}{O}H.$$

Experiments on the exchange of C^{14}-benzoic acid and O^{18}-benzoic acid with phenyl benzoate were carried out in parallel at t = 200° for 5 hours with the percent exchange determined.

The original C^{14}-benzoic acid and the benzoic acid after exchange were analyzed by wet oxidation to CO_2 by a modified Van Slyke-Folch method.

Experimental results. The mean count of BaC^*O_3 samples from C^{14}-benzoic acid before exchange was 733 counts/min (consequently the loss in activity at equilibrium exchange would have been 733/2 = 366 counts/min). The mean count of the same samples after exchange was 581 counts/min (consequently the loss in activity during the experiment equaled 733–581 = 152 counts/min). The degree of exchange = $\frac{152 \cdot 100}{366}$ = 41.5%.

For analysis of the benzoic acid for O^{18} content, it was decarboxylated and the CO_2 obtained analyzed for O^{18} content on an MI-1303 mass spectrometer.*

*The authors would like to thank M. V. Tikhomirov and his co-workers for carrying out the analyses.

Experimental results. The O^{18} content of the benzoic acid before exchange was 8.49 at. % and after exchange, 7.62 at. %. The degree of exchange equaled 21%.

The degree of exchange between phenyl benzoate and O^{18}-benzoic acid was calculated by the formula $x = \frac{A - A_1}{A - \frac{A + 0.22}{2}}$, where A is the O^{18} content before exchange (at. %), A_1 is the same after exchange, and 0.22 is the natural O^{18} content of phenyl benzoate before exchange (at.%).

By comparing the degrees of exchange of phenyl benzoate with C^{14}-benzoic acid and phenyl benzoate with O^{18}-benzoic acid, it can be considered as established that the exchange between them proceeds according to scheme 1, i.e., at the C–O bond between the carboxyl carbon and the ether oxygen.

MEASUREMENT OF SOUND VELOCITY IN DETONATION PRODUCTS

V. M. Zaitsev, P. F. Pokhil, and K. K. Shvedov

Institute of Chemical Physics, Academy of Sciences, USSR
(Presented by Academician V. N. Kondrat'ev, February 20, 1960)
Translated from Doklady Akademii Nauk SSSR, Vol. 133, No. 1, pp. 155-157, July, 1960
Original article submitted February 16, 1960

The velocity of sound in detonation products is an important characteristic of a detonation wave. Direct measurement of the sound velocity permits one to check the Chapman-Jouguet condition at the front of the detonation wave, and also, as will be shown below, to calculate the distribution of density and pressure behind the front of the detonation wave. The present paper presents a short description of a method worked out by us, and gives the results of sound velocity measurements in the detonation products of charges of TNT and TH 50/50 (an alloy of equal parts by weight of TNT and hexogen)*. The method of measuring the sound velocity is based on the reflection of the detonation wave from a plate of inert materials, pressed to the front end of the charge. If the dynamical stiffness of the plate is less than the dynamical stiffness of the explosive substance (paraffin satisfies this condition well), then, upon reflection of a detonation wave from such a plate, a shock wave proceeds along the plate, and a reflected wave of rarefaction along the products. As in the case of any weak shock, the latter propagates with the local speed of sound [1].

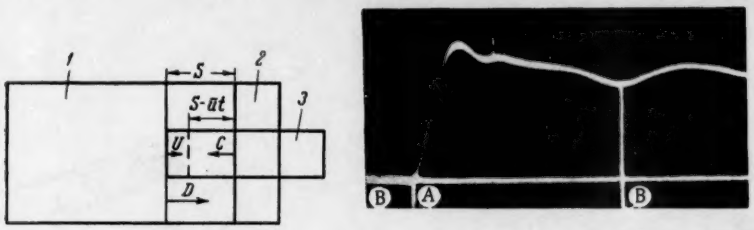

a b

Fig. 1. a) Motion probe; 1) explosive substance, 2) paraffin, 3) probe; D) direction of motion of the plane detonation front, u) direction of motion of the explosion products behind the detonation front; c) direction of motion of the reflected wave of rarefaction; b) photographic record of the emf induced by the moving probe.

By using an electromagnetic method of measuring the velocity of mass motion of the explosion products [2], one can by the very same method, measure the sound velocity in the detonation products.

Let us examine the motion of the probe and the oscillogram in Fig. 1. At the instant t= 0, (point A, Fig. 1b), the front of the detonation wave arrives at the probe and the latter begins to move with the velocity of mass

* s-Triagine, hexahydro-1,3,5-trinitro- [Publisher's note].

TABLE 1

Explosive substance	Diameter of charge, mm	Height of charge from lens, mm	D, km/sec	u_J, km/sec	c_J, km/sec	S, mm	t, μ sec	$\bar{u}$, km/sec	c, km/sec
Cast TNT, ρ_0 = 1.6 g/cm³	40	48	7,00	1,81	5,19	2,53	0,755	1,62	4,95
						4,09	1,255	1,47	4,82
						5,50	1,720	1,36	4,76
Cast TNT, ρ_0 = 1.6 g/cm³	40	90	7,00	1,81	5,19	3,09	0,912	1,68	5,03
						6,16	1,848	1,56	4,94
Pressed TNT, ρ_0 = 1.6 g/cm³	40	90	7,00	1,81	5,19	2,78	0,809	1,71	5,10
						4,84	1,435	1,61	5,02
						6,90	2,080	1,52	4,93
TH 50/50 cast, ρ_0 = 1.68 g/cm³	40	95	7,65	2,03	5,62	2,64	0,706	1,91	5,49
						3,70	1,000	1,87	5,43
						7,30	2,020	1,71	5,32

TABLE 2

Explosive substance	Height of charge mm	t, μ sec	ρ, g/cm³	P·10³ atm.	Explosive substance	Height of charge mm	t, μ sec	ρ, g/cm³	P·10³, atm.
Cast TNT	48	0	2,16	203	Cast and pressed TNT		3,0	1,82	122
		0,5	2,05	175			3,5	1,76	113
		1,0	1,95	151	TH 50/50, cast.	95	0	2,30	262
		1,5	1,84	128			0,5	2,22	237
		2,0	1,74	108			1,0	2,14	216
Cast and pressed TNT	90	0	2,16	203			2,5	2,06	194
		0,5	2,10	188			2,0	1,98	175
		1,0	2,04	173			2,5	1,90	156
		1,5	1,99	160			3,0	1,82	139
		2,0	1,93	147			3,5	1,75	124
		2.5	1.87	135					

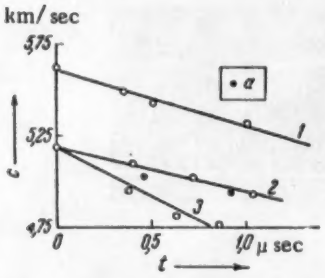

Fig. 2. Time dependence of the sound velocity in the detonation products behind the Chapman-Jouguet plane. Time is reckoned from the front of the detonation: 1) TH 50/50; 2) TNT, length of charge, 90 mm. Point a pertains to a charge of cast material; 3) TNT, length of charge 48 mm.

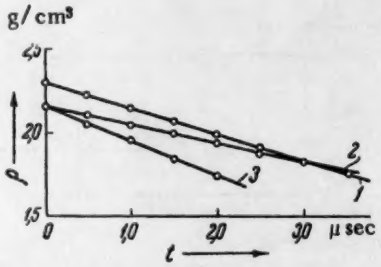

Fig. 3. Time dependence of the density of the explosion products behind the Chapman-Jouguet plane: 1) TH 50/50; 2) TNT, length of charage 90 mm; 3) TNT, length of charge 48 mm.

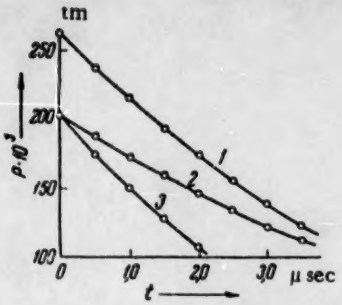

Fig. 4. Time dependence of the pressure of the explosion products behind the Chapman-Jouguet plane: 1) TH 50/50; 2) TNT, length of charge 90 mm; 3) TNT, length of charge 48 mm.

the time interval t:

motion behind the detonation front.

At time t = S/D, the front of the detonation wave arrives at the interface between the explosive substance and the inert material, and the reflected rarefaction wave proceeds through the detonation products. At time $t = \frac{S}{D} + \frac{S - \bar{u}t}{c - \bar{u}}$ (point B, Fig. 1b), the rarefaction wave reaches the probe and it sharply increases its velocity (since the substance in the rarefaction wave moves in the direction opposite to the motion of the wave); this can be seen on the oscillogram. By measuring S, the initial distance from the probe to the interface between the explosive substance and the inert material, D, the velocity of the detonation, $\bar{u}$, the mean velocity of the motion of the probe during the time t – the time of movement of the probe from the instant of passage of the detonation front (point A, Fig. 1b) until it encounters the rarefaction wave (point B, Fig. 1b) – one can calculate the mean velocity of sound during

$$c = \frac{S(D - \bar{u})}{Dt - S}.$$

By changing the distance S, one can obtain the distribution of sound velocity behind the front of the detonation wave. The results of the measurement of sound velocity are presented in Table 1 and Fig. 2, where the dependence of the sound velocity behind the front of the detonation wave on the time is presented graphically. The mean error in the measurement of sound velocity from a series of 3 to 5 tests does not exceed 4 to 5%.

We now make use of the equation of state of the explosion products proposed by L. D. Landau and K. P. Stanyukovich, $P = A\rho^n$; the isentropic relation for sound velocity $c^2 = \partial P/\partial \rho$; and the well known relations at the Jouguet point $\rho_J = \rho_0 \frac{n+1}{n}$, where ρ_0 is the initial density of the explosive substance, and ρ_J is the density of the explosion products at the Jouguet point, and $P_J = \rho_0 \frac{D^2}{n+1}$, where P_J is the pressure at the Jouguet point.

For the case of one dimensional flow, i.e., in the region not enveloped by the unloading wave which comes from the lateral surface, one can obtain the distribution of density and pressure behind the Jouguet point [3]:

$$\rho_* = \frac{n+1}{n}\rho_0 \left(\frac{c_*}{c_J}\right)^{\frac{2}{n-1}}; \quad P_* = \frac{\rho_0 D^2}{n+1}\left(\frac{c_*}{c_J}\right)^{\frac{2n}{n-1}},$$

where ρ_*, P_*, c_* are respectively the local values of density, pressure, and sound velocity in the detonation wave behind the Jouguet point.

As was found in [2], the exponent n remains constant for the explosive substances under consideration in the time range from 3 to 3.5 microsec. Thus, one can calculate the density and pressure distribution behind the Jouguet point from the measured sound velocities in the detonation products, using the above formulas.

The results of the calculations carried out for the indicated charges of explosive substance are presented in Table 2 and in Figs. 3 and 4.

Having investigated the domain of one dimensional flow of the explosion products, we see that these data give the possibility of calculating the impulse of a charge of explosive substance.

LITERATURE CITED

1. Ya. B. Zel'dovich and A. S. Kompaneets, Theory of Detonation (1955)[in Russian].

2. V. M. Zaitsev, P. F. Pokhil, and K. K. Shvedov, Doklady Akad. Nauk SSSR 132, 6 (1960).*
3. K. P. Stanyukovich, Unsteady Motion of a Continuous Medium (1955)[in Russian].

*See C. B. translation.

ADIABATIC THEORY FOR ELECTRON TRANSFER PROCESSES IN SOLUTION

Corresponding Member Acad. Sci. USSR V. G. Levich

and R. R. Dogonadze

Electrochemical Institute, Academy of Sciences, USSR

Translated from Doklady Akademii Nauk SSSR, Vol. 133, No. 1, pp. 158-161, July, 1960
Original article submitted March 28, 1960

The present work was undertaken in an attempt to extend the theory of electronic processes in polar solutions [1].

To represent the solvent we made use of the specific polarization concept, $\mathbf{P}(\mathbf{r})$. Strictly speaking the macroscopic concept of polarization is only significant beyond the limits of the first solvation sphere surrounding the ion. Any precise description of this sphere has to consider its discrete structure, particularly in cases where definite chemical bonding between the ions and the solvent molecules exists. However, considering the present state of solution theory one can not take into account the discrete nature of the solution sphere. In this work we will use the Born model of solution and treat the solvent as a medium with a static polarization $\mathbf{P}(\mathbf{r})$.

In the processes we are interested in, the nonstatic character of $\mathbf{P}(\mathbf{r})$ plays a key role; the polarization would remain static if it were not for an important phenomena: on one hand solvent molecules keep jumping from one temporary equilibrium position to another. From the diffusion data one can readily compute the time between such jumps, and it turns out to be of the order of 10^{-9} sec [2]. This time is very long in comparison with electronic transition periods. Therefore one can freely disregard any mixing caused by molecular diffusion. But as far as the theory developed below is concerned, vibrations about temporary equilibrium positions constitute a more important form of atomic motion. Strictly speaking the atomic vibrations in solution are not harmonic. However, only through a harmonic approximation can the problem of electronic processes be given a quantitative character and solved by quantum mechanical methods.

Let us represent the Hamiltonian for the system: ion + electron + solvent, in the form:

$$H(\mathbf{r}, q) = H_e(\mathbf{r}) + H_s(q) + V_{es}(\mathbf{r}, q). \qquad (1)$$

The Hamiltonian component H_e includes the kinetic energy of the electron, the interaction energy between the electron and the ions, and a term to take into account the effects of static polarization $\mathbf{P}_0$ (produced by the ions in solution) on the electron. The H_s component includes the kinetic and the potential energies of the solvent, the latter being connected with the polarization $\mathbf{P}$ induced by the electron. From now on we will use $\mathbf{P}$ to represent only the inertial component of the total polarization [3]. Finally, V_{es} represents the potential energy of the electron and it also depends on the solvent polarization $\mathbf{P}$ induced by the electron. The Hamiltonian contains no time-independent terms to represent the interaction energy between the ions, the energy connected with the static polarization component $\mathbf{P}_0$, or the intrinsic energy of the noninertial polarization component $\mathbf{P}_e$ due to the electron [3].

Since the chief aim of this work is to study the electron exchange reactions between like-charged ions, all specific calculations will be done exclusively for such cases. As will become apparent later on, the theory

developed here can be readily extended to cases involving other electronic processes in solution. For the case of interest to us,

$$H_e(\mathbf{r}) = -\frac{\hbar^2}{2m}\nabla_r^2 + U_1(\mathbf{r}, R) + U_2(\mathbf{r}, R) \equiv H_{e1} + U_2 \equiv H_{e2} + U_1, \tag{2}$$

where R is the distance between reaction ions; U_1 is the interaction energy involving the electron, the first ion, and the solvent statically polarized by the ion (U_2 is similarly defined). We will try to find the eigenfunctions of operator (1) by using the adiabatic approximation:

$$\Psi_n(\mathbf{r}, q) = \sum_r \Phi_{rn}(q)\, v_r(\mathbf{r}, q), \tag{3}$$

where v_r is the eigenfunction of the operators $H_{e1} + V_{es}$ (when $r = \alpha$) and $H_{e2} + V_{es}$ (when $r = \beta$). Let us substitute Eq. (3) into an exact wave equation, multiply the left side by $v^*(\mathbf{r}, q)$, and integrate with respect to r. Using simple transformations we will get

$$\begin{aligned} &\{H_s(q) + \varepsilon_r(q) - E_n\}\,\Phi_{rn}(q) = \\ &= \sum_{r'} \{L_{rr'}(q) - \Delta_{rr'}(q)\,[H_s(q) + \varepsilon_{r'}(q) - E_n]\}\,\Phi_{r'n}(q), \end{aligned} \tag{4}$$

where we have introduced the terms defined below:

$$L_{rr'} = -\int v_r^*[H_s(q), v_{r'}]\,d\mathbf{r} - \int v_r^* U_{r'} v_{r'}\,d\mathbf{r} \equiv L_{rr'}^{(1)} + L_{rr'}^{(2)};$$

$$U_r = \begin{cases} U_1, & r = \alpha; \\ U_2, & r = \beta; \end{cases} \tag{5}$$

$$\Delta_{rr'} = \begin{cases} 0, & r \text{ and } r' = \alpha \text{ and } \alpha' \text{ or } \beta \text{ and } \beta'; \\ \int v_r^* v_{r'}\,d\mathbf{r}, & r \text{ and } r' = \alpha \text{ and } \beta. \end{cases} \tag{6}$$

The $\epsilon_r(q)$ terms are the eigenvalues of the eigenfunctions $v_r(\mathbf{r}, q)$. In the adiabatic approximation to the excitation theory the operator $L^{(1)}$ (commonly called the nonadiabaticity operator) is small. $L^{(2)}$ represents an exchange integral, which is also very small for large values of R. The second term on the right side of Eq. (4) is also small under these conditions. We can therefore apply to Eq. (4) the usual excitation theory methods by assuming the right side to be small. It can be easily demonstrated that if only the first excitation theory approximation is applied the second term on the right side of Eq. (4) will not give transitions between various electronic states. The electronic transition probability for a case where $L^{(1)}$ represents an excited state has already been calculated [1]. That same paper analyzed the case where the electronic transitions may be induced by the second term in the power series expansion of V_{es} in terms of q, or in other words by the term proportional to q^2; such an approach is in a certain sense equivalent to having considered the vibrational anharmonicity. In the present work we will determine the probability of transitions induced by $L^{(2)}$. In view of the fact that the exchange integral increases with decreasing R it is obvious that for moderately large values of R the term $L^{(2)}$ may assume the principal role in electronic transitions.

The statistical probability for the transfer of one electron from one ion to another (per unit time) can be expressed by the equation:

$$w_{12} = \frac{2\pi}{\hbar} A v_n \sum_{n'} |\langle \Phi_{\beta n'}^0 | L_{\beta\alpha}^{(2)} | \Phi_{\alpha n}^0 \rangle|^2\, \delta(E_{\beta n'}^0 - E_{\alpha n}^0). \tag{7}$$

The subscripts α and β denote the electronic states of the first and the second ions respectively; the Av_n represents an average partition function for the ground states of the surrounding molecules. At the same time we will also get the partition function for the final states n', taking into account the law of conservation of energy by introducing a δ-function. Unfortunately a general solution for w_{12} is not possible. An exact quantitative expression for the transition probability can only be obtained in cases where there is no dispersion of frequencies.

However, it has been shown by Kubo [4] that an approximate solution for an expression of type (7) can be obtained for cases where $kT \gg \hbar\omega_D$. Skipping over the mathematical details we will present the high-temperature approximation to the expression for w_{12}.

$$w_{12} = \left(\frac{8\pi^3}{\hbar^2 kTc\int (D_\alpha^0 - D_\beta^0)^2\, d\tau}\right)^{1/2} |L_{\beta\alpha}^{(2)}|^2 \exp\left\{-\frac{\left[I_\alpha - I_\beta + \frac{c}{8\pi}\int (D_\alpha^0 - D_\beta^0)^2\, d\tau\right]^2}{\frac{c}{2\pi}\int (D_\alpha^0 - D_\beta^0)^2\, d\tau}\,\frac{1}{kT}\right\}; \quad kT \gg \hbar\omega. \tag{8}$$

The quantity c constitutes a fundamental parameter of the theory and is related to the static dielectric constant ϵ_s and the refractive index of light $n = \sqrt{\epsilon_0}$ by the relationship:

$$c = \frac{1}{\epsilon_0} - \frac{1}{\epsilon_s}, \tag{9}$$

where ϵ_0 is the optical dielectric constant. The function I_r used in Eq. (8) can be determined from the equation:

$$I_r = \varepsilon_r(q_r^0) + \frac{c}{8\pi}\int \mathbf{D}_r^0 d\mathbf{r}, \tag{10}$$

where

$$\mathbf{D}_r^0 = \frac{4\pi}{c}\mathbf{P}_r^0 = e\int |v_r(\mathbf{r}', q_r^0)|^2 \frac{\mathbf{r} - \mathbf{r}'}{|\mathbf{r} - \mathbf{r}'|^3} d\mathbf{r}'$$

can be interpreted as the electrostatic field induction, the field being created by a cloud charge with a density of $e|v_r|^2$ (q_r^0 gives the equilibrium configuration of the solvent when the electrons in the latter are in the state r). According to Eq. (8) at high temperatures w_{12} is proportional to $e^{-\Delta E^*/kT}$. According to the theory of absolute reaction rates we can treat ΔE^* as the activation energy for the examined process.

In another limiting case, namely at low temperatures, w_{12} assumes the form:

$$w_{12} = \frac{2\pi |L_{\beta\alpha}^{(2)}|^2}{\hbar^2\omega_0\left(\frac{I_\beta - I_\alpha}{\hbar\omega_0}\right)!} \exp\left[-\frac{c}{8\pi\hbar\omega_0}\int (D_\alpha^0 - D_\beta^0)^2\, d\tau\right] \times$$

$$\times \left[\frac{c}{8\pi\hbar\omega_0}\int (D_\alpha^0 - D_\beta^0)^2\, d\tau\right]^{(I_\beta - I_\alpha)/\hbar\omega_0} \exp\left[-\frac{I_\beta - I_\alpha}{kT}\right]; \quad kT \ll \hbar\omega_0. \tag{11}$$

Thus, the transition probability at low temperatures also acquires the activational form, with the activation energy being replaced by $(I_\beta - I_\alpha)$.

Besides the activation energy ΔE^* we also have to know other thermodynamic functions, such as the free energy of activation ΔF^* and the entropy of activation ΔS^*. A well known statistical physics equation states that

$$\Delta F^* = F^* - F_\alpha = -kT \ln \frac{z^*}{z_\alpha}, \tag{12}$$

where z^* and z_α are the partition functions for the activated and initial states respectively. As has already been pointed out, the activational functions can only be used at high temperatures hence only a quasi-classical approximation to the partition functions has to be computed. The free energy of activation was found to have the form:

$$\Delta F^* = \Delta E^* - kT \ln\left[\frac{\sum_k \hbar^2\omega_k^3 (q_{k\alpha}^0 - q_{k\beta}^0)^2}{(kT)^2\sum_k \omega_k (q_{k\alpha}^0 - q_{k\beta}^0)^2}\right]^{1/2} = \Delta E^* - T\Delta S^*. \tag{13}$$

The expression for ΔS^*, which should be treated as the activation entropy, assumes a particularly simple form when the frequency is not diffused:

$$\Delta S^* = -k \ln \frac{kT}{\hbar\omega_0} < 0. \tag{14}$$

At the present time several papers are known in which the rate constants for the electron exchange in solution are calculated. By starting from the theory of absolute reaction rates the authors of those papers expressed the transition probability w_{12} in the form of a product,

$$w_{12} = w_s w_e, \tag{15}$$

where w_s is the probability for the formation of the activated complex, and w_e the electron transition probability in the activated state. In some papers [5] w_e is calculated while w_s is treated as an empirical function, whereas in others [6] only w_s is calculated. In our opinion the work of R. A. Marcus, who calculated the free energy of activation by purely thermodynamic means, is most interesting and resembles most closely the theory developed in our work. In order to give a quantitative criterion for the applicability of Marcus' formulae we will carry out the following brief analysis. Let us define $\tau^* \approx 2\pi/\omega_0$ as the lifetime of the activated complex, and $\nu_e(R)$ as the frequency of electron exchange between ions separated by a distance R. If R is such that $\nu_e(R)\tau^* \gg 1$ (i.e., $2\pi\nu_e(R) \gg \omega_0$) then we can assume that $w_e \approx 1$.

In concluding it is essential to point out that the electronic mechanism for redox reactions proposed in this work is not the only possible one. Other mechanisms, such as would involve proton transfer for example, are still awaiting a theoretical treatment.

LITERATURE CITED

1. V. G. Levich and R. R. Dogonadze, Doklady Akad. Nauk SSSR 124, 123 (1959).*
2. Ya. I. Frenkel', Introduction to the Theory of Metals [in Russian] (1948).
3. S. I. Pekar, Electronic Theory of Crystals [in Russian] (1951).
4. R. Kubo and Y. Toyozawa, Progr. Theor. Phys. 13, 160 (1955).
5. R. J. Marcus, B. J. Zwolinski, and H. Eyring, J. Phys. Chem. 58, 432 (1954).
6. R. A. Marcus, J. Chem. Phys. 24, 966 (1956); 26, 867 (1957).

* Original Russian pagination. See C. B. translation.

NATURE OF THE CURRENT FALL ON POLAROGRAPHIC WAVES LIMITED BY A PRECEDING CHEMICAL REACTION

S. G. Mairanovskii

Institute of Electrochemistry, Academy of Sciences, USSR and N. D. Zelinskii Institute of Organic Chemistry, Academy of Sciences, USSR

(Presented by Academician A. N. Frumkin, March 9, 1960)
Translated from Doklady Akademii Nauk SSSR, Vol. 133, No. 1, pp. 162-165, July, 1960
Original article submitted March 9, 1960

As has been shown [1, 2], catalytic (and kinetic) currents in polarography are usually the sum of two currents: these components are limited by the rate of the same preceding chemical reaction, but in one case the reaction proceeds in the volume of the solution ("volume" current) and in the other, on the electrode surface ("surface" current). The proportion of the "surface" current increases with an increase in the adsorption of the electrochemically inactive form of the depolarizer [1].

As a rule, adsorption equilibrium is not reached on a mercury dropping electrode at the concentrations used normally in polarography [3]. If the adsorption obeys the Langmuir isotherm,

$$G_e = G_\infty \frac{\beta C_k}{1 + \beta C_k}, \qquad (1)$$

(G_e and G_∞ are the equilibrium and maximum amounts of adsorbed substance, respectively, β is a constant, and C_k is the concentration of adsorbed substance in the solution), then the amount of adsorbed substance at the moment t, $G_t = yG_e$ and the completeness of establishment of equilibrium y depends on the adsorption time, the rate at which the substance is supplied to the electrode, and the value of β [3].

According to A. N. Frumkin [4], the value of β is a function of the electrode potential:

$$\beta = Be^{-\frac{1/2(c-c')}{RTG_\infty}\varphi^2} = Be^{-a\varphi^2}, \qquad (2)$$

where c and c' are the capacities of the electrode double layer in the absence of surface active substance and with complete filling of the electrode surface with molecules, respectively, $\varphi = E - E_M$, E_M is the potential at which adsorption is maximal, and B is a constant. With an increase in φ, the adsorption decreases and due to this there is a fall in the proportion of the "surface" component in the total value of the catalytic (or kinetic) current. Therefore, with the second catalytic wave of quinine, for example, which is observed at high negative potentials (about 1.9 v relative to a saturated calomel electrode), the "surface" and "volume" currents are of the same order [1]. At less negative potentials, the proportion of the "volume" current generally becomes insignificant and the catalytic current observed is practically purely "surface" current.

The dependence of the surface current on the potential is determined on the one hand, by its effect on the rate constant of the electrode process and on the other, by its effect on the amount of adsorbed catalyst. In

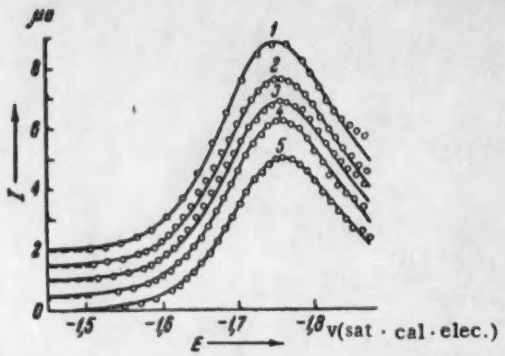

Fig. 1. Catalytic hydrogen waves produced by anabasine in an acetate buffer with pH 6.0; KCl concentration in solution: 1) 0; 1) 0.1; 3) 0.2; 4) 0.5; 5) 1.0 N.

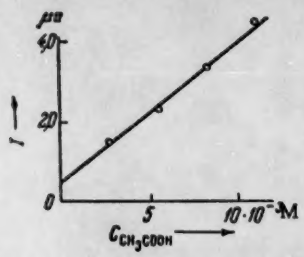

Fig. 2. Relation of the catalytic current in 0.182 mM anabasine solution at E = −1.84 v to the acetic acid concentration in an acetate buffer at pH 6.0.

the case of an adsorbed catalyst, the wave is irreversible [5]. In accordance with the mechanism of the formation of a catalytic wave [6], for the surface current it is possible to write:

$$i = sF\{k_1[DH^+]G - k_2[D]G'\}, \quad (3)$$

$$i_{lim} = sFk_1[DH^+]G, \quad (4)$$

where G and G' are the amounts of adsorbed basic and acidic (electrochemically active) forms of the catalyst, k_1 and k_2 are the rate constants of the reaction of the catalyst in the corresponding form with the proton donor DH^+ or the base D, respectively, s is the electrode surface, and F is the Faraday number.

According to the A. N. Frumkin's theory of retarded discharge [7],

$$i = sk_0G'e^{-\frac{\alpha FE}{RT}}. \quad (5)$$

Were the adsorption independent of potential, then the catalytic wave equation, obtained by substituting the value of G' [found by combining (3) and (4)] in (5), would have the form:

$$E = E_{1/2} - \frac{RT}{\alpha F}\ln\frac{i^0}{i_{lim} - i^0}, \quad (6)$$

where the index zero refers to values corresponding to adsorption at E_M.

The adsorption of the catalyst as a whole depends on the adsorption of its basic and acidic forms, which are in protolytic equilibrium. Judging by the data of Gouy for organic bases determined in neutral and acidic solutions [8], the surface activity of the basic form on mercury is considerably higher than that of the acidic form; in addition, on a negatively charged mercury surface the adsorption of the cationic form changes with the potential comparatively less than for the basic form and therefore the change in adsorption of the catalyst with potential is determined largely by the change in the adsorption of its basic form, though the amount of adsorbed material depends also on the ratio between the forms, i.e., the solution pH.

The catalytic current in an excess of proton donors is proportional to the catalyst concentration at the electrode surface [9]; consequently the change in current with potential solely due to desorption of catalyst may be expressed relative to current i^0, determined from (6), in the following way:

$$\frac{i}{i^0} = \frac{G_t}{G_t^0} = \frac{\gamma\beta}{1+\beta C_k} : \frac{\gamma^0\beta^0}{1+\beta^0 C_k}, \quad (7)$$

where according to (2), $\beta^0 = B$.

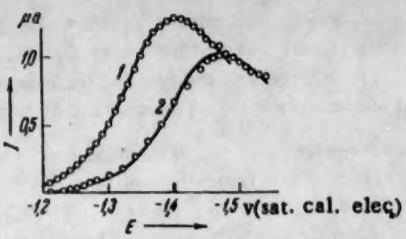

Fig. 3. Catalytic waves of $2.85 \cdot 10^{-6}$ M quinine solution in a citrate–phosphate buffer with pH 3.0 (1) and 4.0 (2).

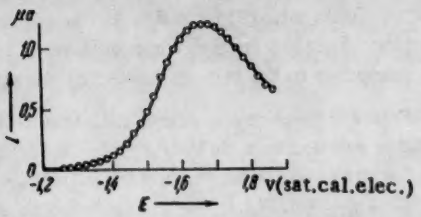

Fig. 4. Catalytic wave of the cysteine complex of Co^{3+} in an ammonia buffer.

Under the conditions of observation of catalytic hydrogen waves, C_k is usually small and the value of $\underline{y}$, especially at low dropping periods, does not exceed 0.5 [3]. As follows from the data of Delahay and Fike [3], with constant C_k and $\underline{t}$, the value of $\underline{y}$ increases in proportion to $1 + \beta C_k$ right up to $y \approx 0.55$. Therefore for $y < 0.55$, Equation (7) may be represented in the form:

$$\frac{i}{i^0} = \frac{\beta}{B} = e^{-a\varphi^*}. \qquad (8)$$

Thus, the surface catalytic hydrogen wave is described by a combination of Equations (6) and (7) or (8). Its characteristic form is caused by the change in adsorption of the catalyst with potential. The accuracy of the equations derived was checked on the catalytic hydrogen waves produced by anabasine, quinine, and the cysteine complex of cobalt.

The value of G_∞ of anabasine, found in [10] from the adsorption prewave of Brdicka [11], equals $2.4 \cdot 10^{-10}$ mole/cm^2, which is close to the value $G_\infty = 3.2 \cdot 10^{-10}$, calculated from the area occupied by an anabasine molecule, which is 58 A^2 (from a model of it). If it is assumed that $G_\infty = 3.2 \cdot 10^{-10}$, $c \approx 15$ and $c' \approx 5\ \mu f/cm^2$, then from (2), for anabasine $a = 6.35\ v^{-1}$.

Due to the desorption of catalyst with an increase in potential, the reciprocal of the slope of the logarithmic graph of the initial section [5] of the catalytic wave $b_k = 2.3RT/\alpha_k F$ is greater than $b = 2.3RT/\alpha F$ of the wave determined from (6). If $\underline{b}$ is known, then from the experimental value of b_k it is possible to find the potential φ_H of the initial section of the catalytic wave ($i = 0.1 - 0.2 i_{max}$) relative to the potential of maximum adsorption E_M and consequently to determine the value $E_M = E_H - \varphi_H$, where E_H is the potential of the beginning of the wave relative to the reference electrode. It is not difficult to show that $\varphi_H = \frac{2,3}{2a} \cdot \frac{b_k - b}{b_k \cdot b} = \frac{(\alpha - \alpha_k)F}{2RTa}$.

For catalytic waves produced by anabasine, $b_k = 0.10$ v [10] so that by assuming for the wave (6), $b = 0.080$ v ($\alpha = 0.738$), we find $E_M \approx -1.15$ v.

In Fig. 1, curve 1 was constructed from the values: $E_M = -1.143$ v (sat. cal. elec.), $E_{\frac{1}{2}} = -1.718$ v, $i^0_{lim} = 97\ \mu a$, and $b = 0.08$ v. The points on the curve are experimental values of the catalytic current (allowing for the prewave of pseudoreduction of anabasine [10]), obtained with an electrode with $m = 1.322$ mg/sec and $t = 0.24$ sec. As Fig. 1 shows, the calculated curve accurately describes the form of the catalytic wave.

With the other conditions the same, the introduction of potassium chloride into the buffer solution somewhat reduces the height of the catalytic wave, apparently due to an increase in the capacity $\underline{c}$ [12]. Calculation shows that for the observed current fall, the capacities $\underline{c}$ at C_{KCl} values of 0.1; 0.2; 0.5, and 1.0 N must be 15.5; 15.6; 15.9, and 16.4 $\mu f/cm^2$, respectively. In Fig. 1, curves 2-5 correspond to calculated values and the points to experimental values.

With a decrease in the buffer capacity of the solution at constant pH and ionic strength, the catalytic current falls. Figure 2 gives the relation of the current in a 0.182 mM solution of anabasine at $E = -1.84$ v (when i^0 reaches more than $0.95 i^0_{lim}$) to the concentration of undissociated CH_3COOH in an acetate buffer with pH 6.0. The slope of the line in Fig. 2 and (4) were used to find the rate constant of the reaction of adsorbed base of anabasine with CH_3COOH (DH^+) and this gave the value $k_1 = 2.9 \cdot 10^5$ liter/mole·sec. The value $G_t = 2.4 \cdot 10^{-11}$ used in the

calculation for E = −1.84 v was found with (1) from G_{∞}, y = 0.13, and β = 7.4 $mmole^{-1}$ (at E = −1.84). The latter was found with (2) from β ≈ 100 at −1.42 v, which, in its turn, was found with (3) from G_t/G_{∞} = 0.62, determined from the height of the prewave of anabasine [10]. The intercept of the line in Fig. 1 on the ordinate axis corresponds to the current limited by the rate of reaction of anabasine base with water and hydrogen ions.

Figure 3 gives experimental data (points) on calculated curves for catalytic waves produced by $2.85 \cdot 10^{-6}$ M quinine solution in a phosphate − citrate buffer with pH 3.0 (1) and 4.0 (2) (electrode with m = 3.82 and t = 0.26 sec). For the calculation we used the values $a = 4.6\ v^{-1}$, b = 85 mv, b_k = 100 mv; for 1: $E_M = -0.812$, $E_{\frac{1}{2}} = -1.325$, $i^0_{lim} = 7.97\ \mu a$; for 2: $E_M = -0.826$, $E_{\frac{1}{2}} = -1.426$, $i^0_{lim} = 9.05\ \mu a$. Curve 2 was much worse in satisfying the experimental data; higher values of a or b should have been used apparently for the calculation of (2). It is interesting that in the given case an increase in the pH had little effect on the value of the catalytic current as the decrease in the rate of protonization of the catalyst was compensated by an increase in its adsorbability due to an increase in the proportion of strongly adsorbed basic form of quinine in this pH region.

In Fig. 4 the points show the catalytic current produced by cysteine ($7.2 \cdot 10^{-6}$ M) in the presence of Co^{2+} ions ($2.9 \cdot 10^{-4}$N) in a buffer of 0.1 N NH_4OH + 0.1 N NH_4Cl with an electrode with m = 1.19 and t = 0.13 sec. To calculate the curves we used the values: b = 128 mv, b_k = 139 mv, $E_{\frac{1}{2}} = -1.576$ v, $i^0_{lim} = 4.67\ \mu a$, E_M = = −0.976, and $a = 2.5\ v^{-1}$, while $G_{\infty} = 6 \cdot 10^{-10}$, c − c' = 7.45.

Strictly speaking, Equations (7) and (8) are accurate only for cases when the adsorption obeys the Langmuir isotherm; in actual fact the adsorption of many substances obeys the more complex sigmoid isotherm of A. N. Frumkin [13]. As the filling of the surface by the adsorbed substance is usually low under the conditions of polarographic investigations, with a certain approximation the section of the Frumkin isotherm may be replaced by a section of the Langmuir adsorption isotherm. It should also be remembered that the value of c is not constant and changes with the potential [12], but c may be regarded as constant at not too negative potentials over a comparatively narrow range.

The author would like to thank Academician A. N. Frumkin for help with the work.

LITERATURE CITED

1. S. G. Mairanovskii, Doklady Akad. Nauk SSSR 132, 6, 132 (1960).*
2. S. G. Mairanovskii and L. I. Lishcheta, Coll. Czech. Chem. Papers (1960) (in press).
3. P. Delahay and C. Fike, J. Am. Chem. Soc. 80, 2628 (1958).
4. A. N. Frumkin, Tr. Fiz.-Khim. Inst. im. Karpova, 5, 3 (1926).
5. S. G. Mairanovskii, Doklady Akad. Nauk SSSR 120, 1294 (1958).*
6. S. G. Mairanovskii, Zhur. Fiz. Khim. 33, 691 (1959).
7. A. N. Frumkin, V. S. Bagotskii, et al., Kinetics of Electrode Processes [in Russian] (Moscow, 1952) p. 174.
8. M. Gouy, Ann. chim. Phys. 8, 9, 116 (1906).
9. S. G. Mairanovskii, Izvest. Akad. Nauk SSSR, Otdel. Khim. Nauk, 5, 805 (1952).*
10. S. G. Mairanovskii, N. V. Barashkova, and F. D. Alashev, Zhur. Fiz. Khim. (in press).
11. R. Brdicka, Coll. 12, 522 (1947).
12. A. N. Frumkin, Tr. Fiz.-Khim. Inst. im. Karpova, 4, 64 (1925).

* Original Russian pagination. See C. B. translation.

ELECTRICAL PROPERTIES OF INNER COMPLEXES

O. A. Osipov and V. M. Artemova

Rostov State University

(Presented by Academician A. N. Frumkin, March 7, 1960)
Translated from Doklady Akademii Nauk SSSR, Vol. 133, No. 1, pp. 166-169,
July, 1960
Original article submitted November 4, 1959

Besides their widespread use in analytical chemistry the inner-complex chelates are of considerable interest in connection with several intriguing problems in the theory of chemical bonding. Yet their physicochemical properties, particularly the electrical properties, have not received adequate treatment [1-4].

The present work deals with the electrical properties of zirconium, thorium, indium, beryllium, and other metal acetylacetonates and hydroxyquinolates. The stereochemistry of inner-complex chelates requires that the acetylacetonates and hydroxyquinolates of the above-listed metals be electrically symmetrical. But a study of the electrical properties of several acetylacetonates in nonpolar solvents indicates that the molecular polarization exceeds considerably the electronic, and in certain compounds the difference may be as large as 30-100 cm^3. The dipole moments computed from these data are of the order of 1.2-2.1 debyes.

Several authors [2-4] have attributed this great difference between the molar and electronic polarizations to an abnormally large atomic polarization, the magnitude of which may constitute 40-60% of the electronic. It was interesting to find out whether these compounds really have abnormally large atomic polarizations or whether their dipole moments are caused by other factors, such as: solvent effects, hindered internal rotation [5], imperfect symmetry in the spatial configuration of the complex. To resolve this problem we investigated the electrical properties of the enumerated complexes both in solution and in the solid phase.

The technique used by us for the determination of the dielectric constant, density, and refractive index has already been described [6]. Dielectric constants in the solid phase were measured by the method described in [7]. We wish to point out, though, that our pellets were compressed for 1 min at 1000 kg/cm^2. The dielectric constant measurements in the solid phase were accurate to within 1-1.5%.

The investigated complexes were synthesized by well known methods [8, 9] and purified through vacuum distillation or repeated recrystallization. We used carefully purified carbon tetrachloride, benzene, and dioxane as solvents for the dipole moment determinations.

In Table 1 we have listed the experimentally determined molar polarizations extrapolated to infinite dilution P_2, the electronic polarizations (refractions) P_e, and the calculated dipole moments (the atomic polarization P_a, determined from the solid phase measurements, was taken into account) of beryllium, aluminum, zirconium, and thorium acetylacetonates in carbon tetrachloride, benzene, and dioxane, and of zirconium 8-hydroxyquinolate in dioxane. The last column lists the ratio of the difference $P_2 - P_e$ between the molar and electronic polarizations to the electronic P_e expressed in percent.

Cryoscopic molecular weight determinations in benzene showed that these complexes were monomeric in solution.

The data presented in Table 1 indicate that the dipole moments of the investigated acetylacetonates are

TABLE 1

Compound	Solvent	P_s	P_e (R)	P_a	μ, in Debyes	$\frac{P_s - P_e}{P_e} \cdot 100$
$(C_9H_7O_2)_2Be$	CCl_4	85,22	58,85	15,40	0,71	44,8
$(C_9H_7O_2)_2Be$	C_6H_6	87,70	59,22		0,79	48,1
$(C_9H_7O_2)_2Be$	$C_4H_8O_2$	88,06	59,04		0,80	50,0
$(C_9H_7O_2)_3Al$	CCl_4	128,59	90,00	17,15	1,03	42,9
$(C_9H_7O_2)_3Al$	C_6H_6	130,52	89,24		1,08	46,2
$(C_9H_7O_2)_3Al$	$C_4H_8O_2$	130,07	88,51		1,11	46,8
$(C_9H_7O_2)_4Zr$	CCl_4	197,50	128,00	24,20	1,45	53,5
$(C_9H_7O_2)_4Zr$	C_6H_6	197,34	128,54		1,46	53,5
$(C_9H_7O_2)_4Zr$	$C_4H_8O_2$	201,03	128,43		1,52	56,6
$(C_9H_6NO)_4Zr$	$C_4H_8O_2$	279,77	189,98	9,85	1,97	47,4
$(C_9H_7O_2)_4Th$	CCl_4	202,21	127,40	23,10	1,58	58,7
$(C_9H_7O_2)_4Th$	C_6H_6	203,60	126,91		1,60	60,4
$(C_9H_7O_2)_4Th$	$C_4H_8O_2$	201,78	127,12		1,57	59,0

TABLE 2

Compound	P_d	P_e (R)	P_a	$\frac{P_d - P_e}{P_e} \cdot 100$	Compound	P_d	P_e (R)	P_a	$\frac{P_d - P_e}{P_e} \cdot 100$
$(C_9H_7O_2)_2Cu$	68,80	65,05	3,75	7,4	$(C_9H_7O_2)_4Th$	150,24	127,14	23,10	18,4
$(C_9H_7O_2)_2Be$	74,62	59,22	15,40	26,5	$(C_9H_6NO)_2Cu$	102,43	96,07	6,36	6,3
$(C_9H_7O_2)_2Cd$	67,41	55,03	12,38	22,4	$(C_9H_6NO)_2Cd$	95,50	89,65	5,85	0,54
$(C_9H_7O_2)_3Al$	106,40	89,25	17,15	19,5	$(C_9H_6NO)_3In$	152,74	145,36	7,38	4,7
$(C_9H_7O_2)_3In$	96,10	88,00	8,10	9,2	$(C_9H_6NO)_3Al$	154,60	144,00	10,60	7,7
$(C_9H_7O_2)_3Cr$	108,23	95,15	13,08	13,7	$(C_9H_6NO)_4Zr$	198,85	189,00	9,85	5,2
$(C_9H_7O_2)_4Zr$	152,70	128,50	24,20	19,3	$(C_9H_6NO)_4Th$	205,90	190,85	15,05	7,8

independent of the solvent. Hence, the great difference between the molecular and electronic polarizations can not be attributed to solvent effects. Moreover, the data also show quite clearly that the difference between these two polarization forms may amount to 60% of the electronic. Unless we can ascribe this difference (after subtracting the atomic polarization determined from our solid phase measurements) to any configurational factors, we will have to assume that the complexes studied by us possess abnormally large atomic polarizations, i.e., that the atomic nuclei become greatly displaced when the molecule is placed in an electric field. To solve this last problem we had to examine the electrical properties of our complexes in the solid phase. The results obtained with beryllium, copper, cadmium, aluminum, indium, chromium, zirconium, and thorium acetylacetonates and hydroxyquinolates are presented in Table 2.

The data presented above indicate that the deformation polarization P_d (which in the solid state is equal to the sum of the electronic and atomic polarizations) differs very little in magnitude from the electronic polarization (refraction). The ratio $(P_d - P_e)/P_e$ in the solid phase is much smaller than the $(P_s - P_e)/P_e$ ratios listed in Table 1 for the solution. From this it would follow that the difference $P_s - P_e$ can not be entirely due to atomic polarization. We detected the largest atomic polarizations in the case of zirconium[20], thorium [23, 10], and aluminum [17, 15] acetylacetonates. However, even these values did not exceed 20% of the electronic polarization of the corresponding acetylacetonates. The listed atomic polarizations are not unusually high, for there exist many compounds with atomic polarizations as high as 20-25% of the electronic [11].

Thus, from the solid phase deformation polarizations determined for the above-mentioned acetylacetonates one can conclude that these complexes do not have abnormally high atomic polarizations.

Our data are in good agreement with the results obtained by Meredith and co-workers [10], who investigated the electrical properties of ferric acetylacetonate in the solid state. According to their data the atomic component

of the polarization is 21 instead of 57 cm^3, as has been previously claimed [11], the latter value being responsible for the abnormally large atomic polarization attributed to ferric acetylacetonate.

With increasing number of atoms and rings per molecule the atomic polarization should increase in magnitude. Yet, the data in Table 2 show that all of the hydroxyquinolates have smaller atomic polarizations than do the corresponding acetylacetonates even though the former contain more atoms per molecule than do the latter.

This also suggests that the atomic polarizations of the investigated complexes can not be abnormally large. After comparing the data in Tables 1 and 2 we are inclined to conclude that the enumerated inner complexes posses orientation polarization.

The assumption would be supported by the experimentally determined electrical properties of uranyl acetylacetonate, nickel di-(ethylthioacetylacetonate), and other inner complexes, in all of which the measured dipole moments were 4-6 D and larger [1-4]. The conclusion, however, would conflict with the interpretations of Coop and Sutton [2], who determined the polarizations of several acetylacetonates in the vapor phase, and with some data indicating that the polarization of beryllium acetylacetonate is independent of temperature [16]. This last complex is the only acetylacetonate for which the temperature dependence of polarization has been reported quite some time ago. Similar work done more recently on ferric acetylacetonate [10] yielded a temperature dependence typical of orientation polarization. This, of course, raises some doubt about the early work and at the same time supports our view that the dipole moment remains constant. The temperature dependence that we found in the case of zirconium acetylacetonate in benzene is of a different nature – the dipole moment increases with temperature:

T°, K	275	283	293	313	333
μ, D	1.39	1.42	1.46	1.58	1.70

This type of dipole moment variation suggests the possibility that the internal rotation of the methyl groups in acetylacetonate is hindered. These results do not conflict with the literature data on thorium and zirconium acetylacetonates [17].

At the same time, the fact that zirconium hydroxyquinolate has a dipole moment (1.97 D) obliges one to assume that the internal rotation is not the only factor responsible for the polarity, since hydroxyquinolate has no groups able to rotate. We can only conclude that the structures of acetylacetonates and hydroxyquinolates are not completely symmetrical.

Recent x-ray work also indicates that there is a certain degree of structural deformation in these compounds [14, 18, 19].

Thus, on the basis of our experimental results and certain literature data one can conclude that the acetylacetonates and hydroxyquinolates of several metals are not completely symmetrical, with the result that the molecules possess a certain constant dipole moment. It should be noted that for several other compounds (diphenyl mercury, p-benzoquinone, and p-dinitrobenzene) to which abnormally high atomic polarizations have been previously ascribed, various factors have since been discovered to account for the existence of orientation polarization [16, 17, 20-22].

Quite recently A. N. Nesmeyanov and co-workers [2, 3] prepared a new zirconium complex, zirconium dinitrodiacetylacetonate. The zirconium has a coordination number of six in this complex and an octahedral structure has been proposed for the molecule. If we assume that the $(C_5H_7O_2)$< radicals are in the same plane then the transconfiguration would be expected to have a dipole moment equal to or close to zero. If on the other hand the radicals should lie in two mutually perpendicular planes the molecule would have a cis-configuration and a large dipole moment. To find which is the case we determined the dipole moment of zirconium dinitrodiacetylacetonate in benzene and in dioxane at 25°. $Zr[(C_5H_7O_2)(NO_2)_2]$ has a dipole moment of 7.34 D in benzene and 7.76 D in dioxane. Such a large dipole moment indicates the presence of a cis-form.

LITERATURE CITED

1. A. A. Grinberg and A. D. Troitskaya, Tr. Radievogo Inst., AN SSSR, 7, 5 (1956).
2. J. E. Coop and L. E. Sutton, J. Chem. Soc.,1269 (1938).
3. A. E. Finn, G. C. Hampson and L. E. Sutton, J. Chem. Soc.,1254 (1938).

4. R. S. Armstrong, C. G. Le Fèvre, and R.J. Le Fèvre, J. Am. Chem. Soc. 79, 371 (1957).
5. J. Draney and M. Cefola, J. Am. Chem. Soc. 76, 1975 (1954).
6. O. A. Osipov, Zhur. Obshch. Khim. 26, 322 (1956)*
7. W. A. Yager, Trans. Am. Electrochem. Soc. 74, 117 (1938).
8. Inorganic Syntheses [Russian translation] (IL, 1951) 2.
9. T. Moeller and M. Ramaniah, J. Am. Chem. Soc. 75, 3946 (1953).
10. G. G. Meredith, L. Westland, and G. F. Wright, J. Am. Chem. Soc. 79, 2385 (1957).
11. C. P. Smyth, Dielectric Behavior and Structure (New York, 1955).
12. K. K. Chatterjee, Anal. Chim. Acta 20, 3, 232 (1959).
13. G. J. Bullen, Nature 177, 537 (1956).
14. D. Grdenic and B. M. Matkovic, Nature 182, 465 (1958).
15. E. A. Shugam, Doklady Akad. Nauk SSSR 81, 853 (1951).
16. F. J. Llewellyn, J. Chem. Soc.,884 (1947).
17. P. Podleschka, L. Westland, and G. F. Wright, Canad. J. Chem. 36, 574 (1958).
18. E. A. Shugam and L. M. Shkol'nikova, Kristallografiya 1, 478 (1956).
19. E. A. Shugam and L. H. Shkol'nikova,, Uspekhi Khim. 28, 889 (1959).
20. L. Paoloni, J. Am. Chem. Soc. 80, 3879 (1958).
21. W. Strohmeier, Z. Elektrochem. 606,58 (1955).
22. S. C. Abrahams and J. M. Robertson, Nature 160, 569 (1947).
23. E.M. Brainina, R. Kh. Freidlina, and A. N. Nesmeyanov, Izvest. Akad. Nauk SSSR, Otdel Khim. Nauk, 937, (1958).*

*Original Russian pagination. See C. B. translation.

KINETICS OF ELECTRODE PROCESSES ON A SILICON ELECTRODE IN ACID AND ALKALINE SOLUTIONS

E. N. Paleolog, K. S. Korotkova, and N. D. Tomashov

Institute of Physical Chemistry, Academy of Sciences, USSR
(Presented by Academician A. N. Frumkin, March 3, 1960)
Translated from Doklady Akademii Nauk SSSR, Vol. 133, No. 1, pp. 170-173, July, 1960
Original article submitted March 3, 1960

There have been no systematic investigations of the electrochemical behavior of silicon in electrolyte solutions. In this respect, however, one may expect quite close analogy with germanium, as silicon and germanium are quite close both in semiconductor and chemical properties. This hypothesis was recently confirmed experimentally by Flynn [1], who showed that holes participate in the anode solution of silicon as with germanium.

The singularity of the electrochemical behavior of a silicon electrode in comparison with germanium should be connected with the presence on its surface of a film of silicon dioxide, which is insoluble in most aqueous solutions. According to the data of Archer [2], under normal conditions in air the surface of silicon is covered with an oxide phase film which is about 30 A thick. An oxide film is also readily formed on silicon during its anode treatment in a number of acid solutions which leads to strong polarization of a silicon anode under these conditions [3, 4]. A film of SiO_2 is insoluble in most aqueous solutions but it dissolves readily in hot alkalis and hydrofluoric acid. These solutions are mainly used for the etching of silicon.

In the present work we studied the rate of discharge of hydrogen ions on silicon and the rate of anode solution of silicon in 0.2 N H_2SO_4, 1.0 N HF, and 5.0 N KOH. The measurements were carried out on silicon monocrystals of the n and p types with various specific resistances (0.2, 10.0 and 23.0 ohm·cm) and a diffusion length of 0.5 mm.

Silicon samples 4-5 mm thick were cut from the central section of a monocrystal and had the same crystal orientation. The silicon surface was cleaned on boron carbide powders No. 100, 180, and 240. For electrical contact, one side of the silicon sample was covered with a layer of electrolytic rhodium to which was soldered a copper wire. Before a measurement, each of the samples was checked for the absence of a rectifying contact. The sample was then sealed with an epoxide resin that was resistant to both acid and alkaline solutions. The experiments were carried out in a thermostat with the solution stirred vigorously in the dark in an air atmosphere. The electrode potential was measured 30 sec after measurement of the current density.

Figure 1 gives curves of the cathode polarization of n-type silicon with various specific resistances on 0.2 N H_2SO_4 and 5.0 N KOH.* The silicon surface was investigated both directly after mechanical polishing and after preliminary etching in a hot alkaline solution (400 g/liter of KOH, temperature 80°, time 1 min).

The results obtained show that in sulfuric acid solution at 25° the discharge of hydrogen ions on silicon with a cleaned (unetched) surface is strongly retarded and the extent of this is greater, the higher the specific resistance of the silicon (Fig. 1, a). In this case the retardation is apparently connected with the presence of the oxide film

*All the polarization curves given below were constructed with allowance for the ohmic potential drop in the volume of the sample. The potential values given are on the hydrogen scale.

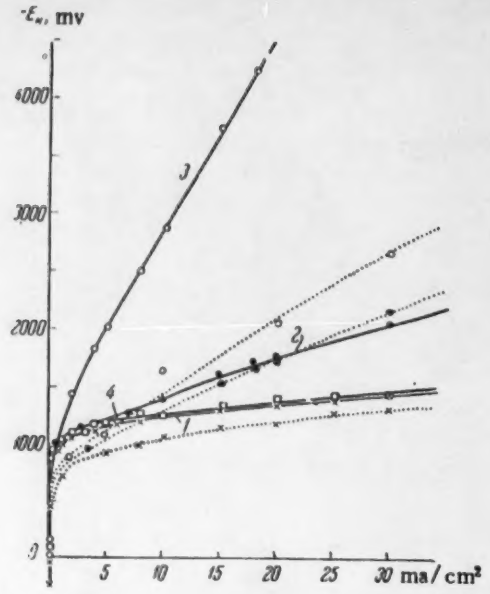

a

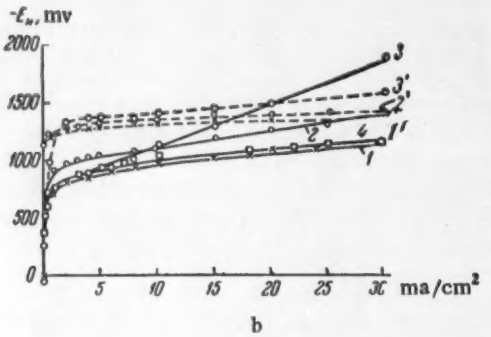

b

Fig. 1. Cathode polarization of n-type silicon. a) Surface after mechanical polishing, t = 25°, solution 0.2 N H_2SO_4, specific resistance: 1) 0.2 ohm · cm; 2) 10 ohm · cm; 3) 23 ohm · cm; 4) 0.2 ohm · cm (hydrogen atmosphere); broken lines – curves from backwards plot. b) Surface after etching, specific resistance: 1-1') 0.2 ohm · cm; 2-2') 10.0 ohm · cm; 3-3') 23.0 ohm · cm; 4) 0.2 ohm · cm (hydrogen atmosphere); 1, 2, 3, 4) 0.2 N H_2SO_4, t = 25°; 1', 2', 3') 5 N KOH, t = 50°.

on the electrode surface as the slope of the polarization curves is much less when they are plotted backward, i.e., after partial reduction of the film, and also after preliminary removal of the film from the sample during etching (Fig. 1, b). The strongest decrease in polarization after etching was shown by silicon with a specific resistance of 23.0 ohm · cm as a particularly complete film is apparently obtained on this silicon.

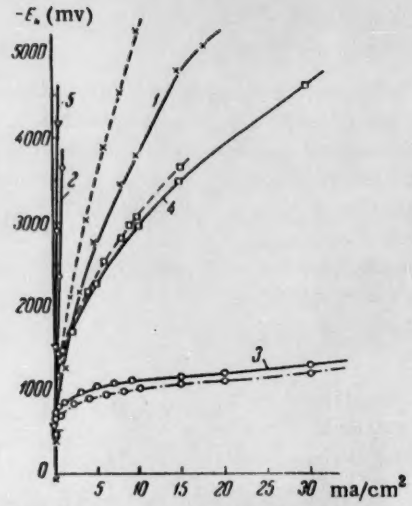

Fig. 2. Cathode polarization of p-type silicon. Solution, 0.2 N H_2SO_4, t = 25°, specific resistance: 1) 0.2 ohm · cm; 2) 10.0 ohm · cm; 3) 0.2 ohm · cm; 1, 2) after etching; 3) without etching. Solution, 5.0 N KOH, t = 50°, specific resistance: 4) 0.2 ohm · cm; 5) 23.0 ohm · cm; 4, 5) after etching. The broken lines are curves plotted backward.

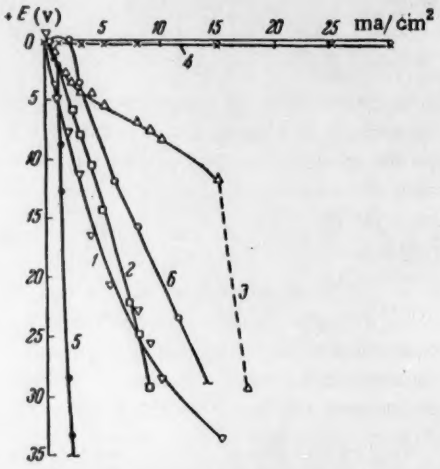

Fig. 3. Anode polarization of n- (2, 5, and 6) and p-type (1, 3, and 4) silicon with a preliminarily etched surface. Solution, 0.2 N H_2SO_4, t = 25°, specific resistance: 1) 10.0 ohm · cm; 2) 1.0 ohm · cm; 3) 10.0 ohm · cm; 3) cleaned under solution. Solution, 1.0 N HF, t = 25°, specific resistance: 4) 10.0 ohm · cm; 5) 1.0 ohm · cm; 6) 1.0 (with illumination).

In 5.0 N KOH at 50° (Fig. 1, b), i.e., under conditions where the oxide film on the silicon is readily soluble, the rate of hydrogen ion discharge on a silicon electrode depends little on the specific resistance, and the cathodic behavior of n-type silicon under these conditions is fundamentally the same as a metallic electrode.

Figure 2 shows curves of the cathode polarization of p-type silicon. It can be seen that both in sulfuric acid and in 5.0 N KOH, silicon of the hole type is polarized more strongly than n-silicon and the slope of the polarization curves is increased with an increase in its specific resistance. The nature of the solution has little effect on the kinetics of hydrogen ion discharge on p-silicon. It should be noted that p-type silicon becomes a strongly polarizable cathode in sulfuric acid solution only after preliminary etching, while for a mechanically polished, unetched surface, the cathode polarization curves differ little for n- and p-type silicons. The latter is explained by the fact that the preliminary etching dissolves not only the oxide film, but also the surface layer of silicon with a deformed (after mechanical polishing) lattice. Preliminary etching of the electrode has no effect for 5.0 N KOH at an elevated temperature (50°) due to the high rate of spontaneous solution of silicon under these conditions.

Analysis of the results obtained shows that the discharge of hydrogen ions on n-silicon apparently involves free electrons. The relatively low cathode efficiency of n-silicon in sulfuric acid solution, which has already been mentioned above, may be connected with the presence of an oxide film with low electrical conductivity on the electrode surface under these conditions and this, in its turn, also has semiconductor properties. All factors promoting the removal or weakening of this film simultaneously increase the efficiency of a cathode of n-type silicon. The sharp reduction in the rate of hydrogen ion discharge on p-type silicon may be explained both by a shortage of free electrons (with their predominant participation in the given cathode reaction) and by an additional ohmic potential drop in the subsurface layer of p-silicon, which is impoverished in holes. In the latter case, electrons from the valence zone must play the major role in the discharge of hydrogen ions on p-silicon. The formation on p-silicon of a subsurface layer with a lower concentration of holes than in the volume occurs during the cathode polarization of a silicon electrode and this is equivalent to connecting a variable ohmic resistance in series in the electrode circuit. The decrease in the rate of the cathode reaction on p-silicon with an increase in its specific resistance which is observed in 5.0 N KOH at 50° (i.e., under conditions when the oxide film is readily soluble) indicates that the second hypothesis, i.e., the predominant participation of electrons from the valence zone in the discharge of hydrogen ions, is more probable. An analogous idea was put forward in [5].

On the basis of the peculiarities of the structure of a lattice with covalent bonds of the diamond type, it might be expected that the anode solution of silicon, like germanium, would involve holes. The latter should be manifested in strong retardation of anode solution of silicon of the electronic type. The singularity of the behavior of a silicon electrode consists of the ready formation on the anode of oxide films, which passivate the electrode and strongly increase its ohmic resistance. The effect of the hole concentration on the anode polarization of n-type silicon can only appear therefore when this anode film is not formed on the silicon electrode (i.e., in electrolytes which readily dissolve silicon dioxide) and when the solution of silicon is the main anode reaction. This film is not dissolved in sulfuric acid of any concentration and therefore regardless of the type of conductivity and the state of the electrode surface, in 0.2 N H_2SO_4 silicon is very strongly polarized and is a practically insoluble anode (Fig. 3). In this case a film of great ohmic resistance is formed on the anode and oxygen is liberated simultaneously.

To confirm the fact that in sulfuric acid the strong anode polarizability of p-silicon is actually determined by the formation of a film on the anode, experiments were carried out on the anode polarization of a silicon electrode (p-type) with simultaneous cleaning of its surface under the solution [6]. The results obtained show (Fig. 3,3) that right up to a current density of about 15 ma/cm^2 the slope of the polarization curve is considerably decreased with cleaning and this is connected with the continuous removal of the film during the polarization process and slight activation of the electrode surface. However, even under these conditions the formation of the film on the anode surface continues. At a current density above 15 ma/cm^2 the polarizability of p-silicon is found to be very high even with cleaning as at this current density the rate of formation of the film apparently begins to be much greater than the rate of its removal by cleaning.

On the basis of the results obtained it may be considered that in sulfuric acid solution over the range of potentials we investigated, the high anode polarizability of silicon both with hole and electronic conductivity is due to passivation of the electrode. The main electrode reaction under these conditions is the liberation of oxygen.

As was to be expected, silicon with electronic and hole conductivity behaved differently under anode polarization in 1.0 N HF. Due to the high solubility of silicon dioxide in hydrofluoric acid, p-type silicon was not passivated up to a current density of 30 ma/cm^2 under anode polarization in this solution.

For silicon of the electronic type, the anode process began to be retarded strongly even at a current density of about 1.0 ma/cm^2 and in analogy with germanium, this may be connected with reaching the limiting current with respect to holes participating in the electrode solution of silicon. For n-type silicon, holes are minority charge carriers and the rate of their transportation to the solution boundary also determines the rate of the anode solution of n-silicon.

Thus, the data obtained show that the electrochemical behavior of silicon in electrolyte solutions is fundamentally similar to that of germanium and, as for germanium, it is determined by the type of its conductivity. The main difference between the electrochemical behavior of silicon and that of germanium is the fact that due to the high chemical inertness of SiO_2, under most conditions silicon has a surface oxide film. The presence of this film, which has a high ohmic resistance, leads to additional retardation of anode and cathode reactions on a silicon electrode.

LITERATURE CITED

1. J. Flynn, J. Electrochem. Soc. 105, 12 (1958).
2. R. Archer, J. Electrochem. Soc. 104, 10 (1957).
3. P. Schmidt and W. Michel, J. Electrochem. Soc. 104, 4 (1957).
4. A. Politycki and E. Fuchs, Zs. Naturforsch 14a, 3 (1959).
5. E. A. Efimov and I. G. Erusalimchik, Doklady Akad. Nauk SSSR 124, 3 (1959).•
6. N. D. Tomashov, G. P. Chernova, et al, Zavodskaya Lab., 3, 299 (1958).••

• See C. B. translation.
•• Original Russian pagination. See C. B. translation.

CONDITIONS FOR THE STABILITY OF A PLANE SOLID-LIQUID INTERFACE DURING CRYSTALLIZATION OF A BINARY MELT

D. E. Temkin

Institute of New Metallurgical Technology of the Central Scientific Research Institute for Ferrous Metallurgy

(Presented by Academician G. V. Kurdyumov, February 12, 1960)
Translated from Doklady Akad. Nauk SSSR, Vol. 133, No. 1, pp. 174-177, July, 1960
Original article submitted February 11, 1960

A small protuberance on a plane crystallization front will advance if the conditions are such that the rate of growth is greater at the extremity of the protuberance than at a point in the plane front far removed from it. The plane front will be unstable under these circumstances. Loss of stability leads to the production of cellular and dendritic structures [1]. The rate of growth is proportional to the total heat flux in the liquid and solid phases, and formulation of the conditions for stability must, therefore, be based on a comparison of the thermal transfer from the extremity of the protuberance and from the plane front itself. The front is stable when the following inequality

$$q_1 + q_2 \leqslant q_{1,0} + q_{2,0}, \tag{1}$$

is valid, $q_{1,0}$ and $q_{2,0}$ being the thermal flux in the solid and liquid phases, respectively, at a point in the plane crystallization front which is far removed from the protuberance, and q_1 and q_2, the corresponding quantities at the extremity of the protuberance. The term "stability criterion" will be used to designate that aggregate of conditions under which there will be a steady state uniform movement of the plane front and the extremity of the protuberance with the appearance of an equality sign in (1).

We will consider a binary melt in which the distribution coefficient $k = C_1/C_2$ is independent of concentration (C_1 and C_2 are the respective equilibrium concentrations of the second component, or solute, in the solid and liquid phases), and the liquidus curve is described by an equation of the form $T_k = T_{k,0} - AC_2$ in which $T_{k,0}$ is the melting point of the pure solvent. The immobile melt of initial concentration C_0, infinite in extent, is crystallizing in such a manner that the plane front with its protuberance is moving forward with a fixed velocity $\underline{v}$. The temperature of the melt at infinity is T_0. The coefficient of diffusion of the solute in the solid phase, D_1, is low and will be considered to be equal to zero.

We will not stop on the possible origin of the protuberance, or the mechanism of its formation, but will suppose it to have semispherical form with radius ρ (Fig. 1). The problem of the stationary distribution of temperature, $T_i(x, y, z)$ ($i = 1$, or 2; the index 1 designating the solid phase and the index 2, the liquid phase), and concentration C_2 (x, y, z) must be solved in order to determine the thermal fluxes q_1 and q_2 which are of interest here. This problem can be formulated in the system of moving coordinates of Fig. 1 through the following equations:

$$\Delta T_i + \frac{v}{a_i}\frac{\partial T_i}{\partial z} = 0, \quad \Delta C_2 = \frac{v}{D_2}\frac{\partial C_2}{\partial z} = 0; \tag{2}$$

$$T_i(x, y, z)|_{z=0} = T_{k,0} - AC_2(x, y, z)|_{z=0} \quad (\text{for} \quad x^2 + y^2 \geqslant \rho^2); \tag{3}$$

$$T_i(x, y, z)|_{z=\sqrt{\rho^2-x^2-y^2}} =$$

$$= g\,[T_{k,0} - AC_2(x, y, z)|_{z=\sqrt{\rho^2-x^2-y^2}}] \quad (\text{for} \quad x^2 + y^2 \leqslant \rho^2); \tag{4}$$

$$T_i(x, y, z)|_{(x^2+y^2+z^2)\to\infty} = T_{i,0}(z), \quad C_2(x, y, z)|_{(x^2+y^2+z^2)\to\infty} = C_{2,0}(z). \tag{5}$$

A condition of thermal balance must be satisfied at the crystallization front

$$\gamma_1 Q v_n = \lambda_1 \frac{\partial T_1}{\partial n} - \lambda_2 \frac{\partial T_2}{\partial n} \tag{6}$$

as well as a condition of balance with respect to the solute

$$(k-1)\,C_2 v_n = D_2 \frac{\partial C_2}{\partial n}. \tag{7}$$

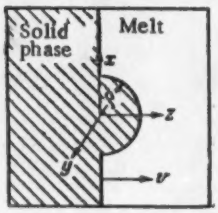

Fig. 1.

Here, $a_i = \lambda_i/c_i\gamma_i$ is the coefficient of thermal diffusivity, λ_i is the coefficient of thermal conductivity, c_i is the heat capacity, γ_i is the density, Q is the heat of crystallization, D_2 is the coefficient of diffusion of the solute in the melt, the multiplying factor $g = [1 - 2\sigma/\gamma_1 Q\rho]$ allows for the diminution in equilibrium temperature arising from the curvature of the surface at the crystal–melt interface and its surface tension σ; $\partial/\partial n$ is the normal derivative, and v_n is the rate of advance along the normal to the surface of crystallization. The stationary distributions of temperature and concentration, $T_{i,0}(z)$ and $C_{2,0}(z)$, in the absence of a protuberance, or at points far removed from the latter, are obtained as solutions of Eq. (3) with the conditions of (4) and (6) - (7) for z = 0:

$$T_{1,0}(z) = T'_k + [(Q/c_1) - (T'_k - T_0)\,c_2\gamma_2/c_1\gamma_1]\,(1 - e^{-vz/a_1}),$$

$$T_{2,0}(z) = T_0 + (T'_k - T_0)\,e^{-vz/a_2}, \quad C_{2,0}(z) = C_0 + C_0 \frac{(1-k)}{k}\, e^{-vz/D_2}, \tag{8}$$

$T'_k = T_{k,0} - AC_0/k$ being the temperature at the crystallization front.

The problem is well defined since the form of the crystallization front is given, and it has a solution for certain values of the parameters of Eqs. (3)-(7). With a view to obtaining an approximation solution it will be supposed that the concentration of the solute on the crystallization front satisfies the equation

$$C_2 = (C_0/k) - Bz/\rho, \tag{9}$$

in which B is, for the moment, an arbitrary constant. Through (9), a solution of Eqs. (3)-(5) can be obtained readily, using spherical coordinates for the liquid phase and toroidal coordinates (with $v\rho/2a_1 \leq 1$) for the solid phase.

Without stopping on the details of the solution, we will simply write down the resulting expressions for the thermal flux at the extremity of the protuberance

$$q_1 = \lambda_1 \left.\frac{\partial T_1}{\partial z}\right|_{\substack{z=\rho \\ x=y=0}} = 0{,}098\,(1-\varepsilon_1)\,q_{1,0} - (0{,}158 - 0{,}256\varepsilon_1)\,(1-g)\,T'_k\left(\frac{\lambda_1}{\rho}\right) +$$

$$+ (0{,}902 - 0{,}519\varepsilon_1)\,gAB\frac{\lambda_1}{\rho}; \tag{10}$$

$$q_2 = -\lambda_2 \left.\frac{\partial T_2}{\partial z}\right|_{\substack{z=\rho \\ x=y=0}} = 3\,(1-\varepsilon_2)\,q_{2,0} - (1{,}42 + 2{,}58\varepsilon_2)\,(1-g)\,T'_k\left(\frac{\lambda_2}{\rho}\right) +$$

$$+ (2 + 1{,}438\varepsilon_2)\,gAB\frac{\lambda_2}{\rho} \tag{11}$$

and for the flow of solute in the melt

$$q_m = -D_2 \frac{\partial C_2}{\partial z}\Big|_{\substack{z=\rho \\ x=y=0}} = \frac{2(1-k)\mu D_2}{k\rho} C_0 \Psi_1(\mu) - \frac{D_2}{\rho} B \Psi_2(\mu). \tag{12}$$

Here

$$\varepsilon_i = \frac{v\rho}{2a_i}, \quad \mu = \frac{v\rho}{2D_2}, \quad q_{1,0} = \lambda_1 \frac{dT_{1,0}}{dz}\Big|_{z=0} = \frac{2\varepsilon_1\lambda_1}{\rho}\left[\frac{Q}{c_1} - (T_k' - T_0)\frac{c_2\gamma_2}{c_1\gamma_1}\right],$$

$$q_{2,0} = -\lambda_2 \frac{dT_{2,0}}{dz}\Big|_{z=0} = \frac{2\varepsilon_2\lambda_2}{\rho}(T_k' - T_0).$$

The functions $\psi_1(\mu)$ and $\psi_2(\mu)$ are plotted in Fig. 2 for the range from $\mu = 0$ to $\mu = 2$. Only members containing the first power of ϵ_i have been retained in Eqs. (10) and (11) since the solution was developed for the case in which $\epsilon_i \ll 1$. Equations (10) and (11) make it clear that there is a difference in the thermal emission at the extremity of the protuberance and at the plane front because of: a) the geometry of the surface of the protuberance (first members of the right-hand terms of Eqs. (10) and (11)); b) the reduction in the equilibrium temperature resulting from the curvature of the interface (second members); and, c) the elevation of the surface temperature of the protuberance arising from diminished (if $k < 1$) concentration of the solute (third members).

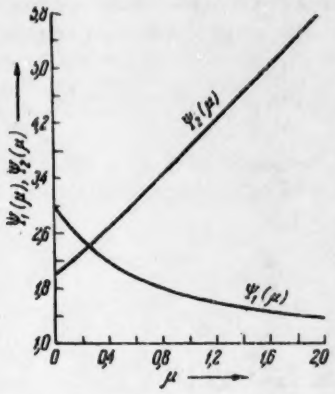

Fig. 2.

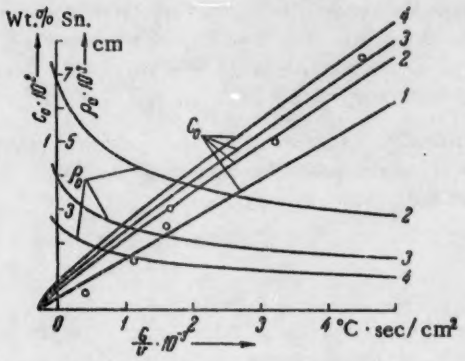

Fig. 3. 1) $v \to 0$; 2) v = 0.003 cm/sec; 3) 0.007 cm/sec; 4) 0.013 cm/sec.

The conditions of balance (6) and (7) have not been drawn on thus far. In fact, these conditions could not be fulfilled over the entire crystallization front since the approximation of (9) enters into the solution. But they will be valid far from the protuberance where $T_1(x, y, z)$ and $C_2(x, y, z)$ pass over into $T_{1,0}(z)$ and $C_{2,0}(z)$. The expression (9) contains a single arbitrary constant and we will therefore require that (6) and (7) be fulfilled at one additional point, namely the extremity of the protuberance. With (9)-(12) we then have:

$$\gamma_1 Q v = q_1 + q_2; \tag{13}$$

$$(1-k)[(C_0/k) - B]v = q_m. \tag{14}$$

The elimination of B from (13) and (14) gives the defined condition for surface stability. When ϵ_1, ϵ_2, and $(2\sigma/\gamma_1 Q\rho)$ are neglected in comparison with unity, this condition can be written as

$$C_0 = \frac{k}{(1-k)A}\frac{Q\gamma_1 D_2}{c_2\gamma_2 a_2} f(\mu) \times$$

$$\times \frac{[0{,}902 + 2{,}902(\lambda_2 G/\gamma_1 Q v) + 2(1{,}42 + 0{,}158\lambda_1/\lambda_2)\lambda_2 a T_k'/(\gamma_1 Q\rho)^2 v]}{2 + 0{,}902\lambda_{12}\lambda_2} \tag{15}$$

where $f(\mu) = [\psi_2(\mu) - 2\mu(1-k)]/[\psi_1(\mu) - 1]$, $G = (dT_{2,0}/dz)_{z=0} = -c_{2,0}/\lambda_2$.

Equations (3)-(7) will have a solution when the parameters are related through (15), and the extremity of the semispherical protuberance will then move with the same velocity, v, as the plane crystallization front. The rate of movement of the extremity is less than v and the plane front stable when C_0 has a lower value than that given by Eq. (15), while the velocity of the extremity exceeds v and the front is unstable at higher values of C_0.

Setting $C_0 = 0$ in Eq. (15) gives an expression for the stability limit in the case of crystallization of a pure material*

$$\frac{G}{v} = -0{,}311\frac{\gamma_1 Q}{\lambda_2} - \frac{2(1{,}42 + 0{,}158\lambda_1/\lambda_2)\sigma T_{k,0}}{2{,}902\gamma_1 Q\rho^2 v}. \tag{16}$$

The stability limit will depend on the radius, ρ, of the protuberance. The concentration C_0 will be at a minimum for a certain value $\rho = \rho_0$ which satisfies the relation:

$$\mu_0^3 F(\mu_0) = \frac{v}{2D_2^2}\frac{(1{,}42 + 0{,}158\lambda_1/\lambda_2)}{(0{,}902 + 2{,}902\lambda_2 G/\gamma_1 Q v)}\frac{\lambda_2\sigma T_k'}{(\gamma_1 Q)^2}, \tag{17}$$

in which $\mu_0 = v\rho_0/2D_2$ and $F(\mu) = f'(\mu)/[2f(\mu) - \mu f'(\mu)]$. Taken together, Eqs. (15) and (17) describe the optimal position of those stability limits for given G and v under which the plane crystallization front will be stable for protuberances of any size whatsoever, provided that the melt concentration is less than C_0.

The points of Fig. 3 designate experimental results on the stability limits in Pb–Sn melts (Sn is the solute) [1] while the curves give results calculated from Eqs. (15) and (17) by using various values of v. The thermal parameters which were chosen were those for pure Pb: $T'_k \simeq T_{k,0} = 600°K$, $\lambda_1 = 0.070$ cal/cm · sec · °C, $\lambda_2 = 0.059$ cal/cm · sec · °C, $\gamma_1 = 11.0$ g/cm^3, $\gamma_2 = 10.7$ g/cm^3, $Q = 5.5$ cal/g, $c_1 = 0.036$ cal/g · °C, $c_2 = 0.034$ cal/g · °C, $k = 0.57$, $\sigma = 7.9 \cdot 10^{-7}$ cal/cm^2, $A = 2.7°$ C/wt.%, $D_2 = 5 \cdot 10^{-5}$ cm^2/sec.

Usually, loss of stability is related to the presence of a zone of "concentrational supercooling" which lies ahead of the crystallization front in the melt [3]. For this reason the equation expressing the condition for the appearance of such supercooling,

$$C_0 = \frac{kD_2 G}{(1-k)Av} \tag{18}$$

is considered to coincide with the equation for the stability limit, although this seems unjustified, physically. It can be shown readily that results from Eqs. (15) and (18) agree to within a multiple of the order of unity when the value of G/v is high. There is, however, an essential difference between (15) and (18) when the G/v ratio is low. This is seen from the fact that (18) shows C_0 to be equal to 0 when G/v = 0 while (15) and (17) indicate that $C_0 = 0$ when $G/v = -0.311\gamma_1 Q/\lambda_2$. Thus, test of the ideas advanced in the present article requires additional experimentation on stability during crystallization of pure melts and melts containing solutes at low concentration.

LITERATURE CITED

1. W. A. Tiller and J. W. Rutter, Canad. J. Phys. 34, 1, 96 (1956).
2. D. E. Temkin, Collected Papers (TsNIICHERMET, 1960), No. 4 [in Russian].
3. W. A. Tiller, K. A. Jackson, J. W. Rutter, and B. Chalmers, Acta Metal. 1, 4, 428 (1953).

*This relation was obtained in [2], but without making any allowance for the effect of surface tension ($\sigma = 0$).

THE NATURE OF SECONDARY CHEMICAL BONDS

D. N. Shigorin, A. N. Rodionov, T. V. Talalaeva, and

Corresponding Member Acad. Sci. USSR K. A. Kocheshkov

L. Ya. Karpov Physicochemical Institute

Translated from Doklady Akademii Nauk SSSR, Vol. 133, No. 1, pp. 178-181
July, 1960
Original article submitted March 25, 1960

In quite a number of compounds the valence electrons initially belonging to a specific primary bond become involved in many-center molecular orbitals which leads to the formation of new (secondary) chemical bonds. This problem has received a considerable amount of attention [1, 2]. Primary (strong) chemical bonds are formed by the direct interaction of valence electrons on adjacent atoms, whereas the secondary (weaker) bonds frequently result from some additional participation of these electrons in a common system of molecular bonds where the energy states of the electrons become substantially changed. Thus, the formation of secondary bonds depends not only on the nature of some specific atom in the molecule but also on the type of electron distribution in the entire molecule. In order to examine the nature of such secondary chemical bonds we carried out a detailed investigation of the I. R. absorption spectra of organolithium compounds and of various acetylene derivatives. The I. R. spectra of R–Li and Ar–Li compounds indicate that a free C–Li group has a characteristic vibrational frequency at 1050-1100 cm^{-1}. Dipole moment measurements in dilute hexane solutions of R–Li compounds yielded a C–Li bond moment of 1.1-1.2 D. The vibrational frequency and the relatively small dipole moment suggest a covalent character for the C–Li bonds in the investigated organolithium compounds. The I.R. spectra of solid (crystalline) organolithium compounds and of their solutions (in benzene, hexane, et al.) show additional bands, absent in the spectra of vapors and displaced from the vapor bands toward longer wavelengths (870 cm^{-1}, 926 cm^{-1}, 970 cm^{-1}). These bands are the characteristic bond vibrations of complexed –C–Li.... groups. The strong shift of the C–Li vibrational bond frequency ($\Delta\nu = \nu_0 - \nu = 1050 - 870 = 180$ cm^{-1}) indicates some indirect participation in complex formation. In its tendency to form complexes, lithium can be classified with elements such as Be, B, and Al. The organolithium compounds resemble the compounds of Be, B, and Al in that they dimerize by forming a lithium bridge, which involves a secondary chemical bond. To the known series of B, Be, and Al complexes we can now add organolithium compounds, as is shown below, for example:

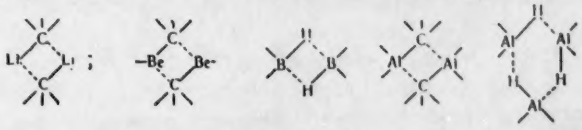

The existence of mixed complexes of the type: $R-Li \cdot BeR_2$, $R-Li \cdot AlR_3$, etc., provides direct experimental evidence for the common character of secondary chemical bonds, which are responsible for the association of organometallic lithium, beryllium, boron, and aluminum compounds [6]. The common nature of the secondary chemical bonds in organometallic compounds of Li, Be, B, and Al can be explained by the special properties of these elements and the primary M–C bonds. A common property of all these elements is the availability of free low-lying p-orbitals and the ability to change the energy state of the valence electrons from $s \rightarrow p$ with very little energy loss. In this manner it becomes possible to form many-center molecular orbitals, particularly three-center ones, as is the case in the enumerated Li, Be, B, Al, and other complexes [12]. Consequently the above-mentioned

elements can not only participate in the formation of chemical bonds by sharing their valence electrons, but also by providing free orbitals for the electrons involved in the formation of primary bonds in other molecules. This leads to the formation of secondary chemical bonds between molecules. For example, in an organolithium dimer each bridge carbon atom can form a three-center orbital with two lithium atoms (two electrons in three nuclear fields). Such an orbital is energetically more stable than an ordinary C–Li bond, since a lithium atom is now able to contribute two orbitals, besides its single valence electron, to the bond formation. The common character of the primary and secondary chemical bonds in the organometallic compounds of Li, Be, B, and Al, is also reflected in the similarity of their physicochemical properties (solubility in nonpolar solvents, small dipole moments, etc.). Therefore it is not surprising that organolithium compounds are good catalysts for the polymerization of ethylene and its derivatives, since they resemble organoaluminum compounds in the formation of primary and secondary bonds. Hence it now becomes obvious that the physicochemical properties and the reactivities of organolithium, organoaluminum, and other similar compounds should be interpreted on the basis of the covalent nature of the C–Li and C–Al bonds and the very pronounced tendency to form secondary chemical bonds with each other and with other molecules. One can therefore assume that a very fundamental step in the initiation of the polymerization of ethylene and its derivatives involves the formation of an adduct between the monomer and the organometallic ompound (R–Li or AlR_3),

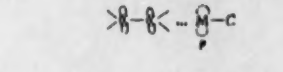

(I)

where p denotes the free orbital of Li, Al, or other similar metals. The secondary chemical bond in such complexes results from the formation of a three-center orbital (two π-electrons in the field of three nuclei). It seems that in certain cases the formation of such a complex can initiate a chain reaction (polymerization). Compounds of the $TiCl_4$ type can also activate the double bonds by disrupting secondary chemical bonds between the Me–C groups thus favoring the formation of the basic complex (I). Using PMR the authors of this paper and V. I. Smirnova showed that $TiCl_4$ reacts with R–Li to yield free radicals. Certain polymerizations can be initiated by compounds such as R–Li even in the absence of $TiCl_4$. The stability of complex (I) will depend on the nature of the π-bond and on steric factors as well as on the type of the primary Me–C bond and the specific properties of the vacant orbitals contributed by the metals (Me). As an indirect experimental proof for the existence of type I complexes one can cite the fact that ethyllithium forms colored complexes with styrene, with α- and β-methylstyrene, and with other unsaturated compounds; the infrared spectra of these colored solutions exhibit a new strong C=C band, strongly shifted toward longer wavelengths ($\sim 1580\ cm^{-1}$), which disappears when the color is destroyed. To the list of such complexes we can also add lithium acetylide adducts [7] and other adducts of acetylene and its derivatives [8]. Another interesting property of lithium in the C–Li group resides in its ability to form secondary bonds, just like B, Be, and Al do, through a donor–acceptor interaction (where the donor provides the free electron pair) which leads to the formation of very stable R–Li . . . X complexes (where X= O , N , etc.). Our I. R. investigation of ethyllithium and butyllithium in hexane, to which various ethers and tertiary amines have been added, and of Ar–Li solutions in ethers, indicate that such complexes are indeed formed and possess varying stabilities. All these results clearly indicate that the catalytic activity of organolithium compounds could be controlled by adding various compounds (ethers, amines, halides, etc.) capable of either altering the nature of R–Li . . . complexes or completely destroying them. The stability of complexes formed through secondary chemical bonds depends on the specific properties of the adjacent primary chemical bonds (polarity, strength). The indicated properties of the Me–C bond depend to certain degree on the interactions between the various groups in the molecule. Thus, for example, σ,π-conjugation $Li \overset{\sigma}{-} C - C \overset{\pi}{=} C-$ in benzyllithium ($C_6H_5-CH_2Li$), fluorenyllithium, and other compounds can affect appreciably the polarity and strength of the C–Li bond. Such a σ,π-conjugation produces changes in the electronic molecular spectra and is responsible for the coloration of several organolithium compounds. Unlike the C–Li, C–Al, and other similar groups the O–H and N–H can not form secondary chemical bonds by forming three-center orbitals with their primary bond electrons since O, N, and H atoms do not possess any low-lying vacant orbitals. Therefore, in systems containing no π-electrons O–H, N–H and similar groups usually form secondary bonds of the donor–acceptor type by utilizing the free electron pairs of the donor atom A–H . . . B. At the same time the O–Li, O–Al, and similar groups can either form secondary chemical bonds of the donor–acceptor type or participate in three-center orbitals by using their primary bond electrons. However, in the case of R–O–Li the formation of secondary bonds in a three-center orbital

would be more favorable energetically and provide for maximum sharing of the valence electrons; this would help explain the vibrational and electronic spectra as well as the unusual electrical properties of R–O–Li compounds.

Groups such as O–Li, O–Al, etc. readily form secondary bonds in molecules containing π-electrons; best examples are provided by the acetylacetonates (inner complexes). In these cases the O–H and N–H bonds behave just like the O–Li and O–Al groups – they form secondary intramolecular (hydrogen) bonds which differ very little fronf other heteroorganic bonds [3, 9]. The energy of secondary intramolecular hydrogen or heterometallic bonds in the systems examined by us is given by the equation: $E = E_d + E_a + E_\pi$ (where E_d and E_a are the dipole and the acceptor–donor interaction energies respectively). The E_π term, which gives the interaction energy between the O–H, O–Li, O–Al, etc. and the π-electrons of the system, constitutes the largest component [3, 6, 1]. In systems such as acetylacetonates π-interaction leads to the formation of pseudoaromatic rings with six electrons shared in common (4 π-electrons from the C=C and C=O bonds and two electrons of the primary M–O bond).

Infrared investigation of metallic inner complexes (Al, Cr, Fe, Cu, Mg, et al.) indicates [9] that the respective bonds in the rings of these compounds are almost equal in length. These results are in good agreement with the x-ray diffraction data [13]. The factors chiefly responsible for the formation of rings with averaged bond lengths and a common π-electron system are: deformations of the electron cloud in the M–O group at right angles to the primary bond ($\sigma \rightarrow \pi$ transitions, which are aided by strong σ,π-conjugation in M–O–C = C– systems) and the availability of vacant p- or d- orbitals on the metal which can be used by the π-electrons of the double bonds (C=O and others). Such a treatment also presumes that the modified p-orbitals of hydrogen are utilized by the π-electrons of the system, though less effectively than are those of the metals (Li, Al, etc.). The electronic spectra of several such systems indicate that in the excited state the use of the hydrogen p*-orbitals by the π-electrons of the system increases considerably [10]. In the systems investigated by us the π-electrons of the C=O group utilize the free orbitals of atom M (H, Li, Al, etc.) to form an unusual three-center orbital, which is also responsible for the redistribution of π-electron densities throughout the system. Similarly, secondary bonds involving π-electrons also appear in simpler systems, such as $\diagdown C{=}O + Al\diagup\!\!-$, which are called π-complexes [11]. Thus, H, Li, Al, and other elements forming inner complexes form bonds not only by utilizing their valence electrons but also by contributing free orbitals. Thus, for example, hydrogen and lithium use one valence electron each and provide in addition one free orbital each, while aluminum contributes three electrons ($3s\ 3p^2$) and provides a total of six orbitals ($3s\ 3p^3\ 3d^2$), which corresponds to six equivalent Al–O bonds. In summing up we can conclude that various types of secondary chemical bonds are possible and that these influence strongly the physicochemical properties and reactivities of the compounds involved.

LITERATURE CITED

1. D. N. Shigorin, Zhur. Fiz. Khim. 25, 737 (1951); Zhur. Fiz. Khim. 32, 1739 (1938); Problemy Fiz. Khim. 1, 171 (1958).
2. Ya. K. Syrkin, Uspekhi Khim. 28, 903 (1959).
3. A. N. Rodionov, D. N. Shigorin, et al., Izvest. Akad. Nauk SSSR, Otdel Khim. Nauk,120 (1958);* Doklady Akad. Nauk SSSR 123, 113 (1958);**Izvest. Akad. Nauk SSSR, Ser. Fiz. 9, 1110 (1958).
4. K. A. Kocheshkov, Problemy Fiz. Khim. 1, 156 (1958).
5. D. N. Shigorin, Acta Spectrochimica (London, 1959) p. 226.
6. G. Wittig and F. Bickelpaupt, Ber. 91, 865 (1958).
7. A. N. Rodionov, G. V. Kazennikova, et al., Doklady Akad. Nauk SSSR 129, 121 (1959).**
8. D. N. Shigorin, M. M. Shemyakin, and M. N. Kolosov, Izvest. Akad. Nauk SSSR, Otdel Khim.Nauk , 1133 (1958).*
9. D. N. Shigorin, Zhur. Fiz. Khim. 27, 554 (1953); Izvest. Akad. Nauk SSSR, Ser. Fiz. 17, 596 (1953).
10. D. N. Shigorin, N. A. Shcheglova, and N. S. Dokunikhin, Doklady Akad. Nauk SSSR 133, 2 (1960).*

*See C. B. translation.

**Original Russian pagination. See C. B. translation.

11. V. N. Filimonov and A. N. Terenin, Doklady Akad. Nauk SSSR 109, 799 (1956).*
12. E. G. Hoffmann and G. Schomburd, Zs. Elektrochem. 61, 1101 (1957).
13. L. M. Shkolnikova and E. A. Shugam, Kristallografiya 5, 1 (1960); E. A. Shugam, Doklady Akad. Nauk SSSR 81, 853 (1951).

*Original Russian pagination. See C. B. translation.

ANODIC DISSOLUTION OF GERMANIUM WITH A p-n JUNCTION

O. G. Deryagina, E. N. Paleolog and N. D. Tomashov

Institute of Physical Chemistry, Academy of Sciences, USSR
(Presented by Academician A. N. Frumkin, February 3, 1960)
Translated from Doklady Akademii Nauk SSSR, Vol. 133, No. 2, pp. 388-391, July, 1960
Original article submitted February 2, 1960

An investigation of the rate and the character of anodic dissolution of germanium with p-n junctions is of interest for the development of an electrochemical method for the manufacture of p-n junctions with a given geometrical shape. At present there exist several empirical methods for selectively etching p-n junctions [1, 2] which are utilized in industry for the manufacture of special semiconducting devices.

An investigation into the kinetics and the mechanism of various electrochemical reactions on a germanium electrode, which has been executed some time back [3-7], enables the planning of a route for a rational choice of conditions in which germanium p-n junctions may be selectively etched. When choosing these conditions not only the physical properties of these junctions must be taken into account, as has been done until now, but the electrochemical characteristics of the separate parts of the rectifier on the boundary with the solution must also be allowed for.

We have investigated the distribution of potential and current density and consequently also the dissolution rate for the separate parts of a germanium rectifier at its anodic polarization under various conditions. All measurements were done on experimental surface p-n junctions, obtained by welding germanium to indium (germanium brand DM was used) and also on a germanium single crystal with a p-n junction. The germanium samples were lined with epoxy resin (compound), ground perpendicularly to the germanium-indium (or p-germanium–n-germanium) contact area, polished with electrocorundum powders Nos. 20 and 7 and, after etching in a hydrogen peroxide solution, exposed to anodic polarization. The latter was done without stirring in a 0.1 N NaOH or H_2SO_4 solution at room temperature and in diffuse daylight. The electrical contact with the positive terminal of the external current source was made on the side of the indium, so that the p-n junction was switched in the forward direction. For each value of the polarizing current density, the potential distribution on the various parts of the rectifier was determined as also the surface relief produced by the dissolution. The potential was measured by means of a narrow capillary probe, which could be moved along the surface [8], and a binocular Linnik microscope [9] was used to determine the depth of corrosion (surface relief). When it is known to what depth the germanium and the indium are corroded anodically at the various points of the surface, then one may calculate the actual distribution of the current densities, that is, determine the fraction of the current responsible for the corrosion of each constituent (indium, p-germanium or n-germanium) of the rectifier. The width of the p-germanium region in the samples investigated was determined by plating it with copper in a solution of pyrophosphate during cathodic polarization of the p-n junction from the side of indium.

The anodic polarization curves of indium, p-germanium and n-germanium in a 0.1 N NaOH solution, obtained with separate samples, are shown in Fig. 1. We see that, in the given circumstances, indium and n-germanium are the most polarizable anodes. Unlike that of indium, here the high polarizability of n-germanium is not connected with the onset of passivity, but with the low concentration of the holes, which are required for its anodic corrosion [3].

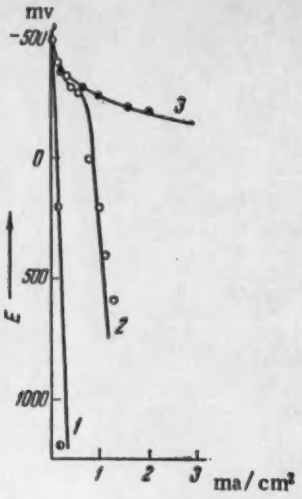

Fig. 1. Anodic polarization of indium (1), n-germanium (2) and p-germanium in a 0.1 N NaOH solution.

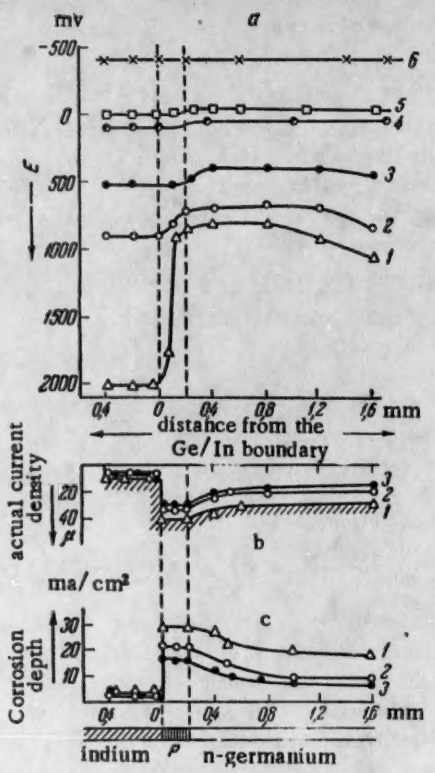

Fig. 2. Potential distribution (a), surface profile (b) and current density distribution (c) along the rectifier surface upon polarizing anodically in 0.1 N NaOH solution. 1) 4 ma, 2) 2 ma, 3) 1 ma, 4) 0.4 ma, 5) 0.1 ma, 6) 0.05 ma.

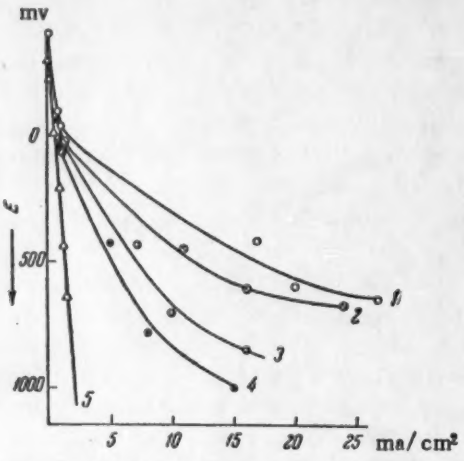

Fig. 3. Anodic polarization of n-germanium at various distances from the In/Ge boundary. 1) 0.1 mm; 2) 0.5 mm; 3) 1.0 mm; 4) 1.5 mm; 5) anodic polarization of n-Ge without injection.

The potential distribution along the surface of the rectifier is shown in Fig. 2a for various currents between 0.05 and 4.00 ma. The potential drop over the ohmic resistance in the p-n junction is not included in the values shown and these represent the actual potentials of the rectifier parts. The surface profiles of the rectifier, observed after polarizing during 60 min at the said currents, are shown in Fig. 2b and the current densities, calculated from these profiles, are given in Fig. 2c. The results obtained show that, in the given circumstances, the rectifier surface appears to be unpolarized. There is not only a considerable difference in potential between the indium and the germanium, which is connected with the presence of a p-n junction (equivalent to a certain ohmic resistance in boundary between p- and n-Ge), but also between the separate regions of germanium itself. Increasing the anodic current of external polarization results in raising this difference in potential. It will be noticed that the potential on Ge becomes the more positive the greater the distance from the p-n junction. At a current density of 4.00 ma the difference in potential over the n-Ge region amounts to 300 mv, that is, considerably surpasses the ohmic potential drop (70-80 mv) over this region at the said current. The current density at the separate parts of the rectifier appears also to be unequal. As was to be expected from the anodic polarization curves shown above, the

lowest corrosion current density is found on indium and the highest on the p-germanium region. The current density on the n-germanium region is not constant, but it is the lower the greater the distance from the p-n junction.

It is interesting to note that the current density on the n-germanium in the rectifier does not correspond to the limiting anodic current density of the n-germanium itself (Fig. 1) but substantially surpasses the latter. In our opinion, this is connected with injection (extraction) of holes through the p-n junction into the n-germanium region, since the anodic polarization of the rectifier is carried out from the side of indium, that is, from the side of p-germanium. If this is really true, then the anodic polarizability of the n-germanium, which is determined by the hole concentration, should vary at various distances from the p-n junction.

Anodic polarization curves for various parts of the n-Ge surface are shown in Fig. 3; they have been calculated from the experimental curves for the distribution of current density and potential along the surface. Curve 5 in this plot corresponds to anodic polarization of the same sample in the absence of injection, that is, at anodic polarization of the rectifier from the side of n-germanium. The results obtained confirm the assumption made above and show that at increasing distance from the p-n junction the anodic polarization of n-Ge is raised owing to the diminished concentration of the injected holes. The latter causes the variation of the potential and the current density along the n-Ge surface. It should be remarked that, in the circumstances of our measurements, hole injection is effective through the whole depth of the germanium owing to the high value (L = 2.6 mm) of the diffusion length for the minority carriers in our germanium (brand DM) and the relatively small thickness of the sample.

Thus, the data obtained show that the p-germanium and the adjoining zone of n-germanium are preferentially corroded, when a germanium rectifier is polarized anodically from the side of indium in a 0.1 N NaOH solution, that is, under such conditions that the anodic polarization of indium is very high. When the polarization of the rectifier is carried out in the same solution, anodically from the side of indium and at the same time cathodically from the side of n-germanium, then the corrosion of the latter may completely stop and the attack may be concentrated on the narrow zone of p-germanium. When the rectifier is anodically polarized in a sulfuric acid solution, in which indium is practically not polarized, we obtain preferential corrosion of the indium and the adjoining region of p-germanium. Substantially analogous results were also obtained for a germanium single crystal with a p-n junction.

When analyzing the results obtained we see that the various parts of a germanium rectifier or transistor may be etched selectively owing to the different anodic polarizabilities of n-germanium, p-germanium and indium in solutions of electrolytes and also because a p-n junction with both electronic and hole conduction exists at the germanium boundary. The presence of a junction is equivalent to inserting an ohmic resistance with a variable resistivity into the circuit.

The aptitude of the p-n junction to inject minority carriers into germanium is an important property. The indicated physical properties of electron-hole junctions have a great influence upon the distribution of the current density along the rectifier surface. When varying the conditions under which the rectifier is polarized anodically, that is, upon varying the anodic current density and the side of the contact and choosing solutions in which the polarizabilities of indium and p-germanium are different, preferential anodic corrosion may be effected either of indium or of the p- and n-germanium region.

LITERATURE CITED

1. E. Billig and J. Down, Nature 172, 115 (1953).
2. J. Lesk and R. E. Gonzalles, J. Electrochem. Soc. 105, 8 (1958).
3. W. Brattain and C. Garrett, Bell System Techn. J. 34, 1 (1955).
4. D. R. Turner, J. Elektrochem. Soc. 103, 4 (1956).
5. H. Gerischer and F. Beck, Z. Phys. Chem. (BRD) 13, 5-6 (1957).
6. E. A. Efimov and I. G. Erusalimchik, Zhur. Fiz. Khim. 32, 2 (1958).
7. E. N. Paleolog, A. Z. Fedotova, and N. D. Tomashov, Doklady Akad. Nauk SSSR 129, 3, 623 (1959).*
8. O. G. Deryagina, "New Methods in Physicochemical Investigations," Transactions of the Institute of Physical Chemistry [in Russian] (Izd. AN SSSR, 1958) pp. 2, 6, 69.

* Original Russian pagination. See C. B. translation.

9. I. L. Rosenfel'd, "Investigations into Metal Corrosion," Transactions of the Institute of Physical Chemistry, [in Russian] (Izd. AN SSSR, 1951) pp. 2, 3, 50.

ELECTROCHEMICAL AND PHOTOELECTROCHEMICAL BEHAVIOR OF THE SILICON ELECTRODE

S. U. Izidinov, T. I. Borisova and V. I. Veselovskii

The L. Ya. Karpov Physicochemical Institute

(Presented by Academician A. N. Frumkin, March 18, 1960)
Translated from Doklady Akademii Nauk SSSR, Vol. 133, No. 2, pp. 392-395, July, 1960
Original article submitted March 16, 1960

The investigation of the electrochemical and photoelectrochemical parameters during the etching of silica in alkali is of some interest because of its contribution toward the explanation of the mechanism of autosolution, and the effects of change in surface composition on the photogalvanic activity of the system. A few published works [1-6] have been devoted to the electrochemical behavior of silicon, but only one of these [6] considers the effect of optical illumination on the silicon electrode in the absence of an external electric field in the alkaline solution.

The material used in the investigation was monocrystalline silicon of the n- and p-types, with a specific resistance of 1 ohm · cm. The crystallographic orientation of the surface was (III). The source of white light of great intensity (about 10^{-1} cal/cm^2·sec) was an incandescent projection lamp. The following methods of treating the surface were employed: etching in hot potassium hydroxide, or in hydrofluoric and nitric acids, and mechanical polishing by means of abrasive powder.

The autosolution of the silicon, accompanied by the evolution of hydrogen, has been studied in potassium hydroxide solutions of various concentrations from 0.01 N to 10 N. Figure 1 gives the change of potential with time for n- and p-silicon in 10 N potassium hydroxide. Curve 1 is for polished samples, for which the potential changes from −550 or −500 mv, the immersion potential, to a constant value of −300 to −320 mv. Curve 2, for an etched sample, approaches the same constant value. With dilution of the potassium hydroxide, a less negative value is found for the stationary potential, which may be from −200 to −50 mv. This is connected with the greater oxidation of the surface owing to the lower rate of autosolution. The autosolution current, measured by the rate of hydrogen evolution, diminishes with time from its highest value of 5 to 6 · 10^{-3} a/cm^2 to a stationary value of 1 · 10^{-3} a/cm^2 at the point where the stationary potential is reached (Fig. 1, Curve 3). It is seen from Fig. 1 that the observed shift of potential during etching in the direction of a less cathodic stationary value for the polished sample is accompanied by a change in the rate of autosolution. This change may be supposed to be due to the reduction in the true surface in consequence of the removal of the mechanically disturbed layer, and also to the increase in the possible oxidation. But the potential displacement is due exclusively to the increased oxidation of the surface under the stationary autosolution conditions. The opposite direction of the change of potential with time for the etched specimens from the less cathodic point toward the stationary value can be accounted for by the appreciable solution of the oxide film produced by the preliminary chemical treatment and standing in air [7]. Figure 2 gives the anode polarization curves for both types, taken immediately after their immersion (Curves 1 and 3), and after the attainment by the same electrodes of the stationary states (Curves 2 and 4), showing the suppression of the autosolution process, and the transition of the silicon into the passive condition. It can be seen from Fig. 2 that, with low rates of autosolution under the conditions of stationary etching, the maximum current necessary for the passivation of the electrode is considerably reduced (6 to 10 · 10^{-6} a/cm^2),

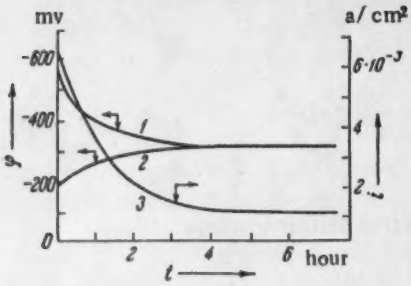

Fig. 1. 1) Change in potential during etching in 10 N KOH of polished samples; 2) the same for previously etched samples; 3) reduction in the autosolution current during the etching of polished samples.

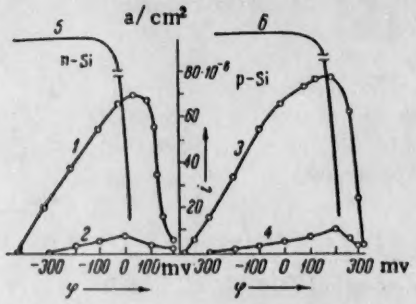

Fig. 2. Anodic polarization curves: 1) and 3) for freshly immersed polished specimens; 2) and 4) after attainment of stationary conditions; 5) and 6) relationship between the rate of hydrogen evolution and the potential.

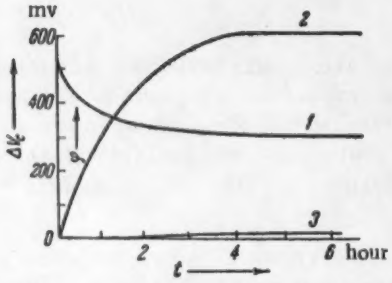

Fig. 3. Increase of ΔV_C with time during the etching of polished specimens: 1) change of potential; 2) p-Si; 3) n-Si.

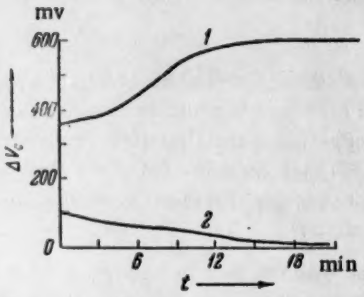

Fig. 4. Change in ΔV_C during the dissolution of the oxide film for: 1) p-Si; 2) n-Si.

in comparison with the current required for the passivation of freshly polished electrodes (75 to 85 · 10^{-6} a/cm²), while in both cases the current required is about a factor of 100 less than the autosolution current. It is interesting that the potential at the maximum on the anode curve for the p-type is some 200 mv more positive than that for the n-type of silicon. Apart from this difference, and the somewhat larger current magnitude for p-silicon, there is no appreciable difference between n- and p-Si on anodic polarization. Measurements of the rate of evolution of hydrogen, made at the same time as the polarization curves were obtained, have shown that the current required to shift the potential by 100 mv in the anodic direction for n- and p-types is some 500 or 600 times smaller than the autosolution current, which is 1 · 10^{-3} a/cm². More than this, it seems that the rate of evolution of hydrogen is practically unaffected by change in potential of 230 mv (n-Si) or 420 mv (p-Si) in the anodic direction (Fig. 2, Curves 5 and 6). The slowing down of the autosolution begins at potentials of 80-90 mv on the cathodic side of the maximum of the polarization curves. Complete cessation of the process of gas evolution occurs in a finite time only in the neighborhood of the potential maximum. A cathodic polarization of −1 to −1.5 v (p-Si), or 0.6 v (n-Si) also has practically no effect on the rate of autosolution. However, the current during cathodic polarization of n-type silicon is of the order of 150 times greater than that for p-Si, and is of the same order as the autosolution currents. In other words, during cathodic polarization the nature of the conductivity is suddenly revealed.

Besides the change in potential and the rate of autosolution during etching, there is also a change in the photogalvanic activity, ΔV_C, of the system. For polished samples of p-type silicon, the value of ΔV_C increases from zero to a constant value of 600 mv at the stationary state of autosolution (Fig. 3, Curve 2). For n-Si under the same conditions, the maximum value of ΔV_C does not exceed 10-15 mv (Fig. 3, Curve 3). The more dilute the alkali solution, the smaller the value of ΔV_C for the p-type, and the larger for the n-type, in comparison with

the value for 10 N potassium hydroxide; and this fact is evidently connected with the greater oxidation of the surface. It should also be noted that the rate of evolution of hydrogen is practically unchanged under the influence of illumination, inspite of the change of the measured potential of the system in the anodic direction by +250 to +300 mv when ΔV_c = 600 mv (p-Si). Oxidation of the surface, both by anodic polarization and by preliminary chemical etching and introduction of oxygen into the solution, has an appreciable influence on the photoeffect, increasing ΔV_c for n-Si (50-100 mv), and diminishing it for the p-type (200-400 mv). In the course of the dissolution of the oxidized film, with simultaneous increase of the potential up to the initial stationary value, the photoeffect is increased for the p-type (Fig. 4, 1), and is diminished for the n-type of silicon (Fig. 4, 2). The nature of the specific electrolyte has much to do with the size of the electrochemical and photoelectric parameters. In sulfuric acid, as distinct from potassium hydroxide, autosolution is practically absent, as a consequence of which the anodic polarization curves do not pass through a maximum, the stationary potentials are positive, and the surface properties produced by the processing are nearly maintained. The shift of potential with time in the anodic direction is independent of the treatment, and is evidently concerned with the further oxidation of the surface in the solution. The maximum value of ΔV_c, 500 mv, is only observed with etching of the p-type silicon; while for the p-type the figure is greatly reduced (150-250 mv), and further diminution takes place under constant illumination. The anodic current returning from the light potential to the dark is reduced from $70\text{-}80 \cdot 10^{-6}$ a/cm^2 to $2\text{-}3 \cdot 10^{-6}$ a/cm^2 because of the growth under these conditions of the oxide film. The anodic polarization causes considerable changes in the parameters of the system, and in the case of sulfuric acid the correlation between the degree of the oxidation of the surface and ΔV_c, which is observed in KOH, disappears.

It thus follows from the results given that the rate of the autosolution process for silicon in alkalis is practically the same for p- and n-silicon, is unaffected by change in the potential over a considerable interval, and is effectively unaltered by optical irradiation.

The practical identity of the rates of autosolution for n- and p-silicon shows that this process is independent of the type of conductivity which is shown. The energy of the controlling stage in the chemical interaction of atoms of silicon with hydroxyl ions in the over-all autosolution process:

$$Si + 2OH^- + H_2O = SiO_3^{2-} + 2H_2$$

ensures the continuation of the compensating associated cathodic reaction in which hydrogen ions are discharged, which takes place with the consumption of the electrons liberated from the valence zone by the anode reaction. Certain difficulties arise in explaining the mechanism of the cathodic autosolution reaction. The observed difference (of an order of magnitude or more) in the currents during cathodic polarization of the two types apparently shows that the autosolution process does not involve the transfer of electrons in the conductivity zone, or the realization of the surface energy levels. Consequently, because of the combination in one stage of the ionization of the silicon and the discharge of a proton, the cathodic autosolution reaction presumably proceeds through the consumption of electrons coming directly from the valence zone. In cathodic polarization, though, the electrons are drawn from the conductivity zone, which reveals itself in the difference in the behavior of the n- and p-types mentioned above. For the explanation of these problems, however, further investigations will be needed.

The absence of an fundamental difference in the form of the anodic curves for n- and p-silicon (Fig. 2), and the passivation of the surface by the currents which are two orders of magnitude less than the autosolution current during oxidation of the surface under stationary etching conditions, may be due to further electrochemical oxidation. The somewhat higher polarizability of the p-type (for which the shift of the maximum of the anode curve is 200 mv in the anodic direction), and the independence of the rate of hydrogen evolution on the rising branches of the curves are linked with the preferred change of the potential jump in the region of the spacial charge. A similar conclusion may be drawn in considering the effect of the optical illumination. The considerable difference in the values of ΔV_c for p-and n-silicon in the absence of an external electrical field is due to the fact that in the autosolution process the surface of p-silicon approximates to that of the n-type, while oxidation affects them in opposite directions: that is, diminution of ΔV_c for p-silicon is produced by oxidation, while the value for n-silicon is increased. It follows from this that although the measured stationary potentials are practically the same for the two types, the distribution of the potential jumps in the silicon-solution interface is different. The etching of the mechanical defect layer, which diminishes the surface recombination, leads to increase in the value of ΔV_c for p-silicon. It is evident that the effect of light will be essentially in the region of the space charge, and this results in the practical invariance of the rate of hydrogen evolution on illumination.

It follows from the matters discussed that the presence of the two associated reactions of oxidation and reduction in the irreversible autosolution process of silica in alkali is the determining factor in the independence of the rate of solution on the type of conductivity; and, side by side with the composition of the surface, also determines the photogalvanic activity of the system.

LITERATURE CITED

1. P. Schmidt and W. Michel, J. Electrochem. Soc. 104, 4, 230 (1957).
2. D. R. Turner, J. Electrochem. Soc. 105, 7, 402 (1958).
3. J. Flynn, J. Electrochem. Soc. 105, 12, 715 (1958).
4. P. F. Schmidt and D. A. Keiper, J. Electrochem. Soc. 106, 7, 592 (1959).
5. E. A. Efimov and I. G. Erusalimchik, Dokl. Akad. Nauk SSSR 130, 2, 353 (1960).*
6. M. Seipt, Z. Naturforsch. 14a, 10, 926 (1959).
7. K. J. Archer, J. Electrochem. Soc. 104, 10, 619 (1957).

* Original Russian pagination. See C. B. translation.

THE OPERATION OF A GALVANIC CELL WITH A SOLID ELECTROLYTE EXHIBITING MIXED CONDUCTIVITY

S. V. Karpachev and S. F. Pal'guev

Electrochemical Institute of the Ural Branch of the Academy of Sciences, USSR
(Presented by Academician A. N. Frumkin, March 7, 1960).
Translated from Doklady Akademii Nauk SSSR, Vol. 133, No. 2, pp. 396-398,
July, 1960
Original article submitted March 7, 1960

It is of interest to consider the influence of electronic conductivity, existing side by side with ionic conductivity, in the solid electrolyte of a galvanic cell, on the electrical power provided by this cell in an external circuit. A solution of this problem would, we believe, widen our understanding of the part played by electronic conductivity of the electrolyte in the operation of galvanic cells with solid electrolytes.

So as to simplify the problem in front of us, we propose its solution for the case of a simple galvanic cell with solid silver bromide acting as the electrolyte. The cell is:

$$\mathrm{Ag} \mid \mathrm{AgBr} \mid \mathrm{Br_2},\ \mathrm{C}. \qquad \text{(I)}$$

Gaseous bromine, when dissolved in solid silver bromide, imparts to the latter electronic conductivity of the p-type [1]. In accordance with this, the electromotive force of our cell is described by the equation [2]:

$$E = (1 - \bar{t})\, E_0. \qquad (1)$$

In this relationship, E_0 is the thermodynamic value of the electromotive force: that is, it is the value which this would have in the absence of electronic conductivity in the solid electrolyte; $\bar{t}$ is the mean value of the transference number of the electrons, or, what amounts to the same thing, of the holes in the solid electrolyte.

We shall assume that the bromine diffuses from the bromine electrode to the silver through the entire thickness of the electrolyte, and that the concentration of the bromine in the immediate neighborhood of the silver electrode is determined by the equilibrium:

$$\mathrm{Ag} + \mathrm{Br} \rightleftarrows \mathrm{AgBr}. \qquad (2)$$

The magnitude of $\bar{t}$ may in such a case be given in the following form [3]:

$$\bar{t} = \frac{\lg \dfrac{\varkappa_0^{(C)} + \varkappa_i}{\varkappa_i}}{\lg \dfrac{C_{Br}^{(C)}}{C_{Br}^{(Ag)}}}. \qquad (3)$$

In equation (3), $\varkappa_0^{(C)}$ is the electronic conductivity in the electrolyte immediately around the bromine electrode; $\varkappa_i$ is the ionic conductivity which we shall regard as being approximately constant in every section of the elec-

trolyte; $C_{Br}^{(C)}$ and $C_{Br}^{(Ag)}$ are the concentrations of bromine dissolved in the electrolyte around the bromine and the silver electrodes respectively: the value of $C_{Br}^{(C)}$ will, evidently, be the equilibrium value in relation to the pressure of bromine at the bromine electrode.

We now compute the ohmic resistance of the electrolyte, regarding the latter as in the form of a cylinder of length L and cross-sectional area of 1 cm^2.

The resistance of a thin layer of the electrolyte of thickness dx will be $\frac{dx}{(\kappa_0 + \kappa_i)}$, so that the total resistance R of the electrolyte will be given by the integral

$$R = \int_0^l \frac{dx}{\kappa_0^{(x)} + \kappa_i}. \tag{4}$$

The quantity $\kappa_0^{(x)}$ may be written thus:

$$\kappa_0^{(x)} = kC_{Br}^{(x)}, \tag{5}$$

where k is a constant, and $C_{Br}^{(x)}$ is the concentration of the dissolved bromine in a cross section of the electrolyte situated at a distance x from the silver electrode.

We shall suppose that the distribution of bromine concentrations along the electrolyte is determined purely by a diffusion process; the gradient of the concentration of bromine will then be constant along the solid electrolyte. In agreement with this we may write:

$$\frac{C_{Br}^{(C)} - C_{Br}^{(Ag)}}{l} = \frac{C_{Br}^{(x)} - C_{Br}^{(Ag)}}{x}, \tag{6}$$

By means of Equations (6) and (5) we may express $\kappa_0^{(x)}$ in terms of x. Inserting the relation so obtained in (4), and integrating, we obtain:

$$R = \frac{2{,}3l}{\kappa_0^{(C)} + \kappa_0^{(Ag)}} \lg \frac{\kappa_0^{(C)} + \kappa_i}{\kappa_0^{(Ag)} + \kappa_i}, \tag{7}$$

If the concentration $C_{Br}^{(Ag)}$ determined by the equilibrium (2) is very small, then we may neglect $\kappa_0^{(Ag)}$ in Equation (7), and we shall obtain:

$$R = \frac{2{,}3l}{\kappa_0^{(C)}} \lg \frac{\kappa_0^{(C)} + \kappa_i}{\kappa_i} \tag{8}$$

The resistance R' of the electrolyte in the case where the electrolyte only possesses ionic conductivity can be written thus:

$$R' = \frac{l}{\kappa_i}. \tag{9}$$

We shall assign the following quantitative relationships, which are close to those actually found:

$$\kappa_0^{(C)} \simeq 10\kappa_i; \quad \frac{C_{Br}^{(C)}}{C_{Br}^{(Ag)}} \simeq 10^{10}.$$

Under such conditions, we obtain the approximate relationships:

$$\bar{t} \simeq 0{,}1, \quad R \simeq 0{,}23R'. \tag{10}$$

We now write the expressions W_0 and W to denote the power given off by the cell into an external circuit,

in the cases where electronic conductivity is absent and present respectively in the solid electrolyte. Let the external resistance be R' in each case. Then:

$$W_0 = 0{,}25\,\frac{E_0^2}{R'}, \quad W = 0{,}54\,\frac{E_0^2}{R'}. \tag{11}$$

It can be seen from this relationship (11) that the power given by our galvanic cell into the external circuit is, in the case where electronic conductivity exists, roughly twice as great as the power given to the external circuit in the absence of electronic conductivity. This circumstance, as is easily seen, arises from the fact that under conditions in which $C_{Br}^{(C)} \gg C_{Br}^{(Ag)}$, because of the appearance of electronic conductivity, the resistance of the electrolyte is reduced considerably more than the electromotive force of the galvanic cell. It should, however, be said that the distribution in the concentration of bromine dissolved in the electrolyte, generally speaking, is disturbed under the influence of the current flowing through the cell. Therefore, the results obtained will be quantitatively accurate only in cases where relatively small currents are flowing, or when a high velocity of diffusion of bromine through the solid electrolyte is found.

Thus, under certain conditions, the occurrence of electronic conductivity in the solid electrolyte of a galvanic cell may be turned to useful account, since it results in an appreciable increase in the power given by the cell to an external circuit.

LITERATURE CITED

1. G. W. Luckey and W. West, J. Chem. Phys. 24, 879 (1956).
2. C. Wagner, Z. Phys. Chem. 21, B, 25 (1933).
3. S. F. Pal'guev, S. V. Karpachev, and L. D. Yushina, Dokl. Akad. Nauk SSSR 129, 1339 (1959).*

*Original Russian pagination. See C. B. translation.

THE MECHANISM OF THE COMBUSTION OF POWDERS

G. B. Manelis, A. G. Merzhanov, and F. I. Dubovitskii

Chemical Physics Institute, Academy of Sciences, USSR
(Presented by Academician V. N. Kondrat'ev, March 2, 1960)
Translated from Doklady Akademii Nauk SSSR, Vol. 133, No. 2, pp. 399-400, July, 1960
Original article submitted February 27, 1960

Experiments by P. F. Pokhil [1] have shown that during combustion, a considerable part of the original powder is dispersed, and is carried away in the form of smoke by the gas stream. Pokhil believes that heterogeneous – homogeneous reactions, which determine the rate of combustion, take place in the smoke – gas mixture thus formed.

In the theory of combustion, considerable interest is attached to the problem of where and how the dispersed particles burn – whether they burn in the hot flame zone at a temperature close to the maximum, or whether they are able to decompose according to the usual laws of reaction in the condensed phase at the powder surface, without reaching the flame.

An exact solution of the problem of the thermal decomposition of dispersed particles in space and time can be obtained from a knowledge of the laws governing the movement of particles and the laws of heat exchange between particles and a surrounding gas. To answer the question posed, however, it has proved sufficient to carry out an isothermal estimation of the lifetime of a particle. In the isothermal estimation, we assume that the particle decomposes at a temperature T_s equal to the temperature at the surface of the hot powder. The value of T_s can be calculated from a formula obtained in one of our earlier works [2], taking account of the dispersion:

$$u^2 = \frac{1}{1-\gamma_d} ak_0 e^{-E/RT_s} \frac{RT_s^2/E}{T_s - T_0 - {}^1/_2 Q(1-\eta_d)/c},$$

where Q is the thermal effect of the decomposition of the powder, C the specific heat capacity of the powder, a the temperature conductance, T_0 the temperature of the powder at a distance from the surface, E and k_0 the activation energy and preexponential term of the rate constant for the decomposition of the powder, and η_d the degree of dispersion.

The lifetime of a particle is

$$t_l = \frac{1}{k_0 e^{-E/RT_s}},$$

and the distance which it is able to travel is

$$x_d = u_g t_l,$$

where $u_g = \frac{\rho}{\rho_g} u$ is the rate of movement of the gases (the maximum possible velocity of the particle), u the rate of combustion, ρ the density of the powder, and ρ_g the density of the gases.

Thus, the experimental values of the rate of combustion u are used to calculate T_s, t_l and x_d, and the calculated values of x_d are compared with the experimental values of the width of the preflame (dark) zone x_g.

p, kg/cm²	u, cm/sec	T_s, °C	t_l, sec	x_d, cm	x_g, exper., cm
20	0,6	385	$1 \cdot 10^{-3}$	0,1	1,3
30	0,9	400	$4 \cdot 10^{-4}$	0,04	0,5
40	1,1	410	$2{,}5 \cdot 10^{-4}$	0,025	0,3
50	1,2	415	$2 \cdot 10^{-4}$	0,016	0,2

The numerical calculation was carried out for the specific case of pyroxylin powder. The initial data used in the calculation were: $a = 1 \cdot 10^{-3}$ cm²/sec; $c = 0.35$ cal/g · °C; $\rho = 1.6$ g/cm³; $Q = 270$ cal/g [1]; $k_0 = 10^{17.8}$ sec^{-1}; $E = 44600$ cal/mole [3]; $T_0 = 20°$ C; $\rho_g = 5 \cdot 10^{-4}\, p$ g/cm³ (where p is the pressure in kg/cm²); and $\eta_d = 0.7$.

The results of the calculation and the experimental values of the width of the preflame zone x_g are given in the Table.

It should be emphasized that the calculated values of x_d represent upper estimated values. If account is taken of autocatalysis in the decomposition process, the heating effect resulting from its own heat evolution, the heating effect resulting from heat transfer from the flame, and the fact that the particles may move with a velocity less than the velocity of the gas, then the calculated value of x_d will be decreased.

Thus, even the upper estimated value shows that the particles do not reach the zone of the flame, but are able to decompose close to the surface of the powder. This result leads to the establishment of a zone in which decomposition of the dispersed particles of the original powder takes place. The existence of this zone is confirmed by experimental data on the transparency of the smoke–gas phase [4] and on the temperature distribution in the hot powder [5, 6] (the sharp increase in the temperature gradient and the maximum heat evolution close to the surface of the powder).

Thus, it can now be assumed that the combustion of a powder base on pyroxylin takes place as follows. In the condensed phase, there takes place an essentially exothermic decomposition reaction, which is accompanied by the dispersion of a considerable quantity of the original powder. The decomposition of the particles of the dispersed powder takes place in a zone close to the surface of the hot powder, and quantities of heat equal to 300 cal/g and above are evolved in the condensed phase in the decomposition zone. In a third zone (the maximum temperature zone), a reaction takes place leading to the formation of the final products and the evolution of the rest of the heat.

LITERATURE CITED

1. P. F. Pokhil, Doctorate Dissertation [in Russian] Chemical Physics Institute, Academy of Sciences, USSR (1954); Collection, The Physics of Explosions [in Russian], 2, 181 (1953).
2. A. G. Merzhanov and F. I. Dubovitskii, Doklady Akad. Nauk SSSR 129, 153 (1959).*
3. K. K. Andreev, The Thermal Decomposition and Combustion of Explosives [in Russian] (1957).
4. V. P. Mal'tsev and P. F. Pokhil, Doklady Akad. Nauk SSSR 132, 3 (1960).**
5. C. A. Heller and A. S. Gordon, J. Phys. Chem. 59, 773 (1955).
6. R. Klein and M. Menster, et al., J. Phys. and Coll. Chem. 54, 877 (1950).

* Original Russian pagination. See C. B. translation.

** See C. B. translation.

THE INTERACTION BETWEEN A MICROIMPURITY AND THE SURFACE OF CRYSTALS

I. V. Melikhov, Chiu Hsiao-Hsi, and M. S. Merkulova
M. V. Lomonosov Moscow State University

(Presented by Academician V. I. Spitsin, February 22, 1960)
Translated from Doklady Akademii Nauk SSSR, Vol. 133, No. 2, pp. 401-404, July, 1960
Original article submitted February 20, 1060

In the present work we have examined the processes which take place during the interaction between an impurity and the surface of a perfect, real heteropolar crystal in contact with a solution.

The first stage in the interaction is the transfer of the impurity to the Volmer phase [1, 2] (the A layer [3]) (secondary molecular and ionic adsorption). At the moment of this transfer, or after displacement along the crystal surface in the A layer, the impurity particle may find itself close to a vacant site formed in the surface layer of the crystal (the S layer), and may fill this vacant site (primary adsorption). We shall assume the particular case where the impurity fills the vacant cationic sites.

We have already shown [3] that the probability W for the appearance, in an adsorption center of the A layer, of an impurity particle which can move into an energetically uniform S layer is determined by the equation

$$W = b_A \nu_A e^{-U_A/kT} p_{S+} A C_L, \tag{1}$$

where b_A is a constant; ν_A the frequency of vibration of the impurity particle in the adsorption center of the A layer; U_A is the activation energy for the transfer of the impurity to the S layer; p_{S+} the concentration of vacant cationic sites in the S layer; $\underline{k}$ the Boltzmann constant; T the temperature of the system; A the adsorption constant, and C_L the concentration of impurity in the solution in contact with the crystal surface. Of the activated impurity particles in the A layer, which are situated close to the vacant cationic sites in the S layer, only a certain fraction φ_A will enter the surface layer of the crystal, since these vacant sites may also be occupied by particles of the macrocomponent. The quantity φ_A is equal to the ratio of the probability for the activation of impurity particles to the sum of the probabilities for the activation of impurity particles and macrocomponent situated close to a vacant site:

$$\varphi_A = \frac{1}{1 + (n-1)\, e^{-\Delta U/kT} C_{MA}}, \tag{2}$$

where $\underline{n}$ is the number of adsorption centers from which direct transfer of particles into the vacant site of the S layer can take place; $\Delta U = U_{MA} - U_A$; U_{MA} is the activation energy for the transfer of the macrocomponent to the S layer; and C_{MA} is the concentration of macrocomponent particles in the A layer. The velocity V_S of transfer of impurity particles to the S layer is given by the equation

$$V_S = n b_A \nu_A e^{-U_A/kT} \varphi_A p_{S+}\, AC_L = M_A p_{S+} C_L, \tag{3}$$

where M_A is a quantity independent of the amount of microimpurity in the system.

In analogous fashion it is possible to determine the velocity V_A of the transfer of impurity particles from the S layer to the A layer, and, by using the surface equilibrium condition $V_S = V_A$, to obtain the equation

$$C_S = M \frac{p_{S+}}{p_{A+}} C_L, \tag{4}$$

where C_S is the equilibrium concentration of microimpurity in the S layer, M is constant for a given solution composition and temperature, and p_{A+} is the concentration of vacant cationic sites in the A layer.

The surface of a perfect crystal containing an impurity cannot, however, always be regarded as uniform. The impurity particles deform the structure of the S layer, so that the values of V_A and V_S for the deformed sections of the surface may differ considerably from the corresponding characteristics of the nondeformed S layer [4, 5].

The concentration of impurity in the deformed and nondeformed sections of the S layer can be determined by Equation (4), and the total concentration C_0 of impurity in the surface layer of the crystal is given by the equation

$$C_0 = \frac{M}{p_{A+}} \left(p_{S+} + \frac{M' m p_{S+}}{M p'_{A+}} p_{A+} C_0 \right) C_L, \tag{5}$$

where the superscript dashes are used to denote the characteristics of the deformed sections of the S layer, referred to above, and m is the number of macrocomponent particles in the deformed section around each impurity particle. The value of m in Equation (5), as a first approximation, is equal to the number of nearest neighbors of the impurity particle in the S layer [6], and is independent of the concentration C_0. The value of p'_{S+} is determined by the deformation and is probably also independent of the quantity of impurity in the S layer. The concentrations p'_{S+}, p_{A+} and p'_{A+} may be dependent on C_0, but only if the following conditions are satisfied

$$C_0 \sim p_{S+}, \tag{6}$$

$$AC_L \sim p_{A+} \sim p'_{A+}. \tag{7}$$

It is reasonable to assume that condition (6) is satisfied when the impurity is present in the system in microconcentrations (the value of p_{S+} is extremely small [6]). The concentration $p_{A+} \gg p_{S+}$, since the structure of the A layer is weakened by adsorbed solvent, and the values of p_{A+} and p'_{A+} can be taken as independent of C_0.

The relationship between the quantities p_{S+} and C_0 can be found by studying the processes leading to neutralization of the surface charge of the crystal relative to the Volmer phase and the solution. The surface charge of a pure crystal may change when the impurity enters the S layer, if the charge of the impurity particles, Z, differs from the charge of the cations of the macrocomponent Z_1 (an "impurity" charge appears), and if the presence of the impurity leads to a change in the value of p_{S+} and the concentration p_{S-} of vacant anionic sites in the S layer. The "impurity" charge and the charge of the vacant sites may neutralize one another or be neutralized by the adsorption of ions of opposite sign from the solution. The condition for electrical neutrality of the surface of separation between the phases may be written in the form

$$p_{S+} + m p'_{S+} C_0 = (1 - \alpha) \frac{Z - Z_1}{Z_1} C_0 + \beta m p'_{S+} C_0 + a_0 + p_{S-}, \tag{8}$$

where α and β are the probabilities of neutralization by adsorption for the "impurity" charge and the charge of the vacant sites produced in the deformed section of the S layer, respectively; $a_0 = p_{S_0^+} - p_{S_0^-}$; and $p_{S_0^\pm}$ represents the concentration of vacant cationic (+) or anionic (-) sites in the S layer of the pure crystal.

From Equations (5) and (8), assuming, after Koch and Wagner, [7], that the vacant cationic and anionic sites interact according to the law of mass action

$$K_S = (p_{S+} + m p'_{S+} C_0) p_{S-}, \tag{9}$$

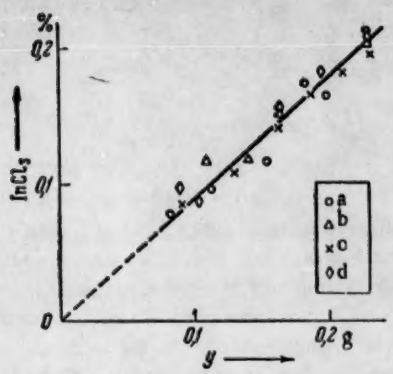

Fig. 1. Relationship between the quantity of $InCl_3$ transferred to the solid phase and the quantity of macrocomponent y in the precipitate. a) Coprecipitation at C_{init} = $= 3.5 \cdot 10^{-7}$ g/ml; b) at $C_{init} = 2 \cdot 10^{-6}$ g/ml; c) at $C_{init} = 2 \cdot 10^{-5}$ g/ml; d) at C_{init} = $3.5 \cdot 10^{-7}$ g/ml in a solution containing $1 \cdot 10^{-4}$ g/ml Al.

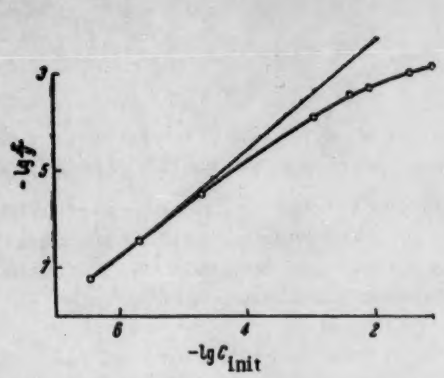

Fig. 2. Relationship between the $InCl_3$ concentration in the NaCl crystals (x/y) and the concentration of impurity in the original solution (C_{init}, g/ml).

we obtain the relationship

$$C_0 = \frac{M\left[a_0 + \sqrt{a_0^2 + 4K_S \dfrac{1 + \frac{M}{p_{A+}}\left[mp'_{S+}(\Gamma - \beta) - R\right] C_L}{1 + \frac{M}{p_{A+}} C_L mp'_{S+}\Gamma}}\right]}{2p_{A+}\left\{1 + \frac{M}{p_{A+}}\left[mp'_{S+}(\Gamma - \beta) - R\right] C_L\right\}}, \qquad (10)$$

where K_S is a constant; $R = \frac{Z - Z_1}{Z_1}(1 - \alpha)$; $\Gamma = 1 - \frac{M' p_{A+}}{M p'_{A+}}$.

Let us examine some particular case for which relationship (10) is simplified.

1. The case where deformation of the S layer by the impurity is slight. In this case, when the quantities of impurity in the system are small, the quantity $(M'/M)mp_{S+}\Gamma C_L \ll 1$ and the relationship (10) becomes

$$C_0 = \frac{M\left(a_0 + \sqrt{a_0^2 + 4K_S}\right) C_L}{2p_{A+}} \approx \frac{Mp_{S_0^+}}{p_{A+}} C_L. \qquad (11)$$

2. The case where the deformation of the S layer by the impurity is large; the "impurity" charge is absent ($Z = Z_1$) or completely neutralized by adsorption ($\alpha = 1$); and the charge of the vacant cationic sites produced close to the impurity particles cannot be neutralized by adsorption ($\beta \to 0$). In this case the concentration C_0 is given by

$$C_0 = \frac{Mp_{S_0^+} C_L}{p_{A+}\left[1 + \frac{M}{p_{A+}} mp'_{S+}\Gamma C_L\right]}, \qquad (12)$$

3. The case where deformation of the S layer is large and the "impurity" charge is completely neutralized by adsorption and by the vacant sites situated close to the impurity particles on the deformed sections of the S layer ($mp'_{S+}\Gamma = R$). In this case, when $\beta \approx 0$,

$$C_0 = \frac{MC_L}{2p_{A+}}\left[a_0 + \sqrt{a_0^2 + \frac{4K_S}{1 + \frac{M}{p_{A+}} mp'_{S+}C_L}}\right]. \qquad (13)$$

When $a_0 = 0$, Equation (13) is analogous to the formula obtained by Kelting and Witt [8] for the equilibrium concentration of impurity in the bulk of the solid phase.

In order to verify these theories experimentally, we studied the coprecipitation of microquantities of $InCl_3$ with NaCl crystals during growth of the latter from slightly supersaturated agitated solutions at 20°. The method of study has been described earlier [9]. The results of the experiments showed that the $InCl_3$ enters the solid phase in considerable quantities (up to 0.2%), while the concentration of microimpurity in the NaCl crystals is independent of the mass of the macrocomponent in the precipitate, and is unaffected by the presence of considerable quantities of foreign polyvalent ions (Fig. 1), but changes slightly with change in the pH of the medium. In the majority of experiments, the acidity was kept at 0.45 N, since an acid medium prevents the adsorption of indium by the walls of the flask, which is always considerable in neutral medium. Microscopic examination of the precipitate showed that the growing NaCl crystals occlude a certain quantity of mother liquor, but the quantity taken up is extremely small. Examination of the change in weight of the precipitate after ignition and fusion showed that the occluded mother liquor amounts to less than 0.24% of the weight of the precipitate, and that less than 0.002% of indium can be entrained in this liquor. It is evident that the $InCl_3$ is coprecipitated not by internal or secondary surface adsorption, but apparently forms solid solutions in the NaCl crystals.

Study of the relationship between the concentration of impurity in the solid phase and the initial concentration of impurity in the solution C_{init} (Fig. 2) showed that the coprecipitation is described by the relationship

$$\frac{x}{y} = \frac{AC_{init}}{(1 + BC_{init})^{1/2}}, \qquad (14)$$

where x and y are the quantities of impurity and macrocomponent, respectively, entering the precipitate, and A and B are constants (A = 0.01 and B = 400).

Theoretical analysis of the diffusion of the macrocomponent and impurity to the surface of the growing crystal shows that when x = 0.2%, the concentration $C_{init} \cong C_L$, and the concentrations of impurity in each S layer being laid down on the surface of the slowly growing crystal are identical and equal to $x/y = C_0$, so that Equation (14) is analogous to formula (13) when $a_0 = 0$.

Thus, the experimental data for the coprecipitation of $InCl_3$, like the data published earlier for the coprecipitation of $PbCl_2$ and $CdCl_2$ [9] with NaCl crystals, are in agreement with the theories presented above.

According to these theories, the interaction of In with the surface of the NaCl crystals can be represented as follows. The indium ions, which in the supersaturated NaCl solution form $InCl_4'$ complexes [10], do not lose all the ligand atoms on transfer to the S layer. One of them occupies the adsorption center of the A layer closest to the impurity particle and neutralizes one of the "impurity" charges of each In ion. The second "impurity" charge is neutralized by the vacant cationic site formed in the deformation zone around each impurity particle: as a consequence, the quantity $mp'_{S+}\Gamma = 1$. Since in all probability $\Gamma \sim 1$ [4, 5], while m = 4 for NaCl crystals $p'_{S+} = 6.5 \cdot 10e^{-\overline{W}/kT} = 0.25$, where $\overline{W}'$ is the work of formation of a vacant site in the deformed section of the layer [6], we have $\overline{W}' \approx 0.14$ ev. From formulas (12) and (14), $p_{S_0+} = A/B = 2.5 \cdot 10^{-5}$. Using the value of p_{S_0+} and the results of experimental studies [9], we calculated the values of $\overline{W}'$ for the $NaCl-PbCl_2$ system ($\overline{W}' = 0.20$ ev) and the $NaCl-CdCl_2$ system ($\overline{W}' = 0.29$ ev). The values obtained for $\overline{W}'$ are reasonable and are in good agreement with the differences in properties of the cations of the impurity and macrocomponent.

LITERATURE CITED

1. M. Volmer, Z. Phys. Chem. 102, 267 (1922).
2. R. H. Doremus, J. Phys. Chem. 62, 1068 (1958).
3. I. V. Melikhov and M. S. Merkulova, Radiokhimiya 1, 6, 627 (1959).
4. I. R. Reitz and I. L. Gammel, J. Chem. Phys. 19, 894 (1951).

5. P. Brauer, Z. Elektrochem. 57, 749 (1953).
6. N. Mott and R. Gurney, Electronic Processes in Ionic Crystals [Russian translation] (IL, 1950).
7. E. Koch and C. Wagner, Z. Phys. Chem. 38, 295 (1937).
8. H. Kelting and H. Witt, Z. Physik. 126, 697 (1949).
9. I. V. Melikhov, M. S. Merkulova, and G. Éval'd, Radiokhimiya 1, 1, 3 (1959).
10. I. A. Schufle and H. M. Eiland, J. Am. Chem. Soc. 76, 960 (1954).

MOLECULAR MECHANISM IN THE DEFORMATIONS OF POLYMER SUBSTANCES

G. A. Patrikeev

(Presented by Academician V. A. Kargin, March 16, 1960)
Translated from Doklady Akademii Nauk SSSR, Vol. 133, No. 2, pp. 405-408, July, 1960
Original article submitted March 15, 1960

1. The theoretical representation of the strained state of a deformed ideal elastic network [1-4] and in connection with deformation relaxation processes in polymer substances [3, 5] were elaborated without using the idea of a molecular mechanism. For instance, in the statistical theory, the change of the state of polymer molecules was considered as a consequence of a change in their configuration [1-4], without considering the possibility of existence of relative displacements of the macromolecules during the deformation of the elastic body. In relaxation theories, the relative displacement of the polymer molecules was considered as a plastic flow [3, 5]. In spite of their great importance, relaxation theories have an insufficiency of principle, because they treat deformations of different nature as independent. The molecular mechanism of the deformation of polymer substances differs essentially from the molecular mechanism of diffusion processes [2, 6-8]. The difference in the behavior upon deformation of polymer links and of polymer chains [7] has been established. New fruitful ideas, like that of "forced elasticity" [6], of "chemical flow" [9], and of "mechanochemical effects" [10, 11] which appear upon deformation of a polymer as a consequence of a local concentration of the tensions, have been proposed. However, the elementary acts which determine the appearance of the above mentioned effects when the polymers are deformed have not yet been explained [7, 9, 10]. In this paper the possibility of explaining a molecular mechanism of deformation of polymer substances by an elaboration of the results of mechanical experiments on a plastic, made on the basis of the application of the methods of macromolecular mechanics [11-13], is discussed.

2. The process of mechanical deformation consists in a relative displacement of the structure elements with different accelerations. The strained state of a polymer must be a consequence of the conservation of the binding of the structure elements strained because of the deformation. In the deformed system in any instant of time the internal mechanical equilibrium must be preserved between the strained elements linked to each other.

According to a structure-mechanical theory, as a result of the important relative displacement of a very small part of the macromolecules the deformation of polymer substances must give rise to a flexible network – a hypothetical frame – which takes on itself the main part of the external load, and also balances an appreciable part of the internal tension of the deformed elastic network, threaded by branched sections of the frame [11-13]. As a way to balance mechanical tensions in the sections of the frame we postulate a mutual redistribution of the tensions along the elastically strained chains. Then the probability of formation of a frame for a corresponding temperature and rate of deformation will be determined by the contour-polycyclic structure of the network by the formation upon deformation of molecular groups and by intermolecular interaction. The strained state must be immediately determined only by the number of the sections of the frame that have been formed and by the degree of their relative elastic lengthening, since the determining influence of the factors just listed can appear only indirectly – through their influence on the structure of the elastic network which is formed [12-13].

3. Important indications concerning the molecular mechanism can be obtained by analyzing the change

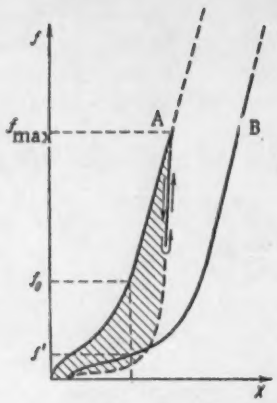

Fig. 1. Structure effects upon deformation of an NK plastic. A) Firststretching with partial contraction (the dotted line shows the outline of the complete contraction); B) second expansion after complete contraction of the stretched sample.

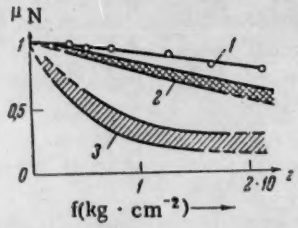

Fig. 2. Thixotropic softening of an NK plastic. 1) "Nonloaded;" 2) channel carbon black (10-30 cm^3); 3) mineral fillers: kaolin, zinc oxide, chalk, mica (10-20 cm^3).

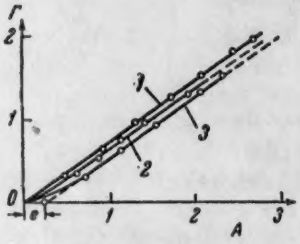

Fig. 3. Structure hysteresis (in kg · m · cm^{-3}). Plastics with channel carbon black (20-25 cm^3); 1) NK; 2) SKB; 3) BSK.

in the area of a cross section (S_x) and of the external surface (S_{xy}) when an elastic body is strained preserving its volume. It is well known that the cross section of a small tube with edges of relative lengths $x = y = z = 1$ decreases when the tube is subjected to a uniaxial tension, according to the law $S_x = x^{-1}$. It is important to know that the area of the external surface must increase upon deformation according to the law $S_{xy} = x^{0.5} = y^{-1}$. Given the decrease of the cross section the elements of the structure must be displaced toward each other along the direction of stretching and simultaneously move from the periphery to the center. In the surface layer, on the other hand, a displacement of the structure elements from the deeper layers to the surface layers muxt be observed, otherwise upon stretching the required increase of external surface would not be ensured. Naturally even according to geometric considerations a uniaxial stretching must be considered as a three-dimensional stretching accompanied by complicated contrary and transversal displacements of the structure elements.

4. In order that a mechanical equilibrium be ensured in the surface layers, the latter must be subjected to a stretching action of the cross sections of the frame [12], which cannot lead to an increase of the deformation of the surface layers at the expense of the local motion of the material from the surface layers to the internal layers. Naturally, in the surface layers the opposite must take place – a counter motion which ensures an increased degree of deformation of the surface layers of the stretched polymer. These considerations apply to the same extent to the internal separation surfaces which are formed for instance when the polymer contains coarse particles of a filler. The ideas in question provide new possibilities for the interpretation of the mechanism of formation and development of the separation surfaces upon mechanical deformations of polymer substances.

5. When the tension is high, the initial contraction stage is characterized by a sharp drop of the tension (Fig. 1 A), which can be explained in terms of an elastic contraction of the frame with conservation of the number of sections [12, 13]. In this "elastic" state the structure of the stretched plastic is characterized by a great stability. For instance, for the multiple alternation of small contractions and expansions which exists after a small contraction of a strongly stretched sample, plastics with a basis of natural (NK), isoprene, sodium-butadiene (SKB), divinylstyrol (BSK), polychloroprene caoutchouc, and butyl caoutchouc retain almost completely their elastic properties (E_β = const.), and plastics with a basis of divinylnitrile and divinylstyrol "carboxylate" caoutchouc

change insignificantly their elastic properties. For a complete contraction a "structure" hysteresis is observed (in Fig. 1 it is indicated by the shaded area), and for a repeated expansion of the polymer a thixotropic softening (Fig. 1 B) takes place, which reflects a significant change in structure. It is essential to note that this change ("fixation") of the structure at room temperature takes place only in the stage of complete contraction of a significantly stretched plastic, and is not observed for a partial contraction of a stretched plastic (Fig. 1 A). It is well known that during the stretching of polymers orientation processes are observed which are due to a change of the structure of the elastic network; the orientation effects spread completely when the polymer undergoes a contraction at a temperature above the vitrification temperature. In our works we established that, together with the restoration of the structure during the contraction process, a further irreversible change of the structure takes place. If the plastic is kept in a stretched state at room temperature, an important increase of the residual deformation is produced, but the value of the hysteresis and of thixotropic structure changes is not affected. Naturally, the residual expansions must be related to displacements of the elements of the elastic network in the stretched samples, whereas "the structure effects" – hysteresis, thixotropic changes, etc. . . – must be determined by changes of the elastic network that take place during the contraction stage. For a high temperature (above 100-120°C) the structure effects determined by changes taking place in the contraction stage practically do not appear when the plastic is deformed.

6. It has been established experimentally* that thixotropic structure changes are always irreversible, if the tension (f) exceeds a critical value (f_k). For the most stable nonloaded plastics of NK, f_k = 20-50 kg · cm^{-2}. "Carbon black" NK plastics are also characterized by a great stability of their mechanical properties; on the contrary, plastics with mineral fillers are characterized by very important irreversible thixotropic changes. In Fig. 2. the irreversible thixotropic changes are evaluated from the value of the highest relative decrease of the conventional moduli $\mu_N = f : f_0$ [14]. The "reversible" part of the thixotropic changes was distributed by heating the samples in glycerin at a temperature of 100-120°C.

7. The nature of structure hysteresis for significant deformations can be interpreted as a consequence of the elastic contraction of the frame sections, and as the impossibility of a spontaneous displacement of these sections. The nature of structure hysteresis must be general for all the polymers in an elastic state, and, therefore, the linear dependence of hysteresis losses (Γ) upon the stretching work (A), already established in 1931. in a study of NK plastics [15], becomes understandable. G. A. Patrikeev and V. M.Fedorov proposed an empirical equation, $\Gamma = k \cdot (A - e)$ kg · cm · cm^{-3} or $\eta = \Gamma : A = k \cdot (1 - e \cdot A^{-1})$, which is valid for $A \geq$ 50-70 kg · cm · · cm^{-3}, where $\underline{k}$ and $\underline{e}$ are constants determined graphically (see Fig. 3). These authors proposed this formula on the basis of the above mentioned [15] and on their own data. In a first approximation the value of the structure hysteresis for significant stretchings, unlike the hysteresis losses for small deformation, depends little upon the type of caoutchouc, the type and the contents of filler, and the degree of vulcanization (for $A \geq 200$ kg · cm · cm^{-3}, $\eta = 0.60 - 0.85$).

8. When the flexible network is eliminated, the action of the external force field must be immediately balanced by the deformed elastic network. Therefore, after the completion of the elastic contraction of the frame, the nature of the stretched state and the molecular contraction mechanism must change in a radical way. It is well known that at this stage of deformation the elasticity modulus becomes less than the "conventional equilibrium" modulus. This can be explained by the counteracting deformation of the elastic network, which is shown by the "weakened" sections of the frame. Therefore a complete contraction must be expected to cause not only a displacement of the elastic network with respect to the frame sections, but also internal tensions.

9. The molecular deformation mechanism of the elastic network in the expansion stage cannot be explained on the basis of the ideas developed [12]. When a plastic is stretched one can expect the appearance of a "hard" displacement of the microvolumes formed by interpenetrating and overlapping frame sections. Subsequently, the microvolumes of the elastic network subjected to a rigid displacement may be deformed according to the molecular "segment" mechanism. The boundary layers between microvolumes rigidly displaced must be deformed very much, although in the absence of mechanical fractures a "healing" effect must take place due to the intermolecular interaction, and therefore, no formation of separation surfaces should be expected.

10. The method of great stretchings is widely used in order to evaluate the mechanical properties of polymer substances. This form of testing may be used as an indirect method for investigating the structure of

*Together with E. A. Abramova and T. S. Dvorkina.

polymer substances, the molecular mechanism of polymer deformation, and the mechanical properties of polymer molecules. Therefore, it is necessary to realize an equipment for mechanical testing of polymers and to continue the elaboration of macromolecular mechanics. An experimental proof of the formation of an elastic network upon deformation of polymers would also be of great interest.

LITERATURE CITED

1. W. Kuhn, Koll. Z. 68, 2 (1934); 76, 258 (1936); E. Gut, G. James, and G. Mark, Chemistry of Large Molecules, Collection 1 [Russian translation] (IL, Moscow-Leningrad, 1948) p. 42.
2. Ya. I. Frenkel', Kinetic Theory of Liquids [in Russian] (Izd. AN SSSR, 1945).
3. P. P. Kobeko, Amorphous Substances [in Russian] (Izd. AN SSSR, 1952); L. Treloar, Physics of the Elasticity of Caoutchouc [Russian translation] (IL, Moscow-Leningrad, 1953); M. M. Reznikovskii, Khim. Nauka i Prom. 4, 1, 79 (1959).
4. M. V. Vol'kenshtein, Configuration Statistics of Polymer Chains [in Russian] (Izd. AN SSSR, 1959).
5. P. P. Kobeko, E. V. Kuvshinskii, G. I. Gurevich, Izv. Akad. Nauk SSSR, Ser. Fiz. 6,3, 329 (1937); A. P. Aleksandrov, Yu. S. Lazurkin, Zhur. Tekhn. Fiz. 9, 1249 (1939); G. Gurevich, P. P. Kobeko, Zhur. Tekhn. Fiz. 9, 1267 (1939).
6. A. P. Aleksandrov, Transactions of the I and II Conferences on High Molecular Weight Compounds [in Russian] (Izd. AN SSSR, 1945) pp. 7, 49; Yu. S. Lazurkin, R. L. Fogel'son, Zhur. Tekhn. Fiz. 21, 257 (1951).
7. V. A. Kargin, Transactions of the I and II Conferences on High Molecular Weight Compounds [in Russian] (Izd. AN SSSR, 1945) pp. 10, 60; V. A. Kargin, D. I. Leipunskaya, Zhur. Fiz. Khim. 15, 1011, (1941); V. A. Kargin, G. L. Slonimskii, Zhur. Fiz. Khim. 15, 1022 (1941).
8. A. Tobolsky, R. Powell, and G. Eyring, Chemistry of Large Molecules [Russian translation] Coll. 2 (IL, Moscow-Leningrad, 1948) p. 206.
9. V. A. Kargin, T. I. Sogolova, G. L. Slonimskii, and E. V. Reztsova, Zhur. Fiz. Khim. 30, 1903 (1956).
10. G. L. Slonimskii, Khim. Nauka i Prom. 4, 73 (1959).
11. G. A. Patrikeev, Doklady Akad. Nauk SSSR 120, 2, 339 (1958).*
12. G. A. Patrikeev, Doklady Akad. Nauk SSSR 120, 3, 562 (1958).*
13. G. A. Patrikeev, Zhur. Fiz. Khim. 33, 9, 2081 (1959).
14. G. A. Patrikeev, Coll.: Aging and Fatigue of Caoutchoucs and Plastics and Increase of their Durability [in Russian] (Leningrad, 1956) p. 65.
15. H. Barron and F. Cotton, Trans. Ind. Rubber J. 7, 209 (1931).

* Original Russian pagination. See C. B. translation.

EQUILIBRIUM POTENTIALS OF ZIRCONIUM IN MIXED FLUORIDE – CHLORIDE MELTS

M. V. Smirnov, V. E. Komarov, and A. N. Baraboshkin

Institute of Electrochemistry, Ural Branch of the Academy of Sciences, USSR
(Presented by Academician A. N. Frumkin, January 28, 1960).
Translated from Doklady Akademii Nauk SSSR, Vol. 133, No. 2, pp. 409-412, July, 1960
Original article submitted January 28, 1960

In previous work in our laboratory [1-3] and also that of other authors [4], the temperature and concentration dependences of the potentials were established for a series of metals in molten mixtures of their chlorides and alkali metal chlorides. However, there is no information in the literature on such measurements in mixed fluoride–chloride melts despite the fact that their results would be of undoubted interest in the electrolysis of K_2TiF_6, K_2ZrF_6, ThF_4, KUF_5, and K_2TaF_7, for example, in molten alkali metal chlorides.

A quantitative relation between the equilibrium potentials and the composition of mixed fluoride–chloride melts could also give very valuable experimental material on complex formation in molten salt media. As already reported in a series of our papers [5-8], the introduction of fluorine ions into chloride melts considerably displaces the potentials of cathode liberation and anode solution of beryllium, titanium, and thorium toward more negative values. This indicates that in mixed fluoride–chloride melts, cations of such metals give stable complex ions with fluorine anions.

In the present communication we present the main results of measurements of the equilibrium potentials of zirconium at 700-950° in an equimolar mixture of sodium and potassium chlorides with the addition of various amounts of fluorides.

Salt mixtures of NaCl + KCl + NaF of definite composition were prepared by fusing chemically pure salts. Zirconium was introduced into the salt melts by anode solution of iodide-refined metal directly into the cell, whose construction is illustrated schematically in Fig. 1. The concentration of zirconium passing into the melt was checked by chemical analysis of the electrolyte in the crucible after the experiment. The gas space in the tube above the melt was filled with argon, freed from traces of moisture, oxygen, and nitrogen. The cell was heated in an electric resistance furnace with automatic regulation of the temperature, which could be maintained at a given value with an accuracy of ±1.5°. The potential of the zirconium electrode was measured relative to a chlorine reference electrode with a high-resistance potentiometer. An emf value which remained constant within the limits of ±1 mv for not less than 30 min under given conditions was considered to be reliable.

Measurements were carried out with melts which contained from 0.17 to 1.05 weight % of Zr and up to 15.82 weight % of F. In this case the ratio of mole fractions of fluorine and zirconium [F]/[Zr] varied from 9 to 75.

The experiments showed that the potential of zirconium depends not only on its concentration in the electrolyte, but also on the fluorine concentration, and to a greater extent on the latter. This dependence follows from the conditions of thermodynamic equilibrium between the metal and the salt melt when fluoride complexes are formed in it:

$$Zr - ne \rightleftharpoons Zr^{n+} \text{ (melt)},$$

$$Zr^{n+} \text{ (melt)} + mF^- \text{ (melt)} \rightleftharpoons ZrF_m^{(m-n)-} \text{ (melt)}.$$

Here m is the mean number of fluorine ions bound in the complex with the zirconium cation and n is the mean valence of the latter in a melt of the given composition.

The first electrode reaction leads to an expression for the equilibrium potential

$$E = E^0_{Zr/Zr^{n+}} + \frac{RT}{nF} \ln [Zr^{n+}],$$

where $[Zr^{n+}]$ is the mole fraction of zirconium cations that are not bound in complex ions. If the instability constant of the latter, expressed in mole fractions of the corresponding ions in the electrolyte, is given by

$$K = [Zr^{n+}][F^-]^m / [ZrF^{(m-n)-}],$$

then the equilibrium potential of the zirconium electrode

$$E = E^0_{Zr/Zr^{n+}} + \frac{RT}{nF} \ln K + \frac{RT}{nF} \ln [ZrF_m^{(m-n)-}] - \frac{m}{n} \frac{RT}{F} \ln [F^-].$$

Where the temperature and zirconium concentration in the melt are constant, considering that practically the whole of the zirconium is in the form of complex ions, we obtain an expression for the relation between the potential and the concentration of free fluorine ions

$$E = \text{const} - 1.984 \cdot 10^{-4} T \log [F^-].$$

In order to check this equation, we measured the zirconium potential in melts with different fluorine concentrations (from 2.04 to 15.82 weight %) at 770° and a zirconium concentration of 1.05±0.2 weight %. In order to compare the results of these experiments with the equation derived, it was necessary to know the mean number of fluorine ions bound in the complex with a zirconium cation. Knowing this, it is possible to calculate the mole fraction of free fluorine ions from the total fluorine content. Only in pure fluoride melts do we have m = 6. In mixtures of them with alkali metal chlorides m < 6 because with a decrease in the ratio of the mole fractions [F]/[Zr] when [Zr] = const, the fluorine in the complex ions is gradually replaced by chlorine:

$$ZrF_6^{(6-n)-} \rightarrow ZrClF_5^{(6-n)-} \rightarrow ZrCl_2F_4^{(6-n)-} \rightarrow \ldots$$

In this case the coordination number remains equal to 6 for tetra- and trivalent zirconium cations.

If the measured potentials are plotted on a graph against the logarithms of the mole fractions of free fluorine ions, calculated with the assumption that m = 6, 5, and 4, straight lines are obtained as is shown in Fig. 2, where graphs are constructed for the case when m = 6. The experimental points fall quite satisfactorily on lines described by the empirical equations:

$$E = -3.055 - 0.309 \log [F^-] \text{ when } m = 6,$$
$$E = -3.057 - 0.321 \log [F^-] \text{ when } m = 5,$$
$$E = -3.062 - 0.334 \log [F^-] \text{ when } m = 4.$$

From a comparison of the experimental and theoretical prelogarithmic coefficients it follows that in melts in equilibrium with metallic zirconium, under our experimental conditions the mean valence of its ions equals 4.01 if it is assumed that m = 6, 3.23 if m = 5, and 2.48 if m = 4. Consequently it changes over the range $4 \geq n > 2.5$ when the fluorine concentration falls so that its content in the complex ions falls from 6 to 4. It should be remembered that the mean values of m and n characterize the melt as a whole and not individual ions, which may differ in valence, and complex ions, which may differ in composition. In mixed fluoride–chloride melts with a relatively large excess of fluorine ([F]/[Zr] > 10), that are in contact with the metal, an overwhelming fraction of the zirconium is present as tri- and tetravalent ions, which form part of the anionic complexes $ZrClF_5^{3-}$, ZrF_6^{3-} and ZrF_6^{2-}. With a decrease in the fluorine concentration ([F]/[Zr] < 10), there is gradual displacement of the equilibrium:

$$3\,Zr^{4+} \text{ (melt)} + Zr \rightleftharpoons 4Zr^{3+} \text{ (melt)},$$
$$2\,Zr^{3+} \text{ (melt)} + Zr \rightleftharpoons 3Zr^{2+} \text{ (melt)}$$

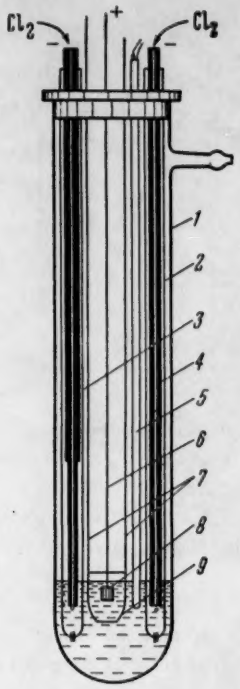

Fig. 1. Measurement cell. 1, 2) Quartz tubes; 3) quartz tube with chlorine reference electrode; 4) auxiliary cathode; 5) thermocouple; 6) molybdenum lead; 7) molybdenum suspension of crucible; 8) zirconium anode; 9) zirconium dioxide crucible.

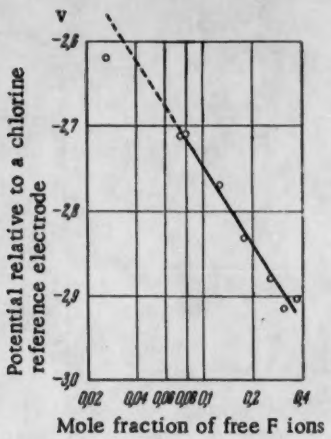

Fig. 2. Change in equilibrium potential of zirconium in relation to the mole fraction of fluorine ions in the melt at t= 770° and a zirconium concentration of 1.05 weight %.

toward the formation of ions of lower valence; appreciable amounts of divalent zirconium appear in the melt.

We also measured the potentials of a zirconium electrode at various temperatures in melts of five compositions. The ratio of the mole fractions of fluorine and zirconium [F]/[Zr] was varied from 45 to 9. The results of these experiments are shown graphically in Fig. 3.

The experimental points fall quite satisfactorily on lines for each of the electrolytes investigated. Empirical equations of these lines were found.

$$E_1 = -3{,}37 + 6{,}39 \cdot 10^{-4} T,$$
$$E_2 = -3{,}50 + 7{,}92 \cdot 10^{-4} T,$$
$$E_3 = -3{,}58 + 9{,}26 \cdot 10^{-4} T,$$
$$E_4 = -3{,}55 + 8{,}95 \cdot 10^{-4} T,$$
$$E_5 = -3{,}51 + 9{,}00 \cdot 10^{-4} T.$$

This linear relation follows from the general expression for the equilibrium potential. It is known [1-3, 9] that $E^0_{Zr/Zr^{n+}} = a + bT$ and $\log K = A - B/T$, where a, b, A, and B are constants that are independent of temperature. By substituting these in the equation for the electrode potential, we obtain

$$E = \left(a - \frac{RB}{nF}\right) + \left(b + \frac{RA}{nF} + \frac{R}{nF} \ln \frac{[ZrF_m^{(m-n)-}]}{[F^-]^m}\right) T,$$

or

$$E = \alpha + \beta T.$$

As can be seen, the constant α is independent of the electrolyte composition. In the equations for melts of various compositions found experimentally, it varied slightly over the range of possible measurement errors:

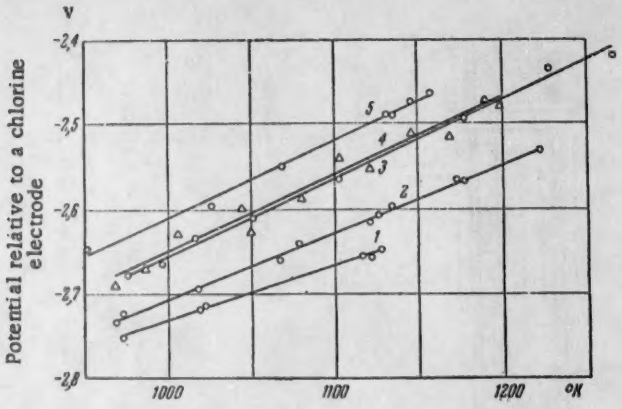

Fig. 3. Temperature dependence of the equilibrium potential of zirconium in melts containing: 1) 0.23 weight % of Zr and 2.16 weight % of F; 2) 0.36 weight % of Zr and 2.08 weight % of F; 3) 1.05 weight % of Zr and 2.04 weight % of F; 4) 0.17 weight % of Zr and 0.75 weight % of F; 5) 0.17 weight % of Zr and 0.64 weight % of F.

$\alpha = -3.50 \pm 0.07$. On the other hand, the coefficient β should vary with composition and increase with an increase in the ratio of mole fractions of zirconium and free fluorine ions, which was actually observed experimentally.

Thus, if it is assumed that mixed fluoride–chloride melts containing up to 10-15 weight % of Zr, like melts with thorium [3], behave as ideal solutions, then to determine the equilibrium potential of zirconium we obtain the equation

$$E = -3{,}50 + 5{,}4 \cdot 10^{-4}T + \frac{1{,}984}{n} \cdot 10^{-4}T \lg \frac{[Zr]}{[F^-]^m},$$

where [Zr] and [F^-] are the mole fractions of zirconium and fluorine ions that are not bound in a complex with it, respectively. In mixed fluoride–chloride electrolytes with a relatively large excess of fluorine ions $75 > [F]/[Zr] > 10$ (in such melts as are used in practice in the electrolysis of fluorozirconate when chlorine is liberated at the anode in an amount equivalent to the zirconium deposited on the cathode and consequently chlorine ions are gradually replaced by fluorine ions), the mean valence of zirconium n and the mean number of fluorine ions in the complex m vary over the range $4 > n > 3$ and $6 > m > 4$. For approximate calculations it is possible to assume that $m = 5$ and $n = 3.2$.

LITERATURE CITED

1. M. V. Smirnov and V. A. Chemezov, Doklady Akad. Nauk SSSR 120, 122 (1958).*
2. M. V. Smirnov, L. E. Ivanovskii, and N. A. Loginov, Doklady Akademii Nauk SSSR 121, 685 (1958).*
3. M. V. Smirnov and L. D. Yushina, Izvest. Akad. Nauk SSSR, Otdelenie Khim. Nauk, 2, 251 (1959).*
4. L. Young and R. G. Hudson, Trans. Met. Soc. AIME 215, 589 (1959).
5. M. V. Smirnov and L. D. Yushina, Izvest. Akad. Nauk SSSR, Otdel. Khim. Nauk, 11, 1285 (1956).
6. M. V. Smirnov and L. E. Ivanovskii, Zhur. Fiz. Khim. 32, 2174 (1958).
7. M. V. Smirnov and N. Ya. Chukreev, Zhur. Fiz. Khim. 31, 2165 (1958).
8. M. V. Smirnov and L. A. Tsiovkina, Izvest. Sibirsk. Otdel. Akad. Nauk SSSR, 9, 17 (1958).
9. M. V. Smirnov and N. Ya. Chukreev, Zhur. Neorg. Khim. 4, 2536 (1959).

*Original Russian pagination. See C. B. translation.

CATALYTIC DECOMPOSITION OF HYDRAZINE ON NICKEL SULFIDE AND ITS SOLID SOLUTIONS

Huang Yu-mei, N. P. Keier, and Corresponding Member
Academy of Sciences, USSR, S. Z. Roginskii

Institute of Physical Chemistry, Academy of Sciences, USSR
Translated from Doklady Akademii Nauk SSSR, Vol. 133, No. 2, pp. 413-416, July, 1960
Original article submitted April 7, 1960

In recent years a series of experimental papers have appeared on the connection between the electronic characteristics of metal oxides and their catalytic [1, 2] and adsorption [3] properties. As yet there has been no experimental work on this relation for metal sulfides.

A number of sulfides, for example, sulfides of Mn, V, W, Fe, Co, and Ni, are used in industry as hydrogenation and dehydrogenation catalysts. Their main advantage is that they are not readily poisoned by sulfur compounds so that they are used in the production of synthetic liquid fuels from sulfur-containing raw material.

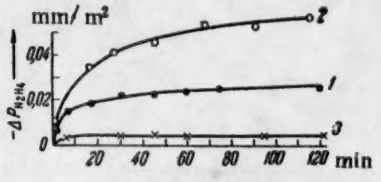

Fig. 1. Kinetic isotherms of N_2H_4 decomposition at 22° C with $P_O N_2H_4$ = 13.0 mm: 1) on NiO; 2) on NiO (1 at.% Li); 3) on NiO (1 at.% In).

As a starting system we chose nickel sulfide, which, due to the similarity between O and S, is analogous chemically to NiO that has been studied thoroughly; however, these compounds differ sharply in electronic properties. According to Hauffe [4], NiS has metallic conductivity in the temperature range from 200 to 700°. The relation between the electronic properties of NiS and its catalytic properties have not been studied previously. In analogy with NiO it seemed interesting to determine whether the addition of sulfides of metals that are not divalent would have an effect in this case. The oxidation of CO with oxygen was not a suitable test reaction for NiS as according to our preliminary data the reaction does not occur right up to 350° and according to literature data the formation of nickel sulfate begins even at 140°. The decomposition of N_2O was unsuitable for the same reason. We chose the decomposition of N_2H_4, which proceeds readily [5] on metals and semiconductors according to the equation

$$3N_2H_4 \rightarrow N_2 + 4NH_3. \quad (1)$$

Our experiments showed (see Fig. 1) that this reaction proceeds at a appreciable rate on nickelous oxide at room temperature and that Li_2O accelerates the reaction while In_2O_3 strongly retards it. The action of the additives differs from that which was observed for the same catalysts in the oxidation of CO at low temperatures.

For the experiments we used chemically pure, doubly distilled hydrazine. The N_2H_4 was freed from traces of dissolved air in a vacuum apparatus by repeated freezing with simultaneous pumping away of the gas liberated. After purification in vacuum, the hydrazine had a vapor pressure corresponding to tabular data. The possible water content did not exceed 0.8%. The nickel sulfide was prepared by passing H_2S over nickel carbonate at 450° C for

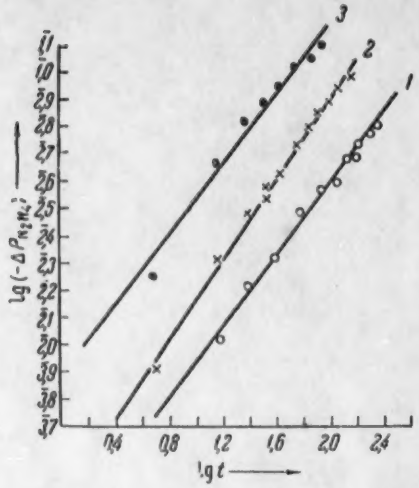

Fig. 2. Kinetic isotherms of N_2H_4 decomposition on NiS: 1) at 60° C; 2) at 75°C; 3) at 100°C.

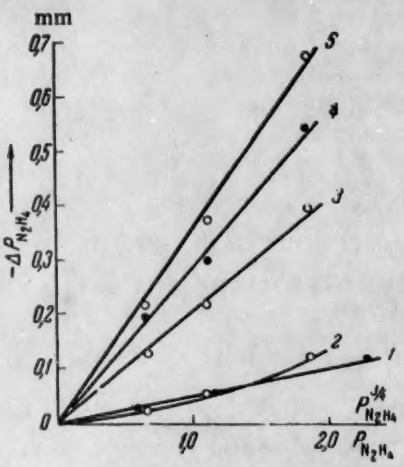

Fig. 3. Relation of the degree of conversion of N_2H_4 to the initial pressure on NiS at 75° C: 1, 2) with t = 5 min; 3) with t = 30 min; 4) with t = 50 min; 5) with t = 70 min.

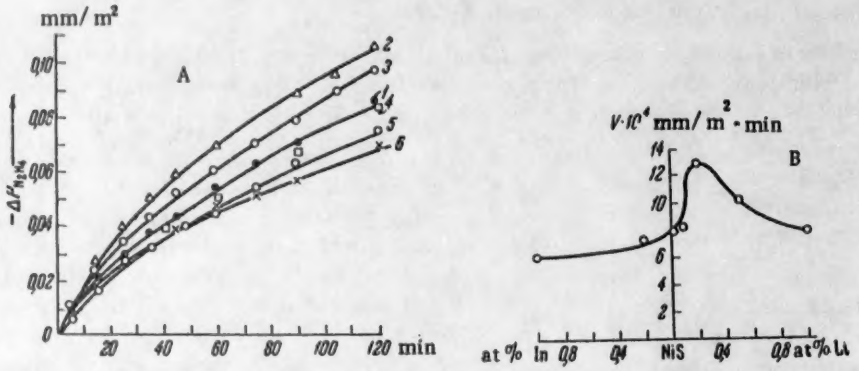

Fig. 4. A) Kinetic isotherms of N_2H_4 decomposition at 75°C. 1) On NiS; 2) on NiS (0.2 at.% Li); 3) on NiS (0.5 at.% Li); 4) on NiS (1 at.% Li); 5) on NiS (0.2 at.% In); 6) on NiS (1 at. % In). B) Relation of N_2H_4 decomposition rate to amounts of additives at 75° C $-\Delta P\ N_2H_4 = 0.03$ mm/ m².

10 hr. The solid solutions were obtained under the same conditions by sulfurization of mixtures of nickel carbonate and lithium carbonate or indium nitrate in definite proportions.

An x-ray analysis carried out by M. Ya. Kushnerev showed that the β-nickel sulfide obtained had the normal hexagonal crystal structure. The lattice parameters of NiS were increased somewhat by the solution of indium sulfide but no regular changes were observed in the parameters when lithium was introduced.

The specific surface was determined by the Brunauer, Emmett, and Teller method from the equilibrium isotherms of the physical adsorption of krypton at liquid nitrogen temperature (−195°C). Solution of lithium sulfide decreased the specific surface from 4.9 m^2/g for NiS to 3.5 m^2/g for NiS (1 at.% Li). The solution of indium sulfide in amounts corresponding to 0.2 and 1 at.% of In produced a variation in the specific surface over a range of ± 10%.

The resistance of tablets pressed from nickel sulfide powder at 4000 atm, measured by means of a dc bridge

circuit, was only 1.2 ohm·cm. Over the temperature range from 78 to 573° K, the resistance increased slightly with an increase in temperature. Thus, nickel sulfide has metallic conductivity over the temperature range studied. Solution of lithium and indium sulfides in amounts corresponding to 1 at.% of foreign atom in the nickel sulfide lattice hardly affected the specific resistance. Measurement of the emf showed that nickel sulfide is an electronic semiconductor.

The decomposition of hydrazine was studied in a vacuum apparatus under static conditions. The catalyst was first heated at 400° C for 1.5 hr.

Oxidation on Pd and passage through a palladium capillary showed that the hydrazine decomposition products did not contain hydrogen and that the decomposition proceeded according to Equation (1) on nickel sulfide. The decomposition kinetics of hydrazine were studied through the volume of nitrogen liberated by decomposition with an initial hydrazine pressure of 1 mm Hg.

As Fig. 2 shows, the kinetic isotherms of hydrazine decomposition on nickel sulfide at 60, 75, and 100°C in the coordinates of log ($-\Delta P_{N_2H_4}$) and log t were linear and obeyed the equation

$$-\Delta P_{N_2H_4} = at^{1/n}, \qquad (2)$$

where $n > 1$. Such kinetic isotherms are characteristics of self-poisoning processes.

Figure 3 shows that with t = 5 min, the decomposition rate increased in proportion to the initial hydrazine pressure to the first power; with t = 30, 50, and 70 min, the rate increased in proportion to $P^{3/4}$. However, the kinetic isotherms of hydrazine decomposition did not obey a first or a simple fractional power law. Investigation of the temperature dependence of hydrazine decomposition showed that over the temperature range from 60 to 150° C the decomposition rate increased with an increase in temperature, while above 150° C there was a fall in the hydrazine decomposition rate. The observed decomposition kinetics and the presence of a rate maximum with respect to temperature may be the results of poisoning by the reaction products. Poisoning by nitrogen is very improbable so that only ammonia remains.

To check this hypothesis we carried out an experiment in which a catalyst that had been heated at 100° C for 15 min was put in contact with ammonia at a pressure of about 1 mm Hg. This reduced the initial hydrazine decomposition rate by a factor of two. The kinetic curve for decomposition on ammonia-poisoned NiS corresponded to a first order reaction.

To determine the nature of the effect of adding Li_2S and In_2S_3 to NiS on hydrazine decomposition, we investigated solid solutions of nickel sulfide containing 0.2, 0.5, and 1 at.% of Li, calculated on the total metal atoms, and nickel sulfide solid solutions containing 0.2 and 1 at.% of In. The investigation showed that the introduction of lithium and indium into nickel sulfide samples did not change the direction or the kinetic equation of hydrazine decomposition.

Figure 4 A gives kinetic isotherms for decomposition at 75° C on nickel sulfide and its solid solutions. This figure shows that the solution of lithium sulfide in amounts corresponding to 0.2 and 0.5 at.% of lithium slightly increased the N_2H_4 decomposition rate; with a further increase in the content up to 1 at.% of Li, the decomposition rate became slightly less than on the original nickel sulfide. With the solution of 0.2 at.% of indium sulfide, the initial decomposition rate was unchanged, but at high degrees of decomposition it was found to be lower than on the original sample of NiS. An increase in the indium content to 1 at.% had a similar action, but to a greater extent than 0.2 at.% of In.

The relation of the N_2H_4 decomposition rate to the lithium and indium contents is shown in Fig. 4B. At a lithium content of about 0.2 at.%, the decomposition rate was maximal. The relation between the work function and the amounts of Li and In added, measured by É. Kh. Enikeev on the same samples, also had a maximum at 0.2 at.% of Li. The form of the relation of the work function to the amount of additive was analogous to the dependence of the hydrazine decomposition rate given in Fig. 4B.

The relation between the N_2H_4 decomposition rate and temperature did not obey the Arrhenius equation, which makes it difficult to determine the effect of Li and In on the activation energy of decomposition.

DISCUSSION OF RESULTS

In the work presented, a comparison was made of the effect of introducing analogous additives including cations differing in charge from the cations of the main compound and the catalytic activity of nickelous oxide and sulfide. In the first case Li_2O and In_2O_3 were introduced into the catalyst and in the second, Li_2S and In_2S_3. Both on NiO and on NiS (pure and with additives) the decomposition proceeded in a direction characteristic of metals and semiconductors with the formation of N_2 and NH_3. The reaction on NiS was retarded by the ammonia formed and had an optimal rate at t~ 150° C. The action of lithium and indium on catalytic activity was considerably stronger for nickelous oxide than for nickel sulfide and was similar in magnitude on the effect of these oxides on the oxidation of CO, though the directions of the change in activity under the action of Li^+ and In^{+3} were opposite for N_2H_4 decomposition and CO oxidation. The different sensitivities of NiO and NiS to analogous additives may be connected with the different nature of their electrical conductivities, i.e., extrinsic semiconductor for NiO and quasi-metallic for NiS. It is possible that in other cases also the sensitivity of degenerate semiconductors and semimetals to impurities which create electronic disorder is lower than for extrinsic semiconductors. In this respect there is a certain correlation with the sharp effect of Me^+ and Me^{3+} on the electrical conductivity of the extrinsic semiconductor NiO and with the extremely low sensitivity of the electrical conductivity of NiS to the same additives.

Figure 4 shows a slight maximum in the activity for N_2H_4 decomposition on NiS at an Li content of ~0.2 at.%. The difference of this preparation from the others is confirmed by their unusual work functions but as the properties of repeat preparations of the same composition were not studied, it is not certain that the high values of the activity and the low values of the work function were not caused by some chance properties of this preparation. Both pure nickel sulfide and nickel sulfide with Li_2S and In_2S_3 added have a high electrical conductivity in the range from 78° K to 700° K; the temperature dependence of the electrical conductivity has a metallic character. The investigation of N_2H_4 decomposition kinetics showed that ammonia formed during the decomposition has a strong retarding action on the reaction.

LITERATURE CITED

1. Problems in Kinetics and Catalysis [in Russian] 8 (Izd. AN SSSR, 1955); Adv. Cat. 7 (1955); S. Z. Roginskii, Khim. Nauk. i Prom. 2, 138 (1957).
2. N. P. Keier, S. Z. Roginskii, and I. S. Sazonova, Doklady Akad. Nauk SSSR 106, 859 (1956);* Izvest. Akad. Nauk SSSR, Ser. Fiz. 21, 183 (1957); G. M. Schwab and I. Block, Z. Phys. Chem. (N.F.) 1, 92 (1955); É. Kh. Enikeev, L. Ya. Margolis, and S. Z. Roginskii, Doklady Akad. Nauk SSSR 130, 807 (1960).*
3. N. P. Keier and G. I. Chuzhikova, Doklady Akad. Nauk SSSR 120, 4 (1958);** N. P. Keier and L. N. Kutseva, Izvest. Akad. Nauk SSSR, Otdel. Khim. Nauk, 5, 797 (1959).*
4. K. Hauffe and H. G. Flindt, Z. Phys. Chem. 200, 199 (1952).
5. O. V. Krylov, Doklady Akad. Nauk SSSR 130, 1063 (1960).*

* Original Russian pagination. See C. B. translation.

** See C. B. translation.

EFFECT OF ADSORPTION OF ANIONS ON THE DISCHARGE OF HYDROGEN ON PALLADIUM AND THE IONIZATION OF HYDROGEN DISSOLVED IN PALLADIUM

L. T. Shanina

M. V. Lomonosov Moscow State University
(Presented by Academician A. N. Frumkin, March 9, 1960)
Translated from Doklady Akademii Nauk SSSR, Vol. 133, No. 2, pp. 417-419, July, 1960
Original article submitted March 7, 1960

The adsorption of halogen ions, especially Br^- and I^-, retards the ionization of molecular hydrogen on a Pt-electrode [1]. The adsorption of these ions also affects the ionization rate of hydrogen adsorbed on platinum, though to a slightly lesser extent [2, 3]. Cl^- anions slightly reduce the overvoltage of this reaction, while Br^- anions reduce or increase it, depending on the contact time. The iodine ion sharply retards exchange between adsorbed hydrogen and hydrogen ions.

In the present work, anode charging curves and polarization measurements on a palladized electrode were used to study the effect of the adsorption of Cl^-, Br^-, and I^- anions on the ionization of hydrogen dissolved in palladium. This process has been studied previously [4, 5], but the effect of the adsorption of anions on it has not been considered in the literature up to now.

The procedure and apparatus analogous to those described previously [6, 7] were used for the measurements. The electrode was a platinum plate with an area of 1 cm^2 on which a definite amount of palladium was deposited electrolytically and the electrolysis conditions were chosen so as to obtain electrodes with a certain standard activity. The temperature was kept at $20 \pm 1°$.

Measurements were made in HCl, HBr, KI + 1 N H_2SO_4, and KI + 1 N NaOH. The charging curves plotted in HCl (0.1 N, 0.5 N, and 2 N) (polarization current density $5 \cdot 10^{-4}$ a/cm^2, amount of palladium black on electrode 0.0053 g) hardly differed from the charging curves plotted in 1 N H_2SO_4 under the same conditions and were close to equilibrium.*

In the presence of Br^- there was slight disruption of the reversibility of the process, which was more strongly expressed the higher the anion concentration and the longer the electrode was in contact with the electrolyte containing Br^-. On such electrodes under cathode polarization, the evolution of gaseous hydrogen began before the electrode was saturated with hydrogen. With a change from Br^- to I^- the deviation from reversibility became even greater. Curves of the relation of the potential to the amount of electricity passed, plotted in KI + 1 N H_2SO_4 solutions, are presented in Fig. 1. Curve 2, which was plotted in 0.01 N KI, still retained a form close to that of the curve in 1 N H_2SO_4, though the overvoltage of the ionization of hydrogen dissolved in the β-phase was considerably higher, the plateau corresponding to the phase transition was deformed, and the width of the hysteresis loop reached 60-70 mv. Curves 3 and 4, which were plotted in 0.1 N and 1 N KI, had a form which differed com-

* In the region of the $\beta \rightleftharpoons \alpha$ transition, in the Pd–H system there are always slight deviations from equilibrium which lead to the appearance of a hysteresis loop when charging curves are plotted in forward and backward directions. This phenomenon is also observed in 1 N H_2SO_4 (see Fig. 1).

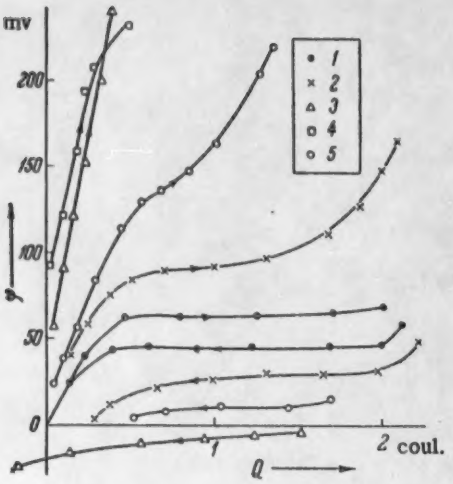

Fig. 1. Curves of the relation of the palladium electrode potential to the amount of electricity passed. 1) 1 N H_2SO_4; 2) 0.01 N KI + 1 N H_2SO_4; 3) 0.1 N KI + 1 N H_2SO_4; 4) 1 N KI + + 1 N H_2SO_4; 5) 0.01 N KI + 1 N H_2SO_4 after the electrode had remained in the solution for 18 hr.

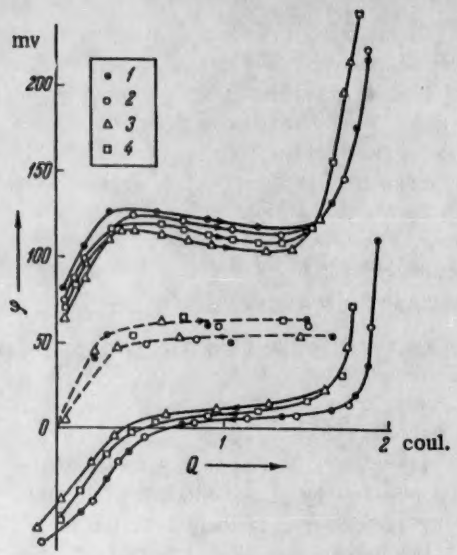

Fig. 2. Charging curves in 1 N NaOH in the presence of KI (forward and backward plots). Polarization current density $I = 5 \cdot 10^{-4}$ a/cm^2. The broken lines show potential values measured after the current had been switched off. 1) 1 N NaOH; 2) 1 N NaOH + $5 \cdot 10^{-3}$ N KI; 3) 1 N NaOH + + $5 \cdot 10^{-2}$ N KI; 4) 1 N NaOH + $5 \cdot 10^{-1}$ N KI.

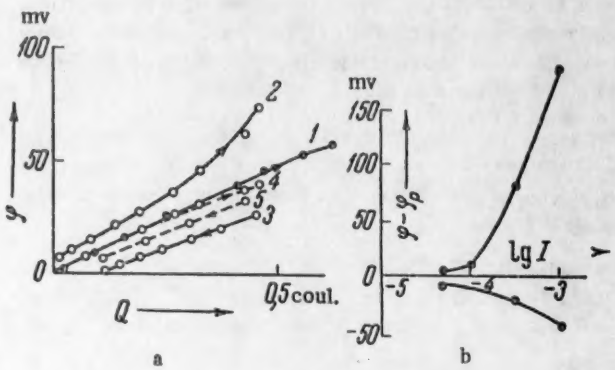

Fig. 3. a) Curves of the relation of the potential to the amount of electricity passed in the region of the β-phase (forward (2) and backward (3) plots) plotted in $5 \cdot 10^{-3}$ KI + 1 N H_2SO_4 at a current density of $I = 5.5 \cdot 10^{-5}$ a/cm^2 and the potential values measured with the current switched off (4 and 5). 1) 1 N H_2SO_4; $I = 5 \cdot 10^{-4}$ a/cm^2. b) Curves of the relation of the overvoltage to the logarithm of the current density.

pletely from the curve in 1 N H_2SO_4. The overvoltage of the beginning of ionization of the dissolved hydrogen was increased by 50-90 mv; the plateau corresponding to the phase transition disappeared and the width of the hysteresis loop increased to 350 mv. It was not possible to plot curves in 0.1 N KI and 1 N KI up to anode potentials higher than 200-300 mv as solution of the palladium began. An increase in the time that the electrode remained in a solution containing KI before the beginning of measurements led to strong deformation of the charging curve (curves 2 and 5, Fig. 1).

On the basis of the data obtained on the effect of the adsorption of KI on the form of the charging curves, it may be considered that the amount of hydrogen dissolved in Pd decreases when I^- is introduced into the solution. In order to check this hypothesis we studied the displacement of the electrode potential due to the adsorption of I^-. When a solution of KI was introduced into the system, the electrode potential, equal to the potential at the beginning of the phase transition (60-70 mv), was displaced in a cathodic direction by 10-15 mv, but rapidly returned to the initial value. Had the amount of hydrogen dissolved in Pd decreased, due to the adsorption of I^-, the observed potential displacement would have been stable. Since this did not occur, the total amount of hydrogen dissolved in the Pd apparently remained constant. The slight displacement of the potential in a cathodic direction was connected with the adsorption of iodine ions; as a result of restoration of the equilibrium between hydrogen in the Pd and hydrogen ions in the solution, the original value of the potential was restored.

We also determined the relation of the potential of a palladized electrode to the amount of electricity passed in 0.005 N KI + N H_2SO_4 with various polarizing current densities for hydrogen-saturated β-phases. Figure 3, a shows curves plotted with anode polarization and with cathode polarization following anode polarization and also gives the values of the potentials after the current had been switched off. As Figure 3 shows, the forward and backward sections of the polarization curves do not coincide, and also curves of the relation between the potential values measured with the current switched off and the amount of hydrogen in the palladium after cathode and anode polarization do not coincide, while in this case complete coincidence was observed in 1 N H_2SO_4. The relation of the magnitude of the deviation of the potential of a palladized electrode from the equilibrium potential of the β-phase of the same composition to log I is linear and has a proportionality coefficient of 180 mv (Fig. 3, b).

Measurements in alkaline solutions with KI added at various concentrations showed (Fig. 2) that the effect of I^- on the ionization of dissolved hydrogen on palladium is very small. The slight effect observed had the opposite sign.

The relation of the overvoltage in the β-phase region to log i at sufficiently high current densities in alkaline solutions was linear with a proportionality coefficient of 0.09-0.1 v. The same relation in the phase-transition region was also linear.

The small magnitude of the effects produced by I^- in alkaline solutions is apparently connected with the fact that the displacement of the electrode potential in a negative direction with a change from acid to alkaline solutions leads to a sharp decrease in the adsorption energy of I^-. The action of the relatively weakly adsorbed I^- ions is determined not by their effect on the energy of the bond of adsorbed hydrogen with palladium, but, as in the adsorption of I^- on mercury, by the change in the structure of the double layer. The slight reduction in the overvoltage in alkaline solutions in the presence of I^- may be explained by facilitation of the orientation of dipolar water molecules with the positive (i.e. hydrogen) end toward the electrode, which promotes their discharge.

We are very grateful to Academician A. N. Frumkin for suggesting the subject and taking interest in the work.

LITERATURE CITED

1. A. N. Frumkin and É. A. Aikazyan, Doklady Akad. Nauk SSSR 100, 315 (1955); Izvest. Akad. Nauk SSSR, Otdel. Khim. Nauk, 202 (1959).*
2. P. I. Dolin and B. V. Érshler, Zhur. Fiz. Khim. 14, 886 (1940).
3. G. P. Birintseva and B. N. Kabanov, Zhur. Fiz. Khim. 33, 844 (1959).
4. A. M. Frumkin and N. A. Aladzhalova, Zhur. Fiz. Khim. 18, 499 (1944).
5. A. I. Fedorova, Zhur. Fiz. Khim. 27, 517 (1953).
6. A. N. Frumkin and A. I. Shlygin, Doklady Akad. Nauk SSSR 2, 176 (1934).
7. A. I. Fedorova, Zhur. Fiz. Khim. 24, 248 (1953).

*Original Russian pagination. See C. B. translation.

THE LUMINESCENCE SPECTRA OF HALOANTHRAQUINONES FROZEN IN SOLUTION

D. N. Shigorin, N. A. Shcheglova, and N. S. Dokunikhin

L. Ya. Karpov Physicochemical Institute

(Presented by Academician A. N. Terenin, February 11, 1960)
Translated from Doklady Akademii Nauk SSSR, Vol. 133, No. 2, pp. 420-423, July, 1960
Original article submitted January 10, 1960

The present work is devoted to the investigation of the structure and interactions between the atoms and radicals in excited molecules by means of their luminescence spectra. We have already shown [1] that such problems may be successfully attacked by using the frozen solution technique (developed by É. V. Shpol'skii [2]) which makes it possible to obtain the vibrational fine structure in the electronic-vibrational spectra.

We investigated the luminescence spectra of α- and β-halo derivatives (F, Cl, Br, and I) of anthraquinone, dissolved in n-paraffins at 77° K ($C = 10^{-4}-10^{-5}$ moles/liter, photoexcitation by $\lambda_{Hg} = 313$ mμ). Considering the structural features of α- and β-haloanthraquinones one would expect the spectra to be substantially different. When an α-hydrogen is replaced by a halogen the two carbonyl groups cease to be equivalent, since in the α-haloanthraquinones one of the carbonyl groups will interact much more extensively with the halogen, which is separated from it by just one carbon atom. This interaction is not serious in the case of β-derivatives, hence their carbonyl groups are practically equivalent. One also must consider the specific effects of each halogen on the spectra of α- and β-substituted anthraquinones. The electronegativity is known to decrease in a regular manner from fluorine (E = 4) to iodine (E = 2.4). The electronegativity of iodine is close to that of carbon (E = = 2.5). Consequently the probability of π-interaction between the free electron pair on halogen and the carbonyl should increase from fluorine to iodine; this is confirmed by the order in which the excitation energy increases.

Thus, the strong inductive effect of the fluorine slightly deforms the π-electron density on the adjacent carbon atoms, the result being equivalent to a slight shortening in the conjugated system. Therefore, the introduction of fluorine should shift the bands toward shorter wavelengths. The main effects of Cl, Br, and particularly I, would involve the participation of their free electron pairs in the molecular π-system; this would lengthen the conjugated chain and consequently shift the bands toward longer wavelengths. The above-mentioned differences between the effects of various halogens should be particularly pronounced in the excited state of the molecule.

When the halogens differ greatly in size their effects on the luminescence spectra of α-haloanthraquinones may also be different. Whereas F being small ($R_b = 1.35$ A) can not lead to any steric interaction with the C=O group, a Cl and particularly Br and I ($R_b = 2.15$ A) can have such steric effects. Repulsive forces arising between the halogens (Cl, Br, and especially I) with large atomic radii and the oxygen in the C=O group will distort the bond angles in >C=O and >C−Hal and somewhat alter the electronic states of these groups. This indeed is the case in such molecules. One would also expect the type and the position of the halogen in the anthraquinone ring to have a strong influence on the intensity and kind of change produced in the molecular electronic-vibrational spectra.

Our experimentally determined luminescence spectra of haloanthraquinones confirmed the assumptions

TABLE 1

The Location (ν in cm^{-1}) of the Components of the Main Maxima in the Spectra of Monohaloanthraquinones Dissolved in Heptane, T = 77° K (ISP-67).

Max. No.	Comp. No.	α-F-anthraquinone	β-F-anthraquinone	Anthraquinone	β-Cl-anthraquinone	β-Br-anthraquinone	β-I-anthraquinone
Initial band	1	—	22064 сл.	22075 сл.	—	21804 оч. н.	21730 оч. н.
	2	—	21991 ср.	21963 сл.	21809 оч. сл.	21732 оч. н.	21659 оч. н.
	3	—	21893 сл.	21826 сл.	21746 сл.	21648 ср.	—
1	1	20915 ср.	20413 оч. сл.	20296 сл.	20188 ср.	20131 н.	20053 н.
	2	20797 н.	20317 н.	20198 н.	20131 н.	20050 н.	19982 н.
	3	20598 ср.	20206 н.	20082 н.	20059 н.	19970 сл.	—
2	1	19257 сл.	18759 оч. сл.	18611 сл.	18523 ср.	18466 ср.	18390 н.
	2	19132 н.	18667 н.	18538 н.	18469 ср.	18396 ср.	18319 н.
	3	18929 н.	18561 н.	18419 н.	18402 ср.	18305 сл.	—
3	1	17598 сл.	17076 оч. сл.	16962 сл.	16886 ср.	16822 ср.	16744 ср.
	2	17458 н.	17010 ср.	16887 н.	16823 ср.	16747 ср.	16670 ср.
	3	17269 н.	16912 ср.	16771 оч. н.	16752 ср.	16663 сл.	—

Note: сл. = weak, ср. = average, оч. сл. = very weak, н. = strong, оч. н. = very strong.

made above. We obtained the vibrational fine structure of all the α- and β-monohaloderivatives.

The corresponding components of the electronic-vibrational bands in the spectra of these and other anthraquinone derivatives with fine structure are set apart from each other by about 1665 cm^{-1} on the average, this distance being characteristic for the C=O bond vibration in the electronic ground state. However, the spectra of α-chloro-, α-bromo-, and α-iodoanthraquinone had fewer lines and a continuous background in the long-wave region of the spectrum (Table 1, Fig. 1). The spectra of these α-haloanthraquinones are all very similar and in many respects resemble those of anthraquinone itself.

The spectrum of α-fluoroanthraquinone is very different from the spectra of other α-haloanthraquinones. The bands become more diffused when octane (the solvent) is replaced by hexane, whereas just the reverse effect is observed in the case of anthraquinone and the other α-haloderivatives. In octane solution the strongest components of the major peaks show a doublet splitting. In contrast with the spectra of other α-monohaloderivatives the spectrum of α-fluoroanthraquinone shows a considerable shift toward shorter wavelengths; the major peaks are shifted by as much as $\Delta\nu$ = 480-630 cm^{-1} from the corresponding maxima in the spectrum of anthraquinone.

We later discovered that certain weak maxima characteristic of anthraquinone are completely absent in the spectrum of the 1,5-difluoroderivative.

On the other hand no vibrational fine structure could be detected in the spectra of 1,5-dichloro-, 1,5-dibromo- and 1,5-diiododerivatives. The spectra of these compounds begin to resemble the continuum region in the spectra of α-Cl-, α-Br-, and α-I-derivatives of anthraquinone. These facts can be explained by assuming that in α-monohaloanthraquinones we are dealing with two distinct $n \rightarrow \pi^*$ electronic transitions due to the presence of two nonequivalent carbonyl groups. The transition probability (intensity) depends to a large extent on the state of these C=O groups. In the case of the α-Cl-, α-Br-, and α-I-monoderivatives of anthraquinone the spectrum with a vibrational fine structure (the one closely resembling the spectrum of anthraquinone) seems to result from a transition in the free C=O group, while the transition connected with the other C=O group has a very small probability and shows up in the form of a continuous spectrum; this last effect is probably connected with a strong deformation of the C=O bond caused by steric factors and interaction with the free electron pairs of the halogen. This interpretation would also explain the absence of vibrational fine structure in the spectra of the dihaloderivatives (Cl, Br, and I).

Both electronic transitions appear in the spectrum of α-fluoroanthraquinone, though the $n \rightarrow \pi^*$ transition has a much greater probability in the C=O group adjoining the halogen.

This can evidently be attributed to the fact that a fluorine, which has a small atomic radius, can not produce any steric deformations in the carbonyl group (α to the halogen) and due to its electronegative nature (inductive effect) it withholds its free electron pairs from participation in the π-electron system.

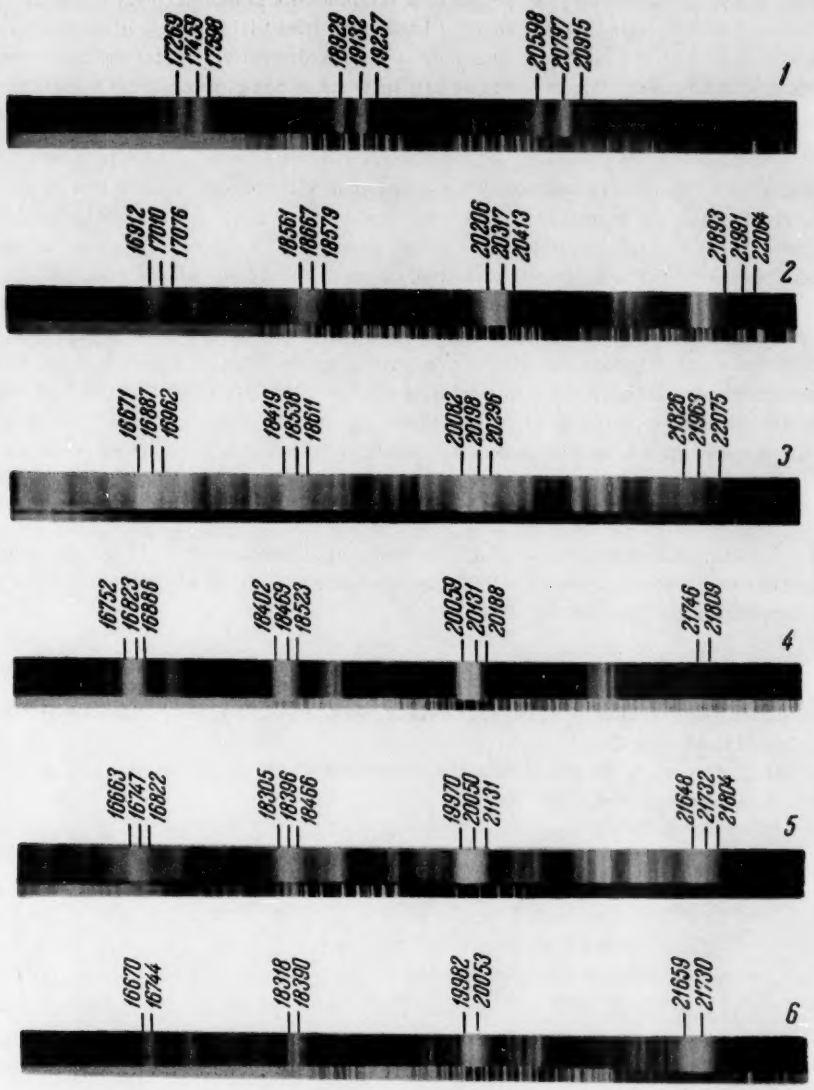

The luminescence spectra of anthraquinone and its haloderivatives in heptane at 77° K. λ = 313 mμ. 1) α-Fluoroanthraquinone; 2) β-fluoroanthraquinone; 3) anthraquinone; 4) β-chloroanthraquinone; 5) β-bromoanthraquinone; 6) β-iodoanthraquinone.

This renders the oxygen in the C=O group more negatively charged which seems to enhance the $n \rightarrow \pi^*$ transition probability in the group.

The luminescence spectra of β-haloanthraquinones also exhibit a vibrational fine structure (Table, Fig.). The multiplicity and the relative intensities of the major components both depend on the solvent. In the β-position each halogen has a distinct effect on the luminescence spectrum of anthraquinone, and if fluorine is

successively replaced by chlorine, bromine, and iodine all the components of the major peaks shift in a regular manner toward longer wavelengths by 100-150 cm^{-1}. The spectrum of anthraquinone itself is intermediate between that of the β-fluoro-derivative and β-chloro-derivative (see Table) which is consistent with the assumptions made above. If the free electron pairs of iodine or bromine should interact with the π-electron system at the instant that the molecules emit light, the spectral band intensities will follow a different distribution law from that observed in the spectra of anthraquinone and other α- and β-derivatives exhibiting vibrational fine structure. Whereas the band intensities in the latter spectra at first increase as one proceeds from the violet to the red region, attain a maximum, and decrease again, the spectra of β-bromo- and particularly β-iodo-derivatives exhibit gradually decreasing band intensities (see Figure).

The β-bromo- and β-iodoanthraquinones give strongest bands at the short-wave end of the spectrum which, according to the Frank-Condon principle, could be explained by assuming that the excitation of the electronic states has very little effect on the interatomic equilibrium distance. Therefore, in the case of the β-bromo- and β-iodoanthraquinones the O"−O' transition is permitted on the basis of the Frank-Condon principle. To determine the exact frequency of the O" − O' transition one has to have the absorption spectra of the compounds under identical conditions, and this, of course, can not as yet be done. If we take the first and strongest short-wave bands in the spectra of β-bromo- and β-iodoanthraquinone as representing the O" − O' transition then the corresponding purely electronic transitions will have the frequencies of 21730 cm^{-1} (β-I) and 21804 cm^{-1} (β-Br) respectively. Thus, due to an effective participation by the free electron pairs of the halogens, the electron density distribution around the C =O groups in the excited β-bromo- and particularly β-iodoanthraquinone molecules remains relatively unchanged, unlike the case of anthraquinone and its other derivatives where the ground and excited states differ considerably.

This fact is evidently responsible for the increased relative luminescence yield from β-bromo- and β-iodo-derivatives. Most monohaloanthraquinones exhibit phosphorescence (with the afterglow lasting from 2 to 10 sec). This problem will require a special investigation.

LITERATURE CITED

1. D. N. Shigorin, and N. A. Shcheglova, et. al., Doklady Akad. Nauk SSSR 120, 1242 (1958);* Izvest. Akad. Nauk SSSR, Ser. Fiz. 23, 37 (1959).
2. É. V. Shpol'skii, E. A. Girdzhiyauskaite, and L. A. Klimova, Results of the Tenth All-Union Conference on Spectroscopy [in Russian] (L'vov, 1957) p. 24.

*Original Russian pagination. See C. B. translation.

THE PARAMAGNETIC RESONANCE OF VARIOUS FORMS OF α,α-DIPHENYL-β-PICRYLHYDRAZYL

Yu. V. Yablokov

Kazan Branch of the Academy of Sciences, USSR

(Presented by Academician A. E. Arbuzov, February 19, 1960)
Translated from Doklady Akademii Nauk SSSR, Vol. 133, No. 3, pp. 424-426, July, 1960
Original article submitted February 12, 1960

While investigating the paramagnetic resonance spectra of microcrystalline samples of α,α-diphenyl-β-picrylhydrazyl (DPPH) at 300 and 9400 Mc frequencies A. E. Arbuzov et al. [1] showed that the absorption band-width depends to a large extent on the solvent used in the last step of the radical synthesis [2], on air oxidation, and on the frequency used in the measurements.

We measured the paramagnetic resonance (at 36,000 Mc, at room temperature) of single DPPH crystals prepared in chloroform, carbon disulfide, and benzene, and of polycrystalline samples prepared in various solvents. Single crystals of DPPH were grown by slowly evaporating the solvent. We noted that this type of crystallization creates favorable conditions for twinning. All the crystals grown in benzene and chloroform and selected for our work turned out to be twins. DPPH crystals grown in chloroform crystallized in the form of elongated flakes. It was therefore easy to locate the twinning plane of these crystals and to separate the individual crystals. With crystals obtained from benzene this was not feasible.

According to the literature data [3] single DPPH crystals grown in benzene solution are monoclinic whereas those obtained from chloroform [3], carbon disulfide, or carbon tetrachloride [4] are triclinic.

In the millimeter region of the spectrum the components which depend on the steady magnetic field show a much poorer resolution than they do at lower frequencies. Therefore, small variations in the g-factor can be determined with a fair degree of accuracy. Our measurements have shown that all of the above-mentioned crystals (even the triclinic ones) possess an axis around which the crystal exhibits a practically constant g-factor.* Allowing for the precision of our measurements we can consider this axis to be the magnetic symmetry axis of the crystal, as was done by W. Gordy et al. [4]. It is reasonable to assume that the magnetic symmetry axis lies along the N–N bond in DPPH. Keeping in mind all that has been said above we used for the paramagnetic resonance of all three types of DPPH single crystals the usual spin Hamiltonian for a case with axial symmetry and spin ½:

$$\hat{\mathcal{H}} = g_{\parallel}\beta H_z S_z + g_{\perp}\beta\,(H_x S_x + H_y S_y)\,. \qquad (1)$$

In Table 1 we have listed the g-factors and the band-widths in the paramagnetic spectra of single DPPH crystals. The band-widths (ΔH) were measured at half the band-height. We used in our apparatus an SP-13B type electromagnet which provided a fairly homogeneous constant field where the sample was located. The single crystals used in our measurements were 0.5 × 0.1 × 0.1 mm in size. When the dimensions of microcrystalline

* When a single crystal of DPPH was rotated around the assumed axis of magnetic symmetry the g-factor varied from 2.0041 to 2.0038.

TABLE 1

The g-Factors and the Widths (in Oersteds) of the Paramagnetic Resonance Bands of Single DPPH Crystals

Solvent	$g_\perp$	$g_\parallel$	$\Delta H_\perp$	$\Delta H_\parallel$
Benzene	2,0039±±0,0003	2,0030±±0,0003	Not over 5	
Chloroform	2,0040	2,0030	1,4±0,1	2,0±0,1
Carbon disulfide	2,0041	2,0031	1,9±0,2	2,4±0,2

TABLE 2

The g-Factors and Widths (in Oersteds) of Paramagnetic Resonance Bands of Various DPPH Samples

Solvent	36,000 Mc, polycrystal		36,000 Mc. single crystal ΔH	300 Mc, ΔH
	g	ΔH		
Benzene	2,0038	7,2±0,2	5	6,8
Chloroform	2,0038	5,4±0,2	1,6	1,7
Carbon disulfide	2,0038	4,7±0,2	2,1	1,3
Carbon tetrachloride	2,0038	5,6±0,2	—	1,9

samples were increased to 0.5 x 0.5 x 0.5 mm the band-width showed no appreciable increase. The steady magnetic field was calibrated during the measurements by means of the proton nuclear magnetic resonance. The g-factors of DPPH were extrapolated from the g-factors of metallic lithium dispersed in rubber for which the value of 2.0023 is accepted [5]. Let us note that our chief interest was not in obtaining the absolute values of g but in finding what effects specific solvents and the orientation of single crystals might have on it. The g-factors could be measured to within ±0.0002.

Table 1 shows that in all of the single DPPH crystals the absolute value of the g-factor remains the same (within the range of experimental errors). All the types of single DPPH crystals exhibit a small (though far outside the range of experimental errors) anisotropy of the g-factor. In crystals obtained from chloroform or carbon disulfide we determined the anisotropy of the paramagnetic resonance band-width which was first detected by Livingston and Zeldes [6]. The existence of anisotropy was not as yet accepted at the time of our work, since Kikuchi and Singer reported [7] that the band-width was independent of the DPPH crystal orientation, but the range of their experimental errors was ±20%. Our data confirmed the existence of such anisotropy. Measurements carried out on DPPH samples obtained from benzene did not yield, however, any such clear-cut results.

Samples prepared in benzene had very many faces. We examined the crystals under a microscope and found no evidence of twinning. However, both the resonance measurements and the x-ray diffraction data forced us to believe that we could not be dealing in this case with single crystals. The DPPH samples prepared in benzene gave resonance curves which most probably consisted of two curves superimposed on each other, with the superposition being very sensitive to the orientation of the relatively constant field. This was apparent from the distorted shape of the curve. At certain orientations two clearly resolved peaks could be detected. At the same time the absorption band was broadened from about 5 to 9 oersteds. After analyzing the results we were also able to detect the anisotropy of the g-factor in the monocrystalline DPPH samples obtained from benzene. We may assume that in this case the resonance band corresponding to a single crystal is not more than 5 oersteds wide. We also measured the paramagnetic resonance in microcrystalline DPPH samples obtained from benzene, chloroform, carbon disulfide, and carbon tetrachloride. These measurements were carried out in order to find out whether the "isotropic" g-factor depends on the specific solvent used and how the absorption band-width varies with frequency. The results are presented in Table 2. The data are for samples with approximately the same grain size; all of the samples were studied in evacuated pyrex capillaries.

We can now assume that the magnitude of the g-factor and its anisotropy do not depend on the solvent used for crystallizing the DPPH samples.

DPPH samples prepared in benzene give paramagnetic resonance with bands much wider than in the case of samples prepared in chloroform, carbon disulfide, or carbon tetrachloride, indicating that exchange interactions are stronger in the last three samples.

The results of our measurements can be compared with data previously obtained at 300 Mc on microcrystalline DPPH samples [1]. At that frequency the weak anisotropy of the g-factor has absolutely no effect on the band shape. Therefore the band-widths obtained for polycrystalline samples at 300 Mc can be directly compared with those calculated for single crystals by means of the formula $\Delta H_{isotope} = 1/3(\Delta H_\parallel + 2\Delta H_\perp)$ where $\Delta H_\parallel$ and $\Delta H_\perp$

are measured in the 36,000 Mc range. Table 2 shows that at higher frequencies the absorption bands of single crystals prepared in benzene (DPPH samples containing cyclic solvent molecules in their crystal lattice) become noticeably narrower, as has already been demonstrated before [1]. On the other hand single crystals containing noncyclic solvent molecules (chloroform, carbon disulfide, and carbon tetrachloride) have a ΔH independent of frequency. In fact the ΔH of single crystals prepared in chloroform has practically the same value at 300 as at 36,000 Mc. The difference between the paramagnetic resonance band-widths of microcrystalline DPPH samples prepared in chloroform and carbon tetrachloride is very small, but the difference remains the same at 300 Mc as at 36,000 Mc. A comparison between the spectra of DPPH samples crystallized from various noncyclic solvents (see [1]) provides convincing evidence that the increased band-width (ΔH) detected at 9400 Mc (relative to that at 300 Mc) corresponds precisely to the magnitude of anisotropy in the g-factor, which becomes important at that frequency. As far as the single DPPH crystal grown in carbon disulfide is concerned we should bear in mind the fact that the samples prepared in this solvent are the ones most exposed to the action of air oxygen; the single crystals used in our present work were very small in size and had been stored in air for 2 months.

Finally, let us note that although air oxidation tends to widen the absorption bands of DPPH obtained from noncyclic solvents [1, 8] it has absolutely no effect on the g-factor of this free radical.

In concluding, the author would like to thank Prof. B. M. Kozyrev for his daily help and thank F. G. Valitova for providing the microcrystalline samples of DPPH.

LITERATURE CITED

1. A. E. Arbuzov, F. G. Valitova, et al., Doklady Akad. Nauk SSSR 126, 774 (1959).*
2. A. E. Arbuzov and F. G. Valitova, Zhur. Obshch. Khim. 27, 2354 (1957).*
3. M. Sternberg, Comptes Rend. 240, 990 (1955).
4. A. van Roggen, L. van Roggen, and W. Gordy, Phys. Rev. 105, 50 (1957).
5. G. Feher and A. F. Kip, Phys. Rev. 98, 337 (1955).
6. R. Livingston and H. Zeldes, J. Chem. Phys. 24, 71 (1956).
7. C. Kikuchi and L. S. Singer, J. Chem. Phys. 23, 1738 (1955).
8. N. S. Garif'yanov and B. M. Kozyrev, Doklady Akad. Nauk SSSR 118, 738 (1958).*

* Original Russian pagination. See C. B. translation.

ELECTROCHEMICAL AND PHOTOELECTROCHEMICAL PROCESSES ON p- AND n-GERMANIUM AT CATHODIC POLARIZATION

R. M. Lazorenko-Manevich, N. A. Aladzhalova and

V. I. Veselovskii

L. Ya. Karpova Physicochemical Institute

(Presented by Academician A. N. Frumkin, March 10, 1960).
Translated from Doklady Akademii Nauk SSSR, Vol. 133, No. 3, pp. 620-623, July, 1960
Original article submitted March 2, 1960

In literature [1, 2] it is pointed out that the nature of the surface has a considerable influence upon the detailed kinetics of hydrogen evolution on a germanium electrode; this is connected with the semiconducting properties of Ge. In this study the influence of illumination together with that of the electrochemical parameters upon H_2 evolution on Ge was investigated. The experiments were done in 1 N solutions of KOH and H_2SO_4 with p- and n-Ge having various specific resistivities (p : 0.5-21.0 ohm · cm, n : 1.1 and 22.9 ohm · cm). The reagents used were prepared from doubly distilled water and chemically pure KOH or triply distilled H_2SO_4. In the apparatus for this study we employed a thick clamped Ge electrode and for the illumination a quartz window was inserted. The surface of the electrode (the (111) face) was etched in CP-4 or in a mixture of HNO_3 and HF (etching reagent No. 8 according to Ellis [3]). All experiments were done in a H_2 atmosphere. A hydrogen electrode in the solution investigated served as reference electrode. The electrode was illuminated by the light of a 300 w bulb which had passed through a layer of ~10 cm water. The entire spectrum of the light was used. The intensity of illumination at the surface of the electrode was $\sim 10^{-1}$ cal/ cm^2 sec.

Overvoltage curves were determined in two ways: the "rapid" and the "slow" way where the stationary equilibrium value of η was attained at each current. Typical stationary curves [1-4], determined after protracted (10-15 hr) cathodic polarization, and also a "rapid" one, determined without previously polarizing p-Ge, are shown in Fig. 1.

The curvature at high currents, which is found in the curves for p-Ge – especially in the "rapid" one –, is connected with the diffusional retardation of electrons [1, 2, 4]; this does not take place on n-Ge, since it has a considerably higher electron concentration in the conduction band than p-Ge has. Several authors [5-7] assume that electrons of the valence band may take part in the cathodic evolution of H_2, just as they may do in the reduction of certain oxidants on Ge [5, 8]. It should be assumed that the transfer of an electron from the valence band to the oxidant ion is only possible if there exists no activation barrier whatever on the semiconductor-solution boundary, that is, for systems in which the electron transfer is a reversible step. Probably, hydrogen evolution on Ge is not such a process.

The presence of hydrogen on the Ge surface, which enhances the surface recombination and generation rate of minority carriers [1, 2, 9], causes blurring of the saturation current region. On the one hand, our experiments confirmed the existence of diffusional retardation in p-Ge at hydrogen evolution; on the other hand, they showed that it does not correspond to a stationary surface state. The dependence of η upon time after switching on a current density of 10 ma/ cm^2 is shown in Fig. 2 a (curve 1). A maximum, the shape and the height of which is

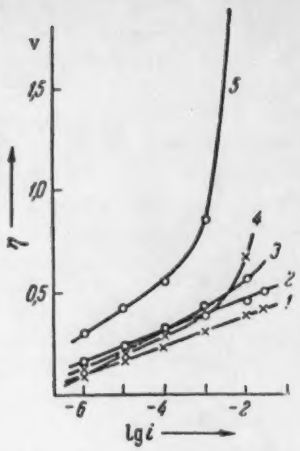

Fig. 1. Overvoltage in 1 N KOH (2, 3, 5) and 1 N H_2SO_4 (1, 4). 1, 2) n-Ge (ρ = 2 ohm · cm); 3, 4, 5) p-Ge (ρ = 0.5 ohm · cm).

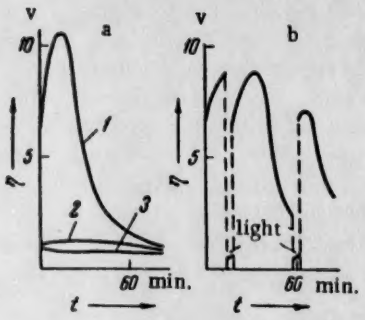

Fig. 2. Typical curves for the relation between the overvoltage at 10 ma /cm² and the time after switching on the current (in 1 N KOH). a) In darkness: 1, 2) p-Ge (ρ = 0.5 ohm · cm); 3) n-Ge (ρ = 1.1 ohm · cm). b) Influence of light, p-Ge (ρ = 0.5 ohm · cm).

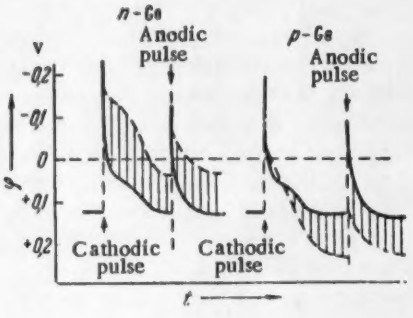

Fig. 3. Influence of adsorbed hydrogen upon the photoeffect on a germanium electrode. Drawn lines) dark potential; dotted lines) potential found when illuminated after a short polarization.

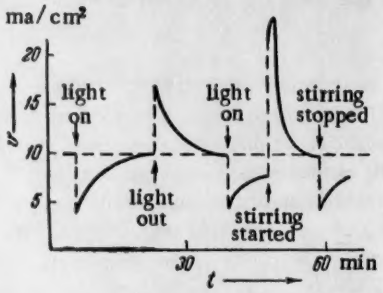

Fig. 4. The influence of light on the rate of hydrogen evolution.

strongly dependent upon the previous history of the electrode surface, deserves attention. Thus, the presence of a thick (~1000-2000 A) oxide layer, obtained by a special etching [3], results in the complete disappearance of the maximum (curve 2). It should be noted that, although the general shape of the curve is retained, η_{max} is considerably lower in acid solutions then in alkaline ones (up to 5-6 v in 1 N H_2SO_4 and up to 20-22 v in 1 N KOH at i = 10 ma/cm²). The descending branch of the curve is inherently connected with the increase in surface generation rate of electrons, caused by accumulation of hydrogen on Ge. The initial increase in overvoltage, which reaches a few volts, cannot be explained by data found in literature. Below we try to give an explanation of the appearance of a maximum by means of the results obtained in certain of our illumination experiments.

Illumination of the polarized p-Ge (when diffusional retardation is still effective) causes the overvoltage to decrease to 0.5-0.6 v (Fig. 2 b). As is well known, this is a result of the generation of electrons on the surface by the action of light. By using interrupted illumination we were able to observe not only the photoeffect already described in literature, but also irreversible phenomena, which are connected with the occurrence of a photoelectrochemical process.

After the light has been switched off (Fig. 2 b), the overvoltage η_d in the dark (when it is situated on the

descending branch of the η_d versus t curve) comes to a value, surpassing the original one (before illumination) by a few tens of volts. When, however, the illumination is made on the rising branch or near to the maximum of the said curve, it causes η_d to decrease to a value lower than the original one, but higher than the overvoltage at time zero. Thus, it seems that illumination tends to bring the surface back to the original state it had before the current was switched on. Since it has been shown that the decrease of η_d with time in the diffusional retardation region is connected with the accumulation of hydrogen on the surface, which enhances electron generation, it is natural to attribute the observed increase in η_d (on the descending branch) to expulsion of hydrogen by the action of light. The mechanism of the observed "photodesorption" cannot be established with certainty from the data given. The occurrence of "photodesorption" shows that the elimination of diffusional retardation is connected with hydrogen which penetrates only a relatively short distance into Ge.

On the rising branch and in the region of the maximum, "photodesorption" also takes place; here, however, it does not manifest itself by an increase but by a decrease in η_d in comparison with the original value. The general shape of the curve for darkness after illumination is the same as that before illumination; consequently, it may be assumed that the increase in η_d at the start of polarization is essentially connected with the accumulation of hydrogen and not with any of the other possibilities for a change in the nature of the surface (as, for instance, reduction of oxidic layers). Hence, it follows from our experiments that both branches of the η_d versus t curve can be explained by the gradual accumulation of hydrogen on Ge.

Further, to explain why a maximum occurs on the η_d versus t curve, it is necessary to look at data on the influence which adsorbed hydrogen has on the photoeffect in Ge, when there is no external current.

The way in which the Ge potential changes in darkness or on illumination, when there is no external current, is shown in Fig. 3 (the initial Ge potential has been shifted in the positive direction, since in these experiments traces of dissolved O_2 were present). As may be seen in Fig. 3, the photoeffect on p-Ge almost disappears or even changes sign after a short (fraction of a second) cathodic polarization and that on n-Ge increases sharply. When intensively stirring the solution (in the case of n-Ge, when illuminating) the potential does not return to its previous value after the same short anodic polarization, but stays (up to 50-100 mv) more negative, which may be connected with dissolution of the oxide layer; however, the photoeffects do not change substantially in comparison with those found before the polarization.

Obviously, the effects observed are connected with the presence of hydrogen on the surface (after cathodic polarization). It is well known that adsorbed hydrogen forms a dipole layer on the surface of many metals, for instance on Pt [10] and Si [11], with the negative pole directed outward. However, it is impossible to explain the phenomenon observed merely by the formation of such a layer. It follows from Fig. 3 that the presence of hydrogen on the Ge surface results in charging the surface more negatively relative to the bulk of the electrode. It may be assumed that this takes place, because, on the adsorption of hydrogen, acceptor levels, situated in the forbidden zone, are formed; electrons may be localized on these levels.

It should be noted that the mere bubbling of H_2 through the solution does not result in the effect described. Obviously, in this respect, molecular hydrogen behaves as an inert gas. A similar difference between the action of atomic and molecular hydrogen has also been observed in the adsorption on Si from the gas phase [11].

The assumption that adsorbed hydrogen has acceptor properties enables the increase in η_d at the start of polarization (Fig. 2 a, curve 1) to be explained as due to a raised concentration of polarizing electrons, which is the result of a decreased equilibrium concentration of conduction electrons on the surface at hydrogen adsorption. The adsorption of hydrogen at the same time increases the number of surface recombination centers, however, up to a certain moment (the maximum in the curve of η_d versus t) the acceptor property of hydrogen probably prevails over its influence as electron generation center.

As has been shown above, the initial state of the surface (determined, obviously, by the thickness and the structure of the oxide layer after etching and by the stay in air) has a strong influence on the quantitative characteristics of the η_d versus t curve (initial η_d, η_{max}, the rate in which η_d changes); however, the presence of a maximum is a characteristic property which always appears.

Finally, we describe one more phenomenon, connected with the action of light upon a semiconductor (it has been observed on p-Ge as well as on p-Si).

When illuminating polarized p-Ge at a constant current density, turning the light on or off is accompanied by a change in the rate of gas evolution (Fig. 4). This phenomenon takes place only in alkaline solutions, when there is a considerable photoeffect (that is, on electrodes having not yet a high surface recombination rate). On n-Ge this phenomenon is not observed. The influence of stirring, shown in Fig. 4, convinces us that the hydrogen "removed" by illumination dissolves in the electrolyte, but is liberated again after some time, when the light is turned off; this makes the liberation rate of gas surpass the value corresponding to the current. Therefore, here slow transfer processes take place from one stationary state (in darkness) to another (in light), which differ by probability of gas bubble nucleation and, therefore, by the content of hydrogen dissolved in the electrolyte. The change in Ge surface tension, caused by the redistribution of charge at illumination, may be the reason for the change in nucleation probability.

LITERATURE CITED

1. J. B. Flynn, J. Electrochem. Soc. 105, 715 (1958).
2. M. Green, Modern Aspects of Electrochemistry 2 (London, 1959) p. 5.
3. S. G. Ellis, J. Appl. Phys. 28, 1262 (1957).
4. W. H. Brattain and C. G. B. Garrett, Bell Syst. Techn. J. 34, 129 (1955).
5. H. Gerischer and F. Beck, Z. Phys. Chem. (N. F.) 13, 389 (1957).
6. E. A. Efimov and I. G. Erusalimchik, Zhur. Fiz. Khim. 32, 1967 (1958).
7. E. N. Paleolog, A. Z. Fedotova, and N. D. Tomashov, Doklady Akad. Nauk SSSR 129, 3, 623 (1959).*
8. Yu. V. Pleskov, Doklady Akad. Nauk SSSR 126, 1, 111 (1959).*
9. N. Holonyak and H. Letaw, J. Appl. Phys. 26, 355 (1955).
10. A. N. Frumkin, V. S. Bagotskii, et al., Kinetics of Electrode Processes [in Russian](Moscow, 1952).
11. J. Eisinger, J. Chem. Phys. 30, 927 (1959).

* Original Russian pagination. See C. B. translation.

FINE STRUCTURE OF THE RAYLEIGH SCATTERING LINE IN SOLUTIONS AND HYPERACOUSTIC DISPERSION

L. V. Lanshina and M. I. Shakhparonov

M. V. Lomonosov Moscow State University
(Presented by Academician V. V. Shuleikin, March 7, 1960)
Translated from Doklady Akademii Nauk SSSR, Vol. 133, No. 3, pp. 624-626, July, 1960
Original article submitted March 7, 1960

Rayleigh scattering of light in solutions is evoked by adiabatic and isobaric density fluctuations, orientation fluctuations, and fluctuations in concentration. In order to separate the total scattering experimentally into its component parts due to these various fluctuations, it is necessary to investigate the fine structure of the Rayleigh scattering line. Such an investigation often permits one in addition to find the velocity of propagation of hyperacoustic oscillations. The fine structure of light scattered by individual liquids has been studied by a number of authors [1]. Up until now to the best of our knowledge only two attempts have been made at qualitative measurement, and these without any definite results [2, 3]. The hyperacoustic properties of solutions have not so far been investigated.

The apparatus that we assembled to photograph the fine structure of the Rayleigh scattering line is essentially similar to the setup described in [1]. The resolving power of the Fabry-Perot interferometer in our experiments was 800,000. The vessel containing the substance to be investigated was thermostatically regulated with an accuracy of $\pm 0.5^\circ$. We studied acetone–water and methyl alcohol–water solutions at 25° and with concentrations in the following molar fractions of acetone: 0.0, 0.06, 0.2, 0.4, 0.7, 1.0; of methyl alcohol: 0.15, 0.36, 0.6, 1.0. For each concentration five or more measurements were made. In each photograph 3 to 4 neighboring interference orders were included. Consequently, the results given later represent the averages of 15-20 or more determinations of the fine structure elements. The measurements were made on the 4358 A line of the mercury spectrum. Moreover, parallel measurements were performed for water at the 4046 A line. The photographs were taken and measured on an MF-4 micrometer and were deciphered by the method described in [1], using several parallel variants. Check was held on the very slight parasitic scattering present by photographs of the fine structure of water (from the absence of a nondisplaced component). A number of photographs was obtained with an interferometer resolving power equal to 1,200,000. In some isolated cases the exposure time was allowed to reach three days.

Curves are shown in Fig. 1 for the velocity of propagation of hyperacoustic oscillations in the acetone–water ($\omega \approx 0.6 \cdot 10^{10}$ sec^{-1}, $\Lambda \approx 22 \cdot 10^{-6}$ cm) and methyl alcohol–water ($\omega \approx 0.5 \cdot 10^{10}$ sec^{-1}, $\Lambda \approx 22 \cdot 10^{-6}$ cm); these curves were calculated according to the equation $\frac{\Delta\nu}{\nu} = 2n\frac{v}{c}\sin\frac{\theta}{2}$. For the sake of comparison, data are shown [4, 5] for the velocity of propagation of ultrasonic oscillations ($\omega \approx 56 \cdot 10^5$ sec^{-1}, $\Lambda \approx 24 \cdot 10^{-3}$ cm). In water and in the solutions large negative dispersion of the hyperacoustic oscillations is observed, $\Delta v/v$ attaining a value of -5%, while the standard deviation in determining $\underline{v}$ was equal to $\sim 1.4\%$. With a decrease in water concentration x_1 the negative hyperacoustic dispersion gradually vanishes, where in the system acetone–water the dispersion is observed to vanish at $x_1 = 0.65$, while in the system methyl alcohol–water this is observed at $x_1 = 0.5$. In more concentrated solutions of acetone and methyl alcohol hyperacoustic dispersion is not observed. As is known,

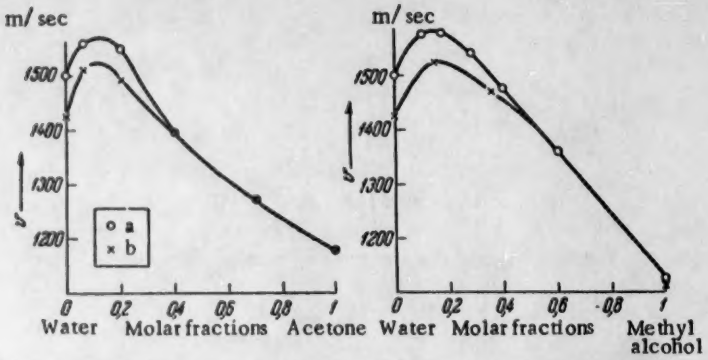

Fig. 1. Dependence of the velocity of ultrasonic oscillations (a) and velocity of hyperacoustic oscillations (b) on concentration for the systems acetone–water and methyl alcohol–water.

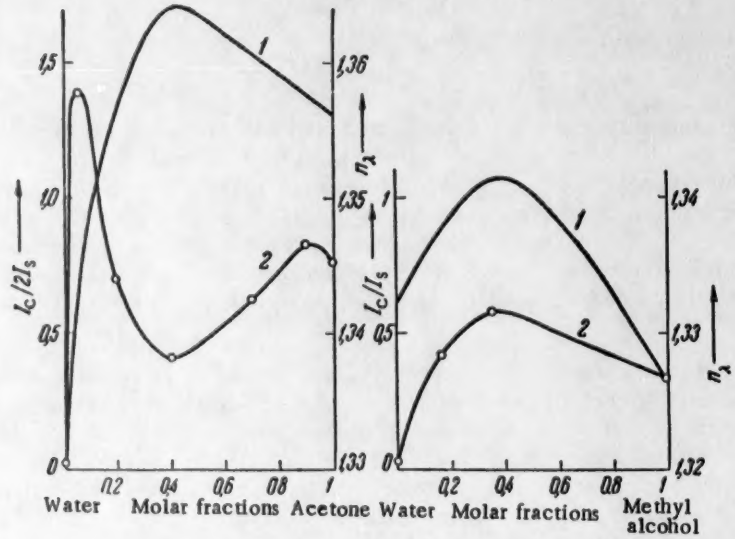

Fig. 2. Dependence of the index of refraction n_λ (1) and ratio of the central component intensity to the summed intensity of the side components $I_c/2I_s$ (2) on concentration for the systems acetone–water and methyl alcohol–water.

no one has until the present time succeeded in observing negative dispersion of acoustic oscillations in individual liquids and solution. The data existing in the literature on negative dispersion of sound in carbon bisulfide, acetone, and certain other liquids have not been confirmed (see [6], pp. 271-272). Our observed negative dispersion of hyperacoustic waves in water and aqueous solutions appears to be due to structural relaxation of the water. The anomalous nature of the dispersion is in accordance with the familiar anomalous properties of water and can be explained on the basis of existing theoretical notions relative to the nature of sound dispersion.

We also made a comparison of the integral intensities of the central component I_c and of the Mandelstam-Brillouin components I_s. Curves are shown in Fig. 2, representing the dependence of the ratio $I_c/2I_s$ on the composition of the solution. For the analysis of these curves it is necessary to make allowance for the dependence of the index of refraction n_λ on concentration. Graphs of $n_\lambda = f(x)$ are also shown in Fig. 2.

In the solutions the central component of the Rayleigh triplet are caused not only by isobaric fluctuations

in density, but by fluctuations in concentration as well, where the intensity of the scattering resulting from concentration fluctuations is

$$I_{\text{con}} \sim \left(\frac{\partial n}{\partial x}\right)^2 \overline{(\Delta x)^2}.$$

In the acetone–water solutions large positive deviations from Raoult's law take place, so that, consequently, the fluctuations in concentration are large, attaining maximum value at $x_1 \approx 0.4$. It is in precisely this interval of concentration that n_λ passes through the maximum ($\partial n_\lambda / \partial x \approx 0$), and, consequently, concentration scattering is almost totally absent. Therefore, in this region of concentrations $I_c / 2I_s$ passes through a minimum. It is interesting to note that in this interval of concentrations $I_c \approx I_s$.

The methyl alcohol–water solutions were nearly ideal, the fluctuations in concentration being very small and not providing any marked contribution to the Rayleigh scattering of light. The dependence of $I_c / 2I_s$ on concentration in this case therefore takes on another form. We note that $I_c / 2I_s$ passes through a maximum, where the maximum value of the ratio $I_c / 2I_s$, as shown in Fig. 2, occurs in the same interval of concentrations as the maximum index of refraction. At the maximum $I_c \approx I_s$. The accuracy in determining I_c and I_s was about $\pm 10\%$.

LITERATURE CITED

1. I. L. Fabelinskii, Uspekh. Fiz. Nauk 63, 355 (1957).
2. K. S. Bai, Proc. Indian Acad. Sci. A 18, 210 (1943).
3. Kh. E. Sterin, Doklady Akad. Nauk SSSR, 62, 219 (1948).
4. I. G. Mikhailov, Doklady Akad. Nauk SSSR 31, 324 (1941).
5. I. G. Mikhailov, Doklady Akad. Nauk SSSR 52, 673 (1946).
6. L. Bergmann, Ultrasonics [Russian translation] (IL, 1956).

INITIATING ACTION OF NITROSYL CHLORIDE IN THE OXIDATION OF PROPANE

Z. K. Maizus and Corresponding Member Acad. Sci. USSR,

N. M. Émanuél'

Institute of Chemical Physics, Academy of Sciences, USSR
Translated from Doklady Akademii Nauk SSSR, Vol. 133, No. 3, pp. 627-629,
July, 1960
Original article submitted April 12, 1960

In studying new methods of achieving oxidative treatment of gaseous hydrocarbons to prepare valuable oxygen-containing substances, we have made wide use of homogeneous catalysis and the transfer of high-molecular gas-phase reactions to mild, low-temperature oxidation conditions at temperatures and pressures close to the critical values [1, 2].

In both cases the aim was to lower the reaction temperature and thus decrease the proportion of unprofitable combustion of hydrocarbons. The action of several homogeneous catalysts and mixtures of them was examined in [2]. In a series of subsequent papers, a more thorough study was made of the chemical possibilities and the mechanism of action of homogeneous catalysts [3-5].

Among the various homogeneous additives (initiators), nitrosyl chloride NOCl attracted our attention as an extremely efficient stimulator of oxidation processes, having an effect on the mechanism of the macroscopic stages which are separate in time [6].

The elementary mechanism of the stimulating action of nitrosyl chloride apparently consists of the ready decomposition of NOCl to two active particles (NO and Cl) due to the comparatively low value of the energy of the N–Cl bond which equals 38 kcal/mole [7]. The present work was devoted to a more detailed characterization of the action of added NOCl in the oxidation of propane and its comparison with added NO_2.

We were mainly interested in the yield of such important oxygen-containing products as acetaldehyde and formaldehyde.

The oxidation was carried out in a static apparatus at 250° and a total mixture pressure of 250 mm Hg. Due to the low temperature, the reaction proceeded quite slowly (in minutes). As we were not concerned with selecting the optimal conditions for the formation of acetaldehyde and formaldehyde in the present work, the reaction rate was not important to us. The stimulating action of the additives appeared quite clearly under these conditions.

First of all, this effect could be seen from the curves of the change in pressure during the oxidation (Fig. 1). Incidentally, the nature of the kinetic curve of the pressure change with NOCl added indicated that the process has macroscopic stages. In actual fact, the existence of macroscopic stages in the oxidation of propane in the presence of NOCl was confirmed by a record of the heat evolution by the reaction mixture during the reaction (Fig. 2).

It should be noted that the stimulating action of NOCl was clearly shown by a fall in the spontaneous ignition temperature of propane–oxygen mixtures. The ignition peninsula of mixtures of propane, oxygen, and NOCl was displaced into the region of lower temperatures by ~100°.

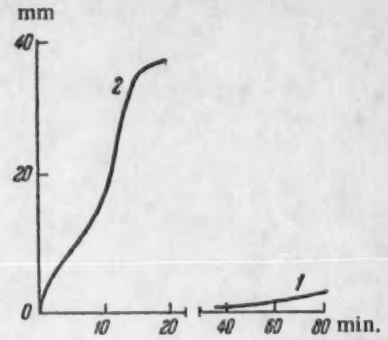

Fig. 1. Kinetic curves of the change in pressure during the oxidation of propane at T = 250° and P = 250 mm. 1) 125 mm C_3H_8 + 125 mm O_2; 2) 120 mm C_3H_8 + + 120 mm O_2 + 10 mm NOCl.

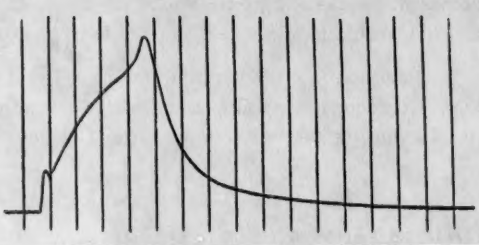

Fig. 2. Photographic record of the heat evolution of a reaction mixture of propane and oxygen in the presence of 10 mm of NOCl with T = 285° and P = 250 mm.

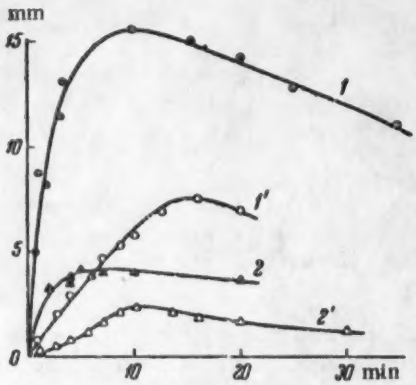

Fig. 3. Kinetic curves of the accumulation of formaldehyde (1) and acetaldehyde (2) in the oxidation of propane initiated by the addition of 10 mm of NOCl (curves 1 and 2) and 10 mm of NO_2 (curves 1' and 2') at T = 250° and P = 250 mm.

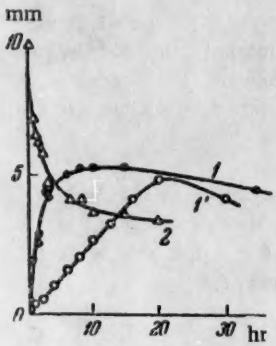

Fig. 4. Kinetic curves of the accumulation of nitropropane (1) and the consumption of NOCl in the oxidation of C_3H_8 initiated by the addition of 10 mm of NOCl (1 and 2) and 10 mm of NO_2 (1').

From data on the temperature dependence of the rate of change in pressure in the temperature range 230-270° we determined the activation energy of propane oxidation in the presence of NOCl as equal to 30 kcal/ mole.

It is extremely important that the addition of NOCl increased not only the rate of formation, but also the maximum concentrations of the main reaction products, acetaldehyde and formaldehyde, both in comparison with the yields of the substances in the uninitiated oxidation and when nitrogen dioxide was used as the homogeneous gaseous initiator (Fig. 3).

The main nitrogen-containing product in the catalysis of propane oxidation by nitrosyl chloride and nitrogen dioxide is nitropropane. A comparison of the kinetic curves of NOCl consumption and $C_3H_7NO_2$ formation (Fig. 4, 1 and 2) indicates that practically the whole of the bound nitrogen in NOCl passed into nitropropane.

The amounts of nitropropane with identical additions of NOCl and NO_2 were equal though the rate of $C_3H_7NO_2$ formation in catalysis by nitrosyl chloride was greater than in the case of NO_2. From the equivalence of the maximum yields of nitropropane in catalysis by NOCl and NO_2, we may draw certain conclusions on the mechanism of the action of NOCl.

Were the catalytic effect only due to the action of NO_2 formed by dissociation of NOCl molecules, as was

proposed, for example, for the reaction of hydrogen with oxygen sensitized by NOCl, then the effects of NOCl and NO_2 should be the same in the systems investigated.

In actual fact the catalytic effect of NOCl is very much greater than the action of equivalent amounts of NO_2. Consequently, an important role in the initiation of oxidation chains in catalysis by NOCl is also played by Cl atoms formed by decomposition of nitrosyl chloride.

LITERATURE CITED

1. N. M. Émanuél', Doklady Akad. Nauk SSSR 110, 245 (1956).*
2. Z. K. Maizus and N. M. Émanuél', Doklady Akad. Nauk SSSR 83, 717 (1952).
3. Z. K. Maizus and N. M. Émanuél', Collection: Chain Oxidations of Hydrocarbons in the Gas Phase [in Russian] (Izd. AN SSSR, 1955).
4. A. A. Babaeva, Z. K. Maizus, and N. M. Émanuél', Izvest. Akad. Nauk. SSSR, Otdel. Khim. Nauk, 8, 1378 (1959).*
5. K. E. Kruglyakova and N. M. Émanuél', Izvest. Akad. Nauk SSSR, Otdel. Khim. Nauk, 1, 18 (1957);* 6, 1005 (1959).*
6. N. M. Émanuél', Izvest. Akad. Nauk SSSR, Otdel. Khim. Nauk, 11, 1298 (1957).*
7. N. N. Semenov, Some Problems in Chemical Kinetics [in Russian] (Izd. AN SSSR, 1958).

*Original Russian pagination. See C. B. translation.

THE MECHANISM OF THE INFLUENCE OF SMALL QUANTITIES OF ADDED ELECTROLYTES ON THE STRENGTH OF A CRYSTALLIZATION HARDENED STRUCTURE

E. E. Segalova, Z. N. Markina, and Academician P. A. Rebinder

M. V. Lomonosov Moscow State University
Translated from Doklady Akademii Nauk SSSR, Vol. 133, No. 3, pp. 630-632, July, 1960
Original article submitted April 23, 1960

The influence of electrolytes on the rate of hydration and strength of structures produced during the hardening of gypsum hemihydrate has been studied by many workers, and the additives have generally been classified on the basis of their effect on the setting time of the gypsum [1]. On the whole, electrolytes accelerate this process, although there are some which retard the setting and hardening process.

Recently, the problem of the influence of electrolytes on the kinetics of the hydration of gypsum hemihydrate has been studied in detail by Ya. L. Zabezhinskii, V. B. Ratinov, and T. I. Rozenberg [2]. These authors have shown that, from a knowledge of the solubilities of gypsum hemihydrate and dihydrate in a solution of a given electrolyte, it is possible to described quantitatively the rate of hydration of the hemihydrate in the presence of this electrolyte. This has enabled them to explain, to a considerable extent, the action of electrolytes in retarding and accelerating hydration.

These theories have not yet made it possible, however, to explain the influence of electrolytes on the strength of the crystallization structure, primarily because the problem of the part played by the magnitude of the supersaturation in the production of the hardened structure has not yet been resolved, and also because the works cited did not take account of the influence of electrolyte on the rate of dissolution of the gypsum hemihydrate. The rate of dissolution of the original binding agent has been shown by work in our laboratory [3], however, to have a significant influence on the strength of the hardened structure produced, even when the magnitude of the maximum supersaturation produced in the hydration process remains unchanged.

The influence of electrolyte on the rate of dissolution of the original binder, and its related influence on the strength of the structure produced, are best studied in the presence of sufficiently small quantities of added electrolytes, when their influence on the magnitude of the supersaturation can be neglected. For this purpose we chose the electrolyte KCl, which has no ion in common with $CaSO_4$ and does not react chemically with it, and which, in small quantities (0.05 g-eq/liter), brings about only an extremely small change in the supersaturation in gypsum hemihydrate suspensions [4].

Fig. 1 shows that a small quantity of added KCl brings about a sharp acceleration in the process of structure-formation in gypsum hemihydrate suspensions, and, at low degrees of dispersion of the initial binder, increases the strength of the hardened structure produced; at high degrees of dispersion, however, the strength is reduced. This is in good agreement with data obtained in [4].

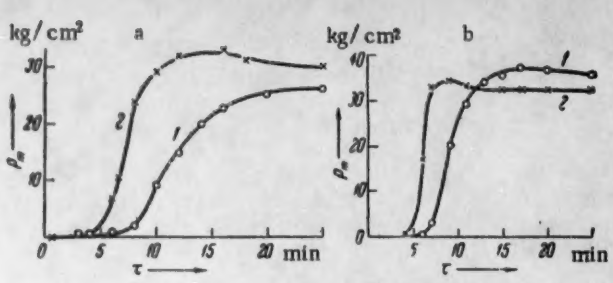

Fig. 1. The kinetics of structure-formation in suspensions of β-gypsum hemihydrate in water (1) and in 0.05 N KCl solution (2). Degree of dispersion of original gypsum hemihydrate: a) S = = 0.34 m^2/g; b) S = 1.65 m^2/g.

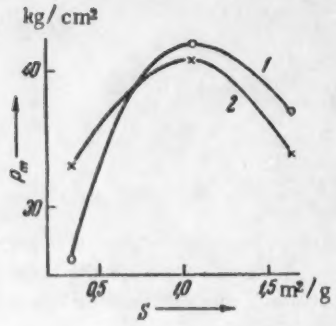

Fig. 2. Relationship between the final strength of the crystallization structure of gypsum dihydrate P_m and the degree of dispersion of the original hemihydrate S when water (1) and 0.05 N KCl solution (2) are used.

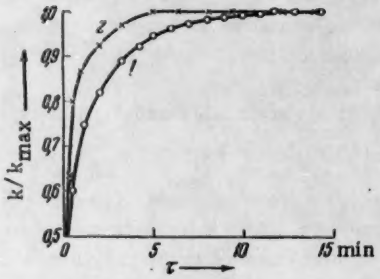

Fig. 3. Kinetics of the change in specific conductance in suspensions of α-gypsum hemihydrate in water (1) and in 0.05 N KCl solution (2).

Fig. 2 shows that a small quantity of added KCl increases the strength of the hardened structure when the degree of dispersion of the original gypsum (or the rate of its dissolution in water) is below the optimum value, and decreases the strength if the rate of dissolution of the original hemihydrate, as a result of a high degree of dispersion, is above the optimum value. In the presence of KCl, the whole of the curve showing the relationship between the final strength of the structure and the degree of dispersion of the original gypsum is displaced, as it were, which indicates a high rate of dissolution of the gypsum hemihydrate in 0.05 N KCl solution compared with the rate of its dissolution in pure water.

This assumption was confirmed by direct comparison of the rates of dissolution of α-gypsum hemihydrate in water and in 0.05 N KCl solution, as determined by the conductometric method [3]. Since the absolute values of the maximum electrical conductivity after dissolution of gypsum hemihydrate in water and in KCl solution are not the same, the values of the specific conductance are given in Fig. 3 as fractions of the maximum value, which corresponds to saturation of the liquid phase of the suspension with $CaSO_4 \cdot 0.5H_2O$. All the measurements were carried out at rates of stirring sufficiently high to ensure that diffusion did not play a limiting role in the process. Under these conditions, the rate of dissolution did not change with subsequent increase in the rate of stirring.

Figure 3 shows that the rate of dissolution of gypsum hemihydrate increases sharply in the presence of KCl. Thus, in the test suspensions, the value of the maximum electrical conductivity is reached after 12 min when pure water is used, and after 5 min when 0.05 N KCl solution is used. The results obtained thus show that the influence of small quantitites of added KCl on the strength of the hardened structure of gypsum hemihydrate is always associated with a considerable increase in the rate of dissolution of the hemihydrate in the presence of the elec-

trolyte. It may be assumed that the action of the added electrolyte involves a change in the structure (decrease in the thickness) of the ionic double layer at the surface of the gypsum hemihydrate crystallites.

LITERATURE CITED

1. J. Traube, Koll. Z. 25, 62 (1919); É. V. Khakimov, Trudy Khim. Inst. Kirg. Fil. Akad. Nauk SSSR, 3, 51 (1950); H. G. Fischer, Bull. ASTM 2, 192, 43 (1953); G. I. Logginov, Doctorate Dissertation [in Russian] (Moscow, 1955); P. P. Budnikov, The Study and Uses of Gypsum [in Russian] (Moscow, 1943); O. O. Roland, Z. f. Elle, 14, 421 (1908); 35, 201 (1903); E. Kanals, J. Rhaum Chim., 30, 1037 (1926); W. C. Riddell, Rock. Prod. 53, 5, 68 (1950); H. B. Weiser and G. Morelland, J. Phys. Chem. 36, 1 (1936).
2. Ya. L. Zabezhinskii, V. B. Ratinov, and T. I. Rozenberg, Doklady Akad. Nauk SSSR 108, 6, 1137 (1956);* B. V. Ratinov, Ya. L. Zabezhinskii, and T. I. Rozenberg, Doklady Akad. Nauk SSSR 109, 5, 981 (1956).*
3. Z. N. Markina, E. E. Segalova, and Ezhi Stoklosa, Kolloid. Zhur. 22, 2, 211 (1960);* E. E. Segalova and P. A. Rebinder, Stroitelnye Materialy, 1, 21 (1960).
4. V. B. Ratinov, T. I. Rozenberg, and N. M. Rubinina, Sborn. Trud. VNII Zhelezobetona (Collected Works of the All-Union Reinforced Concrete Scientific Research Institute) 1, 79 (1957).

* Original Russian pagination. See C. B. translation.

STATIONARY STATES OF DISPERSED ELECTROCHEMICAL SYSTEMS AND THEIR STABILITY

V. P. Smilga and Yu. A. Chizmadzhev

Electrochemistry Institute of the Academy of Sciences, USSR
(Presented by Academician A. N. Frumkin, February 24, 1960)
Translated from Doklady Akademii Nauk SSSR, Vol. 133, No. 3, pp. 633-636, July, 1960
Original article submitted February 22, 1960

Descriptions of self-oscillatory phenomena in some electrochemical systems during the passage of a current are available in the literature [1-6]. In order to explain the mechanism of these phenomena it is necessary to study the problem of the stationary states of dispersed systems and of their stability.

Let us consider the problem of the distribution of the potential in a one dimensional dispersed system whose model, as in [6], is provided by a tube of length $2l$ filled with an electrolyte, on whose walls an electrochemical reaction $j(\varphi)$ takes place. The tube is polarized at the two ends. The potential distribution is described by the equation [7]

$$\varkappa r_0 \frac{d^2\varphi}{dx^2} - j(\varphi) = 0, \tag{1}$$

where κ is the electrical conductivity, r_0 is the radius of the tube, and the coordinate x is measured from the left side of the tube. In reference [6] the stationary states of Equation (1), for the case of a constant polarizing potential φ_1 applied to the ends of the tube, were investigated. Below, we shall carry out an investigation of the case of a given potential φ_1 for an arbitrary function $j(\varphi)$ of a given current, and also of the most general case of a given relationship between current and potential. Let us start with a consideration of a given potential

$$\varphi = \varphi_1, \quad x = 0; \qquad \varphi = \varphi_1, \quad x = 2l.$$

From the symmetry condition of the problem relative to the plane $x = l$ it follows that $d\varphi/dx = 0$ for $x = l$. Let us denote the potential in the point $x = l$ by φ_l. From physical considerations it is evident that $j(\varphi) > 0$ everywhere, except maybe at the points $\varphi = 0$. The general solution of the problem has the form:

$$\frac{l}{\varkappa r_0} = F(\varphi_l) = \int_{\varphi_l}^{\varphi_1} \frac{d\varphi}{\left[\int_{\varphi_l}^{\varphi} j(l)\, dl\right]^{1/2}}. \tag{2}$$

Depending upon the form of the function $j(\varphi)$ the solution $F(\varphi_l)$ will be described by a curve of a family of functions represented in Fig. 1. The behavior of $F(\varphi_l)$ at the origin is determined by the character of the function $j(\varphi)$ for $\varphi \to 0$. If $j(0) \neq 0$ or $j \sim \varphi^n$, where $n < 1$, $F(0)$ is finite (curves a and b). If $j(\varphi)$ has no decreasing portions, the curve b holds. It can be shown that a function of the form a is possible only when there are decreasing sections of the curve $j(\varphi)$. If $j(\varphi)$ for $\varphi \to 0$ is proportional to φ^n, where $n \geq 1$, $F(\varphi_l)$ tends to 0 and infinity (curves c and d). It can be shown that the case c corresponds to a polarization characteristic with a decreasing section.

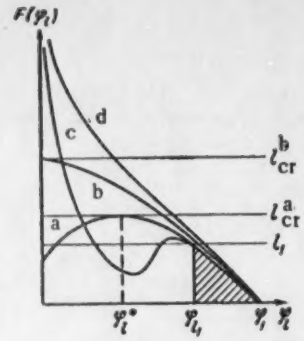

Fig. 1.

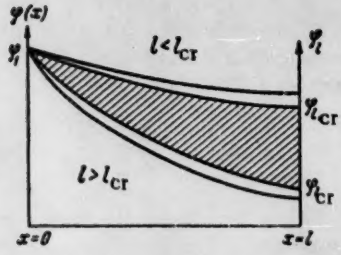

Fig. 2.

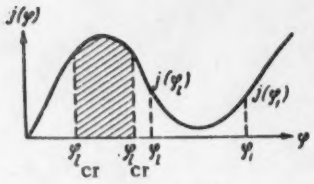

Fig. 3.

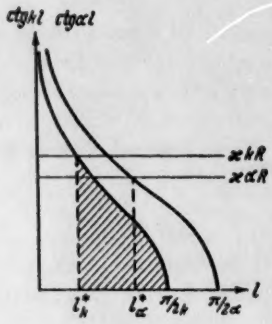

Fig. 4.

Let us consider the case $n < 1$ (curves a and b). In the case b for $l < l_{cr}$ the stationary state lies in the region $\varphi_l < \varphi < \varphi_1$. For $l > l_{cr}$ the entire tube can be divided into two regions: the first – the working region – is equal to l_{cr}; the second, equal to $(l - l_{cr})$, is characterized by the fact that no current passes through it and the potential for $x > l_{cr}$ is equal to zero. Thus, for any l there is a stationary state of the system. In case a for $l > l_{cr}$ there is no stationary state in the system.* In electrochemical problems $n = 1$, so that the curves c and d can be realized, i.e., the function $F(\varphi_l)$ tends to infinity for $\varphi_l \to 0$. This leads to the results that for any l there exists a stationary state. The case c, which is realized when there are decreasing sections of the curve $j(\varphi)$, is characterized by a particular dependence of the potential distribution upon the length of the tube. For $l \neq l_{cr}$ the potential distribution is a continuous function of the length l – with an increase of length φ_l decreases and the whole distribution is displaced to a lower level. However, when l passes through l_{cr} the value of φ_l and also the whole potential distribution change discontinously as is shown in Fig. 2. The shaded area is forbidden. The curves which lie in this region can never be realized. The potential $\varphi(x)$ for any value of l is a continuous function of a coordinate x.

Figure 3 represents the polarization characteristics $j(\varphi)$. The tube is polarized by the potential φ_1 at the point $x = 0$. For a given l the potential in the center of the tube is equal to φ_1; the region of the polarization curve between $j(\varphi_l)$ and $j(\varphi_1)$ is realized along the tube. When l increases, the potential φ_1 is displaced continuously to the left, until the length l reaches l_{cr}. For a further increase of l the working region of the polarization curve changes abruptly, jumping the region shaded in Fig. 3. The approximation of the real polarization characteristics which satisfies the condition $j(0) = 0$ by the linear function $j = K(\varphi_0 - \varphi)$ is equivalent to a transition from the curve c to the curve a. For such a substitution we lose a whole class of solutions and come to the conclusion that, for $l > l_{cr}$ there are no stationary solutions. A stationary distribution requires an additional investigation of the stability. For the case $j = K(\varphi_0 - \varphi)$, and for a given potential, the stability criterion $\sqrt{(K/\kappa r_0)}\, l < \pi/2$ was obtained [6]. This stability criterion coincides with the condition of existence of stationary solutions for the case $j = K(\varphi_0 - \varphi)$. In other words a stationary distribution for the conditions indicated above is stable. The conclusion made in [6] regarding the instability is not correct for $j(\varphi) > 0$. A study of a number of concrete functions $j(\varphi)$ fulfilling the condition $j(0) = 0$ and $j(\varphi) > 0$ showed that the stationary state for a given polarizing potential

*This disappearance of the stationary solutions is analogous to the so-called "thermal explosion" studied in the chemical kinetics of homogeneous systems [8].

is stable.

Let us pass to the case of a given polarizing current $\varkappa \varphi'_{x=0} = -I_0$, when $j(\varphi) = K(\varphi_0 - \varphi)$. As in the case of a given potential, the requirement $j(\varphi) > 0$ leads to the result that a stationary state exists on the decreasing branch only for $\sqrt{(K/\varkappa r_0)}\,l < \pi/2$. The disappearance of solutions, as has been noted above, is related to the approximation used and has no physical meaning. The potential satisfies the time equation.

$$C\frac{\partial \varphi(x,\,t)}{\partial t} = \varkappa r_0 \frac{\partial^2 \varphi\,,(xl)}{\partial x^2} - j(\varphi). \tag{3}$$

As usual, let us represent the solution in the form

$$\varphi(x,\ t) = \varphi(x) + \gamma\varphi_1(x,\ t),$$

where $\varphi_1(x,t)$ is the deviation from the stationary state, and γ is a small parameter. The function $\varphi_1(x, t)$ satisfies the equation

$$\frac{C}{\varkappa r_0}\frac{\partial \varphi_1}{\partial t} = \frac{\partial^2 \varphi_1}{\partial x^2} + k^2\varphi_1, \quad k^2 = \frac{K}{\varkappa r_0}$$

with the boundary conditions $\varphi_1'(0,\ t) = 0$, $\varphi_1'(l\ ,\ t) = 0$. Let $k^2 = \text{const}$, then φ_1 is equal to $\psi(t) \cdot \text{const}$ or $\varphi_1 = \text{const} \cdot e^{\lambda t}$, where $\lambda = \frac{k^2 \varkappa r_0}{C} > 0$. Consequently, in a condition of constant current the state on the decreasing branch is unstable. However, given the current at the input of the tube still does not determine the state on the decreasing branch. As in the case of an equipotential system, the presence of a N-shade characteristic leads to multiple values of the potential for a given current.

Let us show now that the instability can arise only on the decreasing branch. Let us separate the variables in Equation (3):

$$\begin{gathered}\varphi_1(xl) = u(x)\,v(t), \qquad v(t) = v(0)\,e^{\lambda t} \\ u'' - \left[\frac{dj}{d\varphi} + \lambda\right]u = 0, \quad C = \varkappa = r_0 = 1.\end{gathered} \tag{4}$$

Multiplying the equation by u and integrating from 0 to l we obtain

$$\lambda\int_0^l u^2 du = -\int_0^l \frac{dj}{d\varphi}\,u^2 dx - \int_0^l u'^2\,dx,$$

and it follows that $\lambda > 0$ for $dj/d\varphi < 0$ and for

$$\int_0^l \left|\frac{dj}{d\varphi}\right| u^2\,dx > \int_0^l u'^2\,dx.$$

Finally let us consider the case when a relation between the current and the potential is given at the ends of the tube:

$$\frac{E - \varphi(0)}{R} = -\varkappa \left.\frac{d\varphi}{dx}\right|_0,$$

where E is the emf of the battery, R the resistance of the external circuit. Let $j = K(\varphi_0 - \varphi)$. If $E > \varphi_0$, a solution exists in the region $l^* < l < \pi/2k$, where l^* is a root of the transcendent equation represented in Fig. 4. For $E < \varphi_0$ the permissible values of l are limited by the inequality $l < l^*$. For investigating the stability it is necessary to find λ from Equation (4)

$$u'' + \alpha^2 u = 0, \quad \alpha^2 = k^2 - \lambda$$

with the boundary conditions

$$u'_{x=l} = 0, \quad u_{x=0} = \varkappa R u'_{x=0}.$$

The equation for determining α has the form:

$$\operatorname{ctg} \alpha l = \varkappa R \alpha.$$

The solution is unstable if $\lambda > 0$, i.e., $\alpha < k$. Fig. 4 shows that for $E > \varphi_0$ it is possible to find $\alpha < k$ in the region of existence of the solution, and in the case $E < \varphi_0$ no such α exists and the solutions are stable. However, for $E > \varphi_0$ the stationary state ceases to be single, just as in the equipotential case. Thus, in the case chosen by us, the dispersion factor does not lead to the appearance of oscillating solutions.

We express our deep gratitude to Academician A. N. Frumkin and to the Corresponding Member of the Academy of Sciences USSR, V. G. Levich for having suggested the problem and for his participation in very valuable discussions.

LITERATURE CITED

1. M. Thalanger and M. Volmer, Z. Phys. Chem. 150, 401 (1930).
2. J. Butler, Disc. Farad. Soc. 1, 122 (1947).
3. É. A. Aikazyan, Zhur. Fiz. Khim. 33, 5, (1939).
4. A. T. Vagramyan, Electrodeposition of Metals [in Russian] (1950).
5. A. Ya. Gokhshtein, A. N. Frumkin, Doklady Akad. Nauk SSSR, 132, 2 (1960).*
6. Yu. A. Chizmadzhev, Doklady Akad. Nauk SSSR 124, 142 (1959).**
7. A. N. Frumkin, Zhur. Fiz. Khim. 23, 1477 (1949).
8. D. A. Frank-Kamenetskii, Diffusion and Heat Transfer in Chemical Kinetics [in Russian] (1948).

* See C. B. translation.

** Original Russian pagination. See C. B. translation.

DEPENDENCE OF NORMAL AND SHEARING STRESSES UPON THE VALUE OF DEFORMATION AT THE TRANSITION FROM THE REST STATE TO THE STATIONARY FLOW OF A GEL OF ALUMINUM NAPHTHENATE

A. A. Trapeznikov, A. S. Morozov, and G. G. Petrzhik

Institute of Physical Chemistry, Academy of Sciences, USSR
(Presented by Academician S. I. Vol'fkovich, March 24, 1960)
Translated from Doklady Akademii Nauk SSSR, Vol. 133, No. 3, pp. 637-640, July, 1960
Original article submitted March 18, 1960

Weissenberg showed that in various colloid systems and solutions of polymers, stresses orthogonal to the lines of current arise upon shearing [1]. One of the manifestations indicated by Weissenberg of these stresses is the rising of non-Newtonian liquids along the walls of an internal cylinder or stem in the gap between two coaxial cylinders contrary to centripetal and gravitational forces. This effect was investigated also in [2].

Starting with Weissenberg, who used a rheogoniometer, in many subsequent works of a theoretical or experimental nature [3-7] the effect of normal stresses in elastic liquids was considered during the stationary flow of the system without considering the peculiarities of the stage of deformation preceding the achievement of the stationary state. The general opinion is that the system would obey the law of a Hooke (neo-Hooke) body for any deformation and rate of deformation (experimentally not less than 100-300 sec $^{-1}$) which are reached in the stationary flow. Thus, no account is taken of the special value of the initial and intermediate regions from rest to stationary flow, although they are characterized by the disturbance of the structure, and by the influence of this factor on the values of the rheologic constants. This can be attributed to the fact that, according to the opinion of Weissenberg and his followers [5-8], in elasticoviscous non-Newtonian liquids, i.e., in systems flowing with even the smallest shearing stresses, the anomaly of the viscosity is not related to disturbances of the structure, but is only a consequence of a pure orientational (geometric) factor, related to the deviation between the directions of the stress ellipsoid and of the ellipsoid of the deformation rates [5-7]; this, in its turn, can be ascribed to the presence of an elastic deformation in the liquid. However, as a rule, the latter is only calculated in an indirect way from the ratio of the normal and tangential stresses or from the orientation angle and is not measured by a direct method. However, according to Reiner [9], the existing explanations of the mechanism of Weissenberg's effect are certainly not final.

In the work of our laboratory a special attention was given just to the initial state of development of deformation and to the transition from the rest state to a stationary flow for flowing systems, which were called liquid-plastic systems [10]. In investigations carried out before, only concerning shearing deformations, it was shown that for deformation rates higher than some critical rate ($\dot{\epsilon} > \dot{\epsilon}_k$), many systems begin to behave as a rigid body, which has the limit of structural stability P_r. It was noted, in particular, that a lowering of the viscosity (anomaly) is related principally to a disturbance of the structure. In connection with this it is interesting to mention that an attempt recently undertaken by Jobling [5, 6] to correct the increase of the viscosity by a correction on the orientation factor calculated from the normal stresses according to Weissenberg led only to a partial, in some cases very weak, increase of the calculated viscosity.

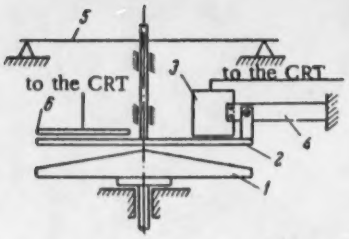

Fig. 1.

In [11] it was noted that visual observations of the rising of a gel or of the solution of a polymer subjected to a shearing stress, along the stem of the internal cylinder in an elastoviscosimeter or an elastorelaxometer, indicated that it started and reached its maximum value only after passing through the stability limit of the structure, P_r, or through the deformation ϵ_m corresponding to the maximum elastic deformation $\epsilon_{e\,max}$, i.e., in the region where the structure of the system is already appreciably distorted. According to this it was assumed that the maximum value of the normal stress P_{nr} would develop only after the passage through the limit of shearing stability and after an appreciable disturbance of the structure. Direct measurements of the elastic deformations of the system, which are a very important characteristic of it, were made possible by the elaboration of special methods and devices [11, 12].

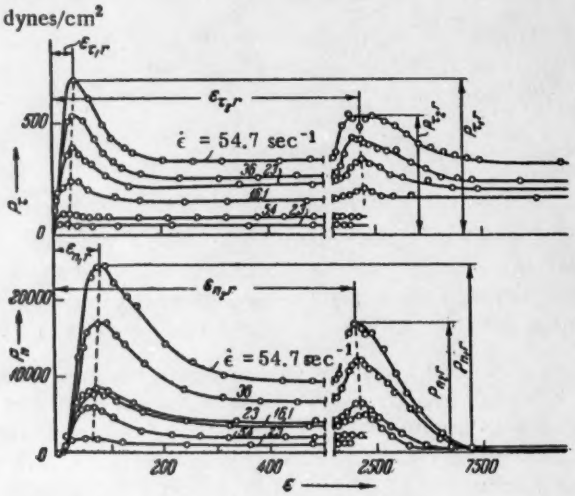

Fig. 2.

The present paper reports a study which was undertaken with the purpose of investigating quantitatively the development of normal stresses during time and depending upon the value of the deformation when there was a continuous transition from the rest state to a stationary flow. A 2% gel of aluminum naphthenate in vaseline oil was investigated; this was one of the gels investigated before [13], aged for three years.

For a simultaneous measurement of the normal stress P_n and of the shearing stress P_τ, a rheogoniometric attachment was built for the elastoviscosimeter which had been used before in our laboratory for investigating shearing stresses. The scheme of the attachment is shown in Fig. 1. The attachment was based on a cone-disc combination (1 and 2), whose diameters were 75 mm. The angle of the conic gap was $\alpha = 3°20'$. The apparatus provided the possibility of measuring simultaneously the vertical displacement of the disc under the action of a normal force F_n and the rotation of the disc under the action of a torsional momentum due to the tangential force F_τ. As dynamometers we used two flat steel springs mutually perpendicular and acting independently, which work by bending (4 and 5). The deflection of the springs was measured by means of two independent capacitor outputs (3 and 6) on a resonance circuit and recorded on a self-recording electronic potentiometer ÉPP-09 or on a loop oscillograph MPO-2. The springs had been graduated previously. The accuracy of the evaluation of the disc displacement was no less than 0.00025 mm. The complete deflection of the springs did not exceed 0.02 mm. The constancy of the deformation rate and its control were ensured by the elastoviscosimetry which switched on through an electromagnet a starting muff.

Figure 2 gives the dependence of the tangential and average normal stress upon the value of the relative

shear deformation ϵ for various deformation rates. The value of $\epsilon = \theta / \operatorname{tg}\alpha$ was calculated from the angle $\theta = \Omega t$ described by the cone during the time t with an angular velocity Ω. The shearing stress was calculated as $P_\tau = 3M/2\pi R^3$ (P_τ corresponds to P_{12} of [5-7]), M is the torsional momentum, R is the radius of the conic gap filled by the gel. The mean normal stress $P_n = 2F_n/\pi R^2$ which, according to [5-7], is the difference of the components of the normal stress $P_n = P_{11} - P_{22}$, was calculated from F_n, the total vertical force, measured with a dynamometer.

From the values of the established tangential stress the viscosity $\eta = P_{\tau s}/\dot{\epsilon}$ was calculated; as usual, it decreased with an increase of $\dot{\epsilon}$ (Fig. 3, 1). For the mean normal stress, one can introduce formally the equivalent ratio $P_{ns}/\dot{\epsilon}$, whose dependence upon $\dot{\epsilon}$ (for the two sections of Fig. 2) is shown by the curves 2 (ϵ = 450) and 3 (ϵ = 10,000). (The symbol s indicates that P_n, P_τ are taken for a stationary flow.) In calculating the value of P_{ns} a correction for the force of inertia decreasing the normal force was introduced; this correction had not been introduced in the data of the curves of Fig. 2, and therefore the latter parts of these curves after the second maximum for higher values of $\dot{\epsilon}$ lie lower than for lower values of $\dot{\epsilon}$.

Figure 2 shows that the curves for both the tangential and the normal stresses have two maxima. Previously, in work concerning the study of shearing stresses in aluminum naphthenate [10-13], one maximum of stability of the structure was described: the maximum arose in the initial part of the deformation, i.e., before the establishment of a stationary flow, although in investigations by A. A. Trapeznikov and T. G. Shalopal'kina in 1955 (unpublished) also a second maximum was observed for high deformations on the curves of shearing stresses. The second maximum, which can now be denoted as $P_{\tau_2 r}$, was lower than the first maximum $P_{\tau_1 r}$. These data, with reference to an aged 2% solution of a sample other than that investigated here, are presented in Fig. 4. It was suggested that the appearance of the second maximum could be related to the attainment of a breaking deformation ϵ_r for the bottom cylindrical part of the gel, in agreement with what was shown in the examination of the maximum elastic deformation $\epsilon_{e\ max}$ [11]. The measurement in a conic gap excludes the possibility of such an explanation, and, consequently, the appearance of the second maximum is related to the presence of special structural changes of the gel.

Comparing the curves of Fig. 2, one should note first of all that the first maximum of the tangential stress, $P_{\tau_1 r}$, corresponds roughly to $\epsilon_{\tau_1 r} \approx 40$, and the first maximum of the normal stress, $P_{n_1 r}$, lies at $\epsilon_{n_1 r} \approx 80$, i.e., the highest normal stress $P_{n_1 r}$ corresponds to the central part of the decreasing branch of the curve describing the tangential stress. Thus, the highest normal stress corresponds to a degree of disruption of the structural network of the system, which is already quite high.

A further deformation of the system leads, after some decrease of both the stresses under consideration, to a new increase of their values. The increase of the stress continues till $\epsilon \approx 1750$, exceeding by factors of 40 and 20 respectively the above mentioned breaking deformations. For this deformation, maxima are observed at the same time on the curves of both stresses. It is interesting to note that the established value of the tangential stress $P_{\tau s}$ is approximately equal to its value in the interval between the two maxima $P_{\tau_1 r}$ and $P_{\tau_2 r}$, whereas the established value of the actual stationary normal stress P_{ns} is very small in comparison with the value of the same stress between the two maxima. The observation of the flowing system was continued up to $\epsilon \approx 40{,}000$.

The experimental data show that for a large ϵ (>1700) the system structure undergoes changes which affect little the values of the tangential stress, but affect very strongly the normal stress.

One may suppose that the normal stresses are related to a very large extent to the "irregularities" and to the "topography" (interlocking) of the particles, when observed in a plane perpendicular to the plane of shearing. In order to shift one chain with respect to another in the plane of shearing, it is necessary to separate to some extent the plane of its original position, i.e., to overcome the normal stresses. The longer and more bent the particles, i.e., the higher the elastic deformations of the system, the stronger must be the normal stresses arising upon shifting. The second maximum of either stress (tangential and normal) may be related to the disruption of structure "residues", formed after the first collapse of the initial network (after the first maximum) and gradually oriented in the flow. Of course, it is possible that particles with free cohesion forces (for polymers, maybe radicals?), formed after the first collapse of the initial structure, form a new structure after combining in new places: the deformation and collapse of this new structure would cause the appearance of the second maximum. According to these considerations, the constancy of the values of $\epsilon_{\tau_2 r}$ and of $\epsilon_{n_2 r}$ for the different values of $\dot{\epsilon}$ used here should be attributed to similar dimensions and to identical orientation conditions for the structural elements.

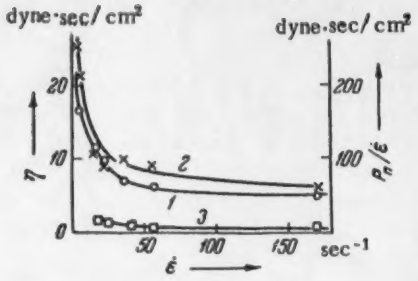

Fig. 3.

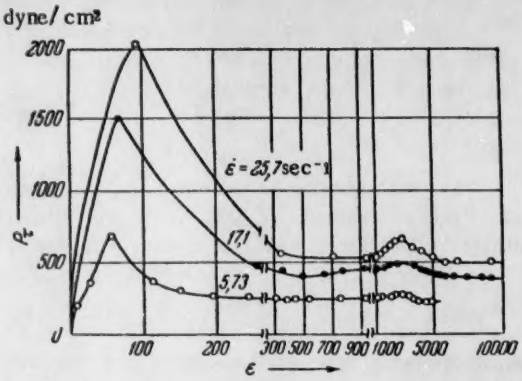

Fig. 4.

This interpretation is preliminary, pending further investigations. One must remark that the action of normal stresses in the shearing of elasticoviscous systems has an important practical significance.

In conclusion, the authors express their gratitude to T. G. Shalopalkina for her permission to use data obtained by her.

LITERATURE CITED

1. K. Weissenberg, Proc. 1st Intern. Congr. Rheologie (Amsterdam, 1948), Vol. 1, p. 29.
2. A. F. H. Ward and P. Lord, 2nd Intern. Congr. Rheologie (Oxford, 1953) (London, 1954), p. 214.
3. M. Mooney, J. Coll. Sci. 6, 96 (1951).
4. N. Pilpel, Trans. Farad. Soc. 50, 1369 (1954).
5. A. Jobling, J. Oil and Color Chem. Assoc. 38, 739 (1955).
6. A. Jobling and I. E. Roberts, Rheologie, Theory and Applications, Ed. F. R. Eirich (New York, 1958), Vol. 2, p. 503; J. Polym. Sci. 36, 421, 433 (1959).
7. W. Philippoff, J. Appl. Phys. 27, 984 (1956); W. Philippoff, F. H. Gaskins, and J. G. Brodnyan, J. Appl. Phys. 28, 1118 (1957); Trans. Soc. Rheol. 1, 95, 109 (1957).
8. B. Rabinowich, Z. phys. Chem. A 145, 1 (1929); A 166, 257 (1933); R. Eisenschitz, Koll. Z. 64, 184 (1933); Z. phys. Chem. A 158, 78 (1931); W. Philippoff, Viscosität der Kolloide (Dresden, 1942).
9. M. Reiner, Handb. d. Phys. (Marburg, 1958), Vol. 6, p. 516.
10. A. A. Trapeznikov, V. A. Fedotova, Doklady Akad. Nauk SSSR 81, 1101 (1951); 82, 97 (1952); 95, 595 (1954); A. A. Trapeznikov, and T. G. Shalopalkina, Koll. Zhur. 17, 471 (1955).*
11. A. A. Trapeznikov, Koll. Zhur. 21, 107 (1959).*
12. A. A. Trapeznikov and T. G. Shalopalkina, Doklady Akad. Nauk SSSR 111, 380 (1956).*
13. T. G. Shalopalkina and A. A. Trapeznikov, Doklady Akad. Nauk SSSR 118, 994 (1958).*.

*Original Russian pagination. See C. B. translation.

CHEMISORPTION ON PURE AND DOPED NiS

Huang Yu-mei, N. P. Keier and S. Z. Roginskii,

Corresponding Member, Academy of Sciences, USSR

Physicochemical Institute, Academy of Sciences, USSR
Translated from Doklady Akademii Nauk SSSR, Vol. 133, No. 3, pp 641-644,
July, 1960
Original article submitted April 14, 1960

In catalysis one has to deal with semiconductors (s.c.) showing extrinsic, intrinsic or degenerate conductivity [1], but the electronic theory of catalysis and chemisorption on semiconductors generally takes only extrinsic semiconductors into consideration. With them were executed the classical experiments which have been performed to establish and test the theory. This made it interesting to extend the investigation to other types of s.c. Nickel sulfide was chosen as one of the substances to be investigated; above 78°K it shows, according to data in literature [2] and our own measurements [3], a degenerate conductivity decreasing at increasing temperatures. NiS crystallizes in an atomic lattice and, as regards chemical properties, it is fairly analogous to the thoroughly investigated nickel oxide which is very sensitive to doping. In this paper are stated the results obtained when investigating the chemisorption of O_2 and C_2H_2 on NiS with and without added Li_2S or In_2S_3. In the s. c. investigated until now, O_2 is an acceptor, C_2H_2 a donor. In literature we did not find any data on the chemisorption of gases on NiS.

The method used for the preparation of pure and doped NiS has been described in a previous paper [3]. The presence of solid solutions was checked by x-ray measurements. When raising the indium concentration the lattice constants increase: a from 3.4199 to 3.4219, c from 5.3052 to 5.3064. The introduction of lithium into NiS has no influence on the lattice constants. This proves that In^{3+} gives solid solutions with NiS. Their formation has not been proved for Li_2S, but is very probable judging from the ease with which sulfides containing foreign cations are introduced into the lattice. We remark that for Li_2O in ZnO there is also no change in the lattice constants, although the change in electric conductivity leaves no doubt about the existence of solid solutions. For NiO–Li_2O with 1 at.% Li the change in the lattice constants lies within the limits of accuracy. Upon dissolving lithium sulfide or indium sulfide in NiS the specific resistivity of nickel sulfide does not change noticeably, which is only natural, if one considers the metallic character of the conductivity of this sulfide and the high carrier concentration. The specific surface area was determined by the BET method from the krypton adsorption isotherm.

The adsorption was investigated by following the pressure drop in a vacuum apparatus. When the pressure was reduced to 10% of the initial value, a fresh amount of gas was admitted raising the pressure to the initial value; this was repeated several times as the adsorption went on. The sulfide was protected against mercury and grease vapors by two U-shaped traps one of which was sealed to the quartz reactor.

The adsorption of oxygen. We investigated NiS, NiS–Li_2S containing 0.2, 0.5 and 1 at.% lithium cations (calculated on the total number of cations) and solid solutions of NiS–In_2S_3 containing 0.5 and 1 at.% indium cations. The adsorption of oxygen was measured in the temperature range 25-65° to avoid the oxidation of the sulfide which takes place at higher temperatures. Before the measurements the catalyst was outgassed at 450° during 1.5 hour at a pressure of 10^{-5} mm Hg.

The adsorption of oxygen did not noticeably influence the electric conductivity.

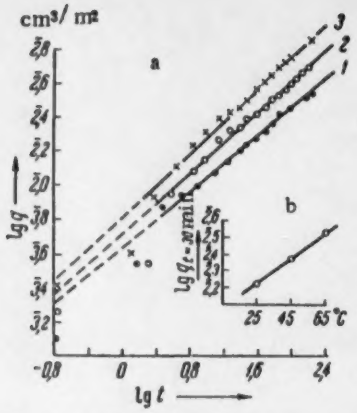

Fig. 1.a) The kinetics of oxygen adsorption on NiS: 1) at 25°, 2) at 45°, 3) at 65°; b) the isochrone of oxygen adsorption.

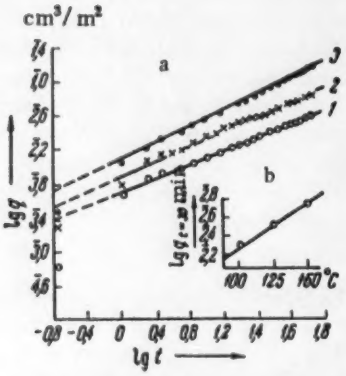

Fig. 3.a) The kinetics of acetylene adsorption on NiS: 1) at 100°, 2) at 125°, 3) at 150°; b) acetylene adsorption isochrone.

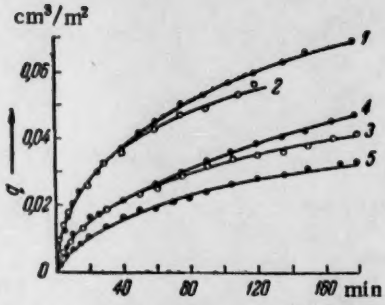

Fig. 2. The adsorption of oxygen at 65°: 1) on NiS, 2) on NiS (0.2 at.% Li), 3) on NiS (1 at.% Li), 4) on NiS (0.5 at.% In), 5) on NiS (1 at.% In).

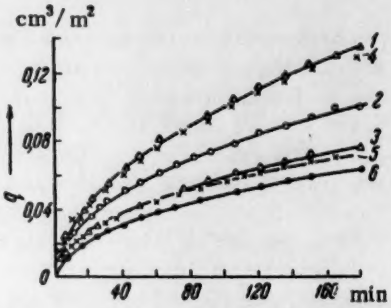

Fig. 4. The adsorption of acetylene at 150°. 1) On NiS, 2) on NiS (0.2 at.% Li), 3) on NiS (1 at.% Li), 4) on NiS (0.2 at.% In), 5) on NiS (0.5 at.% In), 6) on NiS (1 at.% In).

It may be seen from Fig. 1a that the isothermal oxygen adsorption, the very start excepted, follows the kinetic equation [4]

$$q = At^{1/n}. \qquad (1)$$

From Table 1 it is obvious that the values found for 1/n and A increase at increasing temperatures.

In Fig. 1b is plotted the kinetic isochrone of oxygen adsorption, that is, the amount adsorbed after a given time (t = 30 min) in the coordinates log $q_{t=\text{const}}$ and T. Since the points lie on a straight line, the isochrone may be represented by

$$q = q_0 \cdot e^{\beta T}. \qquad (2)$$

Equations (1) and (2) are characteristic for a heterogeneous surface with an exponential distribution of sites [5] with respect to E

$$\rho(E) = H \cdot e^{\alpha E}; \qquad (3)$$

TABLE 1

The Temperature Dependence of A and 1/n for the Oxygen Adsorption on NiS

Temp. °C	A, $cm^3/m^2 \cdot min^{-1}$	1/n
65	$7,4 \cdot 10^{-3}$	0,47
45	$5,8 \cdot 10^{-3}$	0,44
25	$4,7 \cdot 10^{-3}$	0,40

TABLE 2

Temp. °C	A, $cm^3/m^2 \cdot min^{-1}$	1/n
150	$1,1 \cdot 10^{-2}$	0,47
125	$7,2 \cdot 10^{-3}$	0,44
100	$4,5 \cdot 10^{-3}$	0,40

TABLE 3

The Values of the Parameters α and H, which Characterize the Distribution Function with Respect to E, and the Values of k_0 for the Oxygen Adsorption on the Sulfide and its Solid Solutions

Sample	$\alpha \cdot 10^3$, cal/mole	$H \cdot 10^7$, cal/mole	$k_0 \cdot 10^{-3}$, min^{-1}	Sample	$\alpha \cdot 10^3$, cal/mole	$H \cdot 10^7$, cal/mole	$k_0 \cdot 10^{-3}$, min^{-1}
NiS	0,69	1,1	4,2	NiS (1 at. % Li)	0,71	1,8	0,2
NiS (0,2 at. % Li)	0,69	0,9	4,2	NiS (0,5 at. % In)	0,82	0,13	10,0
NiS (0,5 at. % Li)	0,71	1,3	1,0	NiS (1 at. % In)	0,81	0,07	29,0

TABLE 4

Activation Energy Values for the Adsorption of C_2H_2, kcal/mole (100-150° C)

Surface coverage, cm^3/m^2	NiS (1 at. % Li)	NiS (0,5 at. % Li)	NiS (0,2 at. % Li)	NiS	NiS (0,2 at. % In)	NiS (0,5 at. % In)	NiS (1 at. % In)
$6,3 \cdot 10^{-3}$	8,6	10,3	12,5	12,9	13,5	12,2	12,5
$7,9 \cdot 10^{-3}$	9,0	10,7	13,0	13,2	14,0	12,6	12,9
$1,0 \cdot 10^{-2}$	9,5	11,1	13,7	13,8	14,4	13,1	13,3
$1,3 \cdot 10^{-2}$	9,9	11,4	13,8	14,2	14,9	13,5	13,7
$1,6 \cdot 10^{-2}$	10,3	11,8	12,2	14,6	15,3	13,9	14,1
$2,0 \cdot 10^{-2}$	10,7	12,2	14,7	15,0	15,7	14,4	14,4
$2,5 \cdot 10^{-2}$	11,1	12,6	15,1	15,4	16,2	14,8	—

α and H calculated from the adsorption rate at constant temperature [4] do not depend on T and are equal to: $\alpha \cong 0.69 \cdot 10^{-3}$ $(cal/mole)^{-1}$ and $H \cong 1.1 \cdot 10^{-7}$ (mole/cal).* In Fig. 2 the kinetic curves for isothermal oxygen adsorption on nickel sulfide and its solid solutions are compared. It may be seen that the introduction of Li_2S as well as of In_2S_3 into NiS lowers the specific adsorption rate of oxygen, but that in all cases the adsorption kinetics follow the same Equation (1); besides, the introduction of Li_2S or In_2S_3 into nickel sulfide does not alter the type of distribution function but changes the parameters α and H of the exponential distribution. The values of α and H do not depend upon temperature within the limits of accuracy. In Table 3 are given the mean values of these parameters for nickel sulfide and for its solid solutions with lithium or indium sulfide.

From Table 3 it is obvious that α slightly increases when indium sulfide is dissolved in nickel sulfide, and that it scarcely changes when lithium sulfide is dissolved. The pre-exponential factor k_0 in the adsorption rate constant decreases when lithium is dissolved, and increases when indium sulfide is dissolved. The variation in the distribution function parameter H has the effect that the activation energies at a given coverage of the surface

*These figures are very approximate, because the small range of t does not allow an accurate determination.

with oxygen vary on these samples. They are slightly lower on the sample NiS (1 at.% Li) and somewhat higher on the sample NiS (1 at.% In) when compared with NiS.

The adsorption kinetics and the exponential isochrone $q = q_0 \cdot e^{\beta T}$ make it very probable that the change in the activation energy of adsorption is caused by the heterogeneity of the surface.

However, without experiments on the kinetics of isotopic exchange between tagged adsorbed molecules and molecules in the gas and without measurements of the free energy change at adsorption it is impossible to eliminate the possibility that the change in E may be a consequence of an interaction (repulsion) caused by a charge.

The introduction of Li_2S into NiS causes a decrease in the activation energy of oxygen adsorption at a given coverage. The solution of In_2S_3 in NiS increases the activation energy. When dissolving Li_2S the pre-exponential factor k_0 decreases and upon dissolving In_2S_3 the said factor k_0 increases.

The adsorption of acetylene. The adsorption of acetylene on nickel sulfide, on NiS–Li_2S containing 0.2, 0.5 and 1 at.% lithium and on NiS–In_2S_3 containing 0.2, 0.5 and 1 at.% indium was measured at the temperatures 100°, 125°, and 150°. The catalyst was outgassed in the same way as was done for the oxygen adsorption. The adsorption of acetylene also has no influence on the electric conductivity. In Fig. 3a the kinetic curves for the isothermal adsorption of acetylene on NiS are plotted in the coordinates log q and log t. It may be seen that they satisfy the Relation (1), just as oxygen adsorption does.

In Table 2 are given the values of 1/n and A, which increase when the temperature is raised.

In Fig. 3b the isochrone for the adsorption of C_2H_2 on NiS is given in the coordinates $\log q_{(t=\text{const})}$ and the temperature. The points of the isochrone plotted in this way lie on a straight line. This isochrone, just as that of oxygen adsorption, satisfies Equation (2). This shows that in this case also the distribution function of the active sites is of the exponential type (3). The values of α and H practically do not depend upon temperature.

Dissolution of Li_2S or In_2S_3 in nickel sulfide does not change the shape of the kinetic curves for isothermal acetylene adsorption.

In Fig. 4 are given the kinetic curves of isothermal acetylene adsorption on 1 m^2 surface area. The introduction into NiS of Li_2S as well as of In_2S_3 lowers the acetylene adsorption rate. The addition of Li_2S or In_2S_3 to NiS lowers the value of A calculated from Equation (1). When dissolving Li_2S in NiS, 1/n does not change; when dissolving In_2S_3 it increases, that is, α gets higher. In Table 4 are given the values of E, which have been calculated at various coverages from the equation

$$E = RT \ln(t/t_0)[4]. \qquad (4)$$

In all cases they increase with increasing coverage.

From Table 4 it follows that the addition of Li_2S to NiS lowers the activation energy of adsorption at a given surface coverage and that the introduction of In_2S_3 has practically no influence on the said energy.

The dependence of the activation energy upon the degree of coverage is described by the relation

$$E_{ads} = 22.5 + 4.4 \log q \text{ kcal/mole}.$$

The distribution function of the active sites with respect to the activation energy for the acetylene adsorption on NiS is equal to

$$\varphi(E_{ads}) = 0.25 \cdot 10^{-8} e^{0.55 \cdot 10^{-13} E_{ads}}.$$

LITERATURE CITED

1. O. V. Krylov and S. Z. Roginskii, Doklady Akad. Nauk SSSR 118, 3, 526 (1958).*
2. K. Hauffe and H. G. Flindt, Z. Phys. Chem. 200, 199 (1952).
3. N. P. Keier, S. Z. Roginskii, and Huang Yu-mei, Doklady Akad. Nauk SSSR 133, 2 (1960).**
4. S. Z. Roginskii, Adsorption and Catalysis on Heterogeneous Surfaces [in Russian] (Izd. AN SSSR, 1948).

* Original Russian pagination. See C. B. translation.

** See C. B. translation.

5. S. Z. Roginskii, Izvest. Akad. Nauk SSSR, Otdel. Khim. Nauk, 1, 14 (1945).
6. S. Z. Roginskii and O. M. Todes, Acta Physicochim. URSS 21, 519 (1946).
7. S. Z. Roginskii, Zhur. Fiz. Khim. 32, 737 (1958).
8. N. P. Keier, Problems of Kinetics and Catalysis [in Russian] (Izd. AN SSSR, 1957), 9, p. 283.

EFFECT OF METAL AND SOLVENT ON THE FORMATION OF AROMATIC ANION-RADICAL POLYMERIZATION INITIATORS

E. A. Yakovleva, É. S. Petrov, S. P. Solodovnikov,

Corresponding Member Acad. Sci. USSR V. V. Voevodskii,

and A. I. Shatenshtein

L. Ya. Karpov Institute of Physical Chemistry and Institute of Chemical Physics, Academy of Sciences, USSR

Translated from Doklady Akademii Nauk SSSR, Vol. 133, No. 3, pp. 645-648, July, 1960

Original article submitted March 22, 1960

In recent years great attention has been paid to anion-radicals arising as a result of the transfer of an electron from an alkali metal to an organic molecule. Such anion-radicals may initiate polymerization leading to the formation of so-called "living" polymers [1]. It is important to know how the formation conditions of anion-radicals and their stability change in relation to the metal, and also the properties and structure of the solvent molecules. However, available literature information is sparse and fragmentary [2, 3].

Only anion-radicals of polycyclic hydrocarbons have been investigated up to now and sodionaphthalene in 1,2-dimethoxyethane or in tetrahydrofuran is usually used to initiate polymerization, following Scott [4] and Szwarc [5]. It was recently shown [6, 7] that it is possible to prepare anion-radicals of benzene and its homologs by reaction with metallic potassium in dimethoxyethane. Monocyclic hydrocarbons have a lower affinity for an electron than polycyclic hydrocarbons [8] and therefore are more suitable for differentiating the effect of various factors on the formation of anion-radicals.

In the present work we studied the effect of the metal and solvent on the formation of aromatic anion-radicals on the example of benzene and toluene, using the following solvents: 1,2-dimethoxyethane (DME), 1,2-methoxyethoxyethane (MEE), 1,2-diethoxyethane (DEE), tetrahydrofuran (THF), and 1,3-dioxane (DO). We used electron paramagnetic resonance to detect the anion-radicals and determine their stability. The ethers of ethylene glycol were synthesized according to [9 and 10] and 1,3-dioxane was prepared according to [11]. The preparations were fractionated and then boiled for a long time with metallic sodium. The following procedure was used for preparing anion-radicals. A system of ampoules was attached to a high-vacuum apparatus. The ampoules were pumped out and heated, well flushed with carefully purified nitrogen, and again evacuated and then a potassium mirror deposited on their inner surfaces. One of the ampoules contained frozen solvent (1 ml) mixed with hydrocarbon (0.03 ml). This mixture was distilled several times from ampoule to ampoule onto a freshly sprayed potassium mirror. After this purification, the mixture was distilled into a special ampoule onto a metallic mirror surface and the ampoule sealed off. The ampoule was fitted with a special side-arm for measuring the paramagnetic absorption. The electron paramagnetic resonance spectra were measured on the instrument described in [12]. The nature of the electron paramagnetic resonance spectrum [8] was the same for all the solvents and metals studied. The relative concentration of anion-radicals in the solution was determined from the intensity of the same component of the spectrum.

In experiments with benzene, its concentration was about 0.4 mole per liter of solution and the temperature

Relation of the Concentration of Anion-Radicals to the Solvent and Metal (0.4 mole of toluene per liter of solution at about −30°)

Solvent	Metal	C	Solution color	Solvent	Metal	C	Solution color
DME	K	100	Blue-green	MEE	Na	1,5	Colorless
MEE	K	30	Green	DEE	Na	0	Colorless
DEE	K	3	Almost colorless	DO	K	1	Yellow•
THF	K	0,4	Blue				

• As anion-radicals of toluene are formed with difficulty in 1,3-dioxane, the experiment was carried out with benzene. The value of C was calculated with allowance for the difference in the number of components in the electron paramagnetic resonance spectra of benzene and toluene.

Fig. 1.

Fig. 2.

was −30°. Potassium in DME gave a concentration of anion-radicals 4-5 times greater than in DEE. Equilibrium was reached both at higher and at lower temperatures. When sodium was used instead of potassium, in DEE the concentration of anion-radicals was at least two orders lower, which may be partly due to the fact that equilibrium was reached with greater difficulty. Parallel experiments at −70° with lithium and sodium in DEE showed that a considerably higher concentration of anion-radicals of benzene was formed with lithium than with sodium.• We should note that solutions of sodium-benzene, lithium-benzene, and potassium-benzene in DEE have a yellow color in contrast to the green solutions of the latter compound in DME. This is apparently due to the fact that potassium dissolves in DME at low temperature and the blue color of its solution is superposed on the yellow color of the anion-radical.

Experiments with toluene, which has a lower affinity for an electron than benzene, made it possible to characterize more clearly the effect of the above solvents on the formation of anion-radicals. Table 1 gives approximate data which make it possible to assess the relative concentrations of anion-radicals of toluene. The value C expresses the concentration of anion-radicals relative to their concentration in a DME solution of potassium-toluene, which was arbitrarily taken as 100.

In combination with the results given above on the formation of anion-radicals of benzene, the table,

• In the note [8] it was reported that sodium does not add to benzene at all.

makes it possible to draw the following conclusions.

1. Anion-radicals of benzene may be prepared by reaction with Li, Na, and K, and with potassium they are formed in DME, MEE, DEE, THF, and DO.

2. Replacement of the methyl group by an ethyl group in the diether of ethylene glycol reduces the stability of the anion-radicals, which falls in the series DME, MEE, and DEE.

3. The compound of the aromatic hydrocarbon (benzene) with sodium is formed with greater difficulty than those with potassium and lithium.

A comparison of our results with literature data on the solubility of alkali metals in ether [13, 15] shows that there are common traits in the solution of the metals and their reaction with aromatic hydrocarbons. Thus, for example, the solubility of the K–Na eutectic alloy in ethers of ethylene glycol and the stability of the anion-radicals fall in the series DME, MEE, and DEE [13]. Apparently, both processes depend on the solvation of the metal cation, caused by the electron-donor capacity of the oxygen atoms of the solvent molecule with a favorable steric disposition of the atoms in it. Replacement of the methyl groups by ethyl groups in the ethylene glycol ether may create steric hindrance to solvation of the cation.

As regards comparison of the metals, judging by available literature data [13, 14], Li and Na are insoluble even in DME in contrast to K, Rb, and Cs. This may be connected with the higher value of the ionization potential of the first two metals, but as Cafasso and Sundheim reported [14], individual peculiarities are observed in the sequence of solubilities of alkali metals in different solvents. In addition, observations reported in the literature require further checking.*

We carried out a series of experiments on the initiation of styrene polymerization with a solution of potassium-benzene in DME, MEE, and DEE.**

The solutions formed had a red or red-violet color and in a number of cases they showed paramagnetic absorption. The electron paramagnetic resonance spectrum showed a narrow singlet on the background of a broad band (Fig. 1). The electron paramagnetic resonance spectra were obtained at room temperature when potassium-benzene is unstable and does not give a signal. In the initiation of polymerization with a solution of potassium in DME without benzene,*** in a number of experiments we obtained solutions with a green color (at temperatures of the order of −50 to −80°), whose electron paramagnetic resonance spectra at low temperature showed a quintuplet (Fig. 2). This may be due to the formation of an anion-radical as a result of the addition of an electron to the aromatic ring of polystyrene, giving a product similar in structure to the anion-radical of a monoalkylbenzene. The spectra illustrated here differ from the electron paramagnetic resonance spectra of anion-radicals of polystyrene obtained by Japanese authors under somewhat different conditions [16]. The work is being continued.

We would like to thank Yu. P. Vyrskii, E. A. Kovrizhnykh, and A. K. Rusanov for the help given.

LITERATURE CITED

1. M. Szwarc, in the book, Advances in Chemical Physics, Ed. by J. Prigogine (1959).
2. N. D. Scott, J. F. Walker, and V. J. Hansley, J. Am. Chem. Soc. 38, 442 (1936).
3. A. N. Pudovik and A. A. Muratova, Uch. Zap. Kazansk. Gos. Univ. im. V. I. Ul'yanova-Lenina 113, 8, 7 (1953).

* With very careful purification of DME, we obtained a blue solution of Li at low temperature and E. A. Kovrizhnykh observed a blue color from contact of DME with a Na mirror at low temperature. Spectral analysis, which was kindly carried out in A. K. Rusanov's laboratory, showed that the sodium contained less than 0.01% of potassium.

** The polymer samples had molecular weights of 350,000-700,000 and $[\eta] = 1.0$-2.0 in benzene solution. The measurements were carried out by Yu. P. Vyrskii.

*** When these experiments on polymerization with an ether solution of a metal had been carried out, we learned of the brief communication of Dainton and his co-workers on analogous work [15].

4. N. D. Scott, U. S. Patent No. 2181771 (1939).
5. M. Szwarc, Nature 178, 1168 (1956); J. Am. Chem. Soc. 78, 2656 (1956).
6. T. R. Tuttle and S. J. Weissman, J. Am. Chem. Soc. 80, 5342 (1958).
7. V. V. Voevodskii, S. P. Solodovnikov, and V. M. Chibrikin, Doklady Akad. Nauk SSSR 129, 1082 (1959).*
8. L. E. Lyons, Nature 166, 193 (1950).
9. J. V. Capinjola, J. Am. Chem. Soc. 67, 1615 (1945).
10. M. H. Palomaa and J. Honkanen, Ber. 70, 2199 (1937).
11. B. A. Arbuzov and V. S. Vinogradova, Izvest. Akad. Nauk. SSSR, Otdel. Khim. Nauk, 291 (1950).
12. N. N. Bubnov and A. G. Semenov, Pribory i Tekh. Eksp. 1, 92 (1959).
13. J. L. Down, J. Lewis, B. Moore, and G. Wilkinson, J. Chem. Soc., 3767 (1959).
14. F. Cafasso and B. R. Sundheim, J. Chem. Phys. 31, 809 (1959).
15. F. L. Dainton, D. M. Wils and A. N. Wright, Symposium über Makromolekule (Wiesbaden, III sect. A, 1959) p. 7.
16. K. Hirota, K. Kuwata, and K. Mirigaki, Bull. Chem. Soc. Japan 31, 538 (1958); 32, 99 (1959).

* Original Russian pagination. See C. B. translation.

EFFECT OF SPECIFIC RADIOACTIVITY OF CERIUM OXALATE ON ITS SOLUBILITY

Academician Vikt. I. Spitsyn, and N. G. Moshchanskaya

Institute of Physical Chemistry, Academy of Sciences, USSR
Translated from Doklady Akademii Nauk SSSR, Vol. 133, No. 4, pp. 859-861, August, 1960
Original article submitted April 29, 1960

On the basis of [1 and 2] and many later papers, radioactive tracers have been used widely for determining the solubility of sparingly soluble substances. If the solubility of compounds is very low, it is necessary to use preparations of high specific activity. However, as recent investigations have established [3-7], the radioactive radiation of solids has a considerable effect on their physicochemical properties. In particular, V. I. Spitsyn, E. A. Torchenkova, and I. N. Glazkova [8] found that the kinetics of solution of barium sulfate and its actual solubility in water depend on the specific radioactivity of $BaSO_4$ preparations containing S^{35}.

In the present work we studied the effect of the specific radioactivity on the water solubility of cerous oxalate labeled with Ce^{144}. The radioactive isotope of cerium Ce^{144} (maximum energy of β-radiation ~0.3 Mev) has a half life of 282 days and forms a short lived daughter isotope Pr^{144} ($T_{\frac{1}{2}}$ = 17.5 min) with a maximum energy of the β-radiation of 2.97 Mev. We used preparations with four activity levels: 0.0075, 0.046, 0.495, and 4.3 mC/g.

The cerium oxalate samples were prepared under identical conditions by precipitation from an acid (0.5 N with respect to HCl) solution of $CeCl_3$ (pure according to x-ray spectral analysis), containing the radioactive isotope Ce^{141}, at the boiling point with a five-fold excess of oxalic acid. The precipitate obtained was heated at 70-80° for an hour. For better growth of the crystals, filtration was carried out after 24 hr. The precipitate was washed with water to a neutral reaction to methyl orange. After drying in air, the preparations thus obtained corresponded to the hydrate $Ce_2(C_2O_4)_3 \cdot 10H_2O$ in all cases. The cerium content was determined by firing the original oxalate to CeO_2 at 700-800°. The oxalate ion was determined by titration of a hot sulfuric acid solution containing an accurately weighed sample of cerium oxalate with potassium permanganate solution. The water of crystallization content was calculated by difference.

To determine the solubility, we placed 10 mg of cerium oxalate and 80 ml of doubly distilled water in a vessel fitted with a spiral stirrer and an oil seal. The experiments were carried out in a thermostat at 25°. As a rule, saturation was reached after 80-100 hr stirring. Before the removal of a sample, stirring was stopped and the precipitate allowed to settle for 30 min. A solution sample was centrifuged carefully and 0.5 ml portions transferred with a micropipette to special aluminum dishes and then evaporated to dryness. The solution volume was varied from 0.5 to 5.0 ml, depending on the specific activity of the original salt. The minimal counting rate (allowing for background) was 10 counts/min. The solubility was calculated from the formula:

$$L = \frac{I_S Q_{st}}{I_{st} v_S} \cdot 1000, \qquad (1)$$

where L is the solubility in mg/liter, I_S is the activity of the solution in counts/min, v_S is the solution volume in ml, Q_{st} is the cerium oxalate content of the standard in mg, and I_{st} is the activity of the standard in counts/min. The standards were prepared by dissolving an accurately weighed sample of the original cerium oxalate in hydrochloric acid.

Solubility of $Ce_2(C_2O_4)_3 \cdot 10H_2O$ in Water at 25°

Specific activity (N)		Solubility (L), mg/liter
counts/min.g	mC/g	
$5{,}00 \cdot 10^8$	0,0075	0,87±0,02
$3{,}06 \cdot 10^7$	0,046	0,75±0,02
$3{,}30 \cdot 10^8$	0,495	0,50±0,04
$2{,}86 \cdot 10^9$	4,30	0,33±0,03

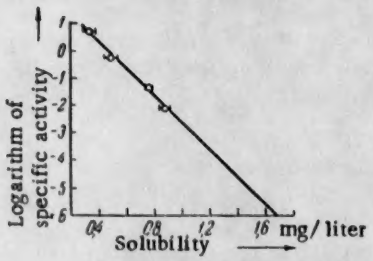

Water solubility of cerium oxalate of various specific activities at 25°.

The results of the four series of experiments are given in the Table and show that with an increase in the specific activity of cerium oxalate, its solubility determined with Ce^{144} as tracer decreases. The composition of the solid phase hardly changes.

As shown in the Figure, the solubility of cerium oxalate is linearly dependent on the logarithm of the specific radioactivity of the preparation and is expressed by the Equation :

$$\lg N = aL + b. \tag{2}$$

In actual fact, if the data in the Table are used for calculating the closeness of the relationship (R) between the solubility (L) and the specific activity (N) of cerium oxalate, we obtain R = 0.99, which indicates the direct functional relationship L = f(log N). The value of R was calculated from the formula

$$R = \frac{n\sum_1^n L \lg N - \sum_1^n L \sum_1^n \lg N}{\sqrt{\left[n\sum_1^n L^2 - \left(\sum_1^n L\right)^2\right]\left[n\sum_1^n (\lg N)^2 - \left(\sum_1^n \lg N\right)^2\right]}}, \tag{3}$$

where R is the closeness of the relationship, L is the solubility in mg/liter, N is the specific activity in mC/g, and n is the number of averaged experimental points. By using the method of least squares it is possible to calculate the parameters a and b in Equation (2) for analytical calculation of the solubility of cerium oxalate at any specific activity. The parameters in Equation (2) were calculated by the formulas:

$$a = \frac{n\sum_1^n L \lg N - \sum_1^n L \sum_1^n \lg N}{n\sum_1^n L^2 - \left(\sum_1^n L\right)^2}, \tag{4}$$

$$b = \frac{\sum_1^n L^2 \sum_1^n \lg N - \sum_1^n L \sum_1^n L \lg N}{n\sum_1^n L^2 - \left(\sum_1^n L\right)^2} \tag{5}$$

which gave the values a = −4.93 and b = 2.235.

By substituting the values of the parameters in Equation (2) it is possible to find the solubility at a very low specific activity. By assuming that $N = 1.0 \cdot 10^{-6}$ mC/g, we obtain L = 1.65 mg/liter.

Literature data on the solubility of cerium oxalate [9-11] disagree considerably; it lies within the limits of 0.55 and 1.45 mg/liter, calculated on the decahydrate. We may regard the most reliable solubility values as

1.32 and 1.45 mg/liter, which were obtained by volumetric and gravimetric methods, respectively [10, 11]. These values agree well with the calculation given above.

In conclusion we should note that the effect of the radiation of the radioactive tracer used on the solubility of sparingly soluble compounds must be considered in using tracer methods.

LITERATURE CITED

1. G. Hevesy and F. Paneth, Z. Anorg. Chem. 82, 323 (1913).
2. Vikt. I. Spitsyn, Zhur. Russ. Fiz. Khim. Obshchest. 49, 357 (1917).
3. Vikt. I. Spitsyn, Izvest. Akad. Nauk SSSR, Otdel. Khim. Nauk, 11, 1296 (1958);* Österr. Chem. Ztg. 60, 130 (1959).
4. Vikt. I. Spitsyn and I. E. Mikhailenko, Doklady Akad. Nauk SSSR 121, 319 (1958);* Atomnaya Énergiya 5, 463 (1958).*
5. A. A. Balandin, Vikt. I. Spitsyn, et al., Doklady Akad. Nauk SSSR 121, 495 (1958).*
6. Vikt. I. Spitsyn and V. V. Gromov, Doklady Akad. Nauk SSSR 123, 722 (1958);* Radiokhimiya 1, 181 (1959).
7. I. E. Mikhailenko and Vikt. I. Spitsyn, Doklady Akad. Nauk SSSR 131, 129 (1960).*
8. Vikt. I. Spitsyn, E. A. Torchenkova, and I. N. Glazkova, Doklady Akad. Nauk SSSR 132, 3 (1960).**
9. E. Rimbach and A. Schubert, Z. Phys. Chem. 67, 183 (1909).
10. R. J. Meyer and O. Hauser, Die Analyse der seltenen Erden und Erdsäuren (Stuttgart, 1912).
11. L. A. Sarver and P. H. M. P. Brinton, J. Am. Chem. Soc. 49, 943 (1927).

* Original Russian pagination. See C. B. translation.

** See C. B. translation.

THE INFLUENCE OF THE STATE OF THE DIFFUSION SIDE OF AN IRON MEMBRANE ON THE RATE OF DIFFUSION OF ELECTROLYTIC HYDROGEN

I. A. Bagotskaya and L. D. Kovba

Electrochemistry Institute, Academy of Sciences, USSR
(Presented by Academician A. N. Frumkin, March 17, 1960)
Translated from Doklady Akademii Nauk SSSR, Vol. 133, No. 4, pp 862-865, August, 1960
Original article submitted March 15, 1960

In the present work we have studied the influence of the state of the surface of the diffusion side of an iron membrane on the rate of diffusion of electrolytic hydrogen v_d, when the polarization conditions on the polarization side are kept constant. As far as we are aware, the literature contains no reports of the study of this problem for the case of an iron electrode. The method of carrying out the measurements, the preparation of the membrane, and the apparatus in which the measurements were made have been described earlier [1]. The diffusion of hydrogen was brought about by cathodic polarization, by a current of $50 \cdot 10^{-3}$ amp/cm^2, of the polarization side in a solution of redistilled HCl, containing traces of $Pb(NO_3)_2$, or in a solution of twice-redistilled 2 N H_2SO_4, containing traces of $Pb(NO_3)_2$ and Na_2S.* The diffusion side of the electrode was in contact with 1 N NaOH solution prepared from chemically pure alkali or from alkali obtained by decomposition of sodium amalgam with twice-distilled water and subsequent purification from traces of mercury by prolonged cathodic polarization at a large Pt electrode. The volumetric method previously described was used to determine the rate of diffusion of hydrogen v_d with cathodic polarization of the diffusion side by currents of $4 \cdot 10^{-6}$ and $2 \cdot 10^{-3}$ amp/cm^2. Since the value of v_d changes slightly with time even when the experimental conditions on the polarization and diffusion sides are kept constant, the measurements were carried out as follows. The diffusion side was subjected to low and high polarization in turn, for periods of 6 min in each case, and measurements were made of the quantity of hydrogen diffusing in 5 min, for a given cathodic polarization of the diffusion side. We determined v_d as the difference between the total quantity of hydrogen evolved from the diffusion side (v) and the quantity of hydrogen evolved from the diffusion side in accordance with Faraday's law (v_f) as a result of its cathodic polarization: $v_d = v - v_f$ (v_d was expressed in cm^3/min). In the case where the diffusion side had a pure iron surface – a surface activated by deposition of platinum or covered with an electrolytic deposit of nickel and copper, cathodic polarization of the diffusion side was found to have no influence on v_d. After the diffusion side had been poisoned with mercury or lead, however, the value of v_d at a current density on the diffusion side $i = 2 \cdot 10^{-3}$ amp/cm^2 was found to be higher than the value for $i_d = 4 \cdot 10^{-6}$ amp/cm^2 (Fig. 1). In the case of iron poisoned with mercury, this effect may amount to 25% relative to v_d for $i_d = 4 \cdot 10^{-6}$ amp/cm^2, and, as shown in Fig. 1, the effect is independent of the absolute value of the flow of diffusing hydrogen. This apparently paradoxical picture of the acceleration of the passage of hydrogen through a membrane with cathodic polarization of the diffusion side, which might have been expected to retard the passage of hydrogen, finds two possible explanations.

It might be suggested that in an alkaline solution, the diffusion side is covered by an oxide film which prevents the diffusion of hydrogen; at $i_d = 2 \cdot 10^{-3}$ amp/cm^2 this film is reduced and the diffusion of hydrogen increases, but with decrease in the cathodic polarization of the diffusion side the oxide film is reformed by the traces

*The $Pb(NO_3)_2$ and Na_2S were added to increase and stabilize the flow of diffusing hydrogen.

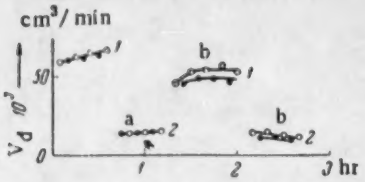

Fig. 1. Relationship between the rate of diffusion and the cathodic polarization of the diffusion side of an iron membrane for different currents of diffusing hydrogen: open circles) $i_d = 2.5 \cdot 10^{-3}$ amp/ cm²; solid circles) $i_d = 4 \cdot 10^{-6}$ amp/ cm²; a) pure iron, b) iron poisoned with mercury.

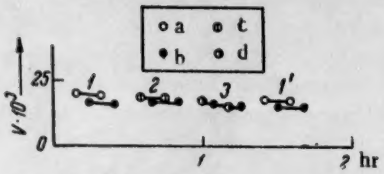

Fig. 2. The relationship between the rate of diffusion and the cathodic polarization of the diffusion side for iron poisoned by mercury: a) $i_d = 2 \cdot 10^{-3}$ amp/ cm², $\Delta\eta = -6$ mv; b) $i_d = 4 \cdot 10^{-6}$ amp /cm²; c) $i_d = 2 \cdot 10^{-4}$ amp /cm², $\Delta\eta = -3$ mv; d) $i_d = 2 \cdot 10^{-5}$ amp/ cm², $\Delta\eta = 10$ mv.

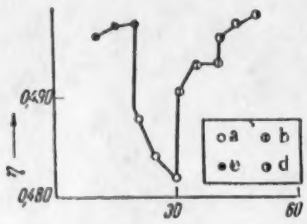

Fig. 3. Relationship between η on the B side of an iron membrane, with cathodic polarization of this side by a current of $5 \cdot 10^{-5}$ amp/ cm², and the cathodic polarization of the opposite A side by currents of:b) $i = 0$; a) $i = 3.5 \cdot 10^{-3}$ amp/ cm²; c) $i = 4 \cdot 10^{-4}$ amp/ cm²; d) $i = 1 \cdot 10^{-4}$ amp/ cm².

of oxygen present in the solution, and the diffusion of hydrogen decreases. The action of the oxide film should be more marked on pure iron than on iron poisoned by mercury or lead. This suggested explanation was rejected on the basis of our experimental study of the influence of anodic polarization of the diffusion side, by currents of $2 \cdot 10^{-6} - 2 \cdot 10^{-4}$ amp/ cm², on the value of v_d for pure iron and for iron poisoned by mercury or lead. The measurements were carried out in such a way that the anodic polarization, of a given current density, was alternated with cathodic polarization by a current of $2 \cdot 10^{-3}$ amp/ cm², for periods of 6 min in each case. It was found that for anodic polarization by a current $i_d = 2 \cdot 10^{-6}$ amp/ cm² on pure iron, the rate of diffusion of hydrogen is the same as for cathodic polarization by a current $i_d = 2 \cdot 10^{-3}$ amp/ cm² and $4 \cdot 10^{-6}$ amp/ cm², and retardation of the diffusion of hydrogen only takes place on further increase in the anodic polarization (by ~ 20 % for anodic polarization by a current of $2 \cdot 10^{-4}$ amp/ cm²). An analogous phenomenon is observed in the case of iron poisoned by mercury and lead, but the retarding action of anodic polarization in this case is less than that for pure iron. These experiments, therefore, refute the above suggestion regarding the part played by oxide film. Another possible reason for the increase in v_d with increase in cathodic polarization may be found in the electrochemical desorption reaction

$$H_{ads} + H_2O + e \rightarrow H_2 \uparrow + OH^-, \quad (1)$$

which takes place readily with high cathodic polarization on iron poisoned by mercury and lead, as has been shown earlier [1]. In order to check this suggestion, we determined the magnitude of the increase in v_d for the case of iron poisoned by lead, for a stepwise increase in the cathodic polarization of the diffusion side up to $2 \cdot 10^{-3}$ amp/ cm², comparing it with v_d for $i_d = 4 \cdot 10^{-6}$ amp/ cm², and compared this with the effect of the diffusing hydrogen on the magnitude of the overvoltage on the diffusion side η, for corresponding cathodic polarizations on the diffusion side. Figure 2 shows that the increase in the rate of diffusion of hydrogen starts to be observed only when the cathodic polarization of the diffusion side reaches the value ($2 \cdot 10^{-4}$ amp/ cm²) at which the diffusing hydrogen brings about a decrease in η, i.e., at which removal of hydrogen from the electrode surface takes place by the electrochemical desorption reaction; the negative value of $\Delta\eta$ corresponds to the decrease in η under the influence of the diffusing hydrogen, and the increase in v_d becomes larger as the decrease in η becomes larger. These data confirm the suggestion regarding the part played by the electrochemical desorption reaction in accelerating the diffusion of hydrogen during cathodic polarization of the diffusion side. If it is assumed that an equilibrium exists between the dissolved hydrogen close to the electrode surface and the adsorbed

hydrogen, then since the rate of diffusion of hydrogen is proportional to the difference in the concentrations of hydrogen dissolved in the metal close to the diffusion and polarization sides, it should follow from what has been said above that, on electrodes poisoned by mercury and lead, the degree of filling of the surface by adsorbed hydrogen θ decreases with increase in the cathodic polarization. In this case we should expect a decrease in the rate of diffusion of hydrogen from an alkaline solution through an iron membrane whose polarization side is poisoned by mercury, as its cathodic polarization increases. The method which we used made it possible to determine v_d volumetrically only within the range of values of i_p from $40 \cdot 10^{-3}$ to $2.5 \cdot 10^{-3}$ amp/cm^2,* whereas we have observed the increase in v_d with increase in i_d in the range of i_d values from $4 \cdot 10^{-6}$ to $2 \cdot 10^{-3}$ amp/cm^2, i.e., at lower current densities. In order to determine at least the direction of the change in v_d with change in i_p at low current densities, we carried out a series of measurements involving the determination of the decrease in the overvoltage η of an iron electrode poisoned by mercury in a solution of 1 N NaOH with increase in the flow of diffusing hydrogen [2]. One of the sides (side A) of the iron membrane poisoned by mercury in 1 N NaOH solution was subjected to cathodic polarization by stepwise application of currents of $i = 0$, $3.5 \cdot 10^{-3}$, $4 \cdot 10^{-4}$ and $1 \cdot 10^{-4}$ amp/cm^2, while measurements were made of the potential of the opposite side B, which also consisted of iron poisoned by mercury in 1 N NaOH solution, but which was subjected to a constant cathodic polarization by a current $i = 5 \cdot 10^{-5}$ amp/cm^2. It was shown (Fig. 3) that when cathodic polarization by a current of $3.5 \cdot 10^{-3}$ amp/cm^2 was applied to side A, the magnitude of η on side B decreased. The subsequent reductions in the cathodic polarization of side A of the membrane lead to an increase in η, which corresponds to a decrease in the flow of diffusing hydrogen. From this experimental material it follows that, at an iron electrode poisoned by mercury in alkaline solution, the increase in v_d with i_d when i_p = const cannot be due to a decrease in θ with increase in the cathodic polarization of an electrode from which the atomic hydrogen is removed by the electrochemical desorption reaction (1). The accelerating action of cathodic polarization on the diffusion of atomic hydrogen when electrochemical desorption takes place is apparently related to the fact that the dissolved hydrogen atoms close to the surface take part in the reaction, and that these atoms do not pass through the "normal" equilibrium state of adsorbed atoms. In other words, the transfer of atomic hydrogen from the metal to the solution takes place in one unit stage of the electrochemical desorption reaction. This result makes necessary some modification of the formulas given in [3].

We wish to thank Academician A. N. Frumkin for valuable advice while this work was being carried out, and for discussion of the results obtained.

LITERATURE CITED

1. I. A. Bagotskaya, Doklady Akad. Nauk SSSR 107, 843 (1956);** I. A. Bagotskaya, Doklady Akad. Nauk SSSR 110, 397 (1956).**
2. A. I. Oshe and I. A. Bagotskaya, Zhur. Fiz. Khim. 32, 6, 1379 (1958).
3. A. N. Frumkin, Zhur. Fiz. Khim. 31, 1775 (1957).

* In this range of i_p values, we observed a linear increase in v_d with $\sqrt{i_p}$ (where i_p is the current density of the cathodic polarization of the polarization side).

** Original Russian pagination. See C. B. translation.

THE EFFECT OF PARTICLE SIZE ON THE RATE OF COMBUSTION OF MIXTURES CONTAINING POTASSIUM PERCHLORATE

N. N. Bakhman and A. F. Belyaev

Institute of Chemical Physics of the Academy of Sciences, USSR
(Presented by Academician V. N. Kondrat'ev, March 12, 1960)
Translated from Doklady Akademii Nauk SSSR, Vol. 133, No. 4, pp. 866-868, August, 1960
Original article submitted March 10, 1960

The problem of the relationship between the rate of combustion in systems made up of a mechanical mixture of a fuel and an oxidizing agent, and the size of the particles, has been considered from a theoretical point of view by O. I. Leipunskii [1], for the case in which combustion of a smoke powder occurs. Leipunskii has come to the conclusion that, in the diffusion region the rate of combustion, u, is proportional to the reciprocal of the particle size: that is $u \sim 1/d$. Novozhilov [3] has come to similar conclusions.

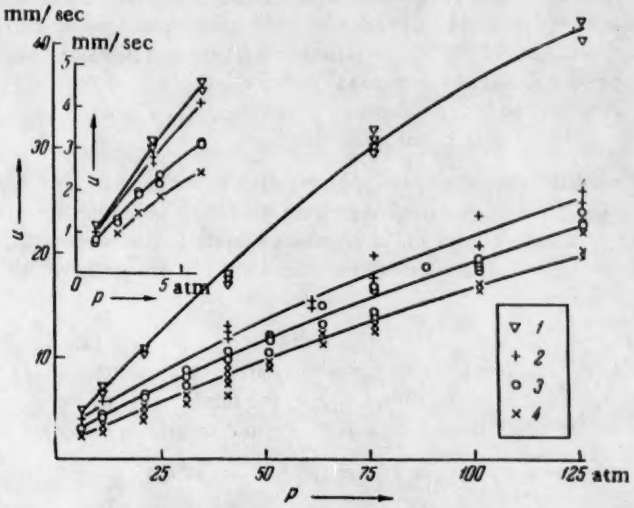

Fig. 1. The relationship between the rate of combustion and the pressure for various particle sizes of the oxidizing agent, using stoichiometric mixtures of potassium perchlorate and bitumen. The size d is: 1) 0.01 mm; 2) 0.07 mm; 3) 0.2 mm; 4) 1.7 mm.

In this paper we give particulars of preliminary experimental results on the relationship between the rate of combustion of heterogeneous systems in which both components are initially in the solid phase, and the degree of heterogeneity. The latter term depends on the size of the particles of both components (and also on the volume

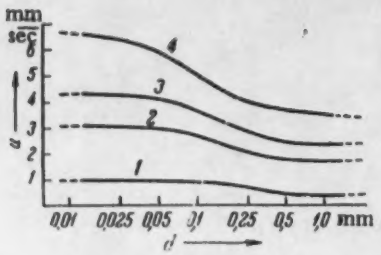

Fig. 2. Relationship of the rate of combustion to the size of particles of oxidizing agent for a stoichiometric mixture of potassium perchlorate and bitumen. Pressures: 1) 1 atm; 2) 3 atm; 3) 5 atm; 4) 10 atm.

ratio between the components, the degree of mixing, and the relative density of the charge. These variables, however, need not be taken into account if they are maintained constant for the system being considered). In a special case, if one of the components exists in the form of a narrow range of particle sizes (with mean diameter d), and the other component is plastic at the time when the charge is prepared, or possesses a particle size much smaller than d, or else goes into the gaseous condition much more easily than the first component, the degree of heterogeneity is determined by the single parameter d.

We have studied in the greatest detail the relationship of u to d for a mixture of crystalline potassium perchlorate with combustible materials which are plastic under the conditions under which the charge is prepared. These include bitumen, hydron and plexiglas. Three screened fractions of potassium perchlorate, with narrow particle size spread, and one fraction prepared in a vibrating mill, were used. The mean microscope diameters were d = 1.7, 0.2, 0.07 and 0.01 mm. The mixture of potassium dichromate and the combustible material, which had been previously diluted with a solvent, was maintained in a state of movement on a vibrating platform during the blending process, and afterward dried out on a water bath and then in a drying chamber. The prepared mixture was compressed to a relative density,* given by $\delta = 0.98$ to 1.00, in the case of bitumen and hydron, and $\delta = 0.90$ in the case of plexiglas. The tablet obtained had a diameter of 6 mm and a height of 8 to 10 mm. Horizontal lengths of glass tubing were stuck onto both ends by means of thin films of a liquid glass containing a filler. The mixture containing hydron, which was distinguished by high plasticity, was compressed in a thick-walled glass tube. The rate of combustion was measured by means of a photorecorder in a bomb of volume 2 liters, and in an atmosphere of nitrogen at pressures varying from 0 to 125 atm.

In this paper we shall only concern ourselves with conditions in which the combustion follows a uniform, laminar course. The disturbing of such conditions by the so-called "penetration" burning may arise, for a given pressure, when the relative density of the charge falls to a sufficiently low value. For a plastic mixture containing hydron at high pressures, a disturbed combustion condition was observed for which the dependence of u on p was considerably greater than when laminar combustion occurred. The rate of combustion under these conditions is not, however, reduced by increase in d, but rather increased.

Figure 1 gives the relationship of the rate of combustion to the pressure for a stoichiometric mixture of bitumen with potassium perchlorate, for different particle sizes of the oxidizing agent. The part played by the size of the particles is shown more clearly in Fig. 2, where the relation between u and d is given directly for the various pressures. It is clear that the relationship between u and d is not uniform: the relevant curve has an S-shaped form.

For sufficiently low particle sizes ($d \leq d_{min}$), the rate of combustion does not generally depend on the value of d. This result could have been predicted from the qualitative considerations in [1]. The magnitude of d_{min} is determined from the equation for the breadth, L_{mix}, of the mixing zone of the vapors of the components, and the breadth L_{heat} of the zone of heating of the vapors. From dimensional considerations:

$$L_{heat} \sim a_{vap}/u_{vap} \sim 1/u; \quad L_{mix} \sim u_{vap}d^2/D_{vap} \sim ud^2/\rho_{vap}D_{vap}. \tag{1}$$

For laminar flow:

$$D_{vap} \sim 1/p \sim 1/\rho_{vap}; \quad L_{mix} \sim ud^2,$$

and therefore the equality of $L_{heat} \sim L_{mix}$ gives

$$d_{min} \sim 1/u. \tag{2}$$

*The relative density $\delta = \rho/\rho_B$, or the ratio of the measured density to that of a solid block from which all air inclusions had been removed.

For turbulent flow,

$$D_{vap} \sim \nu Re^{0.8} \sim u_{vap}^{0.8} d^{0.8},$$

and to a first approximation $L_{mix} \sim d$. From the equality $L_{heat} \sim L_{mix}$, we again arrive at (2).* It therefore follows that, in Fig. 2, the length of the plateau for $d \leq d_{min}$ ought to be the shorter, the higher the pressure (that is, the higher the rate) to which the given curve corresponds.

For intermediate particle sizes, the rate of combustion begins to diminish appreciably in step with the increase in $\underline{d}$. Thus, for p = 10 atm (Fig. 2), increase of particle size from 0.05 mm to 0.25 mm causes the rate of combustion to diminish by a factor of 1.5, which is quite a substantial figure.

Further increase in the particle size, however, causes the dependence of $\underline{u}$ on $\underline{d}$ to fall away again. This is associated with the spreading of the flames along the surface of contact between the grains of oxidizing agent and the combustible material [2]. It seems to be important here to take into consideration the process of heat transfer between the neighboring particles of the oxidizing agent through the intermediate combustible material. It may be assumed that if the ratio d/D, where D is the diameter of the charge, is too great, the combustion will be irregular. (When d/D = 1.7/6 = 0.3, the combustion is still completely steady at pressures greater than 1 atm).

Thus, at each given pressure there exists a definite range of particle sizes within which the rate of combustion diminishes rather rapidly with increase in $\underline{d}$, while outside this range it is either totally independent of $\underline{d}$ (for $d \leq d_{min}$), or depends only slightly (larger values of $\underline{d}$). In such processes the value of $u/_{d \to 0}$ is several times greater than $u/_{d \gg d_{min}}$. With increase in pressure, the region in which there is relatively rapid change of the rate of combustion with the size of the particles is extended, and at the same time is shifted to the left – that is, in the direction of small values of $\underline{d}$.

The complicated form of the relation of the rate of combustion to the dimensions of the particles is linked, apparently, with the fact that when the dimensions of the particles change , the rate of combustion is controlled by various factors. It may be assumed, for example, that when $d \leq d_{min}$, the determining factor is the rate of reaction in the homogeneous mixture of vapors, while at intermediate values of $\underline{d}$ the determining factor is the rate of mixing of the vapor streams, while at large values of $\underline{d}$ the rate is controlled by the velocity of spread of the flame along the boundaries of the particles of the oxidizing agent [2].

As we have already observed at the beginning of this paper, theoretical studies [1, 3] have given a basis for expecting a strong dependence of the rate of combustion on the dimensions of the particles. The results of our experiments on mixtures containing potassium perchlorate show that this dependence is very limited in extent. We have, however, taken account of the fact that in mixtures of potassium perchlorate with bitumen and the other combustible materials, both the components form gaseous phases comparatively easily, while in the work reported in [1, 3] the combustible material was nonvolatile. We have therefore carried out experiments on the system: wood charcoal – potassium nitrate, for which the conclusions of papers [1, 3] were given. We have prepared two mixtures of the same composition, containing 15% carbon and 85% potassium nitrate. One mixture had particles for both oxidizing agent and combustible material from 10-20 μ, while in the other the value was about 400 μ. When $\underline{p}$ had values from 0 to 50 atm the rate of combustion of the coarse-powdered mixture was only about a factor of 2 smaller than that of the finely powdered mixture. At 50 atm, for example, the values were respectively 8 and 16 mm/sec, although the dimensions of the particles differed by a factor greater than 10.

Thus, the conclusions of works [1, 3] do not correctly represent the experimental facts, even with respect to the particular system (smoke powders) for which they were specially intended [1]. It seems that for the most extended mixed systems, the theoretical combustion model ought to be substantially modified as compared with that offered in [1], possibly taking into account the situation discussed in this note.

*In the coordinates (u, p) the situation in which $d_{min} \sim 1/u \sim 1/p^n$ leads to a family of curves for u (p, d), where $\underline{d}$ is the particle size, branching from a point which corresponds to $d \to 0$, of which any given curve of u(p,d) branches to the left from the point of contact where it runs together with the other curves of the family. In other words, the family of curves u (p, d) should have the appearance of a palm branch. In Fig. 1, the curves corresponding to particle sizes 0.01 and 0.07 mm run together into each other at p = 1 atm (u = 1 mm/sec). This signifies that when u = 1 mm/sec, $d_{min} \sim 0.07$ mm.

LITERATURE CITED

1. O. I. Leipunskii, Zhur. Fiz. Khim. 34, 1, 177 (1960).
2. N. N. Bakhman, Dokl. Akad. Nauk SSSR 129, 5, 1079 (1959).*
3. B. V. Novozhilov, Dokl. Akad. Nauk SSSR 131, 6, 1400 (1960).*

* Original Russian pagination. See C. B. translation.

THE MECHANISM OF THE ELECTROLYTIC POLISHING OF METALS, IN THE LIGHT OF ELECTRON MICROSCOPE STUDIES OF THE SURFACE AT DIFFERENT STAGES IN THE TREATMENT

G. S. Vozdvizhenskii, G. A. Gorbachuk, and G. P. Dezider'ev

Chemistry Institute, Kazan Section, Academy of Sciences, USSR
(Presented by Academician A. N. Frumkin, January 28, 1960)
Translated from Doklady Akademii Nauk SSSR, Vol. 133, No. 4, pp. 869-871, August, 1960
Original article submitted January 28, 1960

In the majority of published works on the electron microscope study of the process of electrolytic polishing, use is made only of the surface purity characteristic, when estimating the possibility and limits of the smoothing out of the microirregularities [1]. At the same time the electron microscope can also be used to solve electrochemical problems [2], and in particular to examine the mechanism of the electrolytic polishing of metals [3].

In our earlier work [4], it was shown clearly that, both in the initial stages of the process of anodic dissolution and in the stages corresponding to the external effect of electrolytic polishing, structural etching always takes place, while the scale of this etching shows variations, depending on the electrochemical nonuniformity of the surface. The electron microscope photographs which we obtained show no suppression of the structural etching throughout the whole course of the electrolytic polishing process. We observe merely a regular decrease in the scale of the etching, associated with the decrease in the electrochemical nonuniformity of the surface.

In our later studies we have tried to obtain experimental material relating the process of anodic dissolution to the structure of the metal.. For this purpose we have studied the electrolytic polishing process on specimens of rolled and annealed copper and brass.

The materials studied were mark M1 sheet copper (cold rolled) and mark L59 sheet brass (cold rolled). The electrolytic polishing was carried out in 11.35 M orthophosphoric acid solutions containing 4.8 and 2.9 g/liter respectively. Special experiments showed that the optimum current density (limiting) for the electrolytic polishing was 14.5 ma/cm^2 for the copper specimens, and 19 ma/cm^2 for the brass specimens.

The specimens were etched until a distinct microstructure was revealed (for 4 min at 20° in 10% ammonium persulfate solution in the case of the copper specimens, and for 2-3 min at 20° in a mixture of aqueous ammonia solution and hydrogen peroxide in the case of the brass specimens), subjected to metallographic examination, and suspended in the electrolytic polishing bath. After the required time interval, the specimens were removed from the bath, washed, dried and again subjected to metallographic examination. Lacquer replicas were then taken, shaded at small angles (7-18°) with chromium, and examined by the electron microscope.

The metallographic (200 x) and electron microscope (23,000 x) photographs of the surface of rolled specimens of copper treated under these conditions are shown in Fig. 1, and the corresponding photographs for the brass specimens in Fig. 2.* The figures indicate the times of treatment, in minutes.

* In Figs. 1-4 the upper row of photographs were obtained with the optical microscope and the lower row with the electron microscope.

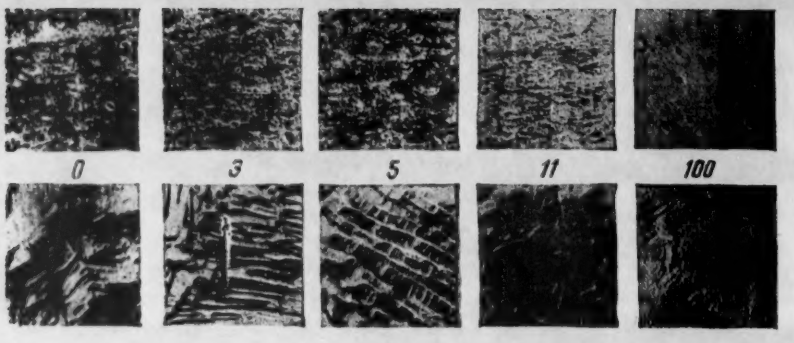

Fig. 1.

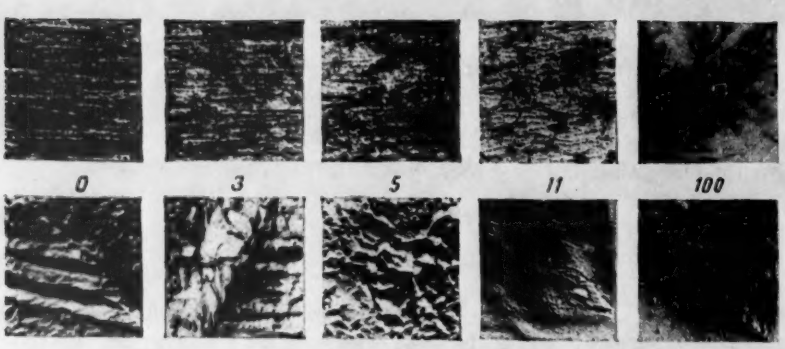

Fig. 2.

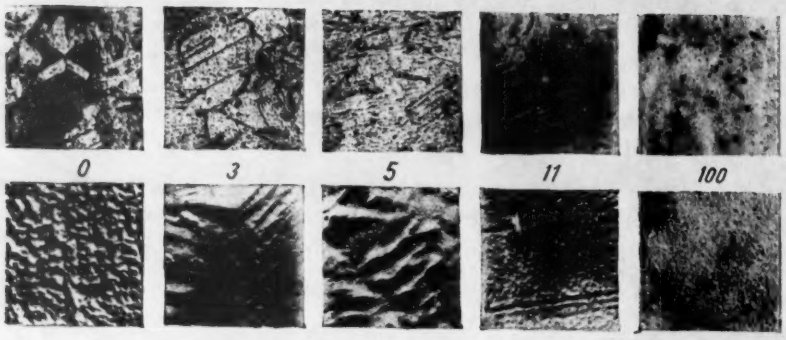

Fig. 3.

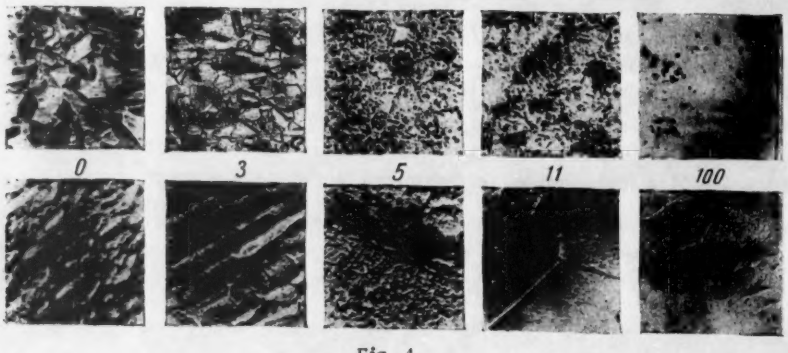

Fig. 4.

Another series of experiments was carried out with specimens annealed in vacuo (at 700° for 1 1/2 hr in the case of copper, and at 600° for 2 hr in the case of brass; the specimens were cooled in the furnace). The optimum current density for the electrolytic polishing of the copper specimens was 21 ma/cm^2, and that for the brass specimens 16 ma/cm^2. The metallographic (200 x) and electron microscope (23,000 x) photographs of the annealed copper specimens treated under these conditions (etched and electrolytically polished for different periods of time) are shown in Fig. 3 and the corresponding photographs for annealed brass specimens are shown in Fig. 4.

The original surfaces of all the specimens studied were, of course, electrochemically nonuniform. For this reason the chemical etching in ammonium persulfate solution in the case of the copper specimens and in the mixture of aqueous ammonia solution and hydrogen peroxide in the case of the brass specimens revealed a distinct structure (Figs. 1-4).

The anodic dissolution of the specimens takes place with the participation of an acceptor present in the electrolyte – apparently the phosphoric acid. At the start of the treatment, the acceptor is able to reach the metal over almost the whole of the surface, so that there are no restrictions on the development of the anodic dissolution shapes. These shapes should also develop on any scale, in accordance with the dimensions of the electrochemical nonuniformity. In subsequent stages of the dissolution, the acceptor is prevented from reaching the foot of the etching pits which are formed, and this leads to a retardation in the increase in the depth of these pits, and the dissolution process should take place on new areas, spreading over the surface of the metal.

The optical photomicrographs (200 x) for the rolled material show that the external effect of chemical etching in the appropriate solutions corresponds to the orientation of the crystals in the direction of rolling (texture). For L59 brass and more heterogeneous materials, which exhibit a high electrochemical nonuniformity, the orientation of the crystallites in the direction of rolling is shown to a much smaller extent than in the case of copper.

The electrolytic polishing not only does not conceal the effect of the chemical etching – the clearly revealed microstructure corresponding to the orientation of the crystallites – but, on the contrary, reveals this effect even more sharply. The treated regions of the surface (which are light in color, particularly for copper) are drawn out in the direction of rolling.

The electron microscope photographs also show that the effect of the chemical etching of the original surface corresponds to the orientation of the crystallites – in this case the etching reveals the large number of orientated displacements inside the crystallites. This is shown particularly clearly on the copper specimen. The clear picture of these regions is again not obscured by the electrolytic polishing. In later stages it is revealed even more clearly, but the affected areas do not become deeper; instead they become wider, as a result of the difficulty experienced by the acceptor in reaching the foot of the etching pits. In electrolytic polishing, therefore, there is none of the so-called suppression of the structural etching, but merely a change in the scale of the anodic dissolution, in accordance with the change in the scale of the electrochemical nonuniformity.

Comparison of the optical photomicrographs for the rolled copper specimen, treated for 11 min, with the electron microscope photograph for the same specimen, is particularly interesting. The former shows bright regions, drawn out in the direction of rolling, which are also shown on the latter, but now in the form of anodic dissolution shapes covered with a finer pattern. The linear dimensions of the bright areas on the first photograph correspond approximately to those of the drawn-out shapes on the second, as can be seen from a comparison of the magnifications (23,000 : 200 ≅ 100). The greater electrochemical nonuniformity of the brass specimens is further shown by the fact that the electron microscope photographs show more readily the joints between crystallites with different orientation. This phenomenon is rare in the case of the copper specimens.

The annealed material (copper and brass) shows the same basic picture of chemical and electrochemical dissolution as in the case of the rolled material, but the picture now corresponds to the structure produced during annealing. In these cases also, there is extensive breakdown of the surface of the crystallites. The large crystals are covered with very fine etching pits which gradually increase in width. Since the crystallites in the annealed material are larger than those in the rolled material, the effects of the treatment become noticeable even at small magnifications (200 x). The annealing process disorientates the arrangement of the crystallites, so that the surface elements which have been subjected to the anodic treatment show no orientation on either the optical or electron microscope photographs.

Although the rolled material shows a significant difference in the results of the anodic treatment of copper and brass specimens, resulting from the marked difference in the degree of electrochemical nonuniformity of the metals, this difference is smoothed out in the case of the annealed specimens, as a result of the fact that during the annealing process both materials become disorientated more or less to the same extent. The higher electrochemical nonuniformity of the brass specimens is shown only by the fact that the joints between crystallites with different orientation are more readily detected on the electron microscope photographs.

Thus, our choice of specimens for the experimental electron-microscope study of the mechanism of the electrolytic polishing of metals has been fully justified. It has made it possible to illustrate clearly the leading part played by the metal structure in this mechanism. The structural etching of the electrochemically nonuniform surface is the basic process in electrolytic polishing, and takes place in all stages of the process. The restriction of the diffusion of the acceptor plays an important part, leading to a gradual change in the scale of the structural etching into the depth of the metal.

LITERATURE CITED

1. A. Politicki and H. Fischer, Z. Elektrochem. 56, 326 (1952); E. Coull and M. Cohen, Canad. J. Chemistry 31, 237 (1953); H. Fischer and L. Koch, Metall, 17/18, 481 (1952); H. Poppa and H. Spähn, Metalloberfläche 10, 11, 329 (1956).
2. E. H. Boult and H. R. Thirsk, J. Photogr. Sci. 3, 5, 140 (1955); cited in Russ. Zhur. Khim., 22, 66 (1956).
3. G. S. Vozdvizhenskii, Trudy Kazanskogo Khim.-Tekhnol. Inst. 21, 15 (1956).
4. G. S. Vozdvizhenskii, G. A. Gorbachuk, and G. P. Dezider'ev, Doklady Akad. Nauk SSSR 120, 101 (1958).*

* Original Russian pagination. See C. B. translation.

ON THE NONEQUILIBRIUM STATE BEHIND A SHOCK WAVE IN AIR

S. A. Losev and N. A. Generalov

M. V. Lomonosov Moscow State University
(Presented by Academician V. N. Kondrat'ev, March 17, 1960)
Translated from Doklady Akademii Nauk SSSR, Vol. 133, No. 4, pp. 872-874, August, 1960
Original article submitted March 15, 1960

At the high temperatures developed behind the front of a shock wave, air is a mixture of atoms and molecules of oxygen, nitrogen, oxides of nitrogen, and other gases; investigation of the process of the establishment of equilibrium in such a mixture is a very complex problem. The present communication gives the results of a preliminary experimental investigation of the state of the gas behind a shock wave in air.

The experiments were carried out in a shock tube [1, 2]. Hydrogen under a pressure of 40 to 130 atm was used in the high pressure chamber of the shock tube. Air, purified by freezing out with liquid nitrogen, at a pressure of 4.4 to 7.6 mm Hg (0.0058 to 0.01 atm) was situated in the low pressure chamber. The velocity of the shock wave was measured by ionization gauges to a precision of 1 to 2%, and, depending on the initial drop of pressure in the chambers, it ranged from 2.4 km/sec to 3.7 km/sec.

Our previous investigation [2] showed that the air behind the shock wave under these conditions is appreciably absorptive in the ultraviolet region of the spectrum ($\lambda < 3400$ A). This property of the heated air was used for studying its state behind the shock wave. For this purpose, the arrangement described in [2] was used; for $\lambda > 2170$ A, the photomultiplier registered practically no scattered light. The resolution time of the over-all recording channel was $\tau \sim 0.2$ microsec.

The distribution of the value of the absorption capability behind the front of the shock wave in air in the 10 angstrom wavelength range near $\lambda = 2200$ A was investigated in the experiments. It turned out that with the aforementioned pressure and shock wave velocity, there was significant absorption immediately behind the front of the wave; then, with increasing distance from the front, the value of the absorption capability decreased, and further, remained constant (Fig. 1). The region of constant absorption corresponds to an equilibrium state of the gas (according to [3], the air temperature measured in this region agrees satisfactorily with the temperature calculated assuming complete chemical equilibrium).

To solve the problem of the cause of the appearance of an absorption maximum immediately behind the shock wave front, it is necessary to know the contribution of the various gases to the observed absorption. Additional control experiments with N_2, O_2, and a mixture of 21% O_2 + 79% A ("air" in which nitrogen was replaced by argon), showed that the absorption observed at $\lambda = 2200$ angstroms in air is primarily determined by O_2 molecules; absorption occurs as a consequence of transitions from vibrationally excited levels of the fundamental state $X^3\Sigma_g^-$ into the state $B^3\Sigma_u^-$ (Schumann-Runge O_2 band). It was established that the absorption capability of air at $\lambda = 2200$ A depends strongly on the concentration of O_2. Therefore, the reduction in the absorption capability in the flow behind the shock wave front can be associated with the nonequilibrium dissociation of the O_2 in the air.

The dimensions of the region of occurrence of the process of O_2 dissociation can be characterized by the

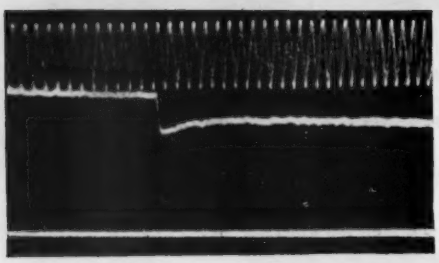

Fig. 1. Oscillogram of the distribution of absorption behind the front of a shock wave propagating in air with a velocity of 3.62 km/sec with an initial pressure of 4.4 mm. The straight line is the zero level. Frequency of the calibrating sine wave – 1 Mc/sec.

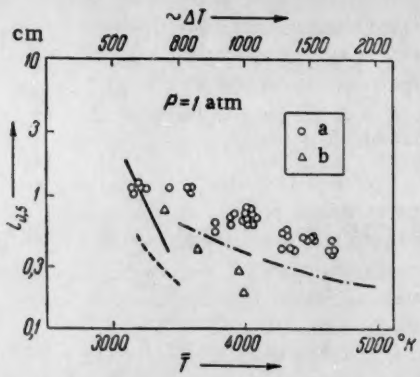

Fig. 2. Experimental dependence of the characteristic length of the nonequilibrium region in air (a) and in oxygen with not more than 1% nitrogen (b) on the mean temperature behind the front of the shock wave with atmospheric pressure behind the wave. Averaged data for oxygen from [7] are shown by the continuous line, and from [1] by the dashed line. The dash-dot line shows the dimensions of the relaxation of vibrations in nitrogen according to the data of [8].

distance $l_{0.5}$ from the leading edge of the front of the shock wave to that point at which the absorption is midway between the maximum value of the absorption capability and the constant level of absorption. The experimental dependence of this length $l_{0.5}$ on the mean temperature behind the front* for experiments in which the pressure behind the shock wave was 1 ± 0.18 atm are shown in Fig. 2a. As is apparent from Fig. 2, the length of the nonequilibrium portion decreases appreciably with increasing temperature, which can be explained by the increase in the dissociation rate of oxygen molecules.

Let us examine the possible mechanism of the reaction leading to the decrease in the concentration of O_2 in air, neglecting, in accordance with [4], the effect of recombination reactions, which begin to play a significant role only near equilibrium:

$$O_2 + O_2 \rightarrow 2O + O_2 \qquad (I)$$

$$O_2 + O \rightarrow 3O + O \qquad (II)$$

$$O_2 + N_2 \rightarrow 2O + N_2 \qquad (III)$$

$$O_2 + N \rightarrow 2O + NO \qquad (IV)$$

To evaluate the effect of nitrogen on the process of O_2 dissociation in air, it is of interest to compare the rate of dissociation of O_2 in pure oxygen (Reactions I, II) and in air. The effect of reactions III and IV is that for the same partial pressure of oxygen, the dissociation of O_2 in air proceeds more rapidly than the decomposition of O_2 in pure oxygen. The ratio r of the dissociation rate of O_2 in pure oxygen and in air will be different if the comparison is carried out at different partial pressures of oxygen. For the same temperature, it follows from I-IV that

$$r = \left(\frac{P'}{P''}\right)^2 \frac{K_I \xi'_{O_2} \xi'_{O_2} + K_{II} \xi'_{O_2} \xi'_{O}}{K_I \xi''_{O_2} \xi''_{O_2} + K_{II} \xi''_{O_2} \xi''_{O} + K_{III} \xi''_{O_2} \xi''_{N_2} + K_{IV} \xi''_{O_2} \xi''_{N}}, \qquad (1)$$

where K denotes the rate constants of the corresponding reactions, ξ_M is the molar fraction of component M, and P is the total pressure; one prime pertains to experiments in O_2, two primes, in air. For the same total pressure ($P' = P''$), the presence of reactions III and IV in air (last two terms in the denominator of the relation (1))

*The mean temperature behind the shock wave front was determined as the arithmetic mean of the equilibrium value and the value obtained without considering the expenditure of dissociation energy. The upper scale in Fig. 2 shows the approximate change of temperature during dissociation of O_2 in air for the corresponding value of the mean temperature.

cannot compensate for the five-fold increase in the partial pressure of O_2 ($\xi'_{O_2} \sim 5\xi''_{O_2}$) – the rate of dissociation of O_2 in air can in this case be smaller than the rate of dissociation of O_2 in pure oxygen. This is also observed experimentally at $P' = P'' = 1$ atm (Fig. 2): the nonequilibrium region of dissociation of O_2 in air at $\bar{T} \sim 3500$ to 4500° K is longer than the dimensions of the region in O_2.* For $P' = 0.5$ atm and $P'' = 1.2$ atm it was observed that with $\bar{T} = 4000$°K, $r \sim 1$-2.

Comparison with [6] showed that the experimentally determined total dissociation rate of O_2 in air, measured at atmospheric pressure, $d\xi_{O_2}/dt$, is approximately equal to $3 \cdot 10^8$ and $1 \cdot 10^9$ $(\text{mole/cm}^3)^{-1} \cdot \text{sec}^{-1}$ at $\bar{T} = 3500$ and 4000°K respectively. However, these values are apparently only an upper limit for the possible values, since the dimensions of the observed region of dissociation of O_2 behind the wave front in air are somewhat lower because of the effect of the process of the delayed excitation of N_2 vibrations, which occurs practically simultaneously with the dissociation of O_2 (Fig. 2). The higher temperature, caused by the lag in the excitation of N_2 vibrations, leads to a shortening of the time required for dissociation of O_2 in air. This probably also affects the dependence of the characteristic length $l_{0.5}$ on $\bar{T}$.

LITERATURE CITED

1. S. A. Losev, Doklady Akad. Nauk SSSR 120, 6, 1291 (1958).*
2. S. A. Losev, N. A. Generalov, and L. B. Terebenina, Optika i Spektroskopiya 8, 4, 569 (1960).
3. F. S. Faizullov, N. N. Sobolev, and E. M. Kudryavtsev, Doklady Akad. Nauk SSSR 127, 3, 541 (1959).**
4. R. E. Duff and N. Davidson, J. Chem. Phys. 31, 4, 1018 (1959).
5. M. Camac, J. Camm, et al., Chemical Relaxation in Air, Oxygen and Nitrogen, I. A. S. Reprint No. 802 (1958).
6. D. Matthews, Phys. Fluids 2, 2, 170 (1959).
7. S. R. Byron, J. Chem. Phys. 31, 2, 420 (1959).
8. V. Blackman, J. Fluid Mech. 1, 1, 61 (1956).

* An analogous result was obtained by Camac and others [5], who found that for the same total pressure ($P \sim 3.5$ atm) the establishment of equilibrium in O_2 also occurs more rapidly than in air.

** Original Russian pagination. See C. B. translation.

THE INFLUENCE OF SELENIUM AND TELLURIUM ON THE CATALYTIC ACTION OF SILVER IN THE OXIDATION OF ETHYLENE

V. E. Ostrovskii, N. V. Kul'kova, and A. D. Nedbaeva

L. Ya. Karpov Physicochemical Institute

(Presented by Academician S. S. Medvedev, March 28, 1960)
Translated from Doklady Akad. Nauk SSSR, Vol. 133, No. 4, pp. 875-877, August, 1960
Original article submitted March 28, 1960

Previously we have investigated the modifying influence [1] of sulfur compounds when added to silver catalyst for ethylene oxidation [2]. There are indications in the patent literature that the addition of selenium or tellurium enhances the selectivity of the silver catalyst, that is, directs the reaction more toward the formation of ethylene oxide, while it decreases noticeably the activity of the catalyst [3]. The results of an investigation into the influence of elements analogous to sulfur on a silver catalyst are stated below.

The catalyst samples were examined in a circulating flow system at 219° C. The ethylene concentration in the ethylene–air mixture fed was maintained between 2.5 and 3.0%. The method of the kinetic measurements and the purification of air have been described previously [2, 4]. The ethylene, obtained by dehydration of ethanol, was purified by passing it in succession through activated charcoal AG-3 and AC, a trap at a temperature of −78°, a furnace with copper oxide at 150° and a tower with soda lime and silica gel. The purification system used made it possible to work more than 300 hours with the catalyst sample without deterioration of the stationary activity. We used selenium and tellurium compounds tagged with the radioisotopes Se^{75} and Te^{127}, so that we could check very small concentrations of admixture in the catalyst, observe the migration of the admixtures to the surface and ascertain whether the admixture is carried off from the surface during the catalytic reaction.

Sponge silver, obtained by a coprecipitation of silver carbonate and silver selenate or tellurate followed by reduction in the ethylene–air mixture at 219°, was used as catalyst.

Selenic acid was prepared from elementary selenium by oxidation in hot hydrogen peroxide [5], the telluric acid by oxidation with hot hydrogen peroxide in an alkaline solution [6]. The surface areas of the catalyst samples were measured by nitrogen adsorption at low temperature and were found to be 0.95 ± 0.15 m^2/g for the samples with selenium added and 0.75 ± 0.1 m^2/g for the samples with tellurium added.

We will characterize the catalytic activity by the reaction rate constant of ethylene oxidation k_1 expressed in relative units. The reaction rate constant for the sample without admixture but with the same specific surface area as the catalyst series considered was taken as the unit rate constant. The rate constant was calculated from the relation [7]

$$\omega_1 = \frac{k_1 [C_2H_4]}{[C_2H_4O] + 0{,}3\,[CO_2]},$$

where ω_1 represents the rate of ethylene oxide formation, $[C_2H_4]$, $[C_2H_4O]$, and $[CO_2]$, the concentration of the corresponding gases in the reaction mixture. The selectivity S is expressed in percent and is defined as the ratio of the rate of ethylene oxide formation to the sum of the rate of ethylene oxide formation and the rate of ethylene

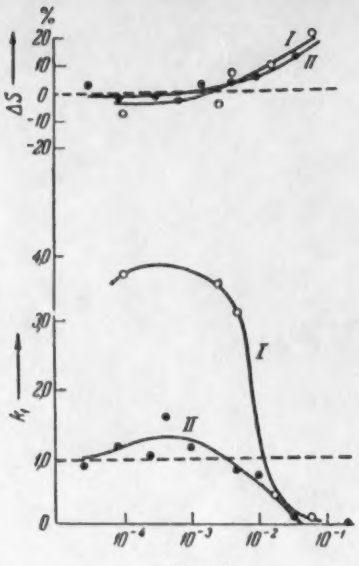

Fig. 1.

oxide oxidation to CO_2 and H_2O. The selectivity change $\Delta S = S - S_0$, where S represents the selectivity of the catalyst with admixture and S_0 the selectivity of the catalyst without admixture. The mean of $S_0 \cong 50\%$.

The catalyst was examined for not less than 55 hours and for the comparison the averages of the k_1 and ΔS values found between the 44th and the 54th hour were used. In Fig. 1, these mean values of k_1 and ΔS are plotted versus the concentration of selenium (curve I) and the concentration of tellurium (curve II) in the catalyst. The dotted line gives the reference level (the catalyst without admixture). As will be shown below, the selenium or the tellurium is mainly found on the surface of the catalyst. The fraction of the silver surface covered by selenium or tellurium was calculated conditionally as the ratio of the number of Se or Te atoms in the catalyst to the number of silver atoms on the surface. As may be seen in Fig. 1, the addition of selenium in a concentration of $10^{-4} - 5 \cdot 10^{-3}$ at.% (0.1 - 5% surface coverage) increases the catalytic activity by about 3.5 times. A further increase in the selenium concentration results in poisoning of the catalyst. At a content of $7.8 \cdot 10^{-2}$ at.% Se (about one monolayer) the catalyst is nine times less active than the catalyst without admixture. The addition of tellurium does not result in a substantial increase in catalytic activity. Tellurium concentrations above 10^{-2} at.% (about 12% surface coverage) poison the catalyst. The activity of the catalyst with $3.3 \cdot 10^{-2}$ at.% Te (about 40% surface coverage) is 15 times lower than that of the catalyst without admixture. A noticeable increase in selectivity is observed only at such high Se or Te contents that the catalytic activity is lowered.

The initial admixture concentration of the catalyst was calculated from the radioactivity of the solution of silver carbonate in nitric acid. The radioactivity was determined by means of a Geiger-Müller counter type MC-4 and the solution was poured into a shielded glass cell with double walls [8]. After the kinetic measurements had been finished, the catalysts with selenium admixtures were extracted with hot water and with a hot 2% NaOH solution; those with tellurium admixtures were treated with hot water, a hot 2% NaOH solution, a concentrated solution of ammonia and a 2% HNO_3 solution. After this the catalysts were dissolved in HNO_3. The radioactivity of all solutions was determined. Water does not extract selenium from the catalysts; the 2% NaOH solution extracts 40-80% of the selenium, whereas not more than one monolayer of silver is dissolved. Water does not extract tellurium; a 2% NaOH solution and a saturated solution of ammonia in water partially extract tellurium only from catalysts containing $3.3 \cdot 10^{-2}$ at.% Te (about 40% surface coverage) or more. A 2% HNO_3 solution extracts 50-90% of the tellurium, whereas not more than two monolayers of silver are dissolved.

Therefore, the selenium and the tellurium, added during the preparation of the catalysts, are found in the outer layer of the used catalyst. It has been found previously [2], that, when sulfur has been added to the catalyst, 80-90% of it can be extracted with water from the used catalyst. The maximum catalytic activity was observed at a concentration of about $5 \cdot 10^{-5}$ at.% S and was about 3.5 times higher than that of the sample without admixture.

Obviously, when small amounts of the elements in the sixth group of the periodic system are added to the silver catalyst, there take place two effects, which are connected with the admixture on the surface or in the outer layer of the catalyst. The first of these effects is connected with the formation of negative ions, such as SO_4^- or SeO_3^-, on the surface, which lowers the energy of oxygen adsorption, so that the oxygen adsorption is retarded and the reaction between ethylene and adsorbed oxygen is accelerated.* For this reason the reaction rate goes through a maximum at a certain optimum binding energy.

The second effect consists in the blocking of the silver surface by foreign atoms and can lead only to a

* In experiments which will be described in another communication it has been established that the binding energy of oxygen on silver is lowered and the oxygen adsorption is retarded, when sulfur is added in amounts corresponding to small surface coverages.

lowering of the activity of the catalyst. To attain the maximum catalytic activity, less sulfur than selenium is required. When tellurium is added to the catalyst, only the second effect is observed, since the affinity of tellurium to oxygen is noticeably lower than that of sulfur or selenium.

LITERATURE CITED

1. S. Z. Roginskii, Adsorption and Catalysis on Heterogeneous Surfaces [in Russian] (Izd. AN SSSR, 1948), p. 511.
2. A. I. Kurilenko, N. V. Kul'kova, V. E. Ostrovskii, and M. I. Temkin, Doklady Akad. Nauk SSSR 123, 878 (1958).•
3. H. H. Voge, Berkeley, and L. T. Atkins, US Pat. No. 2680752 (February 8, 1954).
4. A. I. Kurilenko, N. V. Kul'kova, et al., Zhur. Fiz. Khim. 32, 797, (1958).
5. H. Fonzes-Diaçon, Contribution à l'étude des seléniures métalliques (Montpelier, 1901).
6. Cited from J. W. Mellor, A Comprehensive Treatise on Inorganic and Theoretical Chemistry 11, 85 (1934); A. Gutbier, Z. Anorg. Chem. 32, 257 (1902); A. Gutbier, F. Resenschech 42, 174 (1904).
7. A. I. Kurilenko, N. V. Kul'kova, et al., Zhur. Fiz. Khim. 32, 1043 (1958).
8. V. V. Losev, Doklady Akad. Nauk SSSR 100, 111 (1955).

•Original Russian pagination. See C. B. translation.

A RAPID CHROMATOGRAPHIC METHOD OF MEASURING GAS AND VAPOR ISOTHERMS

S. Z. Roginskii, Corresponding Member, Academy of Sciences, USSR, M. I. Yanovskii, Lu P'ei-chang, G. A. Gaziev, G. M Zhabrova, B. M. Kadenatsi and V. V. Brazhnikov

Institute of Physical Chemistry, Academy of Sciences, USSR
Translated from Doklady Akademii Nauk SSSR, Vol. 133, No. 4, pp 878-881, August, 1960
Original article submitted January 28, 1960

It will be important for practical and scientific purposes to develop rapid and reliable methods of measuring the specific surface area of solids. In heterogeneous catalysis the magnitude of the specific surface area is very important for the efficiency of many technical processes.

Vacuum methods for the determination (by weighing, volumetrical, from pressure drop) of the specific surface area are the most common at present. For an extensive examination of a great number of adsorbent or catalyst samples these methods have the drawback that they require experiments to be made in a complicated vacuum apparatus and that the samples have to be outgassed during a long time (conditioning) before the measurements.

Very promising is the chromatographic method of measuring adsorption isotherms; it is derived from the theoretical work of Wilson who, as early as 1940, had discussed [1] how the shape of the chromatographic curve will depend upon the shape of the isotherm, when equilibrium is established instantaneously and the longitudinal diffusion may be neglected. These conditions are completely satisfied in gas chromatography [2-4].

In this study two versions of chromatographically measuring the adsorption isotherm are compared with the conventional vacuum method.

EXPERIMENTAL

The chromatographic apparatus is shown schematically in Fig. 1. The essential pieces of the equipment are the dynamic tube 3 filled with adsorbent or catalyst, the thermostated bubbler 2 containing the adsorbate and the sensitive gas analyzer 4 the reading of which is automatically recorded by the potentiometer 5. An ionization detector based on Pm^{147} the construction of which has been described recently [5] was used as gas analyzer. Usually we employed nitrogen as carrier-gas. In those cases where a higher sensitivity was required (for the determination of small surface areas) we applied argon, which allowed the raising of the sensitivity by about two times. By means of the needle-valves 7 and 8 the gas flows were adjusted to the proportion required to give the adsorbate concentration, which could be measured by the ionization detector 4. During the time needed for the adjustment of the concentration required, the column and all joints were purged with inert gas through valve 10 and flow meter 14. After the stationary state had been established, the flow of carrier-gas containing adsorbate vapor was directed to the column by turning the four-way stopcock 11. This moment is marked on the record as the start of the experiment. The curve on the record gives the reading of the gas analyzer as a function of time and is called frontal diagram (the right branch of the curve in Fig. 2b). The step height n of the frontal diagram corresponds to the adsorbate concentration C_0 in the feed. When the frontal experiment is stopped, the stopcock

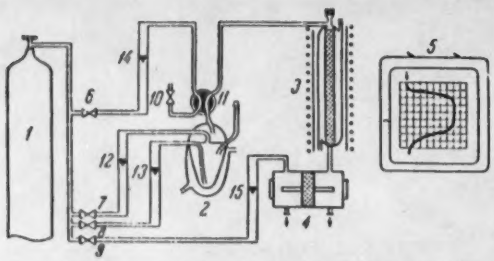

Fig. 1. Scheme of the apparatus. 1) Cylinder with carrier-gas; 2) bubbler with adsorbate; 3) chromatographic column; 4) gas analyzer; 5) recording potentiometer; 6, 7, 8, 9, 10) needle-valves; 11) four-way stopcock; 12, 13, 14, 15) flow meters.

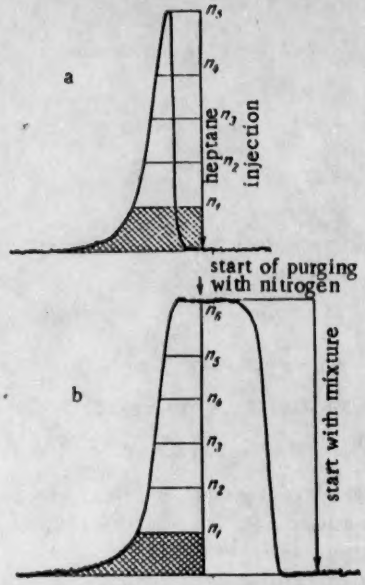

Fig. 2. The breakthrough curve. a) Development version; b) frontal version.

11 is again turned to its original position and pure carrier-gas is passed through the column. To prevent the change in flow rate, which might occur at the moment the flow is reversed by turning stopcock 11, a parallel flow of pure carrier-gas was passed through the needle-valve 10 during the time in which the frontal diagram was taken; the needle-valve was adjusted to have its resistance equal to that of the dynamic tube. In this case only, the reversal of the flow does not give a break in the chromatogram. The moment at which the purging of the dynamic tube with pure carrier-gas is started is marked on the chromatogram as the beginning of the desorption curve (left branch of the curve in Fig. 2b); by an analysis of this branch (see below) the adsorption isotherm may be determined.

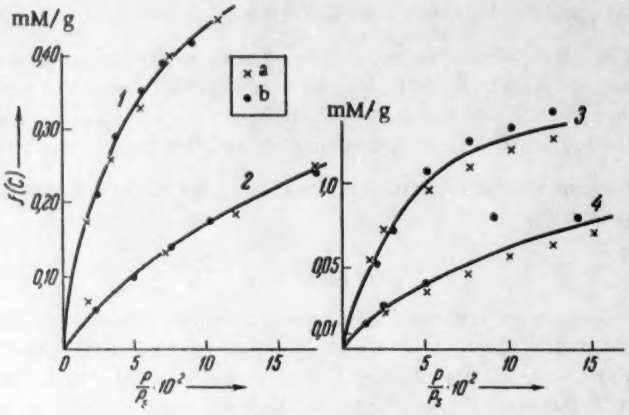

Fig. 3. Heptane adsorption isotherms determined chromatographically (a) or by weight (b). 1) MgO from $Mg(NO_3)_2$; 2) silica gel E; 3) sample 862; 4) brick.

The other version of the chromatographic determination of the isotherm is still simpler. In this case, the adsorbent is not previously saturated with the adsorbate, but by means of a microsyringe a pulse of adsorbate is periodically injected through a rubber gasket into the continuous flow of carrier-gas to the column. The chromatographic curve is shown in Fig. 2a. Such an experiment takes 10-15 min.

Adsorbent or catalyst	Specific surface area, m^2/g	
	determined chromatographically	determined statically
Fireproof diatomaceous brick	34.2	41.4
Silicagel E	103	97.4
Sample 862 (nickel hydroxide gel)	47.5	61.4
Nickel catalyst	16	20
Magnesium oxide from $Mg(NO_3)_2$	220	217
ZnO + 14.5 $ZnSO_4$	6.0	5.3
Carbon black	116	95

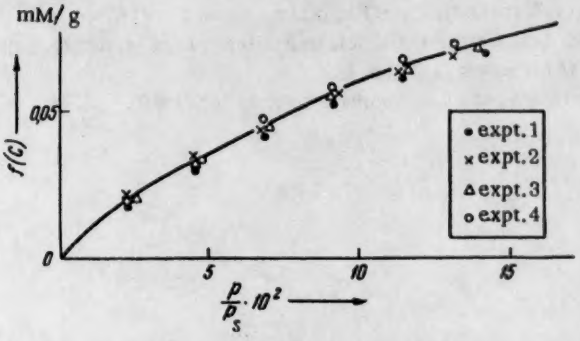

Fig. 4. Heptane adsorption isotherm on fireproof diatomaceous brick determined in four parallel chromatographic experiments.

Analysis of the Experimental Data

As is well-known, the following equation may be derived from the material balance [2-4]

$$\varkappa q \left(\frac{\partial C}{\partial t}\right)_x + (1-\varkappa)\left(\frac{\partial a}{\partial t}\right)_x = \omega \left(\frac{\partial C}{\partial x}\right)_t. \qquad (1)$$

Here C represents the concentration in the flowing gas (mg/cm^3); a, the amount adsorbed (mg per 1 cm^3 adsorbent); q, the cross section of the chromatographic column (cm^2); κ, the fraction of the cross section not occupied by adsorbent; ω, the flow rate (cm^3/min); t, the time from the start of the experiment (min); x, the distance from the inlet in the direction of flow (cm).

We assume that the adsorption equilibrium is established instantaneously and the longitudinal diffusion may be neglected; then, by integrating Equation (1), one may obtain the following simple relation from which the adsorption isotherm may be calculated

$$f(C) = \frac{\omega k}{ug} S_i; \qquad (2)$$

where $f(C)$ represents the amount adsorbed (mM/g) at equilibrium with the concentration C; k, the detector constant ($mM/cm^3 \cdot cm$); u, the rate at which the record is moved (cm/min); g, the adsorbent weight (g); S_i, the area below the desorption curve (Figs. 2a and 2b).

In Figs. 3a and 3b the isotherms of heptane at 23° on various catalysts and adsorbents, determined by means of the chromatographic method, are compared with those obtained by means of a quartz helix in a vacuum apparatus. The specific surface areas were calculated by applying BET theory. In the Table the data obtained are summed up.

In Fig. 4 it is shown that the data obtained in four parallel experiments with brick reproduce satisfactorily. It has been shown in separate experiments that the results obtained for smooth adsorbents with wide pores depend rather little upon the flow rate of the inert gas or on the amount of adsorbent or catalyst.

The chromatographic determination of surface area did not give reproducible results for several adsorbents with a high number of narrow pores (for instance, activated charcoal). For a definite conclusion about the limits of applicability of the methods further investigations are needed.

The authors consider it as their pleasant duty to thank I. E. Neimark and M. A. Piontrovskaya for the preparation of the wide-porous samples of silica gel E and the nickel hydroxide 862.

LITERATURE CITED

1. J. N. Wilson, J. Am. Chem. Soc. 62, 1583 (1940).
2. E. Glueckauf, J. Chem. Soc., 1302 (1947).
3. S. Z. Roginskii and M. I. Yanovskii, Zhur. Fiz. Khim. 24, 2, 137 (1950).
4. a) L. Graf and J. Toth, Acta Chim. Acad. Sci. Hungaricae 13, 3-4, 403 (1958); b) S. J. Gregg, and R. Stock, Gas Chromatography (Amsterdam, 1959) p. 90.
5. S. N. Oziraner, G. A. Gaziev, et al, Zavodskaya Lab. 6, 760 (1959).*

* Original Russian pagination. See C. B. translation.

KINETICS OF THE HYDROLYSIS OF PYRIDINE – SULFUR TRIOXIDE

I. G. Ryss and D. B. Donskaya

Dnepropetrovsk Institute of Railroad Transport Engineers
(Presented by Academician A. A. Grinberg, March 16, 1960)
Translated from Doklady Akademii Nauk SSSR, Vol. 133, No. 4, pp. 882-885, August, 1960
Original article submitted March 4, 1960

As one of us showed [1], the activation energy E of the hydrolysis of coordination compounds of boron trifluoride with amines, which proceeds by an S_N1 mechanism and in which the solvent attacks the B–N bond, increases steadily with a decrease in pK of basic dissociation of the amine; the point expressing the relation between E for the hydrolysis of BF_4^- and pK of the F^- ion lies on a continuation of the same curve although in BF_4^- a B–F bond is hydrolyzed. The entropy of activation $\Delta S^{\ddagger}$ of hydrolysis of compounds of BF_3 with amines increases linearly with an increase in E; the entropy of activation of BF_4^- hydrolysis [2] is extremely small and this is apparently caused by the increase in the order in the structure of water occurring with an increase in the length of the $-B \cdots F^-$ bond at the moment of formation of the transition state.

The data presented above confirm the existence of a relation between the kinetics of hydrolysis of a coordination compound and the thermodynamic properties of the donor. It might be expected that similar relations may also exist for a series of compounds of one particular donor with different acceptors (Lewis acids).

The great similarity in the hydrolysis kinetics of BF_4^- and SO_3F^- [3] is connected both with the similarity in structure of these ions and their activation mechanisms and possibly with the closeness of the strengths of BF_3 and SO_3 as Lewis acids.

If this is so, then one might expect a similarity in the kinetic characteristics of hydrolysis of compounds of boron trifluoride and sulfur trioxide with tertiary amines; the hydrolysis of compounds with secondary or primary amines should differ more sharply due to the strong acidic (protonic) dissociation of compounds of these amines with SO_3.

The hydrolysis kinetics of F_3B : Py, where Py is pyridine, were studied previously by one of us [4]. There are only qualitative indications on the rate of hydrolysis of O_3S: Py. Baumgarten [5] reported that this compound is relatively resistant to the action of water up to 50°; according to A. P. Terent'ev and L. A. Kazitsina [6], pyridine–sulfur trioxide is hydrolyzed by water "so slowly that it may be recrystallized from it."

Synthesis of Pyridine–Sulfur Trioxide. We used the method in [6] with some modifications. Into 75 ml of dichloroethane, stirred with a magnetic stirrer, was distilled 25 g of sulfur trioxide. A solution of 25 g of pyridine in 25 ml of dichloroethane was added dropwise to the solution obtained with external cooling with ice and stirring. The precipitate of O_3S : Py was collected on a Nutsch filter, washed with dichloroethane, and freed from excess pyridine and dichloroethane with a stream of dry air sucked through the filter and then in a desiccator over concentrated sulfuric acid. The product was stored in sealed ampoules and the contents of an opened ampoule were immediately transferred to a reagent bottle in a desiccator.

Carefully purified and dried reagents were used for the synthesis and the apparatus had ground glass joints.

Contact with atmospheric moisture was possible only during the transfer of the substance to the Nutsch filter and the desiccator and during the sealing in ampoules. However, due to the rapid hydrolysis of $O_3S:Py$ according to the equation

$$O_3S:Py + H_2O = [PyH]HSO_4, \quad (1)$$

the substance obtained contained a considerable amount of pyridine hydrosulfate.

The total SO_3 content of the product was determined by precipitation as $BaSO_4$ after complete hydrolysis. We also determined the alkali consumption in titration (in the presence of phenolphthalein) of the products of complete hydrolysis. Found in %: SO_3 48.43; 48.37; 48.39, average 48.40; alkali consumption in mg-equiv/g: 12.17 and 12.18; average 12.715.

The SO_3 content equaled 96.21% and the alkali consumption 96.89% of theoretical. This was due to the content of inert impurity (dichloroethane) and also the $[PyH]HSO_4$ content. As will be shown below, the hydrolysis of dissolved $O_3S:Py$ proceeds relatively slowly at 0°; this made it possible to determine the $[PyH]HSO_4$ content approximately. A sample of substance was added to ice water containing phenolphthalein and rapidly titrated with alkali to the first coloration with vigorous shaking of the suspension. The alkali consumption equaled 2.44-2.46 mg-equiv/g of substance, which corresponds to a content of 21.7% of $[PyH]HSO_4$ or 2.20% of water bound according to Equation (1); consequently the content of inert impurity equaled 1-1.5% (calculated by difference).

Kinetics of Hydrolysis of Dissolved Pyridine–Sulfur Trioxide. The rate of hydrolysis of pyridine–sulfur trioxide according to Equation (1) was investigated by titrimetric determination of the time dependence of the alkali consumption in the titration of $[PyH]HSO_4$ (in the presence of phenolphthalein). Due to the high rate of hydrolysis of $O_3S:Py$, the removal of a solution sample for titration would have led to considerable errors and we therefore carried out successive titrations on the same solution.

For reactions at 10-25°, the reaction vessel was a flask with a ground glass stopper and double walls between which water from an ultrathermostat circulated. Into the flask was placed ~30 ml of water and when the temperature of the latter reached that of the circulating water, a sample of ~0.04 g of $O_3S:Py$ in a small bottle was introduced into the flask, which was shaken vigorously for the precipitate to dissolve more rapidly. When the precipitate had dissolved, 1 drop of a 1% alcohol solution of phenolphthalein was introduced* and the solution periodically titrated with 0.10692 N NaOH from a 5-ml microburette and the moment at which color appeared was read off from a timer. In some experiments, excess alkali (relative to the pyridine hydrosulfate present at the given moment) was added to the solution periodically and the time until the indicator was decolorized recorded. The titration with alkali (or the introduction of excess alkali) was carried out as rapidly as possible in order to decrease the absorption of CO_2 from the air.

The rate of hydrolysis of $O_3S:Py$ measured by the two methods was found to be the same, and consequently the hydrolysis rate was independent of the presence of H^+ or OH^- with moderate concentrations of these ions. The cleavage of $O_3S:Py$ to glutaconic aldehyde derivatives by cold concentrated alkali, which was reported by Baumgarten [5], did not occur under our conditions. The relative content of pyridine–sulfur trioxide in the solution at the moment of time ϑ equals

$$x \equiv \frac{v_\infty - v}{v_\infty},$$

where v and v_∞ are the alkali consumptions at the moment of time ϑ and after complete hydrolysis, respectively. The results of all the experiments are well described by the equation

$$\lg \frac{x_0}{x} = 0{,}4343\, k\vartheta, \quad (2)$$

which is readily derived for processes of the first order.

As is shown readily, x_0 (the value of x extrapolated to $k\vartheta = 0$) should be less than unity as the starting material

* A number of experiments showed that the consumption of $O_3S:Py$ in the sulfonation of alcohol under these conditions was negligibly small; the indicator did not react with pyridine–sulfur trioxide either.

Conditions and Results of Studying the Kinetics of Hydrolysis of Pyridine–Sulfur Trioxide

Expt. No.	°C	Duration of expt. in min.	Number of points measured	2+lg x_0	0.4343k min^{-1}	$\eta \cdot 10^2$
1	0,0	126,8	6	1,8665	$2,41 \cdot 10^{-3}$	2,8
2	0,0	137,2	8	1,8526	$2,42 \cdot 10^{-3}$	1,8
3	10,0	128,2	8	1,8721	$7,31 \cdot 10^{-3}$	7,7
4	10,0	127,3	8	1,8716	$8,06 \cdot 10^{-3}$	9,2
5*	10,0	146,2	8	1,8689	$7,74 \cdot 10^{-3}$	7,7
6	14,9	61,1	"	1,8711	$1,33 \cdot 10^{-2}$	3,8
7	14,9	74,7	"	1,8040	$1,30 \cdot 10^{-2}$	11,2
8*	14,9	75,4	7	1,7766	$1,26 \cdot 10^{-2}$	2,0
9	15,1	64,2	8	1,8112	$1,40 \cdot 10^{-2}$	9,0
10	25,0	34,3	8	1,8437	$4,06 \cdot 10^{-2}$	12,7
11	25,0	18,4	8	1,7871	$4,12 \cdot 10^{-2}$	9,0

contained pyridine hydrosulfate which is neutralized by alkali instantaneously; x_0 may differ somewhat from the relative initial content of O_3S : Py in the substance investigated due to the difference between the rates of heterogeneous hydrolysis (at the beginning of the experiment before the substance had dissolved completely) and hydrolysis of the dissolved pyridine–sulfur trioxide.

For studying the hydrolysis rate at 0°, a sample of O_3S : Py (0.07-0.09 g) was added to 60-70 ml of ice water and lumps of ice in a flask surrounded by ice; the change in concentration of the solution due to part of the ice melting did not affect the results of measuring the rate constants of a first order reaction.

The Table gives the experimental conditions and average values of log x_0 and 0.4343k (in min^{-1}); to characterize the deviation of the points in the Table, we also give the mean error in the determination of log $\underline{x}$, $\eta = \frac{\Sigma|\Delta|}{n}$, where Δ is the deviation of the value of log $\underline{x}$ found for the moment ϑ from that calculated from Equation (2) for the same value of ϑ, and $\underline{n}$ is the number of measurements in one experiment. The maximum value of η corresponded to an error in the determination of log $\underline{x}$ (or the time reading) of ~ 3%.

The asterisks mark experiments (Nos. 5 and 8) in which the pyridine–sulfur trioxide was hydrolyzed in an alkaline medium. The higher values of log x_0 in Experiments 1-6 are explained by the fact that they were determined with a sample of pyridine–sulfur trioxide from a freshly opened ampoule as in all cases log x_0 fell with an increase in the time that the pyridine–sulfur trioxide was stored in a desiccator in a closed bottle.

The mean values of $\underline{k}$ for each temperature apart from 0°, obtained by the method of least squares, were used to derive the following equation for the temperature dependence of the rate constant (in min^{-1}):

$$\log (0.4343k) = (4088.4/T) + 12.3215. \qquad (3)$$

The discrepancies between the values of log (0.4343k) found and those calculated from Equation (3) are given below:

Temp.°C	log (4343k) found	log (4343k) calculated	$\Delta \cdot 10^2$
~0	$\bar{3},3856$	$\bar{3},3543$	31,3
10,0	$\bar{3},8856$	$\bar{3},8817$	4,8
14,9	$\bar{2},1139$	$\bar{2},1286$	—14,9
15,1	$\bar{2},1461$	$\bar{2},1384$	7,7
25,0	$\bar{2},6117$	$\bar{2},6094$	2,3

The value of 0.4343k at ~0°, which was not used in calculating the coefficient of Equation (3), corresponds to that calculated for + 0.57°.

From Equation (3) it follows that the experimental activation energy of the hydrolysis of pyridine–sulfur trioxide E = 18.7 kcal/mole, while the entropy of activation $\Delta S^{\ddagger} = -10.6$ entropy units. The similar values of E = 20.3 and $\Delta S^{\ddagger} = -8.3$ were found [4] for the hydrolysis of F_3B : Py. Consequently, our hypothesis on the similarity of the hydrolysis kinetics of the two coordination compounds is confirmed. At 25°, O_3S : Py is hydrolyzed 5.2 times faster than F_3B : Py.

The results of the investigation show that the hydrolysis of pyridine–sulfur trioxide proceeds much more rapidly than could be judged from qualitative data [5, 6]. At 50° the value of log (0.4343k) should equal 1.670, i.e., the half-decomposition period of dissolved O_3S : Py equals only 1.5 min so that the recrystallization of pyridine–sulfur trioxide from hot water is evidently impossible.

LITERATURE CITED

1. I. G. Ryss, Doklady Akad. Nauk SSSR 120, 797 (1958).*
2. I. G. Ryss and M. M. Slutskaya, Zhur. Fiz. Khim. 21, 549 (1947).
3. I. G. Ryss and T. A. Gribanova, Zhur. Fiz. Khim. 29, 1822 (1955).
4. I. G. Ryss and S. L. Idel's, Zhur. Neorg. Khim. 2, 2716 (1957).
5. P. Baumgarten, Ber. 59, 1166 (1926).
6. A. P. Terent'ev and L. A. Kazitsina, Zhur. Obshch. Khim. 18, 723 (1948).

* Original Russian pagination. See C. B. translation.

THE EFFECT OF TEMPERATURE ON THE CORROSION RATE OF METALS IN ACID MEDIA

V. A. Khitrov, V. I. Shatalova, I. S. Smol'yaninov, and Yu. I. Sadovskaya

Voronezh State Pedagogical Institute
(Presented by Academician V. I. Spitsyn, March 10, 1960)
Translated from Doklady Akademii Nauk SSSR, Vol. 133, No. 4, pp. 886-888, August, 1960
Original article submitted March 3, 1960

The equation established by Arrhenius in 1889 for the reaction rate as a function of temperature is very general and fully applicable to heterogeneous reactions, particularly to corrosion processes. For the latter case the equation can be expressed in the form

$$K = A \exp\left(-\frac{E_{\text{eff}}}{RT}\right), \quad (1)$$

where A is a constant while E_{eff} is the effective activation energy. Converting Equation (1) into a logarithmic expression we will get a linear relationship,

$$\lg K = \lg A - \frac{E_{\text{eff}}}{2{,}303RT}, \quad (2)$$

which can be used to calculate K at intermediate temperatures between experimental points and also to determine the apparent activation energy.

Many workers [1-3] consider the Arrhenius equation satisfactory and sufficiently accurate for relatively active metals in acid media. In several papers [4, 5] a linear relationship between current density and 1/T has been experimentally established and the function resembles Equation (1). If $\Delta\varphi$ is constant this relationship remains linear over a wide range of potentials. However, data can be found in the literature which indicate that the linear relationship does not always hold.

Deviations from the Arrhenius equation are particularly frequent in cases where metal corrosion is accompanied by oxidative depolarization: in open systems where the decreased corrosion rate at higher temperatures is connected with decreasing solubility of oxygen; in such cases Eq. (2) in coordinates $\log K - 1/T$ frequently gives a curve with maximum [5]. Also in cases involving gaseous corrosion the function $\log K = f(1/T)$ occasionally deviates from a straight line, especially if the crystal structure of the metal undergoes a change (for example, α-Fe $\rightarrow$ γ-Fe).

Gutmann and Simmons [6] have suggested that these deviations from linearity are either due to the fact that the constants A and E_{eff} change appreciably with temperature or that several simultaneous equations take place.

While investigating the effects of temperature on the corrosion rates of certain metals (steel, Fe, Ni, Zn, Al, Cu, Cd, Sn, Pb) in acidic media (1N HCl and H_2SO_4) we found that only in very few cases did the equation $\log K = f(1/T)$ deviate from a straight line. In sulfuric and hydrochloric acids the Arrhenius equation was adequate enough for iron, steel, nickel, tin, cadmium, and aluminum (the last one only in 1N H_2SO_4), as can be seen in Fig. 1.

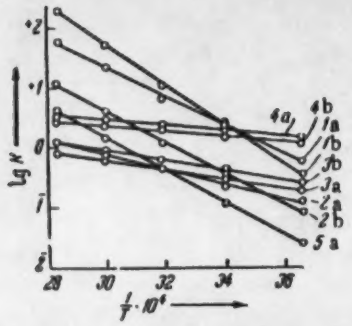

Fig. 1. The common logarithm of the corrosion rate of metals as a function of the reciprocal of absolute temperature. 1) Armco iron; 2) nickel; 3) tin; 4) cadmium; 5) aluminum; a) in 1N H_2SO_4; b) in 1N HCl.

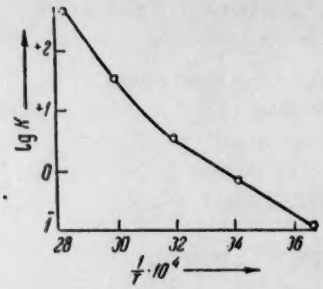

Fig. 2. The common logarithm of aluminum corrosion rate in 1N HCl as a function of the reciprocal of absolute temperature.

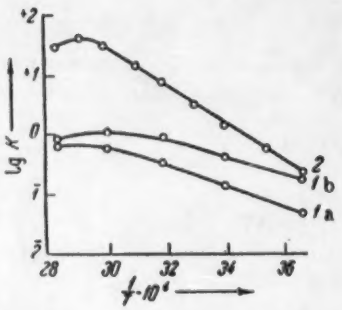

Fig. 3. The common logarithm of the corrosion rate of metals as a function of the reciprocal of absolute temperature. 1a) Copper in 1 N H_2SO_4; 1b) copper in 1N HCl; 2) aluminum in 35N H_2SO_4.

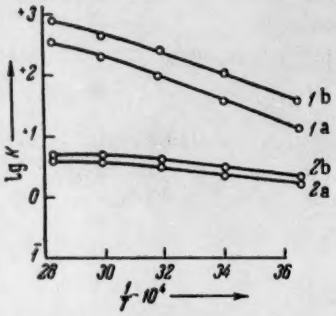

Fig. 4. The common logarithm of the corrosion rate of metals as a function of the reciprocal of absolute temperature. 1) Zinc, 2) lead, a) 1N H_2SO_4; b) 1N HCl.

However, while studying the temperature dependence of the corrosion rate of aluminum in 1N hydrochloric acid we found that the rate increased much faster with temperature than one would anticipate from Equation (2) (see Fig. 2). The deviation becomes apparent only at temperatures above 40°C. It is obvious that E_{eff} must be increasing with temperature. We can explain this behavior of aluminum in hydrochloric acid by assuming that at higher temperatures the chloride ions attack and destroy the oxide coating of aluminum (which is usually stable in dilute acids), particularly the pseudomorphous layer. One must also remember that, as was first established by N. D. Tomashov and T. V. Matveeva [7], the negative differential effect shows up on aluminum under these conditions.

Just the contrary was observed when the corrosion of technical grade aluminum (A1-2) in concentrated (35N) sulfuric acid was investigated. In this case too, below 50-60°C the corrosion rate increases with temperature in accordance with Arrhenius' equation, but at higher temperatures the rate drops off considerably (Fig. 3). When log K is plotted against 1/T the curve exhibits a maximum at about 70°C. Between 60 and 80°C E_{eff} is negative. A transition into passive state would provide a very satisfactory explanation for the behavior of aluminum under these conditions. It seems that both the high acid concentration and the elevated temperature greatly enhance the oxidizing action of sulfuric acid. As a result the film covering the bottom of the pores becomes less permeable to Al^{3+} ions, the pore dimensions decrease, and passivation sets in reducing effectively the corrosion rate of aluminum.

Our observations were very similar in the case of copper; the corrosion rate in a 1N solution of either acid goes through a maximum at a certain temperature which can be explained by assuming that the solubility of oxygen in the open system decreases at higher temperatures.

We also found some cases (zinc and lead in either acid) where at elevated temperatures the equation $\log K = f(1/T)$ deviated from a straight line toward the temperature axis (Fig. 4). Apparently this is due to the fact that at higher temperatures the rates of both the chemical and the diffusion processes increase but the rate of the former increases faster than that of the latter [8]. Consequently at higher temperatures the diffusion factor will become very important and may even control the reaction. This effect becomes particularly pronounced in the case of lead where the surface screening produced by solid salt films is a contributing factor.

On the basis of our experimental results we can conclude that the corrosion rate of metals in acid media changes with temperature in accordance with the Arrhenius equation, unless certain complicating factors enter into play. If the temperature rise is accompanied by changes in the metal structure or a destruction of the oxide film, or if it renders the metal passive, the corrosion rate will not obey the Arrhenius equation and Equation (2) will deviate from a straight line. Two types of deviations are possible. There is also no doubt that at elevated temperatures certain deviations of the log K vs 1/T line toward the temperature axis may be caused by the fact that the increase in diffusion rate does not keep up with the increase in the chemical reaction rate.

LITERATURE CITED

1. N. D. Tomashov, Corrosion Theory and Metal Protection [in Russian] (Moscow, 1959).
2. I. N. Putilova, S. A. Balezin, and V. P. Barannik, Inhibitors of Metallic Corrosion [in Russian] (Moscow, 1958).
3. V. V. Gerasimov and I. L. Rozenfel'd, Izvest. Akad. Nauk SSSR, Otdel. Khim. Nauk, 10, 1166 (1957).*
4. S. V. Gorbachev, Zhur. Fiz. Khim. 24, 7, 888 (1950).
5. A. V. Izmailov, College Sci. Report, Chem. and Chem. Tech. [in Russian] 23, 1 (1958); Zhur. Fiz. Khim. 30, 12, 2813 (1956).
6. F. Gutmann and L.M. Simmons, Proc. Met. Internat. Comm. Electrochem., Thermodyn. and Kinet. (London, 1954).
7. N. D. Tomashov and T. V. Matveeva, Trans. Phys. Chem. Institute, 2, Investigation of Metallic Corrosion, 1, [in Russian] 146 (1951).
8. A. I. Brodskii, Physical Chemistry [in Russian] (Moscow-Leningrad, 1948) 2.

* Original Russian pagination. See C. B. translation.

THE EFFECTS OF LIGHT ON POLARIZED GERMANIUM ANODES

A. A. Yakovleva, T. I. Borisova, and V. I. Veselovskii

L. Ya. Karpov Physicochemical Institute

(Presented by Academician A. N. Frumkin, March 18, 1960)
Translated from Doklady Akad. Nauk SSSR, Vol. 133, No. 4, pp. 889-892, August, 1960
Original article submitted March 18, 1960

The behavior of germanium anodes in electrolytic solutions has been investigated by many workers [1-6], and although the mechanism of anodic dissolution is not yet fully understood one can state with a certain degree of certainty that: first of all, since the reaction involves the use of holes, the number of holes generated in the solid by thermal vibrations determines the actual saturation current in N-type germanium, and second, that germanium goes into solution as a hydroxide complex ion. It is known that polarized N-Ge anodes are very sensitive to light but, with the exception of several papers [1], there is no comprehensive data on the photoelectrochemical relationships involved in such processes.

In this work an attempt was made to determine the effects of light on the structure of the germanium–electrolyte phase boundary and on the anodic dissolution of germanium. In using various forms of radiation it is important that one be able to irradiate the electrode in such a way as to avoid any side effects that might be caused by any of the solution radiolysis products (in cases where ionizing radiation is used).

The apparatus consisted of a Teflon cylinder which was topped by a quartz window at one end and had the investigated germanium samples at the other; the samples were made in the form of discs the thickness and crystal orientations (III) of which were varied. A circular resistance contact was soldered to the dry side of the sample. All of our work was carried out on single crystals of N-type germanium of various specific resistances in 0.1N NaOH and under nitrogen. The samples were polished and dipped in a standard poisoning solution SR-4, then washed thoroughly with twice-distilled water. We used 0.4-0.7 μ monochromatic light from an incandescent lamp. The samples were illuminated either under conditions of steady current or steady voltage. Figure 1 shows that the system remains photosensitive over the entire range of investigated polarizations. When an N-anode is exposed to light the potential barrier disappears completely, i.e., the potential over the entire saturation region drops to a constant value of 0.5 v. Above the breakdown voltage the effect rapidly disappears.

The anodic dissolution can be represented by the over-all reaction [2]:

$$Ge + 2OH^- + 2e \rightarrow Ge(OH)_2^{2+} + 2e.$$

The slope "v" of the initial section of the polarization curve (Tafel region) decreases from 110 mv in total darkness to 80 mv under intense illumination (Fig. 2). In this region the concentration of excess carriers does not as yet control the reaction rate at the anode. However, under nonequilibrium conditions when the anode current is flowing, a part of the measured potential drop occurs in the space charge region of the semiconductor. It has already been demonstrated [7] that in such cases the reaction rate at the anode may be represented by the function

$$i = ke^{-\Delta\varphi F/RT}e^{-\alpha\Delta HF/RT}, \quad (1)$$

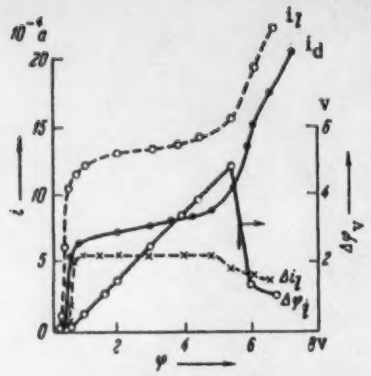

Fig. 1. The effects of polarization on various photoelectrochemical parameters of N-Ge 3/07 in 0.1 N NaOH.

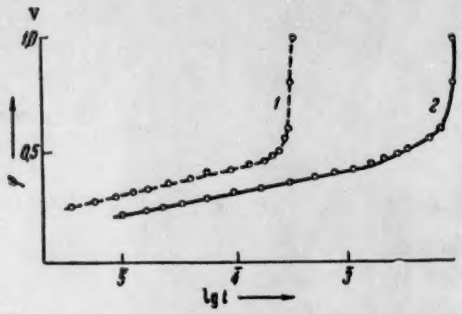

Fig. 2. i_d (1) and i_l (2) as a function of voltage in the Tafel region.

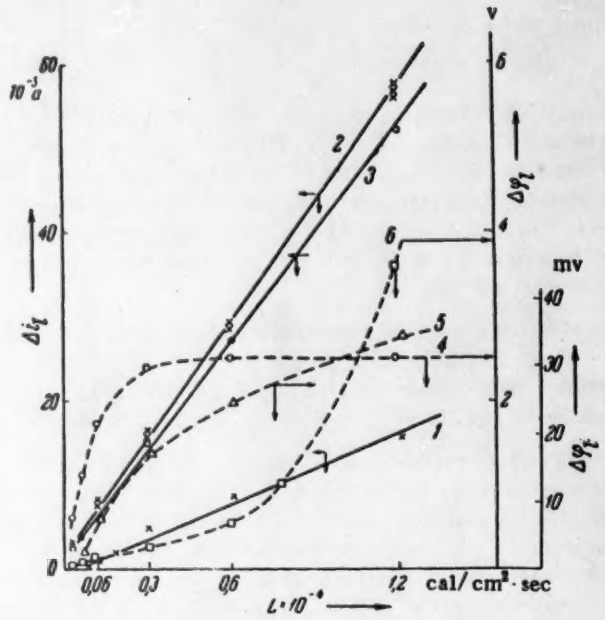

Fig. 3. Δi_l (1, 2, 3) and $\Delta\varphi_l$ (4, 5, 6) as a function of light intensity at 0.5, 3, and 5 v respectively.

TABLE 1

$L_{incid.}$ cal. / cm · sec.	Δi (theoret.)	Δi_l (exper.)	hν, ev.	K
$1{,}2 \cdot 10^{-4}$	$1{,}4 \cdot 10^{-4}$	$3{,}6 \cdot 10^{-4}$	1,8	2,6
$0{,}6 \cdot 10^{-4}$	$7 \cdot 10^{-5}$	$18{,}2 \cdot 10^{-5}$	1,8	2,6
$0{,}3 \cdot 10^{-4}$	$3{,}5 \cdot 20^{-5}$	$9{,}1 \cdot 10^{-5}$	1,8	2,6
$1{,}2 \cdot 10^{-5}$	$1{,}4 \cdot 10^{-5}$	$4{,}55 \cdot 10^{-5}$	1,8	3,2
$0{,}6 \cdot 10^{-5}$	$0{,}7 \cdot 10^{-5}$	$2{,}6 \cdot 10^{-5}$	1,8	3,7
$0{,}3 \cdot 10^{-5}$	$0{,}35 \cdot 10^{-5}$	$1{,}6 \cdot 10^{-5}$	1,8	4,5

TABLE 2

φ_d	L_{abs}	$h\nu$, ev	No. of incident quanta	Δi_l	Current yield	κ
0,45	$0,6\cdot10^{-4}$	1,8	$8,65\cdot10^{14}$	$10,4\cdot10^{-5}$	$6,4\cdot10^{14}$	0,73
3	$0,6\cdot10^{-4}$	1,8	$8,65\cdot10^{14}$	$36,0\cdot10^{-5}$	$22,3\cdot10^{14}$	2,6
6	$0,6\cdot10^{-4}$	1,8	$8,65\cdot10^{14}$	$18,2\cdot10^{-5}$	$11,3\cdot10^{14}$	1,3
0,45	$0,6\cdot10^{-5}$	1,8	$8,65\cdot10^{13}$	$17,5\cdot10^{-5}$	$10,8\cdot10^{13}$	1,24
3	$0,6\cdot10^{-5}$	1,8	$8,65\cdot10^{13}$	$4,55\cdot10^{-5}$	$28,2\cdot10^{13}$	3,2
6	$0,6\cdot10^{-5}$	1,8	$8,65\cdot10^{13}$	$2,5\cdot10^{-5}$	$15,8\cdot10^{13}$	1,8

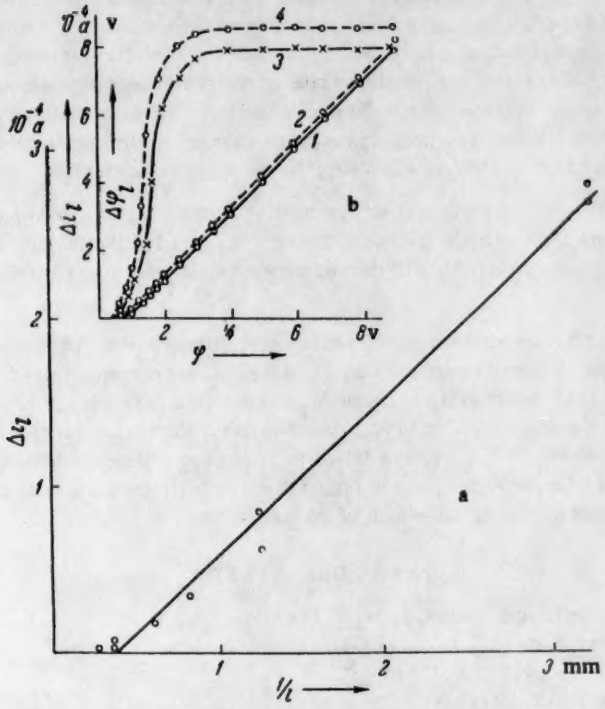

Fig. 4. a) Δi_l as a function of electrode thickness for low-resistance Ge; b) for high-resistance Ge: 1) and 3) $\Delta\varphi_l$ and Δi_l on the dry side; 2) and 4) on the electrolyte side.

where $\Delta\psi$ is the potential drop in the semiconductor space charge region, and ΔH is the potential drop in the ionic double layer.

$\Delta\psi$ and the concentration of charge carriers in the surface layers of the solid are connected by the equation:

$$C_{surf} = C_{bulk}^{-ne\Delta\psi/kT}. \qquad (2)$$

Thus, any factor which might affect the surface concentration of electrons and holes (surface treatment, polarization, illumination) should influence both the $\Delta\psi$ and the total measured potential difference $\Delta\varphi$.

As the light is absorbed in the surface layers, by changing the concentration and distribution of carriers it displaces the energy levels in such a way as to render the measured potential difference on N-anodes smaller since the voltage drop in the space charge region of the semiconductor is now reduced. According to Equation (1) if $\Delta\psi$ decreases during illumination the slope (in "v") should also decrease.

In Fig. 3 we have plotted the photoelectrochemical characteristics Δi_l and $\Delta \varphi_l$ as a function of light intensity for all the polarization regions. In every case the photoelectrochemical current increases linearly with the number of quanta absorbed. The relationship between $\Delta \varphi_l$ and light intensity is more complicated. In the Tafel region $\Delta \varphi_l$ is an exponential function of intensity, in the saturation current region it approaches a limiting value at high intensities, and above the breakdown voltage the potential barrier changes very little when the light intensity is reduced.

An important characteristic of the system is the quantum yield of the photoelectrochemical reaction. Table 1 gives the quantum yields at various intensities of absorbed light in the region of saturation voltage. The quantum yield is inversely proportional to the intensity when L is small and remains constant when L is large. It seems that in the latter case recombination effects become more pronounced. Table 2 gives values of K at two intensities. K has a maximum in the saturation region. It is noteworthy that the quantum yield is greater than one and varies from one and a half to four. This effect seems to be of the same general nature as the so-called "coefficient of charge multiplication" reported by several workers [1-3]. In our experiments the value ranged from one and a half to four depending on the experimental conditions. It is impossible to enter into a full discussion of this problem in the present communication, but it should be noted that though the multiplication itself is connected with the nature of the electrochemical reaction the absolute value of the coefficient depends on the conditions under which the carriers recombine on the surface. Since the excess carriers created by light remain most of the time in a thermal equilibrium with the lattice they participate in the charge multiplication through the same mechanism as do the carriers involved in dark current which explains the high quantum yield.

To extend the applicability of our method it was interesting to determine the relationship between the photoelectrochemical parameters and the electrode thickness when the dry side is illuminated. It is obvious that in this case the photoelectrochemical current Δi_l will depend very much on the recombination effects inside the sample and on the surface.

In the case of high-resistance germanium (ρ = 28 ohm · cm, diffusion path 1.8 mm) when the plate is at least 0.5 mm thick it makes very little difference (as far as Δi_l or $\Delta \varphi_l$ is concerned) whether the dry or the wet side is illuminated (Fig. 4, b). The relationship between Δi_l and the electrode thickness for low-resistance germanium (ρ = 2 ohm · cm, L = 0.5 mm) is shown in Fig. 4a. The figure shows that Δi_l is a linear function of the reciprocal of the electrode thickness. Thus, we have failed to detect any difference between the effects induced by radiation on the dry or the electrolytic side, and when the dry side is illuminated total extinction occurs if the plate is several times as thick as the diffusion path of the excess carriers.

LITERATURE CITED

1. W. Brattain and C. Garrett, Bell. Syst. Techn. J. 34, 129 (1955).
2. D. R. Turner, J. Electrochem. Soc. 103, 4, 252 (1956).
3. J. B. Flynn, J. Electrochem. Soc. 105, 12, 715 (1958).
4. J. Bardeleben, Z. Phys. Chem. 17, 39 (1958).
5. E. A. Efimov and I. G. Erusalimchik, Zhur. Fiz. Khim. 32, 1103 (1958).
6. H. Gerischer and F. Beck, Z. Electrochem. 63, 4, (1959).
7. V. I. Veselovskii, Zhur. Fiz. Khim. 22, 1427 (1948).

THE MECHANISM OF THE RECIPROCAL TRANSFER OF COPPER DURING FRICTION BETWEEN BRONZE AND STEEL

D. N. Garkunov, V. N. Lozovskii, and A. A. Polyakov

(Presented by Academician P. A. Rebinder, March 30, 1960)
Translated from Doklady Akademii Nauk SSSR, Vol. 133, No. 5, pp. 1128-1129, August, 1960
Original article submitted March 24, 1960

Earlier experiments on the study of friction between bronzes (BrOSN and BrOF) and steel, with lubrication by glycerol or an alcohol–glycerol mixture, have shown that a thin layer of bronze, enriched with copper, is formed on the steel surface. During friction, particles of this layer are transferred from the steel surface to the bronze surface, then back from the bronze surface to the steel (reciprocal transfer); this results in an almost complete absence of wear. This phenomenon has been called "atomic pick-up" [1]. The physical processes taking place during atomic pick-up have not been studied.

It appears to us that the processes taking place during friction between bronze and steel, with lubrication by glycerol, can be pictured as follows.

Contact between the parts takes place at isolated contact points, whose total area is much smaller than the nominal friction surface [2], so that it is natural to assume that during friction there are regions on the bronze surface at which intense evolution of heat takes place, and that at these regions, the oxide film which is always present on the surface is reduced to copper (by the glycerol). As a result of the atomic nonuniformity in composition, the reduction of the oxide film to copper takes place at those regions which are enriched with copper. These regions of the bronze are active centers for pick-up by the steel. The regions of the bronze which are not enriched with copper are worn away by the friction and the products of the wear are carried away by the glycerol. As a result, the steel surface gradually becomes covered with a thin layer of almost pure copper. Further treatment leads to the reverse transfer of copper from the steel surface to the bronze surface.

The following experiment was carried out in order to prove the selectivity of the process involved in the pick-up of copper by the steel:

Friction tests were carried out on an "MI" machine with two steel specimens at a specific pressure of 30 kg/cm^2 and a rate of sliding equal to 0.4 m/sec, with lubrication by glycerol containing some powdered black copper oxide CuO, in the form of a suspension. After 20-30 min, a thin deposit of copper was obtained on the surface of the steel specimens. The increase in temperature close to the points of contact between the specimens has thus led to the reduction of copper oxide to copper by the glycerol, followed by pick-up of the copper by the steel.

The following experiment was carried out in order to prove the reverse transfer of copper from the steel to the bronze: a steel rod of 25 mm diameter was fixed in the center of a lathe. Its surface purity corresponded to Class 11, according to State Standard GOST 2789-52. The surface of the rod was cleaned with crocus cloth to remove the thin film of oxide, the surface was lubricated with glycerol, and a rod of BrOF bronze was pressed with a force of 100 kg/cm^2 against the steel rod, which was rotating at a speed of 40 rpm. The experiments on the friction between the bronze and steel rods were carried out in two ways (Fig. 1). In the first case the bronze rod was moved along the steel rod, so that every part of the steel rod made contact only once. No traces of copper

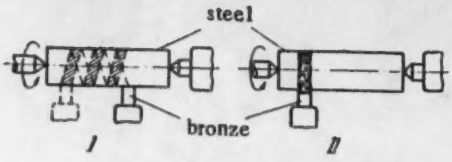

Fig. 1. Diagram illustrating the tests carried out with steel and bronze rods: I) bronze rod making contact only once with every part of the surface of the steel rod; II) bronze rod making repeated contact with a restricted area of the steel rod surface.

were found on the friction surfaces of the steel rod or bronze rod after 200 revolutions. In the second case, the bronze rod was not moved along the steel rod, and made contact with only one section of the steel rod. After 100 revolutions, the surface of the steel rod, and the surface of the bronze rod in contact with it, were covered with a layer of copper.

The experimental results show that the formation of a layer of copper on the surface of the bronze rod is possible only as a result of the transfer of copper from the steel surface. Thus, during friction between bronze and steel in glycerol, transfer of the copper of the bronze onto the steel surface first takes place, followed by transfer in the reverse direction from the steel surface to the bronze surface. The thin compact layer of copper formed on the friction surfaces of the bronze and steel prevents direct contact between the bronze and steel. The copper covering is readily picked up at the points of contact, and this leads to the reciprocal transfer of copper between the friction surfaces and to an almost complete absence of wear.

The friction between bronze and steel in liquids other than glycerol (kerosene, mineral oils, distilled water), including the nonpolar liquid paraffin, is not accompanied by this effect of reciprocal atomic transfer of copper.

These experiments indicate that friction between bronze and steel, with lubrication by glycerol, is accompanied by physicochemical processes which can be made the basis of new methods for treating friction surfaces.*

LITERATURE CITED

1. N. D. Garkunov and I. V. Kragel'skii, Doklady Akad. Nauk SSSR 113, 2 (1957).**
2. I. V. Kragel'skii, L. F. Bessonov, and E. M. Shchvetsova, Doklady Akad. Nauk SSSR 98, 1 (1953).

* Author's Certificate No. 115744.
** See C. B. translation.

THE PROBLEM OF MEASURING THE CONDENSATION COEFFICIENT

R. Ya. Kucherov and L. É. Rikenglaz

(Presented by Academician A. N. Frumkin, March 23, 1960)
Translated from Doklady Akad. Nauk SSSR, Vol. 133, No. 5, pp. 1130-1131, August, 1960
Original article submitted October 14, 1959

Much work has been devoted to the experimental determination of the condensation coefficient, α, [1, 2]. Depending on the vapor pressure, p_0, of the working material, these measurements have involved either a determination of the rate of evaporation in vacuum followed by an evaluation of α through the Langmuir Equation

$$\tau_0 = \alpha p_0 (2\pi mkT)^{-1/2}, \tag{1}$$

or a determination of the rate of vaporization at an interface where the pressure of vapor is p with evaluation of α from the Hertz-Knudsen Equation

$$\tau = \alpha (p_0 - p)(2\pi mkT)^{-1/2}. \tag{2}$$

The first of these techniques is applicable to substances for which $p_0 \lesssim 0.1$ mm of Hg, while the second is used for materials of higher vapor pressures.

Proof will be given in the present paper that Equation (2) is valid only for the limiting case in which $\alpha \ll 1$, and that it must therefore be used with extreme caution. Errors arise here from the fact that the derivation of the equation makes no allowance for the inevitable convectional movement of vapors which accompanies evaporation from, and condensation on, the liquid surface, and neglects the temperature discontinuity which prevails at the liquid–vapor interface.

Corrections for these effects have been carried out by the authors in [3] for the case of slow vaporization at a rate considerably less than the rate of vaporization into vacuum at the same temperature, the condensation coefficient, α, and the accommodation coefficient, β, being, in addition, equal to unity. Similar considerations show readily that the particle flow density for arbitrary values of these coefficients can be expressed through an equation of the form:

$$\tau = \alpha \frac{p_0}{\sqrt{2\pi mkT_0}} - \alpha \frac{p}{\sqrt{2\pi mkT}} + \alpha \frac{\tau}{2}, \tag{3}$$

in which T_0 is the temperature of the liquid surface, T is the temperature of the vapor at this surface, τ is the flow density of the vapor molecules, and m is the mass per molecule.

Simple transformations in which members involving second powers of the ratio τ/τ_0 are neglected give:

$$\tau = \frac{2\alpha}{2-\alpha} \frac{1}{\sqrt{2\pi mkT_0}} \left\{ (p_0 - p) - \frac{p_0}{2} \frac{T_0 - T}{T_0} \right\}. \tag{4}$$

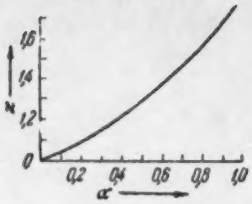

The temperature difference $T_0 - T$ will be determined through an expression for Q, the density of the energy flow. Reasoning in analogy with [3] shows the quantity of thermal energy transferred by the molecules in approaching the surface of evaporation to be given by

$$Q^- = \frac{p}{\sqrt{2\pi mkT}}[2kT + U(T)] - \frac{Q}{2}, \tag{5}$$

U(T) being the internal energy of the molecule at the temperature T and the relation being valid in the immediate neighborhood of the surface itself.

The flow of molecules away from the surface involves two components, the one composed of evaporating molecules and the other of molecules which have been scattered as a result of surface collision. The molecules of this last component make up a fraction $(1 - \alpha)$ of the molecules impinging on the surface. The energy exchange between these molecules and the surface is characterized by the Knudsen accommodation coefficient.

$$\beta = \frac{T_r - T}{T_0 - T}, \tag{6}$$

T_r being the effective temperature ascribed to the scattered molecules.

In view of these facts, the amount of thermal energy carried by the molecules in moving away from the surface is expressed by:

$$Q^+ = \alpha \frac{p_0}{\sqrt{2\pi mkT_0}}[2kT_0 + U(T_0)] + (1-\alpha)\left[\frac{p}{\sqrt{2\pi mkT}} - \frac{\tau}{2}\right][2kT_r - U(T_r)]. \tag{7}$$

The density of flow of thermal energy is equal to

$$Q = Q^+ - Q^-. \tag{8}$$

A contribution from the thermal conductivity is usually insignificant in this case and can be neglected, so that it is possible to set

$$Q = c_p T_0 \tau. \tag{9}$$

Elementary transformations with the aid of (5) – (9) give

$$T_0 - T = \frac{\sqrt{2\pi mkT_0}}{2\rho_0} \frac{\tau[c_p T_0 - 2kT_0 - U(T_0)]}{(c_v + k/2)[\alpha + \beta(1-\alpha)]}. \tag{10}$$

Setting (10) into (4) finally leads

$$\tau = \varkappa\alpha \frac{p_0 - p}{\sqrt{2\pi mkT_0}} \tag{11}$$

where

$$\varkappa = \frac{2}{2 - \alpha + \alpha[c_p - 2k - U(T_0)/T_0]/2[\alpha + \beta(1-\alpha)](c_v + k/2)}.$$

The figure shows the relation between $\varkappa$ and α for the special case of a monatomic gas ($U(T_0) = 0$) with $\beta = 1$. When $\alpha \to 0$, $\varkappa \to 1$, and (11) goes over into the Hertz-Knudsen Equation. Neglect of $\varkappa$ leads to significant error, however, when $\alpha \sim 1$.

The Hertz-Knudsen Equation has been used in working up the data obtained from all of the measurements of α which have been carried out at high vapor pressures. Re-examination should thus be made of such of these experiments as have led to α values approaching unity.

Comparison of the measured values of the condensation coefficient of a single substance for which $\alpha \sim 1$ as

determined through evaporation into vacuum and through slow vaporization would be of interest for an experimental test of the above-outlined considerations. To the best of the authors' knowledge, measurements of this type have not been carried out as yet.

LITERATURE CITED

1. O. Knacke and I. N. Stranski, Progr. in Metall Phys. 6, 181 (1956); Translation, Usp. Fiz. Nauk 68, 261 (1959).
2. A. N. Nesmeyanov and N. É. Sandamirova, Usp. Khim. 28, 117 (1959).
3. R. Ya. Kucherov and L. É. Rikenglaz, Zhur. Éksp. Teor. Fiz. 37, 125 (1959).

MORPHOLOGY OF MOLECULAR PACKING IN LINEAR POLYESTERS

Yu. V. Mnyukh, E. M. Belavtseva, and A. I. Kitaigorodskii

Institute for Heteroorganic Compounds, Academy of Sciences, USSR
(Presented by Academician I. V. Obreimov, March 23, 1960)
Translated from Doklady Akademii Nauk SSSR, Vol. 133, No. 5, pp. 1132-1135, August, 1960
Original article submitted March 3, 1960

Continuing a research on molecular packing in crystals of linear polyesters [1, 2], we used the electron microscopy method, electron photography and small angle x-ray photography. Our interest in this subject arose in connection with the obtainment of small-angle x-ray photographs which indicated the existence of a very strict periodicity of the order of 100-200 A. In addition to this, it was observed that the value of the overperiod increased, in general, with the length of the chemical structure units (see Table).* The x-ray photographs contained clear reflexes up to 4-th order, whereas usually small-angle x-ray photographs of polymers contain only one diffraction order. Only one case is known [3] where it was possible to obtain four orders of reflection from a period of ~100 A in polyethylene, but the latter was prepared by precipitation from a solution under slow cooling conditions, whereas the samples of polyesters were obtained from a fused mass without maintaining special thermal conditions during their hardening.

As is well known [4-8], in recent years monocrystalline formations were detected in linear polymers with regular chains (polyethylene, guttapercha, polyamides, isotactic polyolefins).** The same process was detected by us for the class of linear polyesters. Photomicrographs showed crystals growing in spiral terraces, and also single monocrystalline layers (Fig. 1). Microdiffraction recording (Fig. 2) permitted us to establish the fact that the axes of the molecules were perpendicular to the planes of these monolayers. An investigation of the external form of the crystals, which made the knowledge of the crystal subcell easier (see the Table) showed that the face indices $\{\pm 1, \pm 1, 0\}$ and $\{100\}$ could be attributed to the external contours. These were just those planes where neighboring chains were more densely packed with each other, and therefore were the most probable growth faces from a theoretical point of view.

The fact itself that a monocrystal growth had already been detected for one class of polymers indicated that for polymers with regular chains this phenomenon had quite a general character. The study of the large number of electron-microscope photographs we had at our disposal showed, moreover, a strict connection of these structures with more complicated morphological formations also observed at the electron microscope (see also [9]).

Samples for study at the electron microscope were prepared by dissolving the polymer in hot ethanol of

*The value of the periodicity in question depended upon the thermal hardening conditions. For instance, a sample of decamethyleneglycol with adipic acid, when hardened in a current of liquid nitrogen vapors, gave the period 151 A, and after fusion and slow cooling gave a period of 194 A. However, all the substances listed in the Table were obtained in roughly identical conditions.

**The present investigation relates to crystalline polymers. As to amorphous polymers, geometrically regular forms were also detected in them.

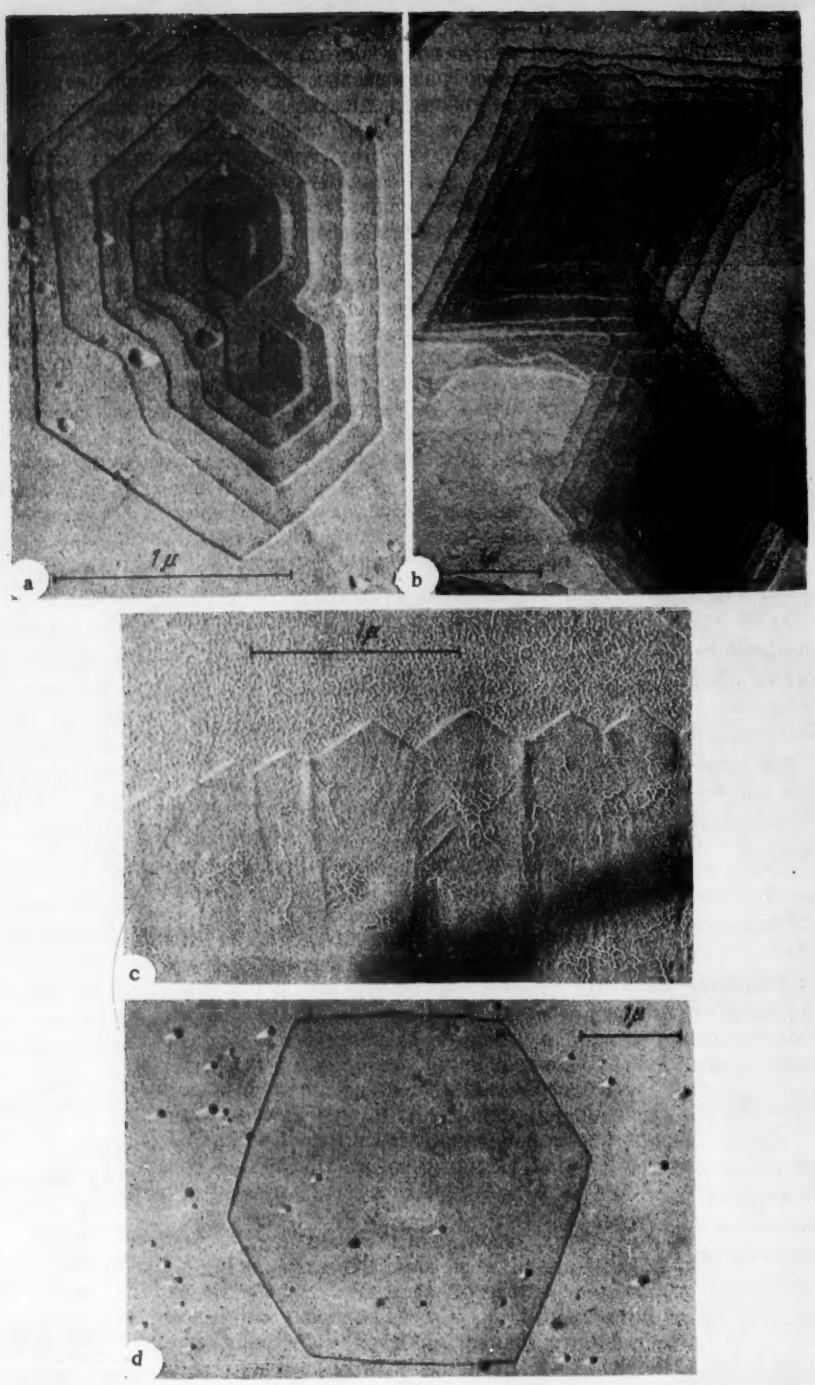

Fig. 1. a, b) Monocrystalline formations in polyesters (samples obtained from a solution); c, d) monocrystalline formations in polyesters, monolayers (from a solution).

Sample	Length of the chemical structure unit,* A	Longest plane to plane distance, determined by the C=O groups, A	Large periods		Parameters of the R-subcell, A		
			A	number of diffraction orders	a_0	b_0	c_0
Polyester of decamethylethyleneglycol and of:							
oxalic acid	17.5	13.2	104	2	6.90	5.24	(?)
succinic acid	20.0	13.0	142	3	7.30	5.04	2.47-2.51
glutaric acid	21.2	18.9	162	3	7.36	4.96	2.46
adipic acid	22.5	10.6	182	4	7.40	5.01	2.48
azelaic acid	26.2	18.3(?); 9.5	208	4	7.45	4.98	2.48
sebacic acid	27.5	12.2	180	4	7.41	4.96	2.47

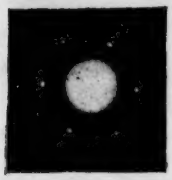

Fig. 2. Diffraction picture of the monolayer shown in Fig. 1d.

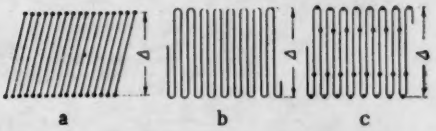

Fig. 3. Thickness of a crystal layer (schematic diagram). The methyl and ester groups are denoted by dots; a) n-paraffin, b) polyethylene, c) polyesters.

amyl acetate. Upon cooling under usual room conditions, crystals separated out of the solutions: in the case of ethanol, they were as a rule hexagonal, in the case of amyl acetate they were rhombic, and the process was easily reproducible. We think that the unusual ease of crystallization was due to the comparatively low molecular weight of the polymers (2000-3000) as well as to their very nature. A slow cooling caused the crystals to grow to a size of a few tens of microns. On the other hand, in less balanced conditions, for which special procedures were sometimes required intermediate forms, corresponding to a transition to spherulites, were obtained. A number of plates showed a structure consisting of monocrystalline layers adjacent to each other passing continuously to sheafs which are, as is well known, the embryonic form of spherulites.

A special consideration is deserved by the height of the steps on the spiral terraces. It is well known that in crystals of normal paraffins the directions of the molecular axes either coincide with the normal to the plane of the crystals or form with it a small angle, and the thickness of the steps therefore corresponds to the length of the molecule [10]. In polyethylene the axes of the chains are normal to the layers; the thickness of a layer [12] corresponds to the "period of torsion" (a term introduced by Keller), i.e., to the distance between two consecutive turns of the molecular chain, usually equal to 100-120 A, although the physical nature of the chain bending with a conservation of an exceptionally rigid periodicity of the value mentioned above has not yet been explained. The structure of a polyester chain differs from that of polyethylene because ester groups are regularly distributed around it. The period of a chemical structure unit for the substances under study of the decamethylene glycol series is equal to 17-30 A and for the eicosamethyleneglycol is 30-43 A.* Measurements of the height of the steps and of single monolayers from electron microscope photographs gave values lying in the limits 15-35 A for objects of the decamethyleneglycol series and 40-70 A for the ercosamethyleneglycol series. A comparison of these

*If the chain is considered as a plane zig-zag with a period c_0 = 2.5 A and the doubling of the period connected to the symmetry of the chain for some terms of the homologous series is not considered.

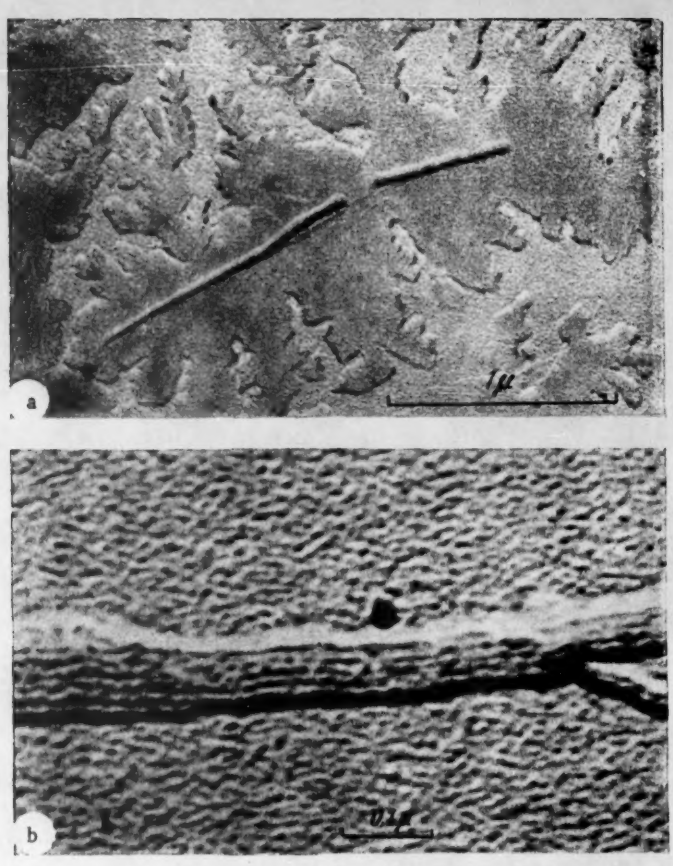

Fig. 4. a) Dendrite formations (from the fused mass); b) fragment of a lens consisting of a few fibers. 140,000 x.

figures gives some ground for thinking that in the packing of polyester molecules we are dealing with a new phenomenon, when the torsion period is determined by the length of the chemical structure unit. We hope to verify this fact more in detail in the future. The three cases mentioned above are shown schematically in Fig. 3. The analysis of a large number of photomicrographs permitted us to suggest that the height of the steps in monocrystals was not a completely stable quantity. This conclusion was supported by x-ray photographs at small and large angles of a sample precipitated from a solution of the same concentration used at the electron microscope. The x-ray photograph contained only the diffraction picture of a subcell, but the overstructural periodicity (~100-200 A), as well as the periodicity determined by the oxygen atoms of the C=O group (~10-15 A), had vanished completely. The periodicity corresponding to the thickness of the crystal layers (~20-30 A for samples of the decamethyleneglycol series) had also vanished.

The photomicrographs also showed some different morphological forms. By changing the conditions of preparation of the objects, it was possible to obtain large dendrite formations, consisting of monocrystals grown together, a spiral growth of unlimited monolayers, the development of globules from a spiral, dendrites in the form of monolayers with wrinkles in the middle, fibrils, etc. Sometimes 2-3 different forms could be noted in one observation field.

Correlation diagrams between the small angle periodicity (100-200 A) and the electron microscope picture led us to investigate at the electron microscope samples crystallized from a fused mass. In order that they should be transparent for an electron beam, they were first prepared in the way described above, laid on their supporting plate, and then fused and subsequently hardened under definite thermal conditions. The picture obtained, which is shown in Fig. 4, shows monolayers in the form of dendrites with wrinkles in the middle, consisting of a number

of parallel fibers. These fibers sometimes lie individually in a line joining in some parts, forming lenses, which in their turn pass gradually to monolayers. In those places where the lenses consisted of fibers lying in one series on the line, it was possible to establish that the width of the individual fibers composing it was equal to ~130 A and their height was ~30 A. We note that the first figure has the same order of magnitude as the periodicity detected in the camera for small angles, and the second coincides approximately with the height of a step in the monocrystal. Thus, regardless of the fact that the section of an individual fiber was very small and exceeded by only two orders of magnitude the size of the section of one molecule, this does not provide any basis for thinking that it is a beam of parallel molecules. On the contrary our data agree better with the data of [12], according to which the axes of the molecules are more likely to be perpendicular than parallel to the axes of the fibers.

Finally it is important that "sheafs" were obtained from a fused mass, and gradually passed to monocrystalline layers, definitely similar to those that had been obtained from samples prepared from a solution, and that from a solution we obtain dendrites, lenses and fibers coinciding in their aspects with those reported in Fig. 4; the fibers had also the same width. Moreover, Fig. 4a shows the appearance of a crystalline boundary of the monolayers for the samples obtained from a fused mass.

The authors express their gratitude to É. I. Fedin for his collaboration in the present research, and also to S. V. Vinogradov for the preparation of the samples.

LITERATURE CITED

1. Yu. V. Mnyukh, Izv. Akad. Nauk. SSSR, Otdel. Khim. Nauk, 9, 1129 (1958);* Zhur. Fiz. Khim. 33, 2076 (1959).
2. Yu. V. Mnyukh, Izv. Akad. Nauk. SSSR, Otdel. Khim. Nauk, 10, 1276 (1958);* Zhur. Fiz. Khim. 33, 2190 (1959).
3. A. Keller and A. O'Connor, Nature 180, 1289 (1957).
4. R. Saccodine, Nature 176, 305 (1955).
5. P. H. Till, J. Polym. Sci. 23, 301 (1957).
6. A. Keller and A. O'Connor, Disc. Farad. Soc. 25, 114 (1958).
7. F. C. Frank, A. Keller, and A. O'Connor, Phil. Mag. 4, 200 (1959).
8. A. W. Agar, F. C. Frank, and A. Keller, Phil. Mag. 4, 32 (1959).
9. R. Eppe, W. Fischer, and H. A. Stuart, J. Polym. Sci. 34, 721 (1959).
10. J. M. Dawson and V. Vand, Proc. Roy. Soc. A 206, 555 (1951).
11. A. Keller, Phil. Mag. 2, 1171 (1957).
12. A. Keller, J. Polym. Sci. 36, 361 (1959).
13. V. A. Kargin, N. F. Bakeev, Kh. Vergin, Doklady Akademii Nauk SSSR 122, 97 (1958).*

*Original Russian pagination. See C. B. translation.

AUTOOSCILLATION PROCESSES IN SOME ELECTROCHEMICAL SYSTEMS

Yu. A. Chizmadzhev

Electrochemical Institute of the Academy of Sciences, USSR
(Presented by Academician A. N. Frumkin, March 28, 1960)
Translated from Doklady Akademii Nauk SSSR, Vol. 133, No. 5, pp. 1136-1139, August, 1960
Original article submitted March 28, 1960

It is well known that electrode reactions consist of a series of successive stages, such as diffusion, adsorption, and the electrochemical reaction proper. In some systems parallel reactions are possible, such as the simultaneous discharge of particles A and B, or the discharge of particle A and the adsorption of particle B. The latter process is a nonstationary one. Each stage of the reaction may be allocated a definite physical magnitude. Thus, the diffusion stage is determined by the concentration, c, of particles near to the electrode (where "near" is to be understood as having a macroscopic significance); adsorption may be characterized by the surface concentration Γ, and the electrochemical reaction proper by the electrode potential φ. We shall designate the number of degrees of freedom in an electrochemical system (or the order of the system) as the number of variables, c, Γ, φ,..., necessary for the full description of the behavior of the system with time. The question naturally arises as to how to determine the number of degrees of freedom in the different systems encountered experimentally. It usually happens that, among the stages of any one reaction, one or two of the stages are slow ones, that is, they are characterized by relatively small exchange current. To solve problems of stationary states, it is sufficient to describe the system with the help of magnitudes which correspond to the slow stages. For example, the reaction involving cathodic discharge of hydrogen at a mercury electrode from a 1 N solution of hydrochloric acid, with a current density of $i = 1 \cdot 10^{-4}$ a /cm^2, is completely described by the overpotential η. In considering the process of establishment of the stationary condition, certain stages are neglected, the velocity of which may be large; this may sometimes lead to qualitative disagreement with experiment. Therefore, in the solution of the problem as to the number of degrees of freedom of an actual system, in the last analysis experiment is the only criterion: if the choice of any particular magnitude as a determining variable does not lead to results in harmony with experiment, it will be necessary to elaborate the model with the introduction of supplementary variables.

We shall consider the process of setting up a stationary state in a system with a single degree of freedom. The law of conservation of charge at the electrode can be expressed in the following form:

$$\frac{dQ}{dt} = \frac{E - \varphi}{R} - j(\varphi), \tag{1}$$

where E is the imposed potential, R is the resistance of the external circuit, $j(\varphi)$ is the polarization characteristic. In this equation, the quantity $(E-\varphi)/R$ represents the current in the external circuit, and $j(\varphi)$ the reaction current. If $(E-\varphi)/R$ is greater than $j(\varphi)$, the charge Q at the electrode increases with time. Introducing the constant capacity, C, of the electrode, we may connect the change in charge, dQ, with the change in potential, $d\varphi$, by the relationship: $dQ = C \cdot d\varphi$, and then rewrite Equation (1) in the form:

$$C\frac{d\varphi}{dt} = \frac{E - \varphi}{R} - j(\varphi). \tag{2}$$

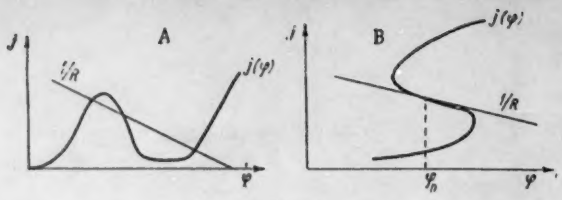

Fig. 1.

In the stationary state, $d\varphi/dt = 0$, and $(E - \varphi_0)/R = j(\varphi_0)$, where φ_0 is the stationary potential at the electrode. Dividing Equation (2) by C, and introducing the relationship $\frac{1}{C}\left[\frac{E-\varphi}{R} - j(\varphi)\right] = F(\varphi)$, we obtain the relationship:

$$\frac{d\varphi}{dt} = F(\varphi). \tag{3}$$

Related equations have been studied in a similar way in the theory of oscillations [2]. The electrochemical systems described by Equation (3) have been investigated by Frank [3]. Depending on the form assumed by $F(\varphi)$, Equation (3) may possess various numbers of stationary conditions. In the presence of descending branches of the function $j(\varphi)$, the stationary conditions may be unstable. We have been interested, however, not merely in the loss of stability, but in the possibility that periodic processes might take place in the system described by Equation (3). We shall assume that Equation (3) described a periodic process. Then, with certain values of φ, the system should proceed in opposite directions: that is, with two different values, $d\varphi/dt$, or which is the same thing, $F(\varphi)$, ought to become a nonsingle-valued function. Only the quantity $j(\varphi)$ can be the source of the nonsingle-valued character. If the polarization characteristics possess a N-shaped form (Fig. 1A), then the function $F(\varphi)$ is everywhere single valued, and a periodic process is impossible. If, however, the polarization curve belongs to the S-type (Fig. 1B), the function $F(\varphi)$ has a region of nonsingle-valued character, and a periodic process becomes possible in the system, the amplitude of which is determined by the depth of the curve loop. Such S-shaped curves have been only little investigated experimentally, and we have been limited to a consideration of curves of the N-type.

There are described in the literature oscillations occurring in the ionization of hydrogen at the platinum electrode under conditions in which passivity arises [4-7]. Equations (1) to (3) have not yet been employed for the description of the behavior of such systems, since the properties of the electrode depend critically on the amount of chemisorption of anions or of oxygen, and the establishment of equilibrium with respect to the adsorbed particles takes place only slowly [8]. It should be said that the platinum electrode is a system with two degrees of freedom. It is known that, in the development of the potential difference at the platinum electrode [1, 9], the adsorption of atoms of hydrogen and oxygen take part. In accordance with this we shall consider the potential of the electrode as a single-valued function $\varphi(Q, \Gamma)$ of the charge of the metallic surface of the double layer, Q, and the surface concentration, Γ, of the adsorbed substances. The exchange current for the adsorption of hydrogen is 10^3 times as great as the exchange current for the oxygen adsorption. It may consequently be supposed that for any value of Q the surface concentration of the hydrogen is an equilibrium value, and the potential may be regarded as a function of the one variable Q or Γ_H; that is, $\varphi = \varphi_1(Q)$, or $\varphi = \varphi_2(\Gamma_H)$. The process of adsorption and disadsorption of oxygen, as well as that of anions, is irreversible [7, 8]. A hysteresis loop is found because of the slowness with which equilibrium is established during the adsorption of oxygen. The loop diminishes with reduction in the current. On the ascending branch $\Gamma < \Gamma_{eq}$, while on the descending $\Gamma > \Gamma_{eq}$. From the fact that the process is irreversible it follows that the electrode potential in the presence of adsorption of anions and oxygen is determined by the combination of the two dynamic variables Q and Γ, which are not connected by any equilibrium relationship. We shall accept the assumptions made in [10], according to which passivation, in solutions containing adsorbable anions, causes a reduction in the number of active points on the electrode because of adsorption. We shall denote, as in [9], the total charge of the metallic surface by Q, and the surface concentration of ions by Γ (including hydroxyl ions among the anions). The total charge Q is equal to $q + \epsilon$, where q is the free charge, compensating the charge of the electrical double layer, and ϵ is the "bound" charge, compensated by that of the adsorbed anions. We write down the law of conservation of total charge thus:

$$\frac{dQ}{dt} = \frac{E-\varphi}{R} - j(\varphi, \Gamma), \tag{4}$$

where $j(\varphi,\Gamma)$ is the discharge current of the hydrogen. We now write the conservation law for Γ as:

$$\frac{d\Gamma}{dt} = I(\varphi, \Gamma). \tag{5}$$

In the stationary condition, $d\Gamma/dt = 0$, and $I(\varphi,\Gamma) = 0$. Equation (5) describes the nature of the change in the number of active points on the surface with time. If it is supposed that the number of active points on the surface is only changed by adsorption and disadsorption of anions, then we may write: $I(\varphi,\Gamma) = I_{ads} - I_{dis}$. The form of the function $I(\varphi,\Gamma)$ is very little known and therefore we make no assumption about this function, but investigate instead what conditions it should fulfil if an autooscillation process is to take place at the electrode. If we express Equations (4) and (5) in terms of the variables φ and Γ, the system of equations assumes the form:

$$\frac{d\Gamma}{dt} = I(\varphi, \Gamma), \quad C\frac{d\varphi}{dt} = \frac{E-\varphi}{R} - j(\varphi, \Gamma) - FI(\varphi, \Gamma). \tag{6}$$

In distinction from the systems with one degree of freedom, the current for the adsorption of anions enters into the equation for the potential. In the stationary state the adsorption current, $I(\varphi,\Gamma)$, becomes zero, and the current in the external circuit is equal to the ionization current of the hydrogen, $j(\varphi_0,\Gamma_0)$. The stationary condition is determined from the condition that $(E-\varphi)/R = j(\varphi,\Gamma)$, and $I(\varphi,\Gamma) = 0$. For the investigation of the stability of the stationary condition φ_0,Γ_0, it is necessary to introduce small deviations from the stationary condition, such that: $\overline{\varphi} = \varphi - \varphi_0$, and $\Gamma = \Gamma - \Gamma_0$. The investigation shows that the stationary condition is unstable if the following inequality is true:

$$\frac{1}{C}\left[-\frac{1}{R} - \left(\frac{\partial j}{\partial \varphi}\right)_\Gamma - \left(\frac{\partial I}{\partial \varphi}\right)_\Gamma F\right] + \left(\frac{\partial I}{\partial \Gamma}\right)_\varphi > 0. \tag{7}$$

The magnitude $(\partial j/\partial \varphi)_\Gamma$ which enters into this equation is always positive, even with falling static characteristics. The required fulfilment of this necessary inequality may only be realized if $(\partial I/\partial \varphi) < 0$, or $(\partial I/\partial \Gamma)_\varphi > 0$.

The instability of the stationary condition is not a sufficient guaranteee that oscillations will arise. In order to achieve the limiting cycle, another inequality must also be satisfied, namely:

$$\left[-\frac{1}{R} - \left(\frac{dj}{d\varphi}\right)_\Gamma\right]\left(\frac{\partial I}{\partial \Gamma}\right)_\varphi + \left(\frac{\partial j}{\partial \Gamma}\right)_\varphi \left(\frac{\partial I}{\partial \varphi}\right)_\Gamma > 0. \tag{8}$$

We note immediately that the derivative $(\partial j/\partial \Gamma)_\varphi < 0$. We assume that the derivative $(\partial I/\partial \varphi)_\Gamma > 0$. Then the product $(\partial j/\partial \Gamma)_\varphi (\partial I/\partial \varphi)_\Gamma < 0$, and for the fulfillment of the condition posed by the inequality (8) it is necessary that the derivative $(\partial I/\partial \Gamma)_\varphi$ be less than zero. But if $(\partial I/\partial \Gamma)_\varphi < 0$, and simultaneously $(\partial I/\partial \varphi)_\Gamma > 0$, the inequality (7) will not be realized. It is therefore necessary, if oscillations are to arise, that $(\partial I/\partial \varphi)_\Gamma$ shall be less than zero. For this the sign of $(\partial I/\partial \Gamma)_\varphi$ is of no importance. For let $(\partial I/\partial \Gamma)_\varphi$ be less than zero. This will always be the case if no interaction occurs between the adsorbed particles. Then we obtain from Equation (7):

$$F\left|\left(\frac{\partial I}{\partial \varphi}\right)_\Gamma\right| > C\left|\left(\frac{\partial I}{\partial \Gamma}\right)_\varphi\right| + \frac{1}{R} + \left(\frac{\partial j}{\partial \varphi}\right)_\Gamma. \tag{9}$$

In this case the condition set by (8) is automatically fulfilled. Since $I_\varphi < 0$ and $I_\Gamma < 0$, then $(d\Gamma/d\varphi)_{stat} < 0$; that is, oscillations may arise only around this stationary condition, if at this point the number of active centers increases as the potential increases. On the static potential curve, correspondingly, there should be observed in this region of potentials a rising portion. A necessary condition for the development of oscillations is that irreversible adsorption shall occur. For assume that the adsorption is reversible: then it may be assumed that at any moment the concentration term Γ is at equilibrium with φ. The system of equations can be converted into a single equation for the potential:

$$C\frac{d\varphi}{dt} = \frac{E-\varphi}{R} - j(\varphi),$$

which does not possess an oscillatory solution. Comparison of theory with experiment is somewhat difficult, since

it is only in paper [7] that polarization characteristics have been obtained. The oscillations observed in that work actually occurred in the region of increase of the polarization curve. This growth, in the opinion of the author, was due to the increase in the number of active centers in the surface because of the dissolution of the platinum. This process can be regarded as formally equivalent to the disadsorption of anions which is required by the theory. It would be considerably easier to test the theory on a liquid cathode with adsorbed organic materials, for which the curve of $\Gamma(\varphi)$ is known. Oscillations are described in the literature on solid electrodes in the presence of surface active substances [11]. It is interesting to note that the oscillations in these experiments were observed in the disadsorption region, in harmony with the conclusions of the theory set out above.

I offer my hearty thanks to Academician A. N. Frumkin for raising the problem and for his numerous valuable contributions to the discussion; and also to Corresponding Member of the Academy of Sciences, USSR V. G. Levich for his helpful advice and constant interest in the work.

LITERATURE CITED

1. A. N. Frumkin, V. S. Bagotskii, Z. A. Iofa, and B. N. Kabanov, Kinetics of Electrode Processes [in Russian] (1952).
2. A. A. Andronov, A. A. Vitt, and S. É. Khaikin, The Theory of Oscillations [in Russian] (1959).
3. U. F. Frank, Z. Phys. Chem. 3, 183 (1955).
4. M. Thalanger and M. Volmer, Z. Phys. Chem. 150, 401 (1930).
5. J. Butler and F. Armstrong, Nature 129, 613 (1932).
6. J. Butler, Disc. Farad. Soc. 1, 122 (1947).
7. É. A. Aikazyan, Zhur. Fiz. Khim. 33, 5 (1959).
8. Ts. I. Zalkin and B. V. Ershler, Zhur. Fiz. Khim. 25, 565 (1951).
9. A. N. Frumkin and A. I. Shlygin, Izv. Akad. Nauk. SSSR, Ser. Khim., 5 (1936).
10. A. N. Frumkin and É. I. Aikazyan, Dokl. Akad. Nauk SSSR 100, 315 (1956);* Izv. Akad. Nauk SSSR, Otdel. Khim. Nauk, 1959, 202*
11. A. T. Vagramyan, Zhur. Fiz. Khim. 22, 1496 (1948).

* Original Russian pagination. See C. B. translation.

SPECIFIC CATALYTIC ACTIVITY OF IRON FILMS TOWARD ISOTOPIC EXCHANGE IN MOLECULAR HYDROGEN

M. A. Avdeenko (Corresponding Member, Acad. Sci. USSR),

G. K. Boreskov and K. N. Zhavoronkova

L. Ya. Karpov Physicochemical Institute

Translated from Doklady Akademii Nauk SSSR, Vol. 133, No. 6, pp. 1354-1357, August, 1960
Original article submitted May 11, 1960

When one ascertains the relation between the specific catalytic activity of metals and their electronic structure, the question always arises to what extent and how the specific activity of one and the same metal may be varied. These variations may be connected both with structural factors (for instance, size and orientation of crystallites) and with possible variations in chemical composition. It has been repeatedly pointed out in literature that films, as regards their catalytic and adsorptive properties, differ considerably from massive metals [1, 2]. It may be assumed that the high activity – when compared with that of massive metals – of films obtained by condensation of metal vapors in vacuum is connected with peculiarities of their structure. Films from massive metals differ in several of their properties (lattice parameters, work function, electric conductivity) according to the evidence given by various authors [3-5]. The aim of this study is the elucidation of the influence which the conditions of evaporation and sintering of iron films have on their catalytic activity toward the isotopic exchange in molecular hydrogen.

Experimental method. The catalytic activity of the iron films was measured by a static method. Most of the experiments were done at a pressure of 0.5 mm Hg. At this pressure the external diffusion has no appreciable influence upon the reaction rate up to an absolute rate of the order of 10^{-7} mole/sec. The reaction order was measured by varying the pressure between 0.05 and 5 mm Hg. The experimental set-up is schematically shown in Fig. 1. The reaction volume (300-400 cm^3) comprises the glass vessel (1), on the inner wall of which the film was deposited, a trap (2), which is cooled by liquid nitrogen during the whole of the experiment, and the bulb (3), in which the concentration of HD molecules is measured continuously by means of heat conductivity. A 4.5 liter flask, containing unreacted $H_2 + D_2$ mixture, could be connected periodically to the reaction volume; this enabled the measuring of the reaction rate to be repeated without pumping away gas from the reaction volume. A gallium seal (6), by which the film could be isolated from the rest of the apparatus, was placed between the reaction vessel and the trap. Before the depositing of a film the reaction volume was thoroughly outgassed at 500° until the residual pressure stayed below 10^{-7} mm Hg. The films were deposited by heating an iron strip (2-3 mm wide and 0.2-0.3 mm thick) by a constant current and condensing the vapor onto the inner wall of the reaction vessel. The surface areas of the films were determined from the adsorption of hydrogen (at pressures between 10^{-2} and 10^{-1} mm Hg) and krypton using the volumetric method. An equimolar $H_2 + D_2$ mixture was used for measuring the rate of exchange. Spectroscopically pure iron (brand Hilger) was used for the deposition of the films. The gas content of this iron was analyzed by melting in vacuum by means of a high-frequency furnace. It appeared to contain 0.12 cm^3/g (mainly hydrogen, nitrogen and oxygen), which is much lower than the gas content of iron samples of other brands. The oxygen content is 0.0015 weight %. The reaction rate constant was calculated using a first order equation [6].

The maximum error in the determination of the specific catalytic activity is 20%, if the surface area of

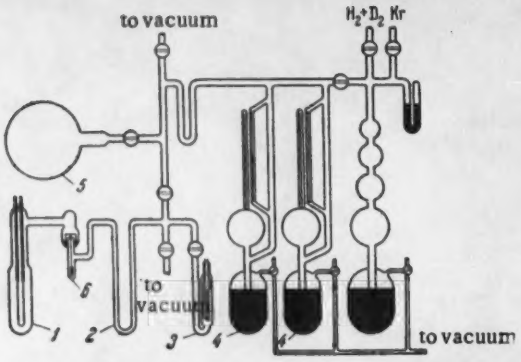

Fig. 1. Scheme of the apparatus.

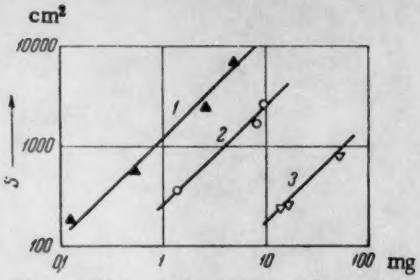

Fig. 2. The relation between the surface area and the film weight. Deposition temperatures: 1) −196°, 2) 20°, 3) 300°.

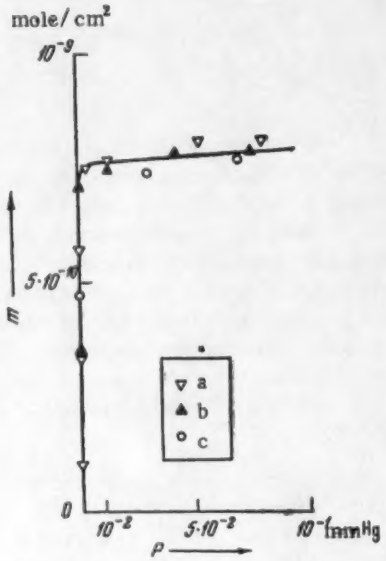

Fig. 3. Hydrogen adsorption at −196°: a) weight 2.1 mg, deposited at −196°; surface area 2500 cm²; b) weight 6.3 mg, deposited at 20°, surface area 1800 cm²; c) weight 53 mg, deposited at −196°, sintered at 300°, surface area 830 cm².

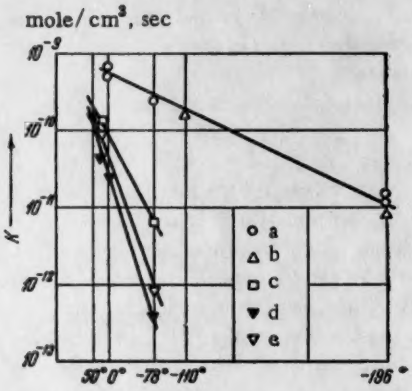

Fig. 4. The dependence of the reaction rate at 0.5 mm pressure upon temperature: a) deposition at 20°, E = 800-900 cal/mole; b) deposition at 300°; c) sintered at 300°, E = 3300 cal/mole; d) sintered at 300°, E = 5200 cal/mole; e) sintered at 550°; E = 7600 cal/mole.

the film exceeds 1000 cm². When the films have a surface area of the order of 100 cm², then the maximum error in the determination of the specific activity will be considerably higher (up to 50%), mainly because it is difficult to measure very small surface areas.

Characterization of the iron films. In our experiments the iron films were deposited at −196°, 20°, and 300°. This enabled the size of the crystallites to be varied in a broad range. The mean size of the crystallites may be estimated, because the weight of the film and its surface area are known. Although the deposition temperature was varied in a broad range (from −196° to 300°) at each temperature a linear relation between the weight of the film and its surface area was observed (Fig. 2). Hence, the growth of film must be ascribed to an increase in the number of crystallites without a change in their size. The size of the crystallites only depends upon the deposition temperature. Just the same, regularities have been found for other transition metals [7]. The crystallite sizes and the specific surface areas of iron films, deposited at the various temperatures, are shown in Table 1.

Hydrogen adsorption was measured mainly at −196°. Typical adsorption isotherms for three different iron

TABLE 1

Temp. of film deposition, °C	a, Å	S_{spec}, m^2/g
—196	60	125
20	300	25
300	4800	1,6

TABLE 2

Temp. of film deposition, °C	K, $\frac{mole}{cm^2 sec}$	a, Å
20	$2,3 \cdot 10^{-12}$ $3,3 \cdot 10^{-12}$ $2,8 \cdot 10^{-12}$	300
300	$2,7 \cdot 10^{-12}$ $2,9 \cdot 10^{-12}$ $2,1 \cdot 10^{-12}$ $3,5 \cdot 10^{-12}$	4800

TABLE 3

Temp. of film deposition, °C	K, $\frac{mole}{cm^2 sec}$	a, Å
20	$8 \cdot 10^{-12}$ $13,7 \cdot 10^{-12}$	300
300	$14,5 \cdot 10^{-12}$	4800
—196	$23 \cdot 10^{-12}$	60

TABLE 4

Sintering temp. °C	K, $\frac{mole}{cm^2 sec}$
—196	$35 \cdot 10^{-12}$
300	$45 \cdot 10^{-12}$ $39 \cdot 10^{-12}$ $48 \cdot 10^{-12}$
550	$20 \cdot 10^{-12}$

films (hydrogen adsorption is referred to 1 cm^2 surface area, as measured by krypton adsorption) are shown in Fig. 3. Apparently, the points lie on the same curve. In all cases, the hydrogen adsorption proceeds very rapidly at −196° and a considerable amount (up to 95% coverage) is adsorbed at very low equilibrium pressures. In the pressure range 10^{-3}-10^{-1} mm Hg an additional small hydrogen absorption is observed. Obviously, in this pressure range hydrogen adsorption is reversible already at −196° and proceeds at a lower rate. The slow adsorption amounts to about 15% of the rapid one. The data on hydrogen adsorption obtained by us are in good agreement with those in literature [8-10].

Influence of the conditions at which the iron films were deposited upon the specific catalytic activity. The results of the first experiments in which the specific activity of iron films was measured at −196° and P = 0.5 mm are given in Table 2.

Although the size of the iron crystallites varies by a factor of 16, the specific activity of the films stays nearly constant. In the first experiments, obviously, the iron samples from which the films were evaporated had been insufficiently outgassed, for the films had a low activity. In later experiments (Table 3) we used one iron sample, for which previously several films had been evaporated in idle runs over a long stretch of time. It is evident that by this procedure the specific activity increased a few times, but that, nevertheless, the films, deposited at various temperatures, differed very little in their activity.

Especially interesting are the films deposited at −196°. Owing to the low mobility of metal atoms at low temperatures one may expect the formation of any irregular structure. In the opinion of certain authors, films deposited at low temperatures will be strongly "disordered" [11]. However, their activity is very near to that of films deposited at higher temperatures, as our experiments have shown. Even when the crystallite size is varied by 80 times, the specific activity changes at most by only two times. The change observed may be partially connected with a variation in the orientation of the crystal faces. The reaction order was measured at −196° in the 0.05-5 mm Hg pressure range and it was found to be 0.6-0.7. The activation energy of the reaction in the range −196° − 0° is 800-900 cal/mole (Fig. 4).

The influence of sintering upon the specific activity of iron films. When the films are sintered, the specific surface area sharply decreases and they approach massive metals in their properties. It was interesting to trace the change in their specific activity at the same time. The first experiments, done with films obtained from insufficiently outgassed iron samples, have shown that the specific activity sharply decreases by the sintering and the activation energy increases (Fig. 4); this is in disagreement with the fact established by us, namely

that the specific activity of films deposited at various temperatures is nearly constant. Therefore, it is impossible to explain the decrease in activity observed in our first experiments by changes in structure. Contamination of the film surface is another possible cause of the decrease in activity. The concentration of impurities may be sharply raised as a result of the sharp decrease in surface area. Therefore, it is necessary that a film which will be exposed to sintering should be as free from impurities as possible. For this reason we used a sample of iron which had been molten previously in vacuum to remove impurities as completely as possible. Before use several blank films were evaporated from it. The results of these experiments are given in Table 4. In all cases, the films were deposited at −196°.

It is evident that, if sufficiently stringent precautions are taken, the specific activity of the films scarcely changes by sintering, while at the same time the surface area sharply decreases (by 50-100 times at 300° and by nearly 400 times at 550°).

From the results obtained by us the conclusion may be drawn that the specific activity of iron films remains nearly constant when the conditions of deposition and sintering are varied within a broad range. The decrease in catalytic activity caused by sintering is mainly connected with contamination of the surface.

LITERATURE CITED

1. B. M. W. Trapnell, Chemisorption [Russian translation] (IL, 1958).
2. A. C. Collins and B. M. W. Trapnell, Trans. Farad. Soc. 53, 1476 (1957).
3. J. H. de Boer, Adsorption Phenomena, Collection: Catalysis, Some Problems of Theory and Technology of Organic Reactions [Russian translation] (IL, 1959).
4. B. M. W. Trapnell, Trans. Farad. Soc. 51, 368 (1955).
5. N. A. Shishakov, Zhur. Éksp. i. Teor. Fiz. 22, 241 (1952).
6. M. A. Avdeenko, G. K. Boreskov and M. G. Slin'ko, Problems in Kinetics and Catalysis, Isotopes in Catalysis [in Russian](Moscow, 1957), 9.
7. B. M. W. Trapnell, Proc. Roy. Soc. A 218, 566 (1953).
8. N. N. Kavtaradze, Zhur. Fiz. Khim. 32, 1055 (1958).
9. N. N. Kavtaradze, Zhur. Fiz. Khim. 32, 909 (1958).
10. A. S. Porter and F. C. Tompkins, Proc. Roy. Soc. A217, 544 (1953).
11. R. Suhrman, Z. Elektrochem. 60, 8, 804 (1956).

EFFECT OF MOLECULAR WEIGHT ON THE LUMINESCENCE OF HIGH-MOLECULAR COMPOUNDS

V. F. Gachkovskii

Institute of Chemical Physics, Academy of Sciences, USSR
(Presented by Academician V. N. Kondrat'ev, April 14, 1960)
Translated from Doklady Akademii Nauk SSSR, Vol. 133, No. 6, pp. 1358-1360, August, 1960
Original article submitted April 5, 1960

Many polymers and biopolymers show bright fluorescence in solid and dissolved states. In the present work we made a qualitative investigation of polymers of very diverse chemical structures both with and without a continuous chain of conjugated bonds: polyphenylacetylenes, poly-p-carboxyphenylmethacrylamides, polystyrenes, polymethacrylates, a number of proteins, amino acids, nucleic acids DNA and RNA, etc. The fluorescence spectra were photographed on "Paninfra" spectral plates with a glass spectrograph with an illuminating power of 1:5 and a reciprocal dispersion in the region of 660-670 mμ of 14 mμ per mm. The excitation source was a PRK-2 lamp with a UFC-4 light filter. Microphotometric measurements on the spectra were made with an MF-4 microphotometer.

Figure 1 gives fluorescence spectra of some of the compounds listed. All the spectra clearly have structural similarities, regardless of the diversity of the chemical composition and structure of the polymers.

The fluorescence spectra of all the polymers given and also of many other polymers not presented here spread as a continuum from 300 to 700 mμ. This fluorescence is not the characteristic fluorescence of molecules. For all the compounds listed above, it consists of maxima which are constant in position in the red part of the continuum and an adjacent broad, diffuse maximum in the blue-violet part. The latter maximum varies in position from compound to compound and with a change in the molecular weight in the same homologous series.

The study of the relation between the fluorescence spectra and the change in molecular weight is of great practical interest since if a relation can be found between the molecular weight and any spectral characteristic of a polymer, this may make it possible to develop a method of determining the molecular weights of polymers in the solid state. We know of no such method though there is a great need for it due to the insolubility of many polymers.

The change in fluorescence spectra with a change in the molecular weight of a polymer with a continuous chain of conjugated bonds in its molecule was investigated with samples of polyphenylacetylene, which has the structure.

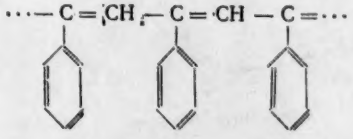

Figure 3 gives photomicrograms of the fluorescence spectra of solutions of polyphenylacetylenes obtained by thermal polymerization in an inert gas at 150, 300, and 400° and with mean isobestic molecular weights of 1100, 1300, and 1500, respectively [1].

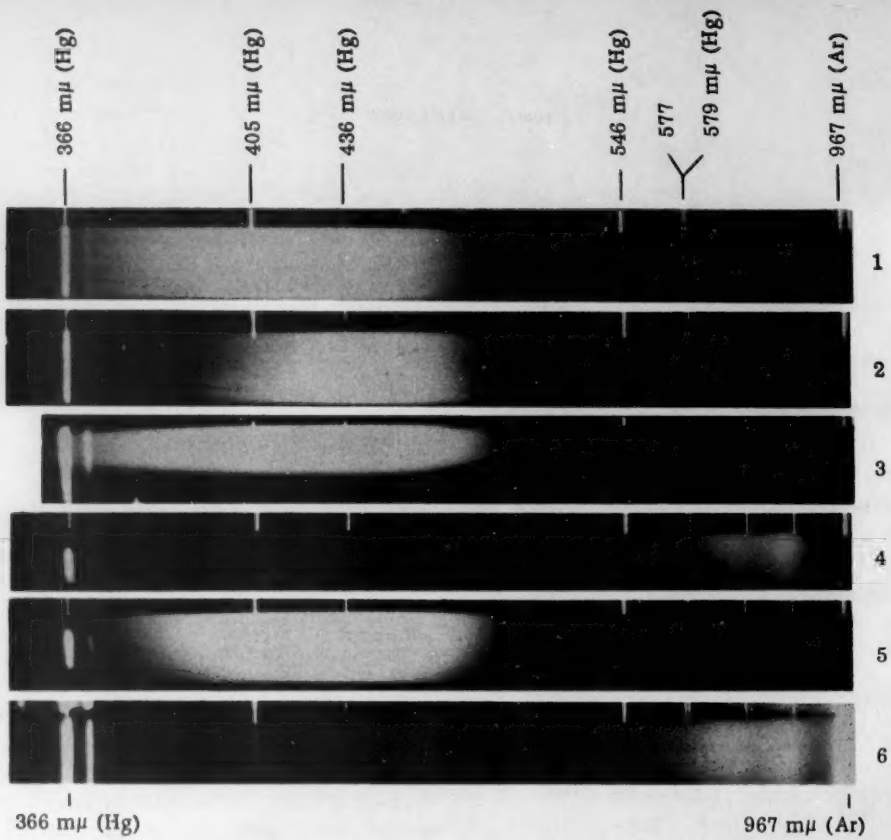

Fig. 1. Fluorescence spectra: 1) polystyrene; 2) serum albumin; 3) poly-p-carboxyphenylmethacrylamide; 4) solution of polyphenylacetylene (mol. weight 1500) in benzene; 5) solution of polyphenylacetylene (mol. weight 1100) in benzene; 6) desoxynucleic acid (DNA).

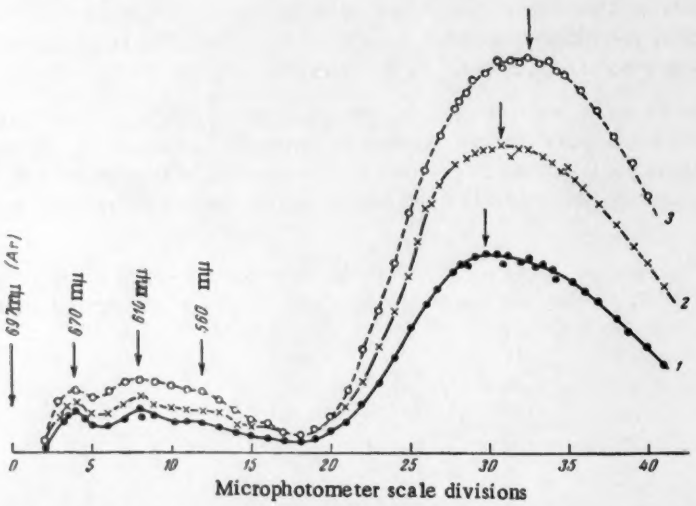

Fig. 2. Microphotograms of fluorescence spectra of polystyrenes in the solid state: 1) mol. weight 180,000; 2) mol. weight 250,000; 3) mol. weight 300,000.

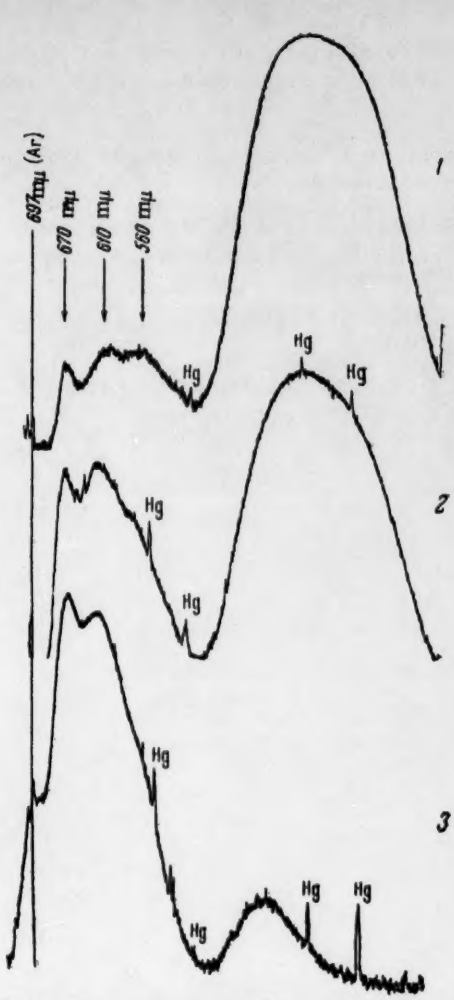

Fig. 3. Photomicrograms of fluorescence spectra of benzene solutions of polyphenylacetylenes: 1) mol. weight 1100; 2) mol. weight 1300; 3) mol. weight 1500.

The photomicrograms show that the spectra of all three samples of polyphenylacetylenes have, as already noted, the same system of fluorescence bands: maxima at 670, 610, and 560 mμ, a few bands in the region of the green and blue lines of mercury* and a broad blue-violet band. It is characteristic that the bands were in the same positions in the spectra of all the samples investigated and analogous fluorescence bands of different polyphenylacetylenes differed only in intensity. The exception was the broad blue-violet maximum which showed a red shift that increased in parallel with an increase in the molecular weight of the polymer. In addition, attention is attracted by the redistribution of the band intensities throughout the whole range of the fluorescence spectrum: as the molecular weight increased, the intensity of the long-wave fluorescence bands increased relative to the intensity of the blue-violet band. In actual fact, for polyphenylacetylene with a molecular weight of 1100, the broad blue-violet band was the most intense while the long-wave bands, which were unchanged in position in the spectrum, were weak. For polyphenylacetylene with a molecular weight of 1300, the broad blue-violet band and the red bands were equivalent in intensity, while for polyphenylacetylene with a molecular weight of 1500, the maximum of the blue-violet band was considerably displaced toward longer wavelengths and much reduced in intensity relative to the long-wave bands, which were stable as regards position in the spectrum and remained intense.

In addition, special photometric measurements showed that with an increase in the molecular weight of the polyphenylacetylenes there was a considerable fall in the fluorescence yield over the whole spectral range. As an example of the change in fluorescence spectrum with a change in molecular weight of polymers without continuous chains of conjugated bonds, let us examine the spectra of polystyrenes of various molecular weights. It is particularly interesting to compare the fluorescence spectra of these polymers with the spectra of polyphenylacetylenes described above as the compounds are hydrogenated polyphenylacetylenes. Figure 2 gives photomicrograms of fluorescence spectra of three polystyrenes with mean viscosity molecular weights of 300,000, 250,000, and 180,000. The spectrum of one of these is also given in Fig. 1. The fluorescence spectra are exactly the same as the spectra of polyphenylacetylenes and other polymers, but have their own particular distribution of band intensities. The broad blue-violet band has the maximum intensity here, and, as with polyphenylacetylenes, its maximum is displaced toward longer wavelengths with an increase in molecular weight and at the same time its intensity falls much more than the intensity of all the other bands. In addition, there was the same redistribution of intensities of all the bands as for all the other polymers, that is, the relative intensity of the longer wave bands increased regularly. This is shown particularly well by the bands at 670, 610, and 560 mμ.

Thus, in the case of polymers both with and without a continuous chain of conjugated bonds, an increase in the degree of polymerization leads to a general fall in the intensity of the fluorescence spectrum, a displacement

*These bands appear clearly on plates which do not have a dead spot in the green region of the spectrum.

of the broad blue-violet maximum toward longer wavelengths, and a set relative redistribution of the intensities of all the fluorescence bands, that is, an increase in intensity of the long-wave bands relative to the decreasing short-wave bands.

All these effects are clearly expressed for polymers containing a continuous chain of conjugated bonds in the molecule and weakly expressed for polymers whose molecules do not contain this.

In conclusion, the author would like to thank M. I. Cherkashin and O. G. Sel'skaya for providing samples of polyphenylacetylenes and also P. Yu. Butyagin, A. M. Dubinskaya, and I. O. Kolbanev for samples of polystyrenes.

LITERATURE CITED

1. A. A. Berlin, L. A. Blyumenfel'd, et al., Vysokomolek. Soed. 1, 9 (1959); A. A. Berlin, M. I. Cherkashin, et al., Vysokomolek. Soed. 1, 12 (1959).

EMISSION OF CHEMICALLY ACTIVE PARTICLES DURING THE OXIDATION OF ALUMINUM

M. Ya. Gen and Yu. I. Petrov

Institute of Chemical Physics, Academy of Sciences, USSR
(Presented by Academician V. N. Kondrat'ev, March 31, 1960)
Translated from Doklady Akademii Nauk SSSR, Vol. 133, No. 6, pp. 1361-1363, August, 1960
Original article submitted March 26, 1960

We observed that an aluminum surface freshly prepared in vacuum gives contact prints on an x-ray plate when kept under atmospheric conditions. The results of an investigation of this phenomenon are given below. The samples were prepared by vacuum spraying of aluminum onto glass plates (4.5 x 4.5 cm^2) fixed along the walls of a Pyrex cylinder (39 cm in diameter and 32 cm in height), in the center of which was fixed a sample with a total weight of 0.5 g in a few turns of tungsten wire.

After the apparatus had been pumped out to a pressure of $\sim 5 \cdot 10^{-5}$ mm Hg and subjected to prolonged outgassing, the samples were sprayed, then air was admitted to the apparatus, and the samples rapidly transferred (25-30 sec) to an x-ray film. The mirror deposits gave reproducible, though very weak blackening of the film. To intensify the effect, instead of a mirror deposit, onto the plates was sprayed a finely disperse aerosol of aluminum, obtained by evaporation of a sample in an argon atmosphere at a pressure of 0.1-1.0 mm Hg [1].

Various commercial light-sensitive photographic plates and films were tested as detectors.

However, no blackening was observed in any case. It was found that only x-ray films of the types X and XX (different factories) were suitable. It was observed that the sensitivity of these films to this effect increased with aging and sharp results were given approximately a year after their preparation. Attempts to use a photomultiplier with an uviol window were unsuccessful both under current and pulse conditions. It was established that thin (1 mm) luminescent crystals of CsI, NaI, KI, anthracene, and naphthalene not only did not increase, but completely eliminated the effect. An oil film likewise showed no sensitizing action.

To determine the role of oxygen in the observed effect, a special instrument was constructed in which a sample could be moved and pressed to an x-ray film in successive positions without breaking the vacuum. After a mirror deposit or an aerosol had been sprayed onto a glass plate, the apparatus was pumped out to a pressure of $\sim 10^{-4}$ mm. Experiments with different exposures (up to 10 hr) in vacuum and under atmospheric conditions showed that the film was blackened only in the presence of air. In addition, these experiments demonstrated the absence of radiation which might have been expected as a result of crystallization of initially amorphous particles of aluminum aerosol [2].

Figure 1 gives a histogram of the relation between the blackening density of a type X film after 1 hr and the time after preparation of samples with an aerosol with a mean particle size of $\sim 10^{-5}$ cm (measured on an ÉMZ electron microscope). The width of the steps corresponds to the time that each of the samples was held in contact with the given section of film. The height of the steps corresponds to the integral density of the blackening produced during the exposure. The blackening density was measured with a DFÉ-10 densitometer and averaged over the area of the sample. The shaded rectangles show the mean square deviation of data from six samples. The solid curve passing through the middle points gives an idea of the kinetics of the process caused by the oxidation of aluminum.

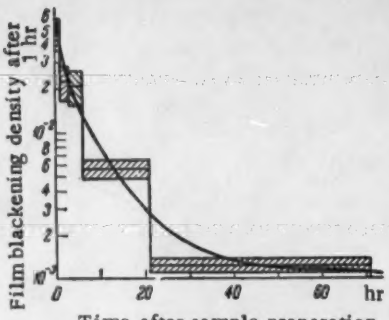

Fig. 1. Kinetics of the oxidation of an aluminum aerosol with a mean particle diameter d ~10^{-5} cm (740 mm Hg, 23°C).

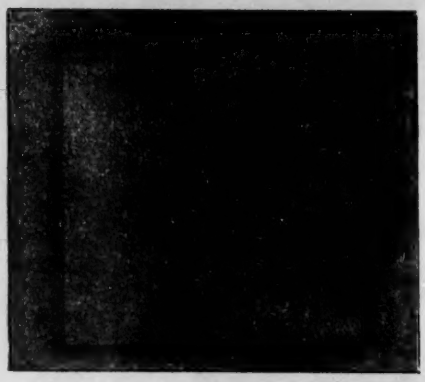

Fig. 2. Burning of a finely disperse aerosol (mean particle size d ~10^{-6} cm) on a heated glass surface.

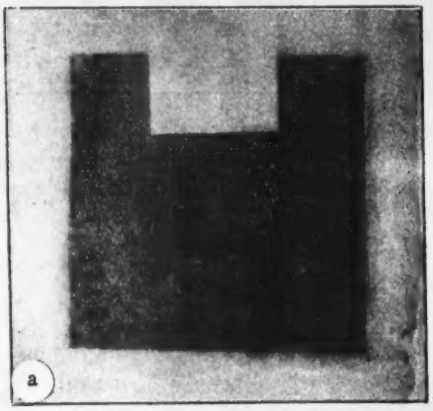

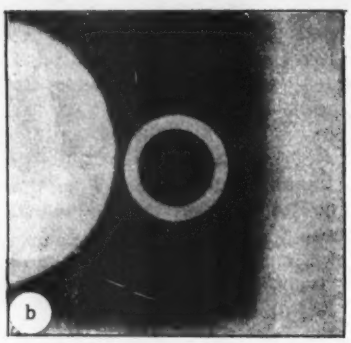

Fig. 3. Prints of a cover glass and a quartz disk demonstrating the absence of light radiation during the oxidation of an aluminum aerosol (d ~ 10^{-5} cm, 2-day exposure).

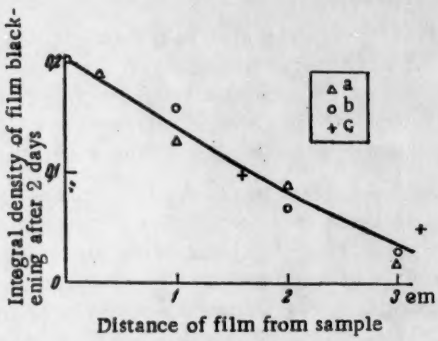

Fig. 4. Absorption of the active agent by an air column inside tubes of various materials: a) brass (d = 16 mm); b) copper (d = 24 mm); c) aluminum (d = 30 mm)

It is interesting to note that finely dispersed aerosols with a particle size of d~10^{-6} cm gave prints in the form of a contour of the plate as is shown in Fig. 2. This is explained by the difference both in heating temperature and in dispersion of the aerosol on the face and edges of the plate. In actual fact, as air was admitted to the apparatus directly after evaporation of samples, due to the heating of the face of the plate, the aerosol was oxidized before the sample was placed on the film. Particles deposited on the edge took a longer route in the argon and consequently grew to a larger size [1].

The reduction in temperature at the edges of the plate and the presence of coarser particles considerably retarded the oxidation process. Aerosols with particle sizes of < 10^{-6} cm sometimes ignited spontaneously at first contact with air. To elucidate the nature of the active agent, various substances were placed between the sample and the film. The experiments showed that the effect was completely eliminated by the following materials: black paper in one layer, mica plate (10 μ), microscope cover glass (0.1 mm), an optical quartz disk (2 mm).

Figure 3 gives typical prints of samples with a shadow from a cover glass and a quartz disk (40 mm diameter) with a two-day exposure (in the latter case, the shadow of a brass ring 2 mm thick is shown). Densitometer measurements showed that the film blackening density under sections of cover glass and quartz covered by the samples did not differ from the background. Measurements of the effect in relation to the thickness of the air layer between the sample and the film were most indicative. In all experiments the film was placed over the sample to prevent aluminum powder from falling from the glass plates (though this was improbable).

Prints of brass rings (2-day exposure) showed that the density of blackening of the film inside the ring, within the accuracy of the given experiments (~20%) was constant over the range of distances from 0 to 3.5 mm (the thickness of the rings was changed in steps of 0.5 mm each). At the same time, the edge of the sample outside the ring gave an increasingly diffuse shadow with an increase in the thickness of the air layer (Fig. 3). In the next experiments we used tubes of aluminum, copper and brass of various lengths and diameters. The tubes were washed carefully in ligroin and alcohol. The relation between the film blackening density and the length of the air column inside the tube is given in Fig. 4 (2-day exposure). The data for different materials lie practically on the same smooth curve.

In a very conclusive experiment, a strong current of compressed air was blown through the gap between the sample and the film (1 mm). The effect was completely absent in this case, though a control sample with the same gap width and the same exposure (8 hr) gave a clear picture.

In summarizing what has been said above, it is possible to draw the following conclusions. The blackening of films is caused by the chemical effect of an extremely active agent produced during the oxidation of aluminum. It is possible that this agent is ozone. The effect of this agent on an old x-ray film may be detected at a considerable distance in air (up to 3 cm inside tubes). No light emission either in the visible or ultraviolet regions of the spectrum was detected during the oxidation of aluminum.

We would like to thank I. V. Eremina and Yu. I. Fedorov for help in carrying out this work.

LITERATURE CITED

1. M. Ya. Gen, M. S. Ziskan, and Yu. I. Petrov, Doklady Akad. Nauk SSSR 127, 2, 366 (1959).*
2. M. Ya. Gen, I. V. Eremina, and Yu. I. Petrov, Zhur. Tekh. Fiz. 29, 11, 1407 (1959).

*Original Russian pagination. See C. B. translation.

A STUDY OF THE SPONTANEOUS CONTRACTION OF POLYMERS WITH A BRANCHED SPATIAL STRUCTURE DURING THEIR BREAKDOWN

V. E. Gul', V. V. Kovriga, and A. N. Kamenskii

M. V. Lomonosov Institute for Fine Chemical Technology, Moscow
(Presented by Academician V. A. Kargin, April 6, 1960)
Translated from Doklady Akademii Nauk SSSR, Vol. 133, No. 6, pp. 1364-1367, August, 1960
Original article submitted March 21, 1960

One of the peculiarities of the breakdown of polymers is the essential change of structure of the material during the process of its deformation and disruption. Changes of the relaxation properties of the material take place with this, and so far we have not been successful in evaluating them.

The present paper reports an attempt to evaluate the relaxation properties of a sample subjected to a breakdown process from the rate of spontaneous contraction. With the help of high speed cinematography we studied the spontaneous contraction of samples of nonfilled vulcanized butadiene-nitrile rubbers SKN-18, SKN-26, SKN-40, which had different contents of nitrile groups, but the same degree of crosslacing.

Two types of samples were used in carrying out the investigation. The sample number 1 was a lamina of vulcanized rubber having the dimensions 60 x 50 x 1 mm. At the center of the larger edge a cut having the dimensions of 2.5 and 1 mm was made. The sample No. 2 was a narrow band of vulcanized rubber of 60 x 10 x x 1 mm. The samples were deformed along their largest dimension. In order to determine the spontaneous contraction rate, the length of the contracted samples was measured by observing their pictures on various frames.

The photographs were taken on a SKS-1 photographic camera. When sample No. 1 was stretched with a definite deformation rate a gradual increase of the cut took place during the loading process. After the rupture the sample started contracting in the place where the collapse had taken place.

In the last moment before breakdown, the sample had only a narrow undisturbed part which then collapsed and started contracting. The rate of contraction of this narrow part of the sample has been studied in the present work. The investigation method with the help of high speed cinematography and the form of the samples during the rupture process were described previously [1]. The spontaneous contraction of samples of the second type took place after the samples had been cut at the lower clamp after they had reached a definite length. In this case the rate of the spontaneous contraction was defined as the rate of motion of the lower boundary of the entire narrow band of the sample.

With the help of this method we obtained data regarding the rates of spontaneous contraction corresponding to definite moments in time. These data served to build diagrams of the dependence of the rate of spontaneous contraction of the end of the sample upon the time t from the beginning of contraction (Fig. 2).

A graphic extrapolation of the values of the rate of spontaneous contraction (v_{sc}) to time 0 led to a value of the initial rate of spontaneous contraction v_0 which also served to characterize the relaxation properties of the material at the moment of disruption. The extrapolation was made plausible by the fact that the first 4-5 points lay well on a straight line with coordinates $\log v_{sc} - t$.

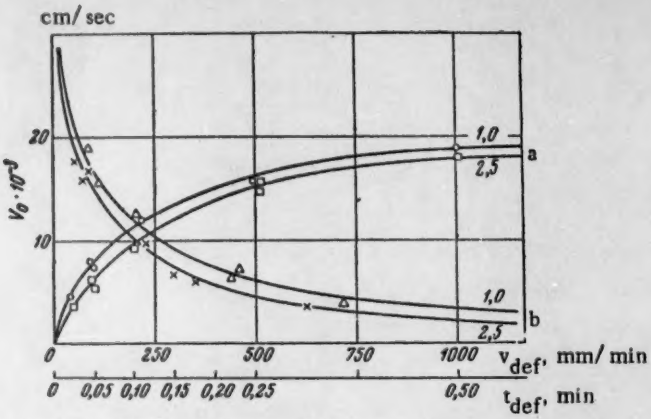

Fig. 1. Dependence of the rate of spontaneous contraction in the initial moments (v_0): a) upon the deformation rate, b) upon the time of deformation for vulcanized rubbers; SKN-18. Sample No. 1. The figures on the diagram correspond to the size of the cut in mm.

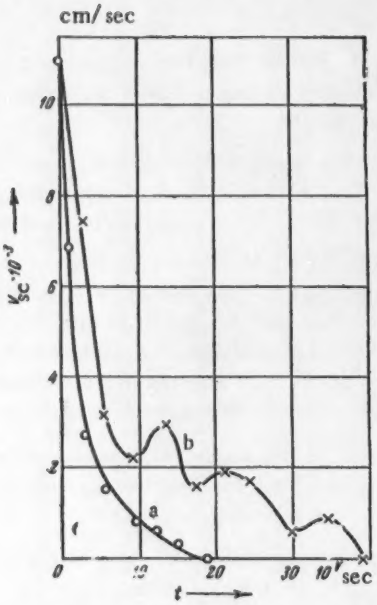

Fig. 2. Dependence of the rate of spontaneous contraction upon time for vulcanized rubbers SKN-18 for a deformation rate of 100 mm/min. a) Sample No. 1, with a cut of 1 mm; b) sample No. 2.

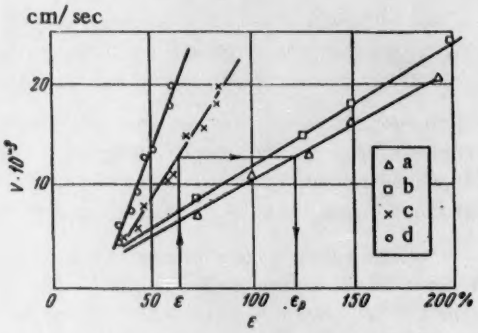

Fig. 3. Dependence of rate of spontaneous contraction in the initial moment upon the elongation for vulcanized rubber SKN-18. a) Sample No. 2, deformation rate 100 mm/min; b) sample No. 2, deformation rate 1000 mm/min; c) sample No. 1 with a cut of 1 mm; d) sample No. 2 with a cut of 2.5 mm.

An examination of the curves reported in Fig. 2 shows that v_{sc} did not decrease in the same way for every type of sample.

In sample No. 2 the curve representing the change of the rate has the form of attenuated oscillations; this fact is connected with the appearance of the already established [2] wave character of the spontaneous contraction. In sample No. 1 the appearance of a wave character of the spontaneous contraction was made more difficult, since the unloading wave was scattered in a large and already quite contracted part of the samples. Sample No. 1 showed a diffusion of the unloading wave along the sample in the form of a thickening. Sample No. 1 was studied in order to find the dependence of v_0 upon the rate of deformation and the time of deformation till the rupture.

Dependence of v_0 and γ Upon the Rate of Deformation and the Value of the Cut for Vulcanized Nitrile Rubbers

Rubber samples	$v_0 \cdot 10^{-3}$ (cm/sec)							γ	
	sample No. 1, for v_{def} = 500 mm/min		sample No. 1, for t_{def} = 0.2 min		sample No. 1, for ϵ = 50%		sample No. 2, for ϵ = 100%		
	a	b	a	b	a	b		a	b
SKN-18	16	15.3	7.5	5.8	9	12.7	11.7	2.8	2.8
SKN-26	13.7	17.7	11.0	9.5	9.5	15.3	12.7	1.9	2.65
SKN-40	19.5	17.9	14.7	10.5	10.0	13.3	13.0	1.76	2.25

Note: a) cut of 1 mm; b) cut of 2.5 mm.

Data of this type for rubber SKN-18 are reported in Fig. 1.

An examination of Fig. 1 shows that, first, when the deformation rate increases the rate of spontaneous contraction also increases, but the higher the values reached by the deformation rate, the smaller is this increase; second, the lower the time of permanence of the sample in a deformed state, the higher is the contraction rate. These dependences are characteristic of materials having relaxation properties.

Fig. 3 shows the dependence of v_0 upon the elongation, studied on samples No. 1 and No. 2.

It should be noted that for the two samples the value of the elongation was determined from the distance between the clamps at the moment of the rupture and before the beginning of deformation. In the case of the testing of sample No. 2 the dependence of v_0 upon the elongation is represented by a straight line passing through the origin of the coordinates, so that the line corresponding to a lower deformation rate would lie lower; this fact is in good agreement with the considerations reported above.

However, as can be seen from Fig. 3, the presence of a cut leads to a faster collapse of the sample No. 1, thus changing the behavior of the dependence in question. The straight lines no longer pass through the origin of the coordinates, and are displaced upward with respect to the straight lines for sample No. 2. An increase of the size of the cut would lead to an increase of the angle of inclination of these curves with respect to the axis of the abscissa. This can be interpreted by the fact that the overstress which is developed till the moment of rupture in the remaining narrow part of sample No. 1 is the higher, the higher the value of the preliminary cut. For large cuts the increase of the deformation would be accompanied by large increases of the stresses at the vertex of the cut and, consequently, by a greater additional deformation and a great rate of spontaneous contraction.

The initial contraction rate of the ends of the narrow part of sample No. 1 is significantly higher than the initial rate of contraction of the edge of sample No. 2 for the same value of the total deformation of the sample. On the basis of this we elaborated a method for evaluating the value of the additional orientation of the material at the top of the growing cut at the moment of rupture, which probably would permit evaluating the overstress.

Knowing the increase in length of sample No. 1 at the moment of rupture and the value of v_0 corresponding to it, one can find, using the diagram of $v_0 = f(\epsilon)$ (Fig. 3) for sample No. 2, the value of the increase in length for which the edge of the band of sample No. 2 has the same rate of spontaneous contraction as the collapsing sample. The picture obtained shows the actual elongation which develops at the top of the collapsing sample No. 1. The behavior of such a determination is shown by the line with an arrow in Fig. 3.

If the increase in length ϵ_p determined in this way is divided by the total increase in length of the sample upon breakdown, we find the value of the additional orientation of the material at the top of the cut [1] $\gamma = \epsilon_p/\epsilon$ in relative units. Since the dependence of v_0 upon ϵ is expressed by straight lines, one can see that the degree of the additional orientation of the material would not depend upon its elongation but upon the size of the cut. Curves similar to the curves reported in Figs. 1, 2, 3 were obtained also for vulcanized rubbers SKN-26 and SKN-40. These data support completely the general character of the dependence obtained. In order to determine

the influence of the polarity of the vulcanized rubbers, the Table shows the values of v_0 and γ for vulcanized SKN with an equal degree of cross linking.

An examination of the Table shows that with an increase of the polarity of the vulcanized rubbers the rate of spontaneous contraction increases if the other conditions remain the same. At the same time an increase in the number of nitrile groups decreases the degree of additional orientation. This is a consequence of the decrease in flexibility of the chain molecules.

LITERATURE CITED

1. V. E. Gul', G. P. Krutetskaya, and V. V. Kovriga, Kauchuk i rezina, 12, 3(1957).
2. G. M. Bartenev, M. M. Reznikovskii, and M. K. Khromov, Koll.Zhur. 18, 395 (1956).*

*Original Russian pagination. See C. B. translation.

THE RATE OF ELECTRON EXCHANGE REACTIONS IN SOLUTIONS

R. R. Dogonadze

Electrochemical Institute of the Academy of Sciences, USSR
(Presented by Academician A. N. Frumkin, April 1, 1960)
Translated from Doklady Akademii Nauk SSSR, Vol. 133, No. 6, pp. 1368-1371, August, 1960
Original article submitted March 28, 1960

On the basis of the adiabatic theory of disorder, there have been calculated [1, 2] probabilities for electronic transfer per unit time, $w_{12}(R)$, between similarly charged ions situated at a distance R from one another. In order to connect w_{12} with the specific rate constant of the reaction, it is necessary to develop the kinetic equation for the reaction. For the sake of simplicity we consider the reaction:

$$Fe^{2+} + Fe^{*3+} \rightarrow Fe^{3+} + Fe^{*2+}. \tag{1}$$

It will be seen, however, from the calculation, that similar results may be obtained also for any electronic exchange reaction.

We shall denote the concentrations of Fe^{2+}, Fe^{*2+}, Fe^{3+}, Fe^{*3+} respectively by the symbols c_2, c_2^*, c_3, and c_3^*. The number of ions of Fe^{*2+} formed in unit volume in time dt may be expressed in the form:

$$dc_2^* = (c_2\rho + c_2^*\rho^*)\,dt, \tag{2}$$

where ρ is the probability that a given Fe^{2+} ion will go over into Fe^{3+} in unit time, and ρ^* has an analogous meaning. Since the number of Fe^{*3+} ions in an element of volume dv, situated at distance R from Fe^{2+}, is given by $c_3^* e^{-\psi(R)/kT}\,dv$, and the probability of the transfer of an electron in unit time is w_{12}, ρ may be presented in the form

$$\rho = \int w_{21}(R)\, c_3^* e^{-\psi(R)/kT}\, dv \equiv k_{12} c_3^*, \tag{3}$$

where $\psi(R)$ is the energy of interaction of the ions Fe^{2+} and Fe^{*3+} situated at a distance R from each other. Similarly, for ρ^* we have:

$$\rho^* = \int w_{21}(R)\, c_3 e^{-\psi(R)/kT}\, dv \equiv k_{21} c_3 = k_{12} c_3. \tag{4}$$

The insertion of (3) and (4) into (2) gives the desired relationship:

$$dc_2^*/dt = k_{12}(c_2 c_3^* - c_2^* c_3). \tag{5}$$

We write down the solution of the equation for the initial conditions:

$$c_2 = c_{20}, \quad c_3 = c_{30}^*, \quad c_2^* = c_3 = 0 \text{ for } \quad t = 0. \tag{6}$$

It is easy to see that at any given moment the following relationships are true:

$$c_2^* = c_3, \quad c_2 + c_2^* = c_{20}, \quad c_3 + c_3^* = c_{30}^*. \tag{7}$$

It follows that (5) may be rewritten in the form:

$$dc_2^*/dt = k_{12}[(c_{20} - c_2^*)(c_{30}^* - c_2^*) - c_2^{*2}] = k_{12}[c_{20}c_{30}^* - (c_{20} + c_{30}^*)c_2^*]. \tag{8}$$

The solution of Equation (8) for the initial conditions shown in (6) has the form:

$$\ln\left(1 - \frac{c_{20} + c_{30}^*}{c_{20}c_{30}^*} c_2^*\right) = -k_{12}(c_{20} + c_{30}^*)t. \tag{9}$$

When $t \to \infty$, as can be seen from Equation (9)

$$c_2^* \to \frac{c_{20}c_{30}}{c_{20} + c_{30}^*} \equiv c_{2\infty}^*, \tag{10}$$

and therefore Equation (9) may be written in the form:

$$\ln(1 - c_2^*/c_{2\infty}^*) = -k_{12}(c_{20} + c_{30}^*)t. \tag{11}$$

Equation (11) was, of course, first obtained by McKay [3].

The quantity k_{12} which was defined in the work of McKay [3] is the specific rate constant of the reaction to be determined by experiment. At low concentrations, $\psi(R)$ may be expressed by using the Debye potential:

$$\psi(R) = 3 \cdot 2e^2 e^{-\varkappa R}/\varepsilon_s R, \tag{12}$$

where κ is the reciprocal of the Debye length, and ϵ_s is the static dielectric constant. From physical considerations it is clear the $1/\kappa$ is much greater than the distance at which $w_{12}(R)$ diminishes, and therefore the exponent in Equation (12) may be replaced by unity; that is, $\psi(R)$ may be expressed by means of the equation:

$$\psi(R) = 6e^2/\varepsilon_s R. \tag{13}$$

Thus,

$$k_{12} = 4\pi \int_0^\infty w_{12}(R) e^{-6e^2/\varepsilon_s RkT} R^2 dR, \tag{14}$$

or, inserting the expression for w_{12} found in the work of V. G. Levich and R. R. Dogonadze [2],

$$k_{12} = \frac{kT}{h} \int_0^\infty \left(\frac{512\pi^6}{h^2\omega_0^2 kTc \int (\mathbf{D}_1 - \mathbf{D}_2)^2 d\mathbf{r}}\right)^{1/2} |L_{21}^{(2)}|^2 e^{-\frac{\Delta F^* + 6e^2/\varepsilon_s R}{kT}} R^2 dR. \tag{15}$$

The quantity $L_{21}^{(2)}$ is the volume integral; $\mathbf{D}_{1,2}$ is the induction of the electrostatic field created by the electron in the initial (or final) state, and c is expressed by the equation:

$$c = 1/\varepsilon_0 - 1/\varepsilon_s, \tag{16}$$

where ϵ_0 is the optical dielectric constant. In the same work [2], it was shown that

$$\Delta F^* = \frac{c}{32\pi} \int (\mathbf{D}_1 - \mathbf{D}_2)^2 d\mathbf{r} + kT \ln \frac{kT}{\hbar\omega_0} \equiv \Delta E^* - T\Delta S^*. \tag{17}$$

So as to make possible the comparison of the relationship obtained for k_{12} with the known equation for the theory of the absolute rates of reactions,

$$k_{12} = \frac{kT}{h} \varkappa e^{-\Delta F^{+}/kT}, \tag{18}$$

we make use of the integral theorem of the mean. The quantity $R^2 e^{-6e^2/\varepsilon_s RkT}$ diminishes suddenly with reduction in R, and increases in proportion to R^2 with increase in R, while the remaining portion of the expression to be integrated diminishes suddenly with reduction in R. The function to be integrated reaches a maximum for some value of R which will be denoted by $\bar{R}$, and has a rather small width $\delta\bar{R}$. Hence the expression lying within the integral sign in (15) may be removed from the integral sign at the point $\bar{R}$, and be multiplied by $\delta\bar{R}$, with the result that we obtain an equation corresponding in accuracy with (18):

$$\Delta F^{+} = \Delta F^{*}(\bar{R}) + 6e^2/\varepsilon_s \bar{R}, \tag{19}$$

and the transmission coefficient is expressed by the equation:

$$\varkappa = \left(\frac{512\pi^6}{\hbar^2\omega_0^2 kTc \int [\mathbf{D}_1(\bar{R}) - \mathbf{D}_2(\bar{R})]^2 d\mathbf{r}}\right)^{1/2} |L_{21}^{(2)}|^2 \bar{R}^2 \delta\bar{R}. \tag{20}$$

In order to compare this with experiment, we used Equation (19) for the free energy of activation, and Equation (20) for the energy of activation:

$$\Delta E^{+} = \Delta E^{*}(\bar{R}) + \frac{6e^2}{\varepsilon_s \bar{R}} = \frac{c}{32\pi}\int [\mathbf{D}_1 - \mathbf{D}_2]^2 d\mathbf{r} + \frac{6e^2}{\varepsilon_s \bar{R}}. \tag{21}$$

Knowing the wave-function of the 3d-electron of the ion Fe^{2+} dissolved in water, the integral of (21) could have been evaluated, and thus ΔE^{*} could have been determined as a function of $\bar{R}$. But in order to evaluate the quantity ΔE^{*}, we must employ a model of a rigid conducting sphere, as was postulated by Marcus [4]:

$$\mathbf{D}_1 = \begin{cases} 0, & r < a; \\ e\mathbf{r}/r^3, & r > a; \end{cases} \qquad \mathbf{D}_2 = \begin{cases} 0, & |\mathbf{r} - \bar{\mathbf{R}}| < a; \\ \dfrac{e(\mathbf{r} - \bar{\mathbf{R}})}{|\mathbf{r} - \bar{\mathbf{R}}|^3} & |\mathbf{r} - \bar{\mathbf{R}}| > a, \end{cases} \tag{22}$$

where a is the radius of the sphere. In this case,

$$\Delta E^{+} = \frac{6e^2}{\varepsilon_s \bar{R}} + \frac{ce^2}{4}\left(\frac{1}{a} - \frac{1}{\bar{R}}\right). \tag{23}$$

So as to determine $\bar{R}$ without making use of the experimental results, a more detailed study of the integral (15) is necessary. At the same time we shall indicate methods by means of which the quantity k_{12} may be evaluated, if the Slater function used is taken as the wave function of the electron. Considering Reaction (1) as an example, then we may write the wave function of the electron in the form:

$$\psi_1(\mathbf{r}) = \psi_2(\mathbf{r} + \mathbf{R}) = \psi_{3d_{z^2}} = {}^1/_8 \alpha^3 \sqrt{2\alpha/\pi}\, r^2 e^{-\alpha r} \cos^2\theta. \tag{24}$$

The parameter α, according to the method of Slater, may for the 3d-electron of Fe^{2+} be equated with

$$\alpha = z_{3d} / n_{3d} a_0 \varepsilon_s = 6{,}25 / 3a_0 \varepsilon_s. \tag{25}$$

Using the method adopted in the theory of semiconductors, instead of the Bohr radius a_0, we have introduced a magnitude ϵ_s times greater, so as to take into account the solvent. The choice of the angular part of the wave-function (24) is based upon the fact that the $\psi 3d_{z^2}$-function gives the greatest correspondence. To simplify the calculations using the functions of (24), we shall use them only for the determination of the volume integral $L_{21}^{(2)}$, and for the remaining quantities we shall assume that it is allowable to make use of (22).

The volume integral $L_{21}^{(2)}$ we write in the form:

$$L_{21}^{(2)} = \int \psi_2^* \frac{3e^2}{\varepsilon_s |r - R|} \psi_1 dr. \tag{26}$$

After simple but lengthy calculations (for the integral must be taken in elliptical coordinates) the following formula was obtained:

$$L_{21}^{(2)} = \frac{\alpha e^2 e^{-\alpha R}}{24\varepsilon_s}\left(48 + 48\alpha R + 20\alpha^2 R^2 + 4\alpha^3 R^3 + \alpha^4 R^4 + \frac{11}{15}\alpha^5 R^5\right) \equiv P_5(R) e^{-\alpha R}. \tag{27}$$

Since the root standing under the integral sign in Equation (15) changes very slowly, it is possible to take this outside the integral sign and to calculate k_{12} in the form:

$$k_{12} = \frac{4\pi}{he}\sqrt{\frac{\pi a}{ckT}}\, e^{-ce^2/4akT} \int_0^\infty P_{12}(R)\, e^{-2\alpha R - (6/\varepsilon_s - c/4)e^2/kTR} dR, \tag{28}$$

where for the polynomial of the 12th degree $R^2P_5^2(R)$ the notation $P_{12}(R)$ is introduced. If we estimate that ϵ_s is independent of R, the integral in Equation (28) may be evaluated accurately. Actually, if we denote $(6/\epsilon_s - c/4)e^2/kT$ by γ, we may present the desired integral in the form of the summation $\sum_{n=2}^{12} A_n I_n$, where [5]

$$I_n = \int_0^\infty R^n e^{-2\alpha R - \gamma/R} dR = 2(2\alpha)^{n-1}(2\alpha\gamma)^{(n+1)/2} K_{n+1}(\sqrt{8\alpha\gamma}). \tag{29}$$

Thus, the integral of Equation (28) may be expressed by means of the MacDonald function. As can be seen from (29), such a calculation is valid for electron exchange between isotopes with charge $\underline{z}$ and $z+1$ only under conditions for which $\gamma > 0$, since α is always positive. This means that $z(z+1)/\epsilon_s - c/4 > 0$, or, after a simple rearrangement:

$$\varepsilon_s < \varepsilon_0 (2z+1)^2. \tag{30}$$

The calculation referred to is sufficiently rigid if the expression to be integrated in Equation (28) reaches a maximum at such a value R_M as permits ϵ_s to be treated as independent of the value of R. It is possible to evaluate R_M by equating to zero the derivative of the exponential index in Equation (28), thus evaluating ϵ_s independently of R:

$$-2\alpha + \gamma / R_M^{0^2} = 0, \quad R_M^0 = \sqrt{\gamma / 2\alpha}. \tag{31}$$

However, because of the presence of $P_{12}(R)$ within the integral, R_M will be somewhat larger than R^0_M.

For Reaction (1), the condition set out in Equation (30) demands that $\epsilon_s < 45$. It is unfortunate that the relationship between ϵ_s and R is difficult to investigate on a theoretical basis. However, the data given by Laidler [6] show that $\epsilon_s < 45$ when $R < 5\text{Å}$. It therefore follows that the most probable separation for the occurrence of electronic transfer in Reaction (1) will be less than 4A. In considering the exchange reaction between ions with charges of 3 and 4, the condition of Equation (30) is automatically fulfilled, and Equation (31) may be written as:

$$R_M^{(0)} = 13{,}9\sqrt{n_{\text{eff}} / z_{\text{eff}}}\ \text{A}. \tag{32}$$

It may therefore be expected that the magnitude of R_M will be sufficient to make it possible to ignore any dependence of ϵ_s on R. For example, in the electronic exchange reaction in the system $Ce^{3+} - Ce^{4+}$, R^0_M is found to be of the order of 8.2A ($n_{\text{eff}} = 4$, and $z_{\text{eff}} = 11.4$): that is, the method developed above for the evaluation of k_{12} may be used with a good degree of accuracy.

It is interesting to note that the expression for the energy of activation for the electronic exchange reaction between ions identical except for valence state, which has been obtained in this paper and given in Equation (23), is in agreement with the free energy of activation calculated by Marcus [4]. For Reaction (1), Marcus obtained the value $\Delta F^{\neq} = 9.8$ kcal/mole, while in our theory it is calculated that $\Delta E^{\neq} = 9.8$ kcal/mole, which is in excellent agreement with the experimental value, $\Delta E^{\neq}_{exp} = 9.9$ kcal/mole.

LITERATURE CITED

1. V. G. Levich and R. R. Dogonadze, Dokl. Akad. Nauk SSSR 124, 123 (1959).*
2. V. G. Levich and R. R. Dogonadze, Dokl. Akad. Nauk SSSR 133, 1, (1960).**
3. H. A. C. McKay, Nature 142, 997 (1938).
4. R. A. Marcus, J. Chem. Phys. 24, 966 (1956); 26, 867 (1957).
5. E. Whittaker and G. Watson, Course in Contemporary Analysis [Russian translation] (1933).
6. K. J. Laidler, Canad. J. Chem. 37, 138 (1959).

* Original Russian pagination. See C. B. translation.

** See C. B. translation.

THE DETONATION OF NITROMETHANE CLOSE TO THE LIMIT

A. N. Dremin, G. A. Adadurov, and O. K. Rozanov

Chemical Physics Institute, Academy of Sciences, USSR

(Presented by Academician V. N. Kondrat'ev, April 2, 1960)
Translated from Doklady Akademii Nauk SSSR, Vol. 133, No. 6, pp. 1372-1374, August, 1960
Original article submitted April 1, 1960

During the measurement of the shock adiabatic curve for nitromethane (NM – CH_3NO_2) [1], one of the authors observed that when the detonation is produced, nonuniformities appear when the process is recorded from the lateral surface of the charge (like those shown in Figs. 2 and 4 of the present work).

In order to examine the nature of these nonuniformities, we decided to record scanning photographs of the process of detonation propagation in NM from the terminal and lateral surfaces simultaneously. The scanning of the process was carried out using a high-speed photorecorder (SFR) with a scanning speed of 2.25 mm/μsec. The slit was placed in position at the center of the charge. All the measurements were carried out according to the scheme illustrated in Fig. 1. A magnesium plate of 5 mm thickness was fixed firmly to the end of the active charge of trotyl, which had a diameter of 40 mm and density $\rho_0 = 1.43$ g/cm^3. A plexiglas cylinder with wall thickness 2 mm, containing NM, was attached to the magnesium plate. A planar detonation wave was propagated through the active charge.

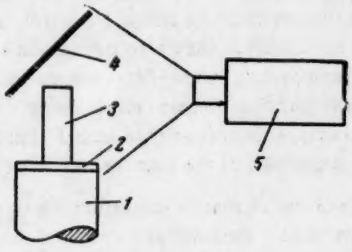

Fig. 1. Experimental scheme: 1) active charge; 2) magnesium plate; 3) plexiglas cylinder with NM; 4) mirror projecting the image of the end surface of the charge onto the film; 5) SFR photorecorder.

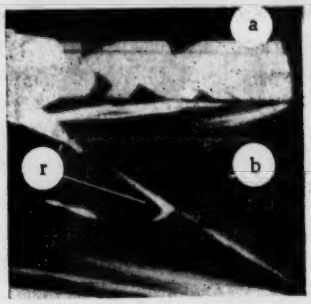

Fig. 2. Scanning photograph of the detonation propagation process in NM from the terminal (a) and lateral (b) surfaces. NM charge diameter 20 mm, height 50 mm; r denotes the retonation wave.

Figures 2, 3, and 4, show some of the photographs obtained by this method.* It should be noted that analogous photographs were obtained in casings and from other materials, and also in cases where the detonation of the NM was produced by shock waves of different intensities

* Photographs analogous to those obtained during our scanning of the end surface have been given in [6], without any explanation of the phenomenon.

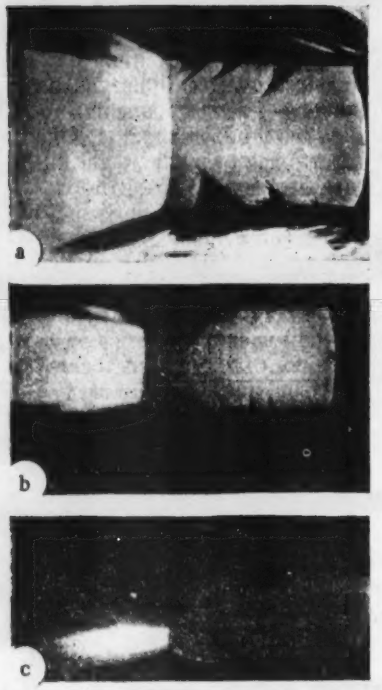

Fig. 3. Scanning photographs of the process of NM detonation from the terminal surface of the charge. a) Charge diameter 30 mm; b and c) diameter 20 mm.

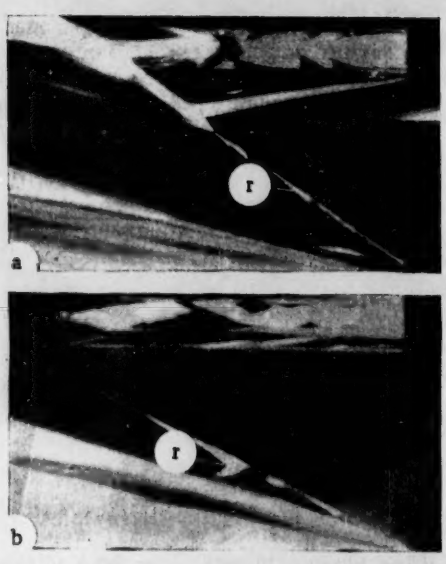

Fig. 4. Scanning photograph of detonation propagation. a) NM charge diameter 17 mm, height 50 mm; b) diameter 17 mm, height 100 mm; r denotes the retonation wave.

and directly from the active charge. A characteristic feature of these photographs is the presence of dark regions (the nonuniformities) on the light background which the detonation front leaves on the film with end surface scanning (Figs. 2, 3, and 4). In the majority of cases these regions originate at the periphery and spread into the depth of the charge. As the detonation spreads through the NM charge, the nonuniformities increase. It can be clearly seen that the dark regions on the end surface scanning correspond to regions of low luminosity on the lateral surface scanning. As the dark regions increase, there is a smooth decrease in the luminosity on the lateral surface scanning, followed by a sharp change to an increased luminosity, which also spreads out in a direction opposite to that of the normal detonation propagation (a reverse detonation, resembling a retonation wave; Figs. 2 and 4). The appearance of the bright luminosity on the lateral scanning corresponds to the production of luminosity on the terminal scanning. (When examining these photographs, it is necessary to bear in mind the fact that the lateral scanning of the detonation process corresponds to the upper part of the terminal scanning).

When the detonation wave comes out onto the terminal surface of the charge, a bright luminosity is observed over the whole cross section (Fig. 2). This luminosity is absent when a dark region comes out onto the terminal surface of the charge (Fig. 3).

These facts lead to the following explanation of the observed phenomenon. The absence of luminosity in the regions corresponding to the dark sections, together with the fact that the detonation is propagated in these sections in a direction opposite to the normal propagation direction, indicate that these sections consist of undetonated NM. The NM in the dark regions apparently loses its transparency under the action of the shock wave moving from the detonating section of the charge. In all the experiments in this work, the NM detonation velocity, measured from the lateral scanning, remained constant at 6300 m/sec until detonation stopped. During the detonation of NM close to the limit, however, the front of the detonation wave did not cover the whole cross section of the charge, but left zones of unreacted material, capable of subsequent detonation. In the case where the cross section of the charge is completely covered by the region of no reaction, or by several such regions, the detonation stops (Fig. 4, b).

The results obtained do not make it possible to reach any conclusions regarding the width of the region in

which no reaction takes place, since the photographs were obtained through a slit; they give information only on the local development of the process. Thus, it can be seen from Fig. 4,b that the zone of no reaction cuts across the whole of the cross section, but detonation nevertheless proceeds. In this case the detonation apparently spreads along the edges of the charge and afterward brings about reaction in the central region of the NM. The mechanism of the production of centers of no reaction, and that of the subsequent excitation of reaction in these centers, are not yet clear.

It has been shown in theoretical work by Yu. N. Shchelkin [2] and experimental work by Yu. N. Denisov and Ya. K. Troshin [3] on gas detonation that the planar front of a moving wave is unstable, and that reaction is initiated not over the whole cross section of the charge, but in isolated centers. Comparison of the results obtained in the present work with the recording of the detonation propagation in gases close to the limit reveals a certain similarity. This similarity lies in the fact that, although a strict periodicity in the production of the above nonuniformities has not yet been observed, each separate nonuniformity on the lateral scanning photographs resembles the scanning photograph of "pulsating" gas detonation [4]. In [2] it has been suggested that the detonation of condensed explosives should be analogous to gaseous detonation. This may in fact be true. In any case, it has been possible, to a considerable extent, to examine the mechanism of detonation combustion in gases by studying the phenomenon close to the limit of detonation propagation. It is not impossible that the results obtained in the present work on the detonation of a weak explosive close to the limit will assist in the further study of the mechanism of detonation combustion of condensed explosives.

In conclusion it should be noted that nonuniformities in the recording of detonation by photographic methods from the lateral surface of the charge were observed by A. Ya. Apin and V. K. Bobolev [5] in work on the detonation of powder explosives.

LITERATURE CITED

1. V. S. Plyukhin, P. F. Pokhil, et al., Doklady Akad. Nauk SSSR 131, 4 (1960).*
2. K. I. Shchelkin, Zhur. Éksp. i Teor. Fiz. 36, 2 (1959).
3. Yu. N. Denisov and Ya. K. Troshin, Doklady Akad. Nauk SSSR 125, 1 (1959).**
4. Yu. N. Denisov and Ya. K. Troshin, Zhur. Prikl. Mekhaniki i Tekh. Fiziki SO Akad. Nauk SSSR, 1 (1960).
5. A. Ya. Apin and V. K. Bobolev, Doklady Akad. Nauk SSSR 58, 2 (1947).
6. A. W. Campbell, T. E. Holland, M. E. Malin, and T. P. Cotter, Nature 178, 4523, 38 (1956).

* Original Russian pagination. See C. B. translation.

** See C. B. translation.

THE MECHANISM BY WHICH MODIFYING ADMIXTURES INFLUENCE THE SELECTIVITY OF ZINC OXIDE FOR THE DEHYDROGENATION AND THE DEHYDRATION OF ISOPROPYL ALCOHOL

G. M. Zhabrova, V. I. Vladimirova and O. M. Vinogradova

Physicochemical Institute, Academy of Sciences, USSR
(Presented by Academician M. M. Dubinin, March 21, 1960)
Translated from Doklady Akademii Nauk SSSR, Vol. 133, No.6, pp. 1375-1378, August, 1960
Original article submitted March 8, 1960

In previous investigations [1-5] it has been established that zinc oxide may noticeably alter its catalytic activity and selectivity for the decomposition of isopropyl alcohol, when it sorbs microamounts of admixtures from electrolyte solutions. It was of interest to investigate in more detail the way in which modifying admixtures influence the dehydrogenation and the dehydration of isopropyl alcohol and this was done by comparing kinetic, chemisorptive and electronic data on the catalyst samples investigated.

Modified samples of the zinc oxide catalyst were prepared by introducing in a base a dosed amount of admixture to the zinc oxide surface. Addition of sodium or lithium oxide was effected by an impregnation of the zinc oxide with the corresponding oxalates followed by their topochemical decomposition at relatively low temperatures (450-500°). Zinc sulfate was added by chemisorbing it from solutions containing various concentrations of the said substance [4, 5].

The specific surface areas of the catalyst samples investigated were determined by n-heptane adsorption using the chromatographic method [6], developed in the Catalysis Laboratory of the Physicochemical Institute of the Academy of Sciences,USSR,and for some samples by krypton adsorption at T = 196° using the BET method. Both methods gave concordant results.

The catalysts were tested in the form of adsorbed layers.

It was found that the kinetics of isopropyl alcohol dehydrogenation and dehydration obeys the bi-logarithmic equation characteristic for an inhomogeneous surface

$$q = At^{1/n}, \tag{1}$$

where q represents the amount of alcohol decomposed, while 1/n and A are constants.

As values characterizing the activity of the catalysts investigated we chose the initial rates, that is, the decomposition rate in the first minute. The activation energy was calculated from the initial rates and also from the formula:

$$E = -\frac{4{,}57\,(\ln t_{1q} - \lg t_{2q})}{1/T_2 - 1/T_1}, \tag{2}$$

The Dependence of the Kinetic Parameters for the Isopropyl Dehydrogenation and Dehydration Upon the Introduction of Modifying Admixtures into Zinc Oxide.

Catalyst	S, $\frac{m^2}{g}$	$V_{spec} \cdot 10^{-3}$, cm^3/min					E $\frac{kcal}{mole}$ (from initial rate)	$\lg V_0$
		130°	150°	180°	200°	220°		
Dehydrogenation								
ZnO without admixture	2,1	—	—	0,4	0,87	3,3	23	7,6
ZnO + 0,114% Na_2O	3,0	1,9	7,0	20	—	—	17,7	6,8
ZnO + 0,38% Na_2O	3,0	—	2,3	14	24	—	18,0	6,7
ZnO + 6,2% Na_2O	3,0	—	1,7	8,0	13,3	—	17	6,0
ZnO + 3,1% Li_2O	4,9	—	1,2	10,2	22,4	—	27	10,8
ZnO + 14,5% $ZnSO_4$	7,9	—	—	0,27	1,9	4,8	32	12,1
Dehydration								
ZnO without admixture	2,1	—	—	2,3	7,9	22	26	9,9
ZnO + 14,5% $ZnSO_4$	7,9	—	—	4,6	16,5	51	27	10,7

where q represents the amount of alcohol decomposed or the percentage of the catalyst surface covered by chemisorbed alcohol.

In Fig. 1 are compared the kinetic curves of the isopropyl alcohol dehydrogenation on zinc oxide samples into which admixtures have been introduced. The reaction was carried out at 180°. The whole series of samples was prepared from a luminescent zinc oxide which has dehydrogenating as well as dehydrating properties [7]. The dehydrogenation rate sharply increases, when sodium or lithium oxide is introduced and decreases, when zinc sulfate is introduced. In Fig. 1 the kinetic data are given in more detail. It follows from the Table that the introduction of 0.114% sodium oxide increases by 50 times the specific dehydrogenation rate, that is, the rate per 1 m^2 surface area. At the same time the activation energy of dehydrogenation decreases. The introduction of 0.38% and of 6.2% sodium oxide also increases noticeably the specific catalytic activity, although these points, obviously, lie past the optimum concentration of the said modifying agent. The introduction of lithium oxide also effects a noticeable increase in the specific catalytic activity. On the contrary, the introduction of zinc sulfate lowers the specific dehydrogenation rate and increases the activation energy for the said process. As to the dehydration of isopropyl alcohol, it is almost completely suppressed by the introduction of 0.114% sodium oxide into the sample of luminescent zinc oxide. The specific dehydration rate increases at increasing zinc sulfate concentration, whereas the activation energy of dehydration practically does not change.

It was of interest to investigate the adsorption and desorption kinetics of isopropyl alcohol and of its decomposition product – acetone – on the samples of pure and modified zinc oxide. It was found that the chemisorption of isopropyl alcohol at temperatures near to those at which the catalytic decomposition occurs and the chemisorption of acetone at the same temperatures take place practically instantaneously. The desorption of the chemisorbed isopropyl alcohol and acetone proceeds slowly. Typical kinetic curves for the isothermal acetone desorption from zinc oxide at various temperatures are shown in Fig. 2. These kinetic curves do not turn into straight lines when plotted on a double-logarithmic scale, as should be the case for an inhomogeneous surface. The activation energy of acetone desorption from zinc oxide at ~2% monolayer coverage was calculated by means of relation (2) and was equal to 32 kcal/ mole. The introduction of 14.5% $ZnSO_4$ increases the activation energy to 41 kcal/ mole (at approximately the same coverage) and the introduction of 6.2% Na_2O lowers the activation energy to 10.0 kcal/ mole.

In Fig. 3 are compared the curves characterizing the relation between the work function change in electron volts and the modifying admixture content of zinc oxide. The work function was determined from the contact potential difference measured by the method of the vibrating condenser [8]. The measurements were carried out by É. Kh. Enikeev. The accuracy of the measurement was 0.01 v. It may be concluded from Fig. 3 that the work function decreases when the concentration of the sodium or lithium oxide admixture in zinc oxide is raised. Upon raising the zinc sulfate content the work function increases.

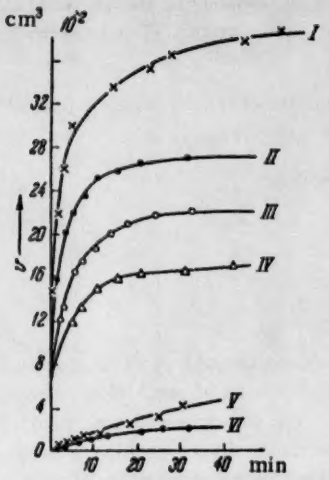

Fig. 1. Kinetic curves of isopropyl alcohol dehydrogenation on samples of modified zinc oxide: I) ZnO + + 0.114% Na_2O; II) ZnO + 0.38% Na_2O; III) ZnO + 3.1% Li_2O; IV) ZnO + 6.2% Na_2O; V) ZnO without admixture; VI) ZnO + 14.5% $ZnSO_4$.

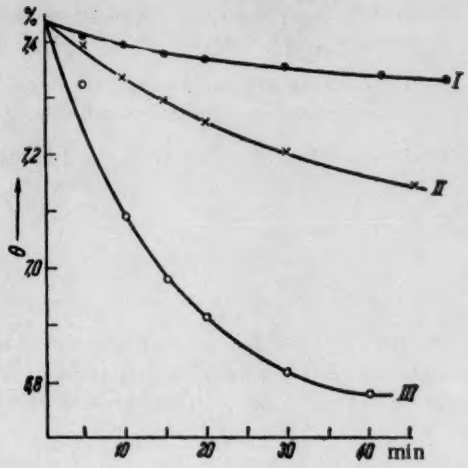

Fig. 2. Kinetic curves for the isothermal acetone desorption from zinc oxide: I) at 120°; II) at 150°; III) at 190°.

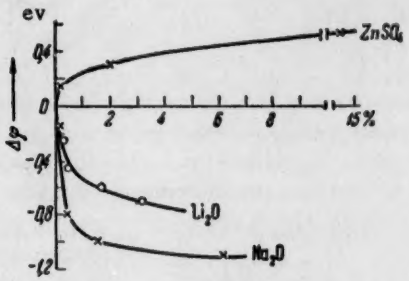

Fig. 3. The relation between the work function of zinc oxide and the modifying admixture content.

According to electronic conceptions, this means that the added sodium and lithium oxides act as donors, since they shift the Fermi level on the surface in the direction of the conduction band. As a result of these additions the zinc oxide surface is positively charged. The addition of zinc sulfate or thorium dioxide introduces acceptor levels which shift the Fermi level in the direction of the valence band and hamper the transfer of electrons to the conduction band. At the same time the zinc oxide surface becomes negatively charged. We note that additions acting as donors have a basic character and those acting as acceptors have an acid character.

To study the influence of the chemisorption of isopropyl alcohol and its decomposition products upon the surface charge of the zinc oxide samples investigated the electric conductivity and the work function were simultaneously measured in an atmosphere of alcohol, acetone and water vapor and even of hydrogen and propylene (pressure 10 mm Hg) at temperatures near to the temperature where catalytic decomposition occurs (100°). It has been established previously that under these conditions there is a considerable chemisorption of isopropyl alcohol and acetone (~60% of a monolayer).

It has been found that the chemisorption of isopropyl alcohol and acetone at temperatures near to that of catalytic decomposition results in an increase by 0.1 ev in the work function both for the sample of original zinc oxide and for samples modified by sodium oxide or zinc sulfate. The chemisorption of acetone has the same effect. Consequently, isopropyl alcohol and acetone act as electron donors and their chemisorption is accompanied by a transfer of electrons from the adsorbed molecules to the conduction band of zinc oxide. The chemisorption of water vapor at 20° even on the samples showing maximum dehydration ability (as, for instance, zinc oxide containing 14.5% zinc sulfate) does not change the electric conductivity and the work function. At a temperature of 100° small variations of the work function lying within the inaccuracy of the measurement were observed. The

presence of hydrogen or propylene has no influence on both of the above-mentioned electric properties. The data obtained by us agree very well with the results of F. I. Vilesov and A. N. Terenin [9] and also with the data of É. Kh. Enikeev, L. Ya. Margolis and S. Z. Roginskii [10].

From the results obtained one may draw conclusions on the mechanism of the dehydrogenation and on the way in which the modifying admixtures influence a step in this reaction.

Obviously, dehydrogenation takes place in the following three steps:

$$(CH_3)_2CHOH \rightarrow (CH_3)_2CHOH^+ + \ominus, \quad \text{(I)}$$

$$(CH_3)_2CHOH^+ \rightarrow (CH_3)_2CO^+ + H_2, \quad \text{(II)}$$

$$(CH_3)_2CO^+ + \ominus \rightarrow (CH_3)_2CO. \quad \text{(III)}$$

The first step, namely, the chemisorption of isopropyl alcohol is a donating step and it is accompanied by the transfer of an electron from the chemisorbed molecule to the conduction band of zinc oxide. The chemisorbed isopropyl alcohol molecule is charged positively. According to our data, this step proceeds practically instantaneously with a very high rate. In the second step a chemisorbed acetone molecule is formed, which has also a positive charge, and hydrogen is liberated. The third step – the desorption of the chemisorbed acetone – is an accepting step requiring the transfer of an electron from the conduction band of zinc oxide to the chemisorbed acetone. As has been shown (see Fig. 2), the desorption of acetone proceeds extremely slowly. Obviously, the desorption of acetone is the rate determining step of the dehydrogenation of isopropyl alcohol.

The activation energy of acetone desorption decreases when a donating admixture – sodium oxide – is added. On the contrary, the addition of an accepting admixture – zinc sulfate – increases the activation energy of acetone desorption. This is in accordance with the established fact that the addition of sodium oxide lowers and that the addition of zinc sulfate raises the activation energy of the dehydrogenation (see Table).

Thus, one may presume from the whole body of data obtained that the dehydrogenation of isopropyl alcohol is an electronic (donor-acceptor) process and that the accepting step of acetone desorption acts as the rate determining step. The results obtained by us do not confirm the assumption of Hauffe [12], Schwab [13], and Garner [14] that the donating step of isopropyl alcohol dehydrogenation on zinc oxide is rate determining.

The dehydration of isopropyl alcohol, obviously, may be treated as an acidic process, which proceeds by the transfer of protons from the catalyst to the reacting molecule and vice versa.

LITERATURE CITED

1. G. M. Zhabrova, L. N. Kutseva, and S. Z. Roginskii, Doklady Akad. Nauk SSSR 94, 78 (1954).
2. G. M. Zhabrova, Problems of Kinetics and Catalysis [in Russian] (Izd. AN SSSR, Moscow, 1955) p. 209.
3. G. M. Zhabrova, Uspekhi Khim. 24, 598 (1955).
4. G. M. Zhabrova and E. V. Egorov, Radiokhimiya 1, 538 (1955).
5. G. M. Zhabrova, V. I. Vladimirova, and E. V. Egorov, Zhur. Fiz. Khim. 33, 2451 (1959).
6. S. Z. Roginskii, M. I. Yanovskii, Lu P'ei-chang, G. A. Gaziev, G. M. Zhabrova, B. M. Kadenatsi, and V. V. Brazhnikov, Doklady Akad. Nauk SSSR 133, 878 (1960).*
7. G. M. Zhabrova, V. I. Vladimirova, and O. M. Vinogradova, Contribution to the Conference on Organic Catalysis [in Russian] (November, 1959).
8. V. F. Bogolyubov, Radiotekhnika i Élektronika 3, 323 (1957).
9. F. I. Vilesov and A. N. Terenin, Doklady Akad. Nauk SSSR 125, 1058 (1959).*
10. É. Kh. Enikeev, L. Ya. Margolis and S. Z. Roginskii, Doklady Akad. Nauk SSSR 124, 606 (1959).*
11. E. Wicke, Z. Electrochem. 53, 279 (1949).
12. K. Hauffe, Advances in Catalysis 7, 213 (1955); Collection: Electronic Phenomena [Russian translation] (IL, 1958) p. 241.
13. G. M. Schwab, Semiconductor Surface Physics, Edited by Kingston (1956) p. 283.
14. W. E. Garner, Advances in Catalysis 9, 169 (1957).
15. F. F. Vol'kenshtein, Uspekhi Khim. 27, 1304 (1958).

* Original Russian pagination. See. C. B. translation.

CAPILLARY RISE OF A LIQUID IN POROUS MEDIA AND CAPILLARY HYSTERESIS

D. N. Nekrasov and M. M. Kusakov

Physicochemical Institute, Academy of Sciences, USSR
(Presented by Academician A. V. Topchiev, April 11, 1960)
Translated from Doklady Akademii Nauk SSSR, Vol. 133, No. 6, pp. 1379-1380, August, 1960
Original article submitted April 11, 1960

As have been shown in [1], in circular tubes with varying cross section there exist several equilibrium heights dependent upon the form of the capillary for the capillary rise of a liquid with a low viscosity. For the case of a porous medium consisting of an infinitely high number of capillaries interconnected, with different cross sections and an intricate shape, the problem of capillary rise cannot be solved analytically. However, if one starts by assuming a vertically erected equivalent capillary with a varying circular cross section,* then, using the method explained in [1] and experimental data on the capillary rise or depression of the liquid in actual porous media, it may be shown that the capillary hysteresis in this case results in the existence of an infinite number of equilibrium heights confined between two limiting (minimum and maximum) values.

For such an equivalent capillary the set of equations

$$\begin{aligned} h\rho g &= \frac{2\sigma}{r}; \\ r &= f(h), \end{aligned} \tag{1}$$

where $\underline{h}$ represents the capillary rise, ρ the density of the liquid, $\underline{g}$ the acceleration due to gravity, σ the surface tension of the liquid against its saturated vapor and $\underline{r}$ the radius of the capillary, will have an infinite number of roots $(h_1)_{min} < h_2 < \ldots < (h_n)_{max}$. The potential energy U for this case will be given by the relation

$$U = -\rho g \int_0^V (p_k - h)\, dV, \tag{2}$$

where p_k represents the capillary pressure expressed in the same units as the height $\underline{h}$ of the column of liquid and V the volume of the liquid in the capillary. For an actual porous medium the potential energy U will be given by an analogous relation and the values $p_k - h$ and V may be measured experimentally. Having obtained the relation $V = f(p_k - h)$ in the form of a graph one may calculate graphically the value of U for each value of the mean height $\bar{h} = V/S$ where S represents the porosity of the medium (which may be taken to be constant) and in this way obtain the graph of $U = f(\bar{h})$. From the condition $\frac{\partial U}{\partial \bar{h}} = 0$ the equilibrium height of capillary rise may be found.

*For this the shape of the capillary described by the equation $r = f(h)$ may be as intricate as desired.

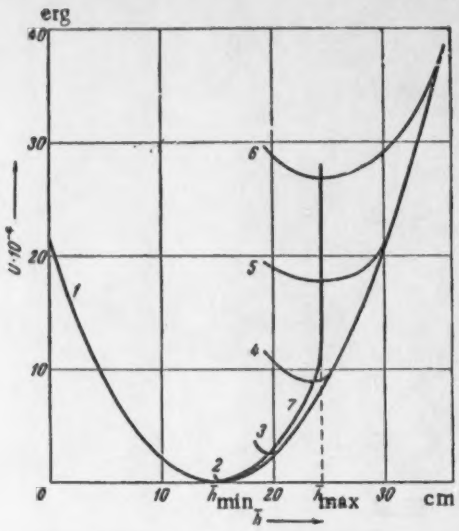

The potential energy of gravity and capillary forces acting on the liquid in a porous medium versus the mean height of capillary rise.

This method was tested experimentally on the capillary in porous media consisting of hydrophilic quartz sand with grain sizes varying from 0.075 to 0.45 mm. The set-up made it possible to observe the capillary rise or retreat of the liquid in the porous medium and to measure very accurately the change in the volume of water in the porous medium at various values of $p_k - h$.

The Figure shows the graph of $U = f(\bar{h})$ for one of the porous media (grain size between 0.35 and 0.42 mm). Curve 1 corresponds to the capillary rise. The minimum value $U = 0$* corresponds to the minimum mean equilibrium height, $(\bar{h}_1)_{min} = 15.42$ cm, of the capillary rise of water in the porous medium. The curves 2-6 calculated as examples (the number of similar curves may be extended infinitely) correspond to the retreat of water from heights $h > (\bar{h}_1)_{min}$. An advance of the liquid to a height higher than $(\bar{h}_1)_{min}$ was effected by a corresponding change in the value and the sign of $p_K - h$.

As is obvious from the Figure each of the curves 2-6 shows a minimum which corresponds to an equilibrium height of capillary retention of the liquid when it retreats in the porous medium. Curve 7, which merges into the straight line $h = (\bar{h}_n)_{max}$, is the locus of the minima in the potential energy; $(\bar{h}_n)_{max}$ represents the maximum mean value of the capillary rise of water in the porous medium. When the liquid retreats after having been raised to a height $h > (\bar{h}_n)_{max}$, it is retained in the position corresponding to the height $h = (\bar{h}_n)_{max}$. For the case shown in the Figure $(\bar{h}_n)_{max} = 24.28$ cm. All other experimentally observed heights of the capillary rise of water in the porous medium satisfy the inequality 15.42 cm $\leq \bar{h} <$ 24.28 cm. The minimum height $(\bar{h}_1)_{min}$ corresponding to the lowest value of the potential energy U is the most stable position.

Thus, it follows from a consideration of general equilibrium conditions and from an experimental test of these conditions that, in the case of porous media, the capillary hysteresis results in the existence of an infinite number of equilibrium heights for the capillary rise, which are confined between a minimum and a maximum value.

LITERATURE CITED

1. M. M. Kusakov and D. N. Nekrasov, Doklady Akad. Nauk SSSR 119, 1, 107 (1958).**

* In the graph of $U = f(\bar{h})$, just as in [1], the minimum energy was chosen as $U = 0$.

** Original Russian pagination. See C. B. translation.

EFFECT OF β-RADIATION OF S^{35} ON ISOTOPIC EXCHANGE OF OXYGEN IN THE SYSTEM $Na_2SO_4{}^{16}-O_2{}^{18}$

Academician Vikt. I. Spitsyn and V. G. Finikov

Institute of Physical Chemistry, Academy of Sciences, USSR

Translated from Doklady Akademii Nauk SSSR, Vol. 133, No. 6, pp. 1381-1383, August, 1960
Original article submitted May 21, 1960

The application of preparations with high specific activities has attracted the attention of investigators to the change in the physicochemical properties of substances and the kinetics of heterogeneous reactions under the action of radioactive radiation of high intensity [1-4]. The purpose of the present work was to study the effect of the β-radiation of S^{35}, introduced in various amounts into sodium sulfate, on the rate of isotopic exchange of oxygen in the system $Na_2{}^{*}SO_4{}^{16}-O_2{}^{18}$ at 600-800°. The investigation procedure was the same as in [5]. In the experiments the temperature was kept constant with an accuracy of ±0.5°.

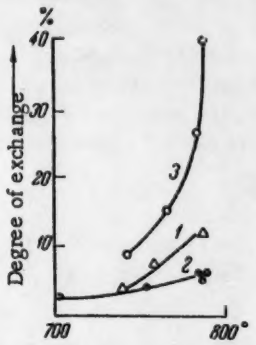

Fig. 1. Temperature dependence of the degree of oxygen exchange in the system $Na_2{}^{*}SO_4{}^{16}-O_2{}^{18}$. Specific activities of preparations (mC/g): 1) 0.08; 2) 0.50; 3) 10.

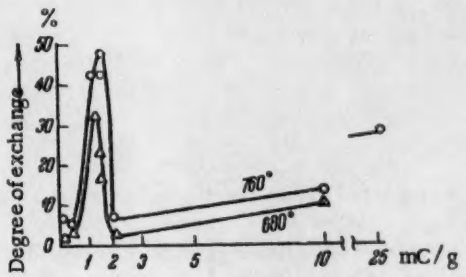

Fig. 2. Relation between the degree of oxygen exchange in the system $Na_2{}^{*}SO_4{}^{16}-O_2{}^{18}$ and the specific activity of the solid phase.

Active sulfate (4-6 g for each series of experiments) was prepared by mixing solutions of active and inactive sodium sulfates with subsequent evaporation of the solutions and firing of the crystals to constant weight at 600°. All the preparations had the same specific surface, which was approximately equal to 5 m^2/g.

For studying the isotopic exchange we used oxygen containing about 1.5 at.% of O^{18}. The isotopic composition of the gas phase was determined with an MS-1 mass spectrometer and the amount of O^{18} in the solid phase was determined with an accuracy of about 2%. The isotopic exchange was studied with preparations with specific activities of 0.08, 0.50, 1.25, 1.50, 1.58, 1.94, 10, and 25 mC/g. Curves of the time dependence of the composition of the gas phase made it possible to calculate the degree of exchange, the rate constants of the reaction,

Dependence of the Degree of Exchange on the Time the $Na_2\overset{*}{S}O_4$ Preparations Were Stored.

Preparation No.	Experiment temp. in °C	Specific activity in mC/g	Storage time in days	Degree of exchange after 8 hr in %	
				before storage	after storage
1	786	0.50	4	5.6	6.3
2	782	10.0	15	26.8	–
	785			–	40.6
3	780	25.0	8	18.5	38.6
	760		6	24.8*	29.6

*The preparation was stored for 2 days before the first measurement.

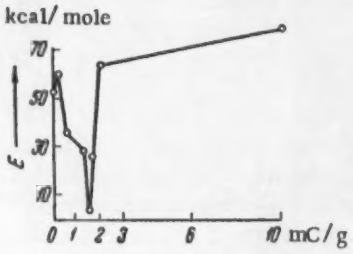

Fig. 3. Relation of the activation energy of the isotopic exchange of oxygen in the system $Na_2\overset{*}{S}O_4{}^{16}-O_2{}^{18}$ to the specific activity of the solid phase over the temperature range 700-800°.

and the activation energy of the process. Figure 1 gives as an example the temperature dependence of the degree of exchange reached after 8 hr for three series of experiments. From this type of data we determined the degrees of exchange for 680 and 760°, and the results are compared in Fig. 2.

Without the effect of radioactivity, the degree of oxygen exchange at 750-800° over the given time interval is only 1-1.5% and the activation energy equals 54 kcal/ mole [5]. As isotherms of the degree of exchange show (Fig. 2), the introduction of S^{35} into sodium sulfate led to an increase in the exchange rate in all cases. With a gradual increase in the specific activity there was a sharp increase in the degree of exchange, which reached a maximum at 1.5 mC/g, after which the rate of the process fell equally sharply and then, as a result of a further increase in the specific activity from 2 to 25 mC/g, there was a slower increase in the rate of the process. A similar effect of radioactive radiation on isotopic exchange has also been observed in other heterogeneous systems [2, 6].

As Fig. 3 shows, the activation energy changed in such a way that it passed through a minimum (4 kcal/ mole) in the region of $Na_2\overset{*}{S}O_4$ specific activities of 1-2 mC/g, while at specific activities of 0.08, 1.94, and 10 mC/g its values equaled 61, 65.5, and 80 kcal/ mole, respectively, i.e., exceeded the value found for isotopic exchange in the absence of radioactivity. The change in the activation energy indicates a change in the reaction mechanism with a change in the intensity of the radioactive radiation.

A peculiar accumulation of the radiation effect with time was observed in active preparations of sodium sulfate. The data in the Table show that isotopic exchange proceeded more rapidly, the higher the initial specific activity of the $Na_2\overset{*}{S}O_4$ samples and the longer their storage time.

A certain fall in the activity of the $Na_2\overset{*}{S}O_4$ preparations as a result of decay of the S^{35} should have decreased the degree of exchange if the radiation had an effect on only the gas phase. Radiochemical phenomena evidently have a substantial effect on the properties of the surface of the solid phase. Radioactive preparations of $Na_2\overset{*}{S}O_4$ acquire a grey-violet color with time and the intensity of this depends on the storage time and the specific activity. When heated to 600°, such preparations become colorless again in a short time. Comparing this fact with the data in the Table indicates that defects in the crystal lattice, arising under the action of radioactive decay, may be divided into two groups: those which are readily restored (change in electron density) and those which cannot be "annealed" (for example, the appearance of Cl^{35} instead of S^{35}). The accumulation of defects which are retained at high temperature must facilitate diffusion processes and thus promote isotopic exchange.

The authors would like to thank V. A. Kiselev and V. L. Litvakov for carrying out the mass spectrometric analyses.

LITERATURE CITED

1. Vikt. I. Spitsyn, Izvest. Akad. Nauk, SSSR, Otdel. Khim. Nauk, 11, 1296 (1958);* Österr. Chem. Ztg. 60, 130 (1959).
2. Vikt. I. Spitsyn and I. E. Mikhailenko, Doklady Akad. Nauk SSSR 121, 319 (1958);* Atomnaya Energiya 5, 463 (1958).*
3. A. A. Balandin, Vikt. I. Spitsyn, et al., Doklady Akad. Nauk SSSR 121, 495 (1958).*
4. Vikt. I. Spitsyn and V. V. Gromov, Doklady Akad. Nauk SSSR 123, 722 (1958);* Radiokhimiya 1, 181 (1959).
5. Vikt. I. Spitsyn and V. G. Finikov, Doklady Akad. Nauk. SSSR 108, 491 (1956).*
6. I. E. Mikhailenko and Vikt. I. Spitsyn, Doklady Akad. Nauk SSSR 131, 129 (1960).*.

*Original Russian pagination. See C. B. translation.

THE MOBILITY OF MODIFYING ADDITIVES IN SILVER

Yu. N. Stepanov, L. Ya. Margolis, and Corresponding Member,
Academy of Sciences, USSR, S. Z. Roginskii

Physical Chemistry Institute, Academy of Sciences, USSR
Translated from Doklady Akademii Nauk SSSR, Vol. 133, No. 6, pp. 1384-1387,
August, 1960
Original article submitted May 18, 1960

Work on the gaseous modification of metals [1-5] has shown that it is possible to bring about a considerable change in the catalytic activity of solids by the action of small quantities of added nonmetals (oxygen, nitrogen, etc.). Sharp maximum values of the activity in ethylene hydrogenation reactions are observed at a definite concentration of additive in the metal (1 atom of nonmetal per 100 atoms of metal). The introduction of sulfur ions into nickel [6], and of phosphate ions into palladium [7], has also shown a modifying action on the hydrogenation reaction.

In later work [8] on the action of additives on metals and oxide catalysts, it was shown that the gaseous promoting action is a particular case of the general modification of catalysts, which is a fundamental method for controlling their activity and selectivity. The use of sensitive radioactive tracer methods of study has extended the range of observations on the modifying action of nonmetal additives on metals, and has shown that halogens have a high efficiency in this respect [9, 10]. Measurement of the work of removal and the electrical conductivity of different metals and semiconductors has shown that one of the principal reasons for the modifying action is the change in the activation energy of the chemisorption and of the catalytic process under the influence of the charging of the surface [11]. Other cases of kinetic modification exist, however, for which the basic change in the activity is due to a large change in the preexponential factor K_0 [12].

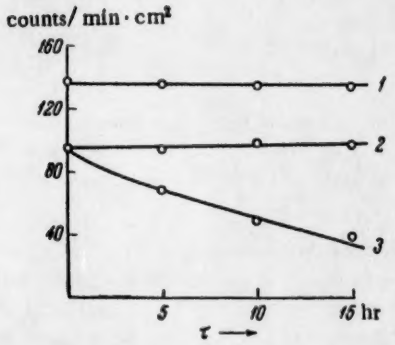

Fig. 1. Change in the specific activity of the silver catalyst after being heated at 300° in different gas media: 1) in nitrogen (without oxygen); 2) in air; 3) in a mixture of air + 3% C_2H_4.

In the analysis of the modification phenomenon, it is usual to examine additives which are irreversibly attached to the solid. These may be solid solutions or mixed phases. As far as modification by nonmetal additives is concerned, however, this picture is too categorical, since displacement of the nonmetal additive in the solid has been observed [4, 13]. In this connection, it was considered of interest to study the mobility of nonmetal additives introduced into a silver catalyst during the catalytic process.

The aim of the present work was to examine two particular problems: the displacement within the layer, and the removal into the bulk, of nonmetals added to a solid, and the uptake of nometals from gaseous molecules and their behavior in the layer (subsequent communication).

TABLE 1

The Influence of Different Reducing Agents on the Change in the Specific Activity of Silver

Composition of gas mixture	Average specific activity of catalyst, counts/(min · cm²)		Rate of removal of chlorine, min^{-1}	Concentration of chlorine in silver, %		
				determined nephelometrically		determined radiometrically after heating
	initial	after heating		initial	after heating	
Hydrogen	260	48*	$0.68 \cdot 10^{-2}$	$1.0 \cdot 10^{-2}$	$1.6 \cdot 10^{-3}$	$1.8 \cdot 10^{-3}$
Ethylene	360	100	$0.24 \cdot 10^{-2}$	–	–	–
Nitrogen + 5.3% isopropyl alcohol	330	56	$0.27 \cdot 10^{-2}$	$7.7 \cdot 10^{-3}$	$2.6 \cdot 10^{-3}$	$1.9 \cdot 10^{-3}$
Nitrogen + 2% ethylene oxide	330	88	$0.25 \cdot 10^{-2}$	$7.7 \cdot 10^{-3}$	$3.7 \cdot 10^{-3}$	$2.2 \cdot 10^{-3}$
Carbon monoxide	330	340	0.0	$7.7 \cdot 10^{-3}$	$7.9 \cdot 10^{-3}$	$8.0 \cdot 10^{-3}$

*Specific activity after heating for 2 hr.

TABLE 2

Rate of Removal of Different Additives From a Silver Catalyst. Medium: C_2H_4

Additive introduced into the silver	Quantity of additives introduced, wt.%	Initial specific activity, $\frac{\text{counts}}{\text{min} \cdot \text{cm}^2}$	Specific activity after heating, $\frac{\text{counts}}{\text{min} \cdot \text{cm}^2}$	Rate of removal of additive, min^{-1}	Quantity of additive removed, %
I^-	$8 \cdot 10^{-3}$	2000	630	$0.23 \cdot 10^{-2}$	70
Cl^-	$8 \cdot 10^{-3}$	385	135	$0.22 \cdot 10^{-2}$	65
SO_4^{2-}	$9 \cdot 10^{-2}$	277	180	$0.12 \cdot 10^{-2}$	35

Labelled isotopes of the nonmetal additives (Cl^{36}, I^{131}, and S^{35}) were introduced into silver powder, with thorough mixing, by adsorption from salt solutions (NaCl, KI and Na_2SO_4). The silver powder was compressed to form tablets of diameter 10 mm and height 5 mm, after which the radioactivity of the surface was determined using an end window counter with mica window of thickness 1.5 mg/cm².

The uniformity of distribution of the additive through the tablet was checked radiometrically. The silver tablets obtained in this way were placed in a glass reaction vessel heated by means of an electric coil, after which mixtures of gases were drawn through the reaction vessel at different speeds; the temperature in the catalyst layer was measured with a thermocouple. The specific activity (per 1 cm² of geometrical surface) was determined at 5 hr intervals while the tablets were heated in different gas media.

Figure 1 gives data showing the change in the specific activity of silver containing chloride ions, after heating in nitrogen purified from oxygen, in air, and in a mixture of air with 3% ethylene, at 300°.

No migration of chlorine in the silver catalyst was observed in nitrogen and air over a period of 15 hr. Increase in the temperature to 400-450° had no effect on the movement of additive in these media. In the 3% ethylene–air mixture at the temperature of the catalysis, a slow decrease in the radioactivity was observed. It is probable that, on the surface of the silver grains, reduction of the chloride ion takes place under the influence of the ethylene, as a result of which hydrogen chloride should be formed. If this is the case, all reducing agents containing hydrogen atoms should facilitate the removal of chlorine from the silver surface. Table 1 gives data showing the influence of different reducing agents on the process of the removal of chlorine from silver at 300°, for a heating time of 5 hr and a rate of flow equal to 16 liter/hr.

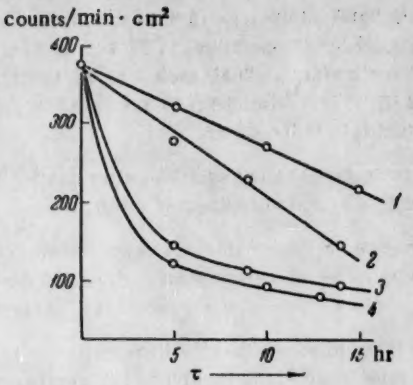

Fig. 2. Change in the specific activity of silver during heating in ethylene–nitrogen mixtures at 300°. 1) In 3% ethylene–nitrogen mixture; 2) in 10% ethylene–nitrogen mixture; 3) in 36-60% ethylene–nitrogen mixture; 4) in ethylene.

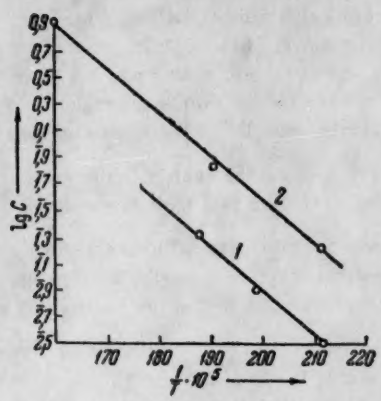

Fig. 3. Relationship between the logarithm of the initial rate of removal of chlorine from silver and the reciprocal of the temperature: 1) in 3% ethylene–air mixture; 2) in 35% ethylene–air mixture.

The rate of removal of chlorine from the silver surface is greatest in hydrogen, and also under the influence of reducing agents containing a hydrogen atom in the molecule. It is known that carbon monoxide exhibits reducing properties and reacts readily with halogens. Treatment of silver containing chlorine with carbon monoxide did not lead to any change in the radioactivity of the catalyst. Nephelometric analysis of the silver for chloride after treatment with carbon monoxide confirmed the radiometric data, and showed that no removal of halogen took place in this case. Special experiments were carried out to determine the hydrogen chloride content of the reaction products. A silver plate was placed in the reaction vessel at a distance of 15 cm from the layer of silver tablets containing Cl^{36} at 300°; the temperature of the plate was kept below 40° by cooling the walls of the upper part of the reaction vessel with water.

After the silver plate had been heated at 300° in ethylene for 5 hr, the radioactivity of the plate was found to be ten times greater than its initial background. A considerable increase in the radioactivity of the silver plate placed above the catalyst layer was also observed when $S^{35}O_4^{2-}$ was introduced into the silver. In a number of experiments, the silver plate at the outlet from the reactor was replaced by a trap containing distilled water and an indicator (methyl red). When the gases were passed through this trap, the products of the reaction between hydrogen or ethylene and the chloride ion present in the silver were found to have a considerable acidity. When the water in the trap was replaced by silver nitrate solution, it was possible to carry out a nephelometric determination of the chloride removed from the catalyst. These results indicate that a reaction takes place involving the formation of hydrogen chloride at the silver surface.

In order to examine the change in the radioactivity throughout the volume of the tablet, sections of silver, of thickness 0.2 mm, were cut. Measurement of the radioactivity of the surface section showed that the reduction takes place throughout the whole volume of the tablet. The possibility of diffusion of chloride ions through the silver lattice was studied using a single crystal of silver. A hole of 5 mm diameter was drilled in the surface of a cylindrical single crystal of thickness 5 mm and diameter 11 mm; this hole was then filled with a small quantity of compressed calcium chloride labelled with Cl^{36}. The single crystal was heated in hydrogen at 300° for 5 hr. Measurement of the radioactivity of sections of the silver monocrystal at a distance of 3 mm from the plane containing the Cl^{36} showed that no appreciable diffusion of chloride ions through the silver lattice took place under these experimental conditions (T = 300°, rate of flow of gas 8 liter/hr).

Thus, the removal of nonmetal from the silver proceeds as a result of the reduction reaction which takes place at the surface of the silver grains. The influence of the ethylene concentration in the ethylene–nitrogen mixture on the rate of change of the radioactivity of the silver, i.e., on the rate of removal of the chlorine from the surface, is shown in Fig. 2. The rate of removal of additive increases with increase in the concentration of

ethylene in the gas mixture. Increase in the concentration above 35% has only a small effect on the rate of removal of chlorine from the silver. Fig. 3 shows the relationship between the logarithm of the initial rate of the process of removal of chlorine from the silver and the reciprocal of the temperature, in 3% and 35% ethylene–air mixtures. The activation energy of the process amounts to approximately 15 kcal/mole. It was considered of interest to examine the rate of the reduction of sulfur labelled with the S^{35} isotope (in the form of SO_4^{2-}), and of iodine labelled with I^{131}, when these elements are present as additives in the silver.

Table 2 shows the change in the activity of silver containing the labelled additive, after heating in ethylene at 300° for 5 hr. The data show that reduction is also observed in the case of iodine and sulfur.

Under the conditions of the catalytic oxidation of ethylene to ethylene oxide, the concentration of nonmetal additive introduced into the silver to increase the selectivity of the oxidation process gradually decreases, as a result of the reduction of the additive by ethylene and subsequent removal of the products of this reaction.

Increase in the concentration of ethylene in the mixture leads to a considerable increase in the rate of reduction of chlorine and hence to a more rapid decrease in the selectivity of the catalyst. The continuous supply of nonmetal additive in the gaseous reaction mixture is thus a more rational method of introducing the nonmetal into the silver.

LITERATURE CITED

1. K. S. Ablezova and S. Z. Roginskii, Doklady Akad. Nauk SSSR 1, 487, 490 (1935).
2. S. Z. Roginskii, Doklady Akad. Nauk SSSR 30, 23 (1941).
3. K. Zhadanovskaya, V. Korolev, and M. Mochan, Doklady Akad. Nauk SSSR 30, 26 (1941).
4. A. Ravdel' and F. Yudin, Doklady Akad. Nauk SSSR 30, 37 (1941).
5. S. Z. Roginskii, Zhur. Obshch. Khim. 15, 1 (1941).
6. S. Z. Roginskii, Adsorption and Catalysis on Nonuniform Surfaces [in Russian](Izd. AN SSSR, 1948).
7. S. Z. Roginskii, Adsorption and Catalysis on Nonuniform Surfaces [in Russian] (Izd. AN SSSR, 1945).
8. L. Ya. Margolis and O. M. Todes, Doklady Akad. Nauk SSSR 58, 421 (1947); Izvest. Akad. Nauk SSSR, Otd. Khim. Nauk, 443 (1947); L. Ya. Margolis, Dissertation [in Russian] (Moscow, 1959); S. Z. Roginskii, Zhur. Obshch. Khim. 21, 1143 (1947).
9. G. M. Zhabrova, Uspekhi Khim. 24, 5, 498 (1955).
10. V. A. Pokrovskii, Uspekhi Khim. 21, 796 (1952); 25, 1448 (1956).
11. S. Z. Roginskii, Problemy Kinetiki i Kataliza 10, 10 (1960).
12. W. H. Hall and P. H. Emmet, J. Phys. Chem. 63, 402 (1959).
13. A. I. Kurilenko, N. V. Kul'kova, et. al., Doklady Akad. Nauk SSSR 123, 878 (1958).•

• Original Russian pagination. See C. B. translation.

THE THERMODYNAMIC PROPERTIES OF CHLORINATED SILANES

M. I. Shakhparonov, S. L. Lel'chuk and K. M. Korchemskaya

The M. V. Lomonosov Moscow State University

(Presented by Academician V. I. Spitsyn, April 4, 1960)
Translated from Doklady Akademii Nauk SSSR, Vol. 133, No. 6, pp. 1388-1390, August, 1960
Original article submitted April 2, 1960

Chlorinated substitution products of silane are well known as basic intermediate products in the laboratory and industrial synthesis of silicoorganic polymers. A systematic study of the thermodynamic properties of solutions of these substances would be of great practical and theoretical value. In the current communication we give the principal results of investigations of the pressure, P, and the density, γ, of saturated vapors of the following systems: CH_3SiHCl_2–$SiCl_4$; $SiHCl_3$–C_6H_6; CH_3SiCl_3–$SiCl_4$; $(CH_3)_3SiCl$–CH_3SiHCl_2; $(CH_3)_3SiCl$–CH_3SiCl_3, and also solutions of CH_3SiHCl_2 and CH_3SiCl_3 in azeotropic mixtures containing 45.93 moles percent of $(CH_3)_3SiCl$ and 54.07 moles percent of $SiCl_4$.

Constants of the Antoin Equation

X_1	A	B	C
CH_3SiHCl_2(1) — $(CH_3)_3SiCl$(2)			
1,000	19,6410	18222,2	1046,2
0,900	4,1838	116,03	46,72
0,500	8,9130	2390,0	347,7
0,216	8,4039	2153,5	336,1
0,100	6,7000	1036,2	215,0
0,000	6,2424	829,4	188,6
$SiHCl_3$(1) — C_6H_6(2)			
1,000	4,5403	188,85	81,79
0,900	5,9874	669,1	180,6
0,640	7,0797	1280,32	262,9
0,4995	5,8702	684,14	180,53
0,300	7,6490	1757,6	311,7
0,230	5,4023	523,72	146,55
CH_3SiHCl_2(1) — $SiCl_4$(2)			
0,895	6,4484	887,76	206,45
0,690	8,3908	2103,5	337,3
0,495	9,7062	3204,5	422,8
0,200	8,6719	2369,5	356,9
0,060	7,5487	1572,95	281,63
0,000	7,4042	1442,8	261,7
CH_3SiCl_3(1) — $(CH_3)_3SiCl$(2)			
1,000	8,6655	2380,6	345,16
0,850	8,5799	2324,9	343,17
0,532	9,7555	3371,9	428,20
0,150	8,12392	2057,4	324,50
CH_3SiCl_3(1) — $SiCl_4$(2)			
0,900	7,8405	1774,6	293,2
0,600	9,2407	2877,7	391,27
0,300	13,0808	7291,1	656,1
0,100	7,0783	1274,9	245,4
Azeotrope(1) — CH_3SiHCl_2(2)			
1,000	8,4765	2210,91	340,23
0,950	6,3505	847,59	197,91
0,500	22,3568	26090,1	1292,9
0,050	6,2535	793,8	193,48
Azeotrope (1)—CH_3SiCl_3(2)			
0,900	8,5736	2449,2	361,6
0,500	9,8962	3458,1	432,9
0,208	7,8291	1790,65	298,06

The method of measuring P and γ is described in [1]. The individual liquid components, after chemical purification and distillation, had the following densities, d^{20}_4 and boiling points at 760 mm mercury:

Compound	d^{20}_4	B.P. °C
$SiHCl_3$	1.3451	31.9
C_6H_6	0.8787	80.1
CH_3SiHCl_2	1.1049	41.1
$(CH_3)_3SiCl$	0.858	57.6
$SiCl_4$	1.483	56.8
CH_3SiCl_3	1.2770	65.9

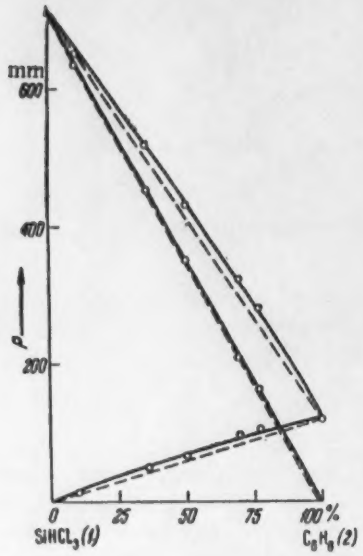

Fig. 1.

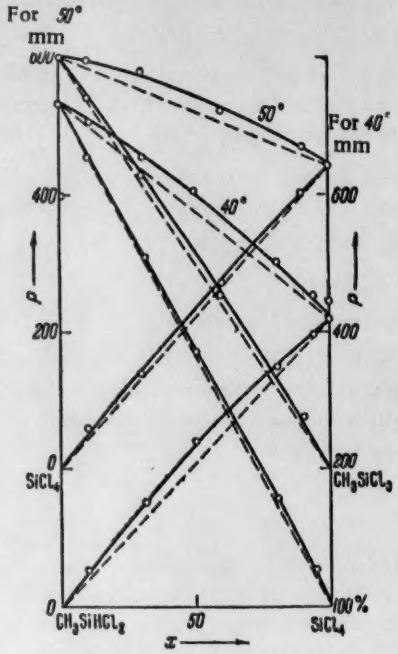

Fig. 2.

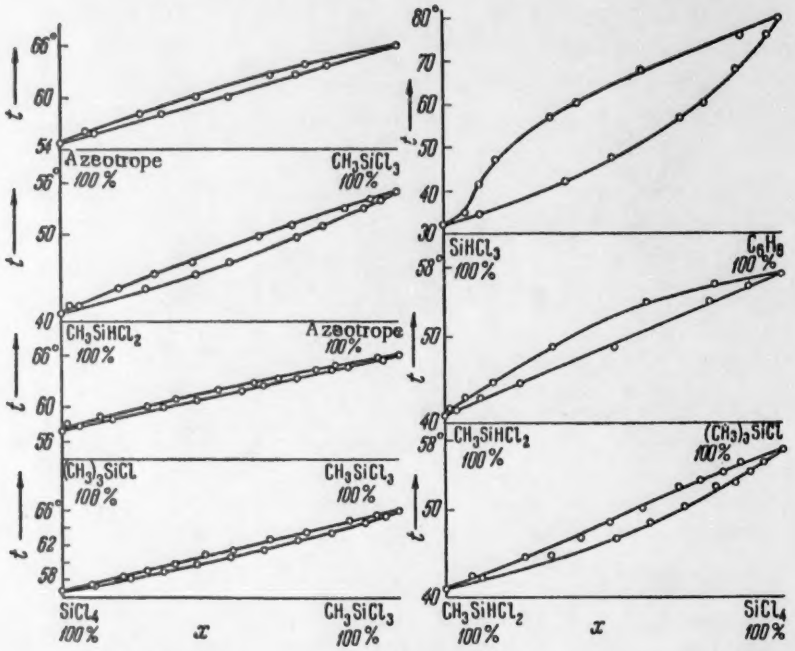

Fig. 3.

The Table gives the constants of the Antoin Equation:

$$\log P = A - B(C + T),$$

calculated from the experimental data for the pressure P for the individual components and their solutions.

From the equation, $\overline{M} = \gamma RT/P$, the mean molecular weight of the saturated vapors has been calculated, and subsequently, from the formula, $\overline{M} = \sum_i M_i x'_i$, their composition has been determined. Together with this, the partial pressures, P_i of the components of the vapors has been calculated. The values of P_i and x'_i were independently checked by the conditions of thermodynamic compatibility, which permitted us to determine these values with an accuracy of 1-2%.

Figure 1 gives the relationship between the total and partial pressures of the vapor in the system $SiHCl_3$–C_6H_6 and the composition of the solutions at 30°.

Figure 2 gives the isotherms for P and P_i for the system CH_3SiHCl_2–$SiCl_4$ at 40°, and the system CH_3SiCl_3–$SiCl_4$ at 50°.

It can be seen from Figs. 1 and 2 that the solutions under consideration are distinguished by only a small positive deviation from ideal behavior.

The solutions $(CH_3)_3SiCl$–CH_3SiCl_3 CH_3SiHCl_2–$(CH_3)_3SiCl$ azeotrope–CH_3SiCl_3 and azeotrope–CH_3SiHCl_2, within the limits of accuracy of our measurements (1-2%) conform to Raoult's Law over the whole range of concentration. Figure 3 gives the isobars of the solutions investigated by us for P = 760 mm.

LITERATURE CITED

1. M. I. Shakhparonov, E. A. Balamutova, et al., Zhur. Fiz. Khim. (1960).

SIGNIFICANCE OF ABBREVIATIONS MOST FREQUENTLY ENCOUNTERED IN SOVIET PERIODICALS

FIAN	Phys. Inst. Acad. Sci. USSR.
GDI	Water Power Inst.
GITI	State Sci.-Tech. Press
GITTL	State Tech. and Theor. Lit. Press
GONTI	State United Sci.-Tech. Press
Gosenergoizdat	State Power Press
Goskhimizdat	State Chem. Press
GOST	All-Union State Standard
GTTI	State Tech. and Theor. Lit. Press
IL	Foreign Lit. Press
ISN (Izd. Sov. Nauk)	Soviet Science Press
Izd. AN SSSR	Acad. Sci. USSR Press
Izd. MGU	Moscow State Univ. Press
LEIIZhT	Leningrad Power Inst. of Railroad Engineering
LET	Leningrad Elec. Engr. School
LETI	Leningrad Electrotechnical Inst.
LETIIZhT	Leningrad Electrical Engineering Research Inst. of Railroad Engr.
Mashgiz	State Sci.-Tech. Press for Machine Construction Lit.
MEP	Ministry of Electrical Industry
MES	Ministry of Electrical Power Plants
MESEP	Ministry of Electrical Power Plants and the Electrical Industry
MGU	Moscow State Univ.
MKhTI	Moscow Inst. Chem. Tech.
MOPI	Moscow Regional Pedagogical Inst.
MSP	Ministry of Industrial Construction
NII ZVUKSZAPIOI	Scientific Research Inst. of Sound Recording
NIKFI	Sci. Inst. of Modern Motion Picture Photography
ONTI	United Sci.-Tech. Press
OTI	Division of Technical Information
OTN	Div. Tech. Sci.
Stroiizdat	Construction Press
TOE	Association of Power Engineers
TsKTI	Central Research Inst. for Boilers and Turbines
TsNIEL	Central Scientific Research Elec. Engr. Lab.
TsNIEL-MES	Central Scientific Research Elec. Engr. Lab.–Ministry of Electric Power Plants
TsVTI	Central Office of Economic Information
UF	Ural Branch
VIESKh	All-Union Inst. of Rural Elec. Power Stations
VNIIM	All-Union Scientific Research Inst. of Metrology
VNIIZhDT	All-Union Scientific Research Inst. of Railroad Engineering
VTI	All-Union Thermotech. Inst.
VZEI	All-Union Power Correspondence Inst.

Note: Abbreviations not on this list and not explained in the translation have been transliterated, no further information about their significance being available to us. – Publisher.